50 Copies

NATIONAL AERONAUTICS AND SPACE ADMINISTRATION

Technical Report 32-1196

A Critical Review of the Magnetoplasmadynamic (MPD) Thrustor for Space Applications

Noble M. Nerheim
Arnold J. Kelly

JET PROPULSION LABORATORY
CALIFORNIA INSTITUTE OF TECHNOLOGY
PASADENA, CALIFORNIA

February 15, 1968

NATIONAL AERONAUTICS AND SPACE ADMINISTRATION

Technical Report 32-1196

A Critical Review of the Magnetoplasmadynamic (MPD) Thrustor for Space Applications

Noble M. Nerheim
Arnold J. Kelly

Approved by:

D. R. Bartz, Manager
Research and Advanced Concepts Section

JET PROPULSION LABORATORY
CALIFORNIA INSTITUTE OF TECHNOLOGY
PASADENA, CALIFORNIA

February 15, 1968

TECHNICAL REPORT 32-1196

Prepared Under Contract No. NAS 7-100
National Aeronautics & Space Administration

Contents

Part I. Application of the MPD Thrustor to Solar Electric Space Missions

Part II. Scope of the Survey

Part III. Existing Technology

Contents (contd)

Part IV. Theory

Part V. Discussion

Contents (contd)

Part VI. Conclusions

Tables

Contents (contd)

Figures

Contents (contd)

Figures (contd)

Contents (contd)

Figures (contd)

Abstract

A comprehensive review of the published performance data and proposed acceleration mechanisms of the magnetoplasmadynamic (MPD) plasma accelerator has been made to estimate its capacity to operate in a spacecraft propulsion system. The ability of the MPD thrustor to perform a specific space mission is compared with that of the ion engine for a Mars-orbiter mission for which mission analyses have been made by others. This comparison is based primarily on the reported performance data; however, other required characteristics, such as lifetime, reliability, compatibility with a solar electric power supply, and the associated weight requirements of the power-conditioning equipment, are discussed. The best results have been obtained with lithium, ammonia, and hydrogen; however, many of the data are of questionable validity because of entrainment or other interactions with the test environment.

The definition and attainment of the proper test environment remain one of the biggest problems. Tests conducted at low pressure are less likely to be in error; however, no reliable method exists to determine whether or when entrainment occurs. The thrust-production mechanisms are poorly understood, as indicated in the number of conflicting assumptions, approximations, and processes that have been proposed. The theoretical difficulties stem from the complexity of the analytical problem, the possible masking of the true operating characteristics by experimental ambiguities, and the difficulty of performing the necessary diagnostic measurements with sufficient accuracy.

In spite of the uncertainties associated with the MPD engine, it may be concluded that the ion engine operates more efficiently than the MPD, with the possible exception of operation at a specific impulse of less than 300 s. If the MPD thrustor is to compete with the ion engine as a spacecraft propulsion system, the weight savings gained with the MPD must be enough to offset the higher overall efficiency that can be obtained from the ion engine at present. Before such a comparison can be meaningful, however, the experimental uncertainties surrounding the MPD thrustor must be eliminated and its true performance established.

A Critical Review of the Magnetoplasmadynamic (MPD) Thrustor for Space Applications

Part I. Application of the MPD Thrustor to Solar Electric Space Missions

I. Introduction

The potential of electric propulsion systems for significantly increasing the scientific payload of specific space exploration missions over the payload attainable with a pure chemical propulsion system has been demonstrated in several recent studies (Refs. 1–3). The mission analyses were based on the use of existing launch vehicles, existing ion engines, and the current technology for the design and development of large, deployable solar panels to power the ion engines. These analyses show, for example, that the useful payload that can be put into Mars orbit may be nearly doubled if the chemical propulsion system used to provide the heliocentric ΔV is replaced by an electric propulsion system (Ref. 4).

The possibility of applying electrical propulsion to space missions in the very near future has resulted from recent developments in lightweight solar photovoltaic power sources. Because the power available from the solar panels depends on the distance of the spacecraft from the sun, the determination of the optimum spacecraft trajectories for specific missions using these sources is more complicated than for those using the previously considered nuclear power sources. In addition, this characteristic of the solar power supply imposes the requirement that the propulsion system be capable of throttling efficiently to match the changing supply of electrical power.

The feasibility of using ion engines on prolonged missions has been demonstrated by endurance tests of both the thrustor and the power-conditioning equipment under vacuum conditions. Several thrustors have exceeded 2000 h of operation and one has exceeded 8000 h of vacuum operation (Ref. 5).

Two factors contribute to the advantage of electric propulsion for space missions. The first is the high specific impulse at which an electrically powered engine may operate, and the second is a consequence of the low

level of acceleration, over long periods of time, that can be obtained. Because of the second factor, the approach velocity of the spacecraft at the destination is significantly reduced from that which would result from the usual chemically powered spacecraft trajectories. Using the Mars-orbiter mission as an example again, it is typically found from mission analyses that the weight of the chemical propulsion system needed to achieve capture at Mars is reduced from 60% of the total spacecraft weight for an all-chemical system to only 20% for the electrical propulsion system. It is largely because of this saving in the weight of the propulsion system that the increased payload is gained. For other missions, e.g., a Jupiter flyby mission, the high specific impulse represents the primary advantage (Ref. 4).

All the systems and mission analyses conducted to date have assumed the use of ion thrustors because the ion thrustor is in an advanced state of development and no other electrical propulsion systems have, as yet, demonstrated the performance and reliability to compete with the ion engine. However, there are two major limitations to the solar-powered ion engine propulsion systems. First, the ion thrustors show a rapid fall-off of efficiency at a specific impulse below 4000 s. This characteristic drives the mission-required specific impulse above that which would be optimum if the efficiency remained constant. Second, ion thrustors are characterized by high-voltage (kV range), low-current (mA) power requirements. Because the solar-array power supply is typically a low- to moderate-voltage ($<$200 V) and medium- to high-current (A) source, a considerable amount of dc-to-dc power-conditioning equipment has to be employed to properly match the solar panels to the ion thrustors. A thrustor system that does not share these disadvantages, that demonstrates performance which is competitive, or nearly so, with the ion engine, and that meets the mission requirements of reliability and lifetime could be employed to advantage on space exploration missions.

II. Purpose of the Survey

A thrustor that may be competitive with the ion engine is the MPD arc, which has indicated some potential for high specific impulse, efficiency, and lifetime. Because this continuous thrustor is characterized by low voltage ($<$100 V) and high current ($>$100 A), it is more easily matched to the solar panel power supply and would require less power-conditioning equipment than does the ion thrustor. Other potential advantages and favorable characteristics of the MPD thrustors are (1) the ruggedness and simplicity of the engine, (2) the potential for efficient, high-specific-impulse operation, (3) the throttlability of both the propellant feed rate and the power level, (4) the adjustable operating voltage level, and (5) the capacity for much higher thrust densities than are possible with ion engines. The high thrust density is not of particular advantage for the relatively low-powered engines considered in the missions referred to above, but could be a very definite advantage in future missions that may require greater power levels.

This survey evaluates the current status of the MPD arc, outlines its operating problems, and attempts to determine the course of its future development, particularly its potential as a solar electric thrustor. A parallel objective of the study is a realistic assessment of the potential of the MPD arc as a thrustor suitable for application to more general types of spacecraft propulsion systems.

III. Solar Electric Spacecraft Characteristics

To illustrate the power supply characteristics of the solar electric spacecraft, a typical mission profile will be described (Refs. 1, 4). A chemical booster is used to launch the spacecraft to earth-escape velocity and, perhaps, to supply a small excess velocity to optimize the mission. After the spacecraft is free from the influence of the earth, the thrustors are activated. The analysis of the Mars-orbiter mission shows flight times of between 150 and 400 days to be typical. The flight time depends upon the excess velocity desired at Mars, the propulsion efficiency, the specific weight of the power plant, and the specific impulse of the thrustor. Once in the vicinity of Mars, the electric propulsion system, having operated continuously (or quasi-continuously with modest periods of coasting), is jettisoned and Martian orbit is obtained by means of chemical propulsion.

During powered transit to Mars, the mean solar energy reaching the solar panels decreases as the inverse square of the radial position of the spacecraft from the sun. However, as the spacecraft proceeds away from the sun, the solar cells become cooler and, as a consequence, more efficient. Analysis indicates that for typical lightweight solar panel construction, solar cell efficiency should continue to increase out to approximately 3 AU. This increase in efficiency is manifest as an increase in solar-cell voltage. Therefore, as the spacecraft travels

toward Martian rendezvous, the solar cell current decreases and the voltage increases. The overall effect is such that the net solar cell output varies not as the inverse square of the distance from the sun but rather approximately as $r^{-1.7}$, where r, the radial distance from the sun, is measured in astronomical units.

The power level of the solar electric spacecraft depends on the specific mission and on the size of the launch vehicle. It may vary from as low as 2.5 kW for a Mars-orbiter launched by an *Atlas/Agena* to more than 50 kW for a Jupiter flyby spacecraft launched with a *Saturn 1B/Centaur* (Ref. 1).

IV. Requirements for a Solar Electric Propulsion System Thrustor

To be compatible with the solar electric power supply and the mission requirements, a thrustor must satisfy a number of requirements that include lifetime, reliability, thrust levels, throttlability, and matching of the thrustor's operating characteristics with the power supply characteristics. The studies referred to above have shown the feasibility of matching the ion thrustor to the solar electric power system. The general requirements that an MPD thrustor has to satisfy in order to be not only compatible with the solar electric spacecraft but also competitive with the ion thrustor can be inferred from these studies. These requirements are based on a detailed analysis of the Mars-orbiter mission with a spacecraft using ion thrustors; the ability of the MPD thrustor to meet the requirements could possibly be improved if the analysis were made using the characteristics of the MPD thrustor. For the present comparison, it is assumed that the trade-offs among the various system parameters determined from the studies using the ion thrustor are applicable to a system using the MPD thrustor.

A. Lifetime

With indicated flight times in the range of 150 to 400 days, thrustor life (defined as the time before a significant change occurs in the operating characteristics) should be equal to, or in excess of, 10,000 h.

B. Performance

A propulsion system may be considered competitive with the ion engine if it can deliver an equal or larger payload at the mission destination. The mission analysis referred to above showed that the maximum payload for the Mars-orbiter mission would be achieved if the ion engine were to operate at a specific impulse of approximately 4000 s. The efficiency of the ion engine used in the analysis was about 60% at 4000 s.

The thrustor efficiency and the specific impulse are defined by Eqs. (1) and (2), respectively:

$$\eta = \tfrac{1}{2}\frac{\dot{m}v^2}{P_i} = \tfrac{1}{2}\frac{T^2}{\dot{m}P_i} \tag{1}$$

$$I_s = \frac{v}{g} = \frac{T}{\dot{m}g} \tag{2}$$

where

$\dot{m}$ = propellant mass feed rate

v = average axial jet velocity

P_i = input power to propulsion system

T = accelerator thrust

g = gravitational constant

The performance a competing thrustor must have to equal the capacity of the ion engine, operating at the optimum specific impulse, to deliver a payload into Mars orbit has been calculated (Ref. 1). The results are shown in Ref. 1 as a curve of specific impulse versus the minimum overall efficiency required to deliver an equal payload. Two of the parameters which were used to make this comparison, and which may vary for different propulsion systems, are the system specific weight α_I, taken as 34 kg/kWe, and the power conversion efficiency, which was assumed to be 93%. A decrease in the specific weight or an increase in the power conversion efficiency of a competing system will lower the required minimum overall efficiency. The result of this trade-off is shown in Fig. 16 of Ref. 1 by a second curve of specific impulse versus the required minimum efficiency for a specific weight of 0.8 of that assumed for the ion engine.[1] The value of α_I, 34 kg/kWe, includes the specific weight of the solar panels, which was assumed to be 23 kg/kWe. The remaining 11 kg/kWe comprised the specific weight of the propulsion system and was assumed to consist of

[1]Both of the curves, for $\alpha = \alpha_I$ and for $\alpha = 0.8\,\alpha_I$, are included on each of the graphs, Figs. 22–28 of the present report, depicting the MPD performance.

3 kg/kWe for the thrustor system, 1 kg/kWe for the propellant tankage, and 7 kg/kWe for the power conditioning and controls.

C. Thrust Level and Throttlability

Because of the variation of the solar panel output, the electrical power will vary during the course of a typical mission. For the Mars-orbiter mission, this variation of electrical power for propulsive purposes is approximately a factor of 2.2. That is, only about 45% of the electrical power available at earth orbit is produced at Mars orbit. At the distance of Jupiter, only about 6% of earth orbit power is available. Therefore, if one were to consider using but a single thrustor, the normal variation of available electrical power during the course of a mission would set rather stringent throttling requirements. This is particularly true for Jupiter missions.

Considerations of overall propulsion system reliability would argue for a modularized thrustor system with a modest degree of redundancy. Furthermore, in order to minimize problems associated with thrust-axis control, it may be desirable to employ pairs of thrustors. The use of thrustor pairs carries with it a subtle benefit. Should the thrustor produce a torque, as there is some evidence to suggest that the MPD thrustor does, then by pairing thrustors of opposite torque, a potentially serious objection to the use of this device can be eliminated.

Although the throttling requirements could be significantly reduced for a Jupiter mission by using a number of thrustors, this is not necessarily true for a Mars mission. If two thrustors are used for the Mars mission, the second engine must be able to double its thrust at the time the first engine is turned off. Thus, the throttling requirement for two engines calls for the ability to operate an engine over a 50% range of thrust, which may be compared with the 45% range required of a single engine. In general, unless more than one thrustor (or thrustor pair) is to be in use at the destination, the engine, assuming all are alike, must be capable of throttling to at least 50% of the maximum thrust produced by that engine.

The power levels of the power systems under discussion range from less than 3 kWe to more than 50 kWe at earth orbit. As will be discussed later, most of the MPD engines that have been tested operate at an input power level considerably greater than the minimum power level contemplated in the mission analyses. Consequently, the ability to scale the experimental engines to smaller sizes becomes of some importance.

Part II. Scope of the Survey

I. Sources of Information

The primary sources of the information used in this survey have been the results of NASA and United States Air Force contracts and the results of investigations at the NASA Lewis Research Center and the NASA Langley Research Center. The primary recipients of the agency contracts were Giannini Scientific Corporation, Santa Ana, California; Electro-Optical Systems (EOS), Pasadena, California; Avco Research Laboratory, Everett, Massachusetts (Avco-Everett); and the Space Systems Division of the Avco Corporation (AVSSD), Wilmington, Massachusetts.[2] A number of other investigations, not necessarily devoted to the development of a propulsion device, have also been reviewed and are included in the following discussions.

II. A Description of the MPD Thrustor

The MPD thrustor is an electrically powered engine that has potential for spacecraft propulsion. This engine produces thrust by ionizing incoming propellant and then accelerating the resulting neutral plasma to high exhaust velocities. The acceleration results primarily from electromagnetic forces.

The electrode geometry of all of the devices considered consists of a central tungsten cathode that is surrounded by a coaxial anode. The propellant is generally injected into the annular region between the cathode and anode well upstream of the cathode tip. (Propellants that are normally stored in a condensed state, such as lithium and ammonia, are vaporized before injection into the discharge region.) The external magnetic field, which is a part of most MPD thrustors, is supplied by a solenoidal coil that surrounds and is concentric with the electrodes. The devices are steady-state, direct-current engines that are operated at current levels usually above 100 A and are characterized by operating voltages, generally below 100 V, that are relatively insensitive to the current level.

Although the individual thrustor power levels required for some of the missions discussed in Part I may be as low as 1 kW, nearly all the experimental thrustors have

[2]For most of the time covered by this survey, the last named laboratory was called the Research and Development Division of the Avco Corporation (AVCO/RAD).

been operated at much higher levels; consequently, this survey is primarily concerned with thrustors designed to operate in the range of 10–200 kW. In addition, the data indicating performance in excess of about 2000 s at reasonably high overall efficiency command most of the interest. The last-named factor limits the preponderance of the performance data considered to only a few propellants. High values of specific impulse have been obtained with hydrogen, deuterium, ammonia, and lithium. Other propellants have been investigated, and, although the high performance capabilities of these propellants are probably limited, very valuable information concerning the acceleration mechanisms has been obtained from experiments with argon, nitrogen, and alkali metals other than lithium.

III. History

With one exception, the laboratories listed in Section I above as having participated in the development of the MPD thrustor were, prior to 1963, investigating plasma accelerators whose geometry and mode of operation differed significantly from the MPD thrustor of today. The investigations that preceded the present effort at each of these laboratories were devoted to studies of either the conventional thermal arc jet or accelerators that were designed to exploit primarily electromagnetic forces.

At two laboratories, Giannini and AVSSD, the primary effort was devoted to the development of the thermal arc jet. The first reports of the attainment of very high values of specific impulse with a steady plasma accelerator, which was called a Thermo-Ionic Accelerator, were published by Ducati in 1963 (Ref. 6). Values of specific impulse up to 10,000 s at an overall efficiency of 46% were obtained with a hydrogen-fed engine by the end of 1963 (Refs. 7, 8). These very encouraging results rewarded the efforts to improve the efficiency and extend the performance of the thermal arc jet. A primary reason given (Refs. 7, 9) for this accomplishment was the lowering of the arc chamber pressure, by increasing the anode throat diameter, from several atmospheres to a fraction of an atmosphere. A typical maximum chamber pressure was about 50 torr. Another reason given was the removal of the supersonic nozzle that had been used to expand the electrically heated plasma (Ref. 9). The stated goal of obtaining a uniform discharge of very high current (greater than 3000 A) is credited to the lowering of the pressure, thereby obtaining diffuse arc attachment at the cathode. The electromagnetic effects associated with the large arc current were stated (Ref. 8) to aid both the acceleration and the containment processes. In later work, described in Refs. 10–17, externally applied magnetic fields were used, and other propellants were investigated.

A quantitative relation of the discharge pressure and the desired diffuse arc attachment has not been obtained, and recent tests (Refs. 15 and 16) at Giannini indicate that the chamber pressure can be higher than the 1963 results. The variation in the chamber pressure was the result of changes in the electrode geometry, which, in some respects, resembles the constricted geometry of the conventional thermal arc jet. An interesting development at Giannini has been the observation that the efficiency is increased as the arc chamber pressure is increased (Ref. 16). This observation followed the recent investigation of the effects of varying the electrode geometry at a fixed value of the feed rate. The increased pressure, which was found to be proportional to the power level, resulted from decreasing the throat diameter. The maximum value of the chamber pressure reported was about 200 torr (Ref. 16), and the limitation on the chamber pressure was a consequence of the damage to the anode that occurred at the higher power levels. These tests were conducted with a strong applied magnetic field.

The first published results of MPD thrustor research at AVSSD (then AVCO/RAD) appeared in 1964. In the initial report (Ref. 18), one of the listed goals was "to explore increases in specific impulse and efficiency which appear to be associated with operation at lower propellant mass flow rates and high current levels." In this initial work, both ammonia and hydrogen were used as propellants, and the research was concerned primarily with the self-field effects; however, a weak (less than 500 G) externally applied magnetic field was found necessary to obtain arc stability and reasonable lifetimes of the electrodes. Strong applied fields were used in nearly all the subsequent work, which included the testing of other propellants, particularly lithium and cesium (Refs. 19–29). The most recent investigations have been devoted almost exclusively to the testing of ammonia (Ref. 29).

At both Avco-Everett and EOS, the use of electromagnetic forces to accelerate the plasma has been emphasized.[3] Hall currents and plasma rotation, caused by

[3]The immediate predecessor (Refs. 30 and 31) of the present Avco-Everett accelerator, which is called the MAARC (magnetic annular accelerator) is shown in Fig. 2a.

$\mathbf{J} \times \mathbf{B}$ forces, were identified as being important in the production of the high-energy plasma stream. A strong magnetic field was used, and helium and argon were the first gases investigated (Ref. 31). By 1962, the configuration which, with but very minor modifications, was used in all subsequent experiments was adopted (Ref. 32). The reasons given for choosing this configuration and operating with a magnetic field were to increase the stability and the electrical impedance of the arc, to reduce energy transfer to the containing walls, and to add momentum, both azimuthally and axially, to the plasma by $\mathbf{J} \times \mathbf{B}$ forces. The initial experiments were made with argon, and the performance was inferred from measurements made with impact pressure probes and other probes. In later experiments (Refs. 33–40) results were obtained with hydrogen and ammonia.

During the period of 1961 to 1964, the group at EOS conducted experiments on a Hall Current Accelerator (Ref. 41). In this device, the applied electric field was axial and the applied magnetic field was radial in a wall-confined annular channel. The thrustor was designed to operate by Hall acceleration of the plasma in the annular channel. The overall efficiency of the device was poor (Refs. 42 and 43), and it was concluded that most of the energy and momentum contained in the exhaust had been transferred to the gas downstream of the accelerator and not to that in the annular channel. As a consequence of this conclusion, design changes, which included the elimination of the annular channel and a revision of the electrode and magnet configurations, were made to enhance Hall acceleration in the region downstream of the accelerator. The devices that were developed with these design changes, all of which have been designated as Hall accelerators, incorporate the features that are used here to describe the MPD thrustor. The first configurations (Refs. 42 and 44) were designed for high-power operation (about 100 kW) with hydrogen and were characterized, along with other features, by an open electrode configuration that had no minimum flow area that could be identified as a throat. However, hydrogen-fed accelerators that were designed for operation in the range of from 1 to 10 kW were constructed with a constricted flow area to increase the pressure at the cathode tip (Refs. 44 and 45). The studies on hydrogen-fueled MPD accelerators at EOS are described in Refs. 42–47.

Because of the potential advantages (which include low frozen-flow losses and easy storability) of the use of lithium as a propellant for space missions, most of the recent effort at EOS has been devoted to investigations of lithium and other alkali metals (Refs. 48–53). The electrode configuration of the alkali metal thrustors has evolved from an open design that resulted in very low pressures at the cathode to a more constricted design with a minimum flow area, or throat, between the anode and cathode. The most recent investigations have been made with a hydrogen-lithium bipropellant (Ref. 51). The EOS engines are now designated ALPHA for "Alkali Plasma Hall Accelerator."

In 1960, Hess (Ref. 54) reported experimental evidence of continuous steady acceleration of a low-density plasma in a Hall accelerator. Using air as the propellant, Hess reported operating voltages between 500 and 1200 V at a current level of about 1.0 A. The exhaust velocity was inferred from the deflection of a thin mica vane placed in the exhaust jet, and the axial acceleration was attributed to the interaction of Hall currents with an applied magnetic field. The confining force to be expected, as well as the rotation of the plasma by $\mathbf{J} \times \mathbf{B}$ forces, was also discussed. In later experiments, current levels of up to 40 A were used (Ref. 55). In more recent experiments with Hall current accelerators (Refs. 56–58), the thrustor configurations that were investigated at NASA Langley were typical of the MPD thrustors discussed in the present report. For most of the experiments, argon has been used as the propellant, and the experiments have emphasized diagnostic measurements. More recently, hydrogen and ammonia have also been tested (Ref. 61). The behavior of engines using a hollow cathode and a porous anode, through which part of the argon was injected, has also been investigated (Ref. 59). Hassan (Refs. 60 and 61) and others (Refs. 62 and 63) have reported theoretical and experimental investigations of engines very similar to those tested at NASA Langley.

The testing of engines developed by AVSSD and EOS at NASA Lewis has produced much useful information concerning thrustor operation at very low pressure (Refs. 64–68). In addition, the group at NASA Lewis has designed and tested a low-thrust continuous plasma accelerator that typically operates at about 2 A (Ref. 69). This device was originally described as a "magnetic expansion engine;" however, in a recent publication, it is designated a "low-power MPD engine" (Ref. 70). The operating characteristics of this engine are very different from those of the engines described above. For example, the voltage is a very strong function of the current. This engine, designed for low-power station-keeping duties,

has been operated on argon and xenon. Very thorough diagnostic measurements, including the measurement of the ion density and the electromagnetic field configurations, have been made.

The operation of MPD engines under transient conditions has also been reported (Refs. 71 and 72). The transient mode of operation allows thrustor operation at very low pressures and also permits the use of diagnostic techniques not applicable to steady-state operation.

Recent surveys and summary articles that include or are devoted to MPD accelerators may be found in Refs. 73–77.

Part III. Existing Technology

I. Early Development

In the early stages of the MPD thrustor development, experimental tests were almost entirely devoted to obtaining performance data, and the emphasis was placed on increasing the overall efficiency, the range of specific impulse, and the lifetime of the electrodes. A number of propellants were investigated. The parallel theoretical studies, in varying degrees of thoroughness at the different laboratories, have been notably ineffective in improving the initial designs. Rather, the changes in thrustor design, made almost entirely on the basis of the experimental results, have been for the purpose of improving the arc stability, increasing the electrode lifetime, and increasing the overall efficiency of the engine.

The scaling of engines to operate at different power levels has also proceeded with little theoretical guidance. The basic axisymmetric engine configuration of a central cathode and coaxial anode has remained unchanged. The major variables in the development have been the strength of the applied magnetic field, variations in the geometry of the electrodes, and the type of propellant tested.

The early progress in increasing the specific impulse was phenomenal, and a large amount of performance data was published that enhanced the future predicted for the device as an efficient engine for space flights. The early optimism was quickly dampened, however, when it became apparent that, at least for some operating conditions – particularly those that produced the highest performance – the measurements were significantly influenced by the interaction with the test environment. Hence, the calculated performance was not the performance to be expected from an engine operating in space. Attention was then directed toward defining the proper test environment, and increased emphasis was placed on purely diagnostic measurements to further the theoretical effort and to provide verification of the measured performance.

In the following sections the development of the existing MPD technology will be described, including the engines tested, the test procedures, and the performance reported with the various propellants. In Section IV the important trends in the theoretical studies are discussed, and the results of these studies are compared with the experimental observations.

II. Propellant Selection

The major considerations in the selection of propellants for electric propulsion systems are the achievement of high overall efficiency at the optimum specific impulse, reliable operation, and the ease of storage during the time required for a particular mission. The condensable propellants that have been tested, ammonia and some alkali metals, require less weight for tankage than do the gaseous propellants. However, hot alkali metal vapors are much more reactive with the materials normally used for electrodes and insulators than are the gaseous propellants, and achievement of the required lifetime may be more of a problem with the alkali metals (Refs. 15, 48, and 51). Furthermore, with the easily condensable exhaust products (Ref. 15), there is a greater possibility of interference with normal spacecraft operations, if any deposition of the propellant on the vital components of the spacecraft should occur.

Because of the lack of an adequate theoretical description of the MPD engine, it is not possible to select the optimum propellant for maximum efficiency on the basis of the known properties of the propellants, and the various propellants must be compared experimentally. However, some qualitative information is obtained from a consideration of the different losses that limit the thrustor efficiency. For example, it is not anticipated that much of the energy invested in ionization or dissociation will be recovered as useful thrust. However, as discussed later in this report, it is not obvious at present that only charged particles may be effectively accelerated in MPD thrustors. Many of the experimental data to be discussed indicate that the ionization of the propellant may be far from complete at the lower values of the specific impulse range.

In addition to the ionization losses, the fraction of the input power that is lost to the electrodes, which is the determining factor for the thermal efficiency, appears to be a function of the propellant type.

For the purpose of identifying losses, a number of partial efficiencies have been defined. The propulsion efficiency, as defined in Part I, is generally called the overall efficiency and is given by Eq. (3):

$$\eta_0 = \frac{\text{total thrust power}}{\text{total electrical input power}} = \frac{\frac{1}{2}\frac{T^2}{\dot{m}}}{IV} \tag{3}$$

where T is the measured thrust, $\dot{m}$ is the propellant feed rate, I is the applied current, and V is the thrustor voltage. Another measurable efficiency, the thermal efficiency, is defined by

$$\eta_{th} = \frac{\text{total power in exhaust}}{\text{total electrical input power}} \tag{4}$$

Because the total power in the exhaust beam is seldom measured, the thermal efficiency is usually calculated from the cooling losses to the electrodes, according to Eq. (5):

$$\eta_{th} = 1 - \frac{\dot{w} c_p \Delta T}{IV} \tag{5}$$

where $\dot{w}$, c_p, and ΔT are the flow rate, heat capacity, and temperature rise, respectively, of the electrode coolant fluid. When the thermal efficiencies of radiation-cooled engines are measured, the coolant is passed through a radiation shield that is located to intercept the radiant energy from the anode (Refs. 15 and 47).

The ratio of the overall efficiency and the thermal efficiency defines a partial efficiency that is sometimes called the thrust efficiency:

$$\eta_T = \eta_0 / \eta_{th} = \frac{\text{total thrust power}}{\text{total power in exhaust}} \tag{6}$$

That part of the propellant power that is used to dissociate and ionize the propellant and is not recovered as useful thrust is called the frozen-flow loss. The partial efficiency that reflects this loss is the frozen-flow efficiency η_F. Because the exhaust composition cannot be correlated with the engine operating parameters at present, it is not possible to predict the frozen-flow losses with any degree of accuracy. To obtain some qualitative information, the calculation of the frozen-flow efficiency is frequently made with the aid of the assumption of complete, single ionization of the propellant. With this assumption, the expression for η_F becomes

$$\eta_F = \frac{\frac{1}{2}\dot{m} v^2}{\frac{1}{2}\dot{m} v^2 + V_i \frac{\dot{m}}{M}} = \frac{I_s^2}{I_s^2 + \frac{2g^2 V_i}{M}} \tag{7}$$

where V_i and M are the ionization potential and molecular weight, respectively, of the propellant. The dissociation energy is added to V_i for molecular propellants, but

the heats of fusion and vaporization of the condensed propellants are seldom included. The ionization potentials and the value of I_s at which η_F is equal to 0.5 are listed for a number of propellants in Table 1.

The assumption of complete, single ionization is probably unrealistic for light propellants at low values of I_s because it overestimates the loss, and for heavy propellants at nearly all values of I_s because it underestimates the loss. For example, spectroscopic observations have indicated the presence of atomic species in the exhaust of hydrogen- and ammonia-fed engines (Refs. 65 and 66) and the presence of multiply ionized species in the exhaust of argon-fed engines (Ref. 56). Furthermore, the performance with hydrogen indicates that the degree of ionization may be as low as 5% (Ref. 39), and with ammonia the performance indicates that the degree of ionization may be between 2 and 20% (Ref. 19). To minimize frozen-flow losses, a propellant with a low first ionization potential is desirable if the second ionization can be suppressed. However, the use of this same criterion to select a propellant for maximum overall efficiency is not universally accepted. Patrick (Ref. 39), for example, has suggested that high performance is more easily obtained with a propellant having a high ionization potential (Part IV, Section II-C-2).

Frozen-flow losses have been calculated by other methods also. For example, the equilibrium composition of hydrogen (Refs. 7 and 21), at a specified pressure, has been used to relate the frozen-flow efficiency to the specific impulse. In addition, multiple ionization has been included, in a very approximate manner, to estimate the frozen-flow losses of cesium (Refs. 20 and 21).

The frozen-flow efficiency is part of the thrust efficiency. To account for the difference between η_T and η_F, another partial efficiency, called the expansion efficiency (Refs. 19 and 21), is sometimes introduced.

The terminology and nomenclature used in the literature to describe the different efficiencies are not standardized. The terms "overall efficiency" and "thermal efficiency" invariably refer to the definitions given by Eqs. (3) and (4), respectively. However, other terms are also used for these efficiencies. Some of the more commonly used expressions are listed in Table 2.

The molecular weight of the propellant may also influence the performance. The directed kinetic energy of a thermally expanded hot gas is proportional to the stagnation temperature and inversely proportional to the molecular weight. If a temperature limitation exists, higher values of specific impulse may be obtained with the lighter gases. Although MPD thrustors are designed to eliminate the necessity of high temperatures, at least near the physical confines of the engine, Cann (Ref. 49) has suggested that the acceleration mechanism of the electromagnetic accelerators may still impose a maximum kinetic energy per unit particle or a maximum temperature. If this is true, it would be advantageous to use a propellant with low molecular weight. A collisional energy addition process, in which the momentum is

Table 1. Some properties of commonly used propellants

Propellant	Atomic weight M, g/g mole	Ionization potential, eV			Dissociation energy D, eV/atom	$\frac{V+D}{M}$	I_s, s ($\eta_F = 0.5$)[a]
		V_1	V_2	V_3			
H_2	1.008	13.6			2.26	15.86	5600
He	4 003	24.58	54.33			6.14	3500
NH_3	4.25[b]	13.83[b]			3.15[b]	3.99[b]	2800
Li	6.94	5.39	75.62			78	1250
N_2	14.008	14.54			5.59	1.435	1700
Na	22.991	5.14	47 29			0.22	660
K	39.100	4.34	31.81	46		0.11	470
Ar	39 994	15.76	27.62	40.9		0.39	800
Cs	132 91	3.87	23.4			0.029	240

[a] I_s at $\eta_F = 0.5$, calculated according to Eq. (7).

[b] Average value per dissociated particle.

Table 2. Nomenclature used to describe various efficiencies

Source	Thrust power / Electric power	Propellant power / Electric power	Thrust power / Propellant power	Available propellant power / Propellant power
Method of calculation[a]	$\frac{T^2}{2\dot{m}\ IV}$	$1 - \frac{\dot{w}\ c_p \Delta T}{IV}$	$\frac{T^2}{2\dot{m}\ (IV - \dot{w}\ C_p \Delta T)}$	Various
This report	Overall efficiency η_0	Thermal efficiency η_{th}	Thrust efficiency η_T	Frozen-flow efficiency η_F
Giannini[b]	Overall η^{eh}	Thermal η^{eq}	Thrust η^{ph}	
AVSSD	Overall ε_0	Arc or thermal ε_{arc}	Propulsion ε_{prop}	Frozen ε_f
Avco-Everett	$\eta_{overall}$	$\eta_{thermal}$	η_{thrust}	
EOS	Thrust η_T or overall (sometimes acceleration) η_0	η_{th}		Frozen-flow η_F
NASA Lewis[d]	Thrust η_T	Energy η_K	Beam η_B	

[a]where

T = thrust — $\dot{w}$ = flow rate of coolant

$\dot{m}$ = mass feed rate — c_p = heat capacity of coolant

I, V = arc current and voltage — ΔT = temperature rise of coolant

[b]Superscripts may be interpreted as "electric-to-gas," "electric-to-kinetic," and "gas-to-kinetic."

[c]An expansion efficiency ε_{exp} defined by $\varepsilon_{prop} = \varepsilon_f \varepsilon_{exp}$ is also used.

[d]The thrust obtained by expelling the unheated propellant is subtracted from the total thrust to obtain T.

transferred from electrons to ions in a prescribed direction instead of randomly, was discussed by Cann (see Part IV, Section II-B-1).

III. Thrustor Configurations

The MPD thrustor consists of a central cylindrical cathode made of tungsten and a concentric axisymmetric anode that is usually surrounded by a solenoidal magnetic field coil. The anode is either made of copper and water-cooled or made of tungsten and radiation-cooled. The propellant is injected radially, axially, or tangentially upstream of the electrodes, or it is injected either through the cathode tip or through the anode. The variations in the geometry of engines designed for operation with a given propellant and of comparable power levels are mainly concerned with the position of the cathode, relative to the anode, and the general configuration of the anode.

Some typical geometries of hydrogen-fueled engines are shown in Figs. 1–9. After preliminary experiments

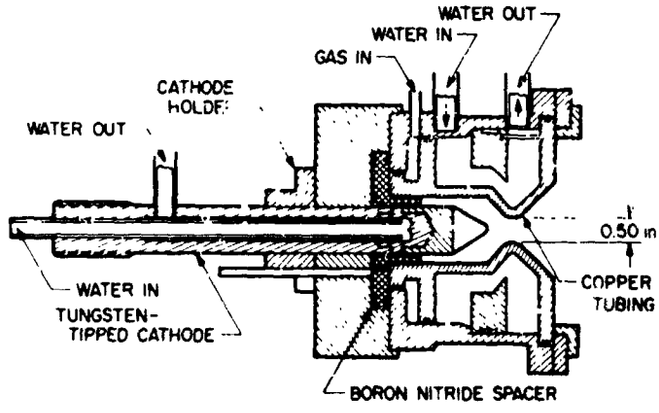

Fig. 1. AVSSD X-2C MPD thrustor used with hydrogen and ammonia (Ref. 19)

with anodes having a straight-through channel, the workers at AVSSD found that better performance (Ref. 18) was obtained with the design shown in Fig. 1 that features an anode throat. This design has been used with both strong and very weak applied magnetic fields and with ammonia as well as hydrogen. In the most recent

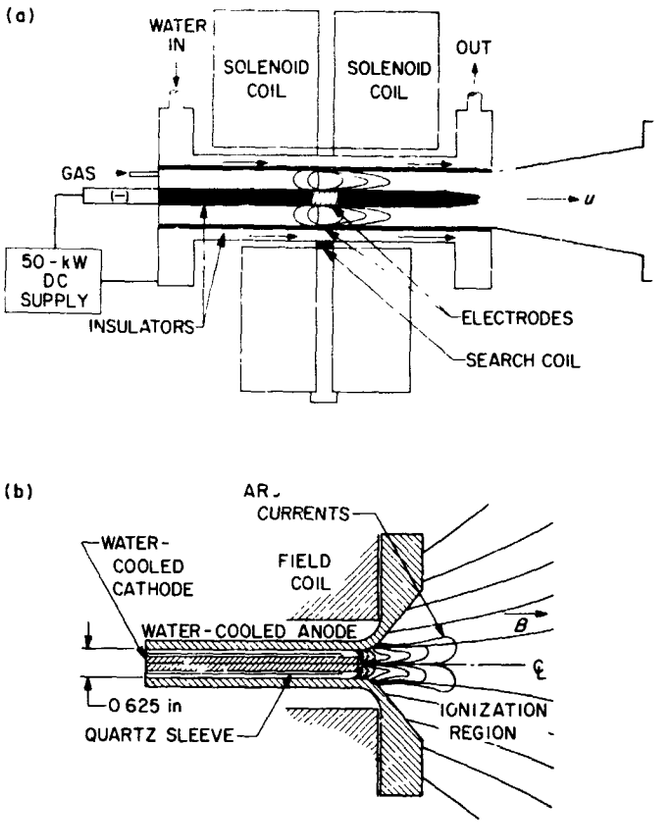

Fig. 2. Avco-Everett Magnetic Annular Arc: (a) Early (1961) configuration used with argon and helium (Ref. 31) and (b) present MAARC used with hydrogen and ammonia (Ref. 40)

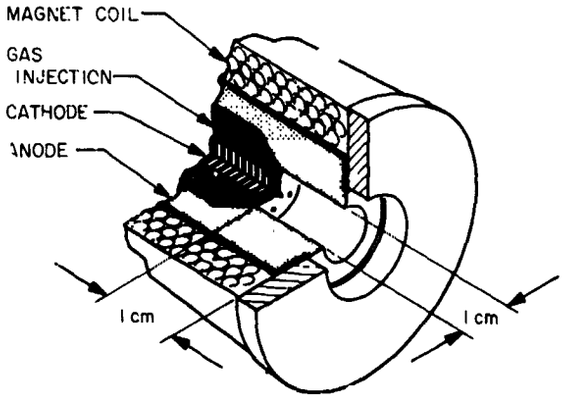

Fig. 3. Early (1964) model of EOS hydrogen-fed MPD accelerator (Ref. 42)

investigations conducted by the group at AVSSD (Ref. 29), the need for a throat was not demonstrated. The performance of the AVSSD engine shown in Fig. 10, which was designed for the recent experiments with ammonia, was comparable with the performance of the

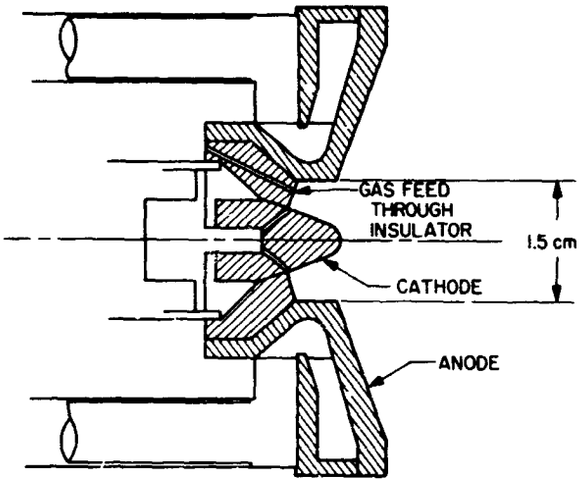

Fig. 4. EOS H_2-1 hydrogen-fed Hall current accelerator (Ref. 47)

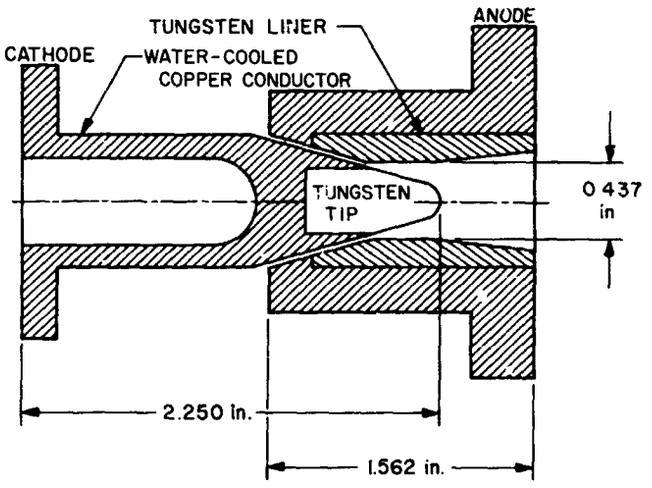

Fig. 5. Giannini hydrogen-fed Thermo-Ionic Accelerator with tungsten-lined anode (Ref. 10)

engine shown in Fig. 1. The Avco-Everett design of Fig. 2b, which followed a less efficient, earlier model in which the anode had a smaller divergent angle (Ref. 32), was found to operate in one of two different voltage modes (Refs. 37 and 40), depending on the axial position of the cathode. One of the earliest MPD engines operated at EOS is shown in Fig. 3 (Ref. 42). The electrode configuration of the later versions was more open. A tungsten anode insert was removed from a previous design to give the EOS H_2-1 engine shown in Fig. 4 (Refs. 44 and 47).

The tungsten liner shown in the anode of the Giannini engine of Fig. 5 was added to improve efficiency

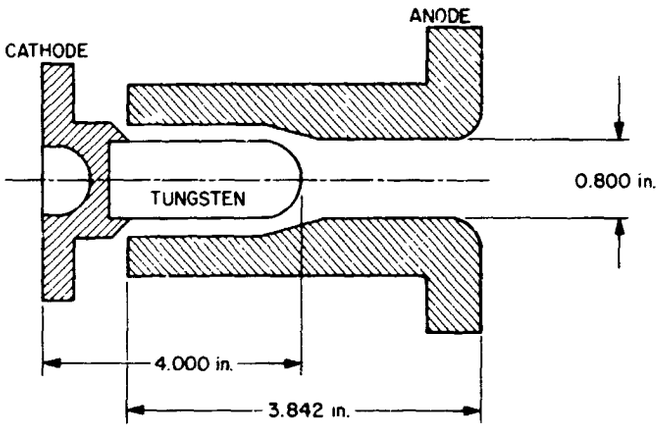

Fig. 6. Giannini hydrogen fed Thermo-Ionic Accelerator. This model was used for one of the early 50-h endurance tests (Ref. 11)

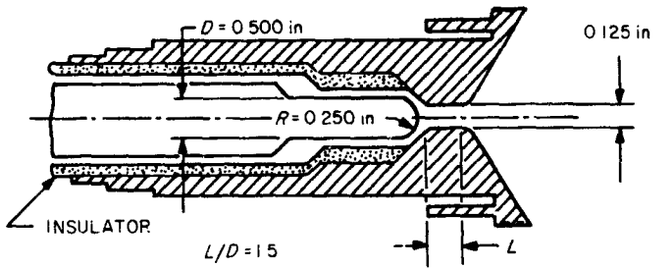

Fig. 7. Giannini hydrogen-fed MPD accelerator. This geometry was used for a systematic study of the engine configuration for a number of anode throat diameters and *L/D* ratios (Ref. 15)

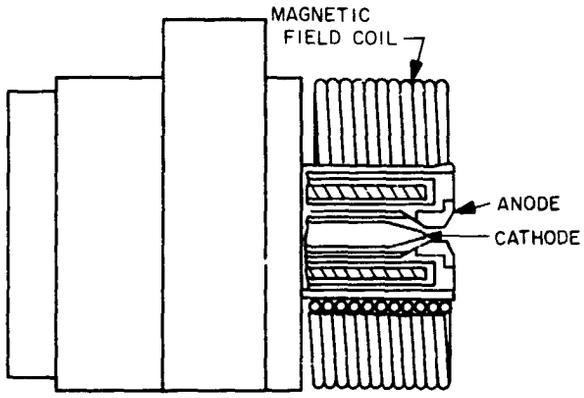

Fig. 8. Low-power (5 kW) Giannini hydrogen-fed accelerator (Ref. 12)

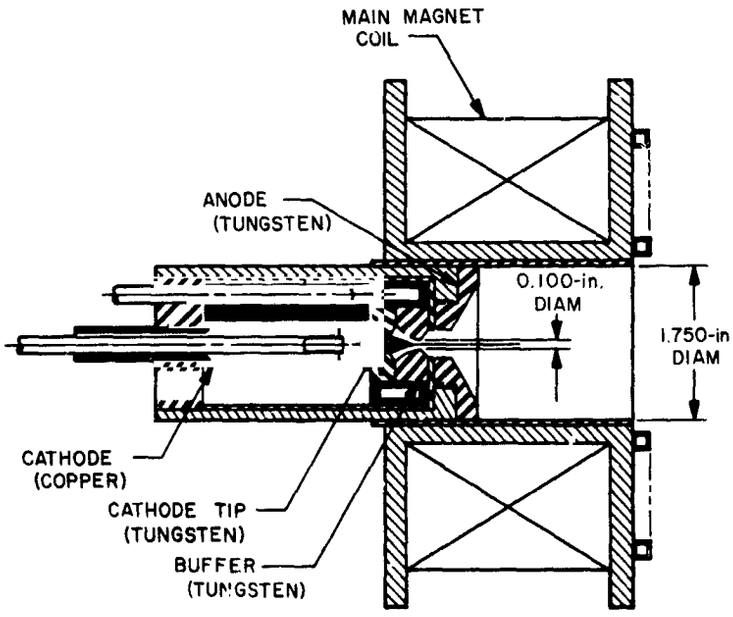

Fig. 9. Low-power (10 kW) EOS H_2-4 hydrogen-fed Hall current accelerator. A tungsten buffer was placed between the anode and the cathode to increase the pressure at the cathode tip (Ref. 47)

(Ref. 10) but was later discarded (Ref. 11) to improve lifetime (Fig. 6). More recently (Refs. 15 and 16), the group at Giannini has begun an experimental program to evaluate the effects of engine geometry by a systematic variation of the anode throat diameter and the throat L/D ratio. The basic geometry of this series of engines is shown in Fig. 7. Two engines designed for low-power operation (less than 10 kW) with hydrogen are shown in Figs. 8 (Refs. 12 and 15) and 9 (Refs. 45 and 47).

The thrustors shown in Figs. 1, 2, and 7 have also been used with ammonia propellant. Two engines (Ref. 29) designed by AVSSD specifically for operation with ammonia are sketched in Figs. 10 and 11. The design shown in Fig. 10 has been used primarily for endurance tests to demonstrate the feasibility of ammonia-fed, radiation-cooled engines. Most of the parametric studies were performed with the water-cooled thrustor (Fig. 11). Various anode diameters, of from 0.4 to 1.25 in., have been tested with the water-cooled design.

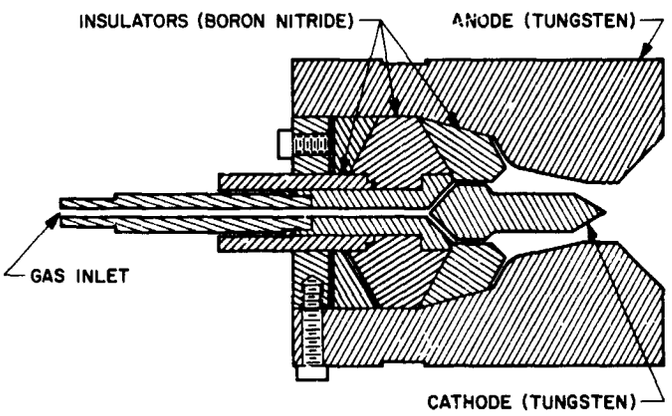

Fig. 10. AVSSD X-7CR radiation-cooled MPD thrustor used with ammonia (Ref. 29)

A much greater variation in the electrode geometry is apparent among the engines designed to operate on alkali metal propellants. To insure stable arc attachment (Ref. 48), the alkali metal vapors must be injected in a manner to prevent the introduction of a condensed phase into the discharge region. The group at AVSSD used cathode-tip injection (Ref. 20), Figs. 12 and 13, for both cesium and lithium, whereas the group at EOS reported better performance for radiation-cooled, anode-fed lithium engines than for cathode-fed engines (Ref. 49). The increase in the length of the cathodes, as depicted in Figs. 14 and 15, was made in an effort to force arc attachment on the cathode at a point away from the insulator placed between the anode and cathode. A determining factor of the engine lifetime was the rate at which the insulator eroded.

A hydrogen–lithium bipropellant was used with one of the earlier (Ref. 49) cathode-fed engines designed at EOS and also with the later anode-fed models. Longer life and increased arc stability were reported for the buffered-cathode design shown in Fig. 16 (Refs. 50 and 51). In this model, an electrically neutral tungsten buffer was placed between the anode and the cathode, and the alkali metal propellant was fed into the cathode region in vapor form. Because of the increased pressure at the cathode, the arc attachment was at the cathode tip. Spot attachment at the cathode tip was found to be more satisfactory than diffuse attachment because the cathode losses were smaller, the discharge was more stable, the erosion was less severe, and the maximum current capacity of the engine was larger.

The EOS thrustor (Ref. 51) shown in Fig. 17 was designed to take advantage of both anode feed and spot attachment of the arc at the cathode tip. In this model,

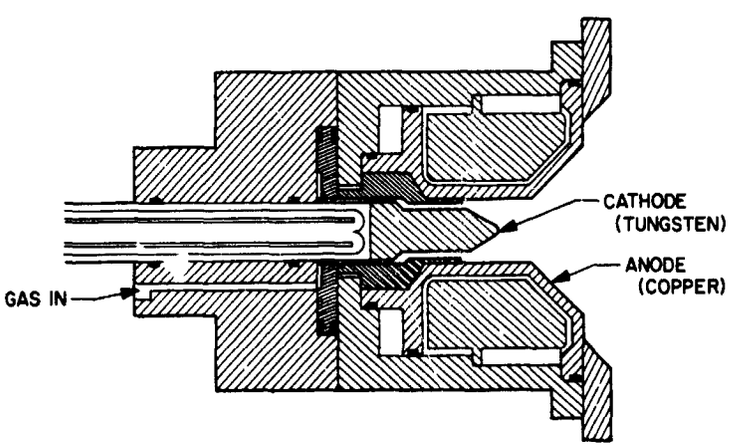

Fig. 11. AVSSD X-7C MPD thrustor used with ammonia. This configuration was used to test the effects of varying the thrustor throat diameter

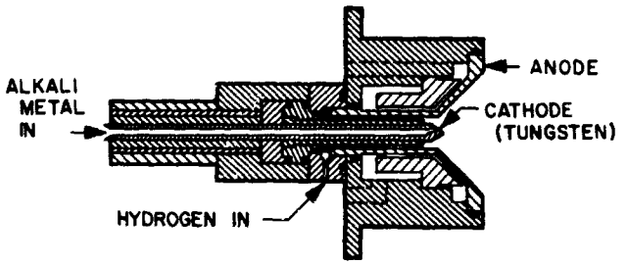

Fig. 12. AVSSD alkali metal MPD thrustor used with cesium and lithium (Ref. 24)

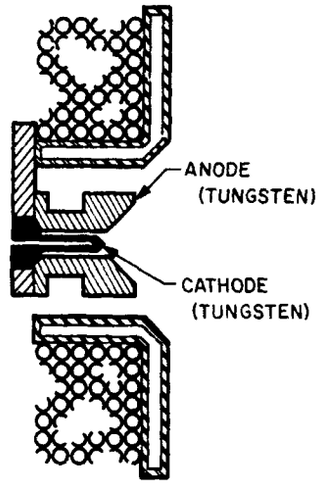

Fig. 13. AVSSD radiation-cooled alkali metal MPD thrustor (Ref. 21)

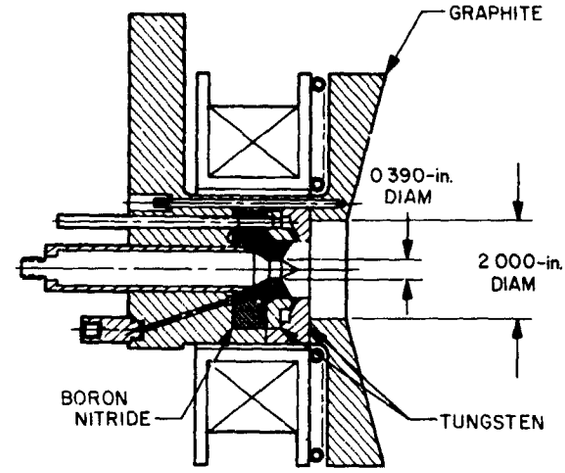

MODEL LAJ-AF-2

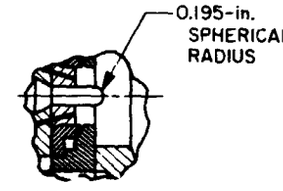

MODEL LAJ-AF-4

(IDENTICAL TO MODEL LAJ-AF-3,
EXCEPT AS INDICATED)

Fig. 14. EOS lithium-fed Hall current accelerators (Ref. 49)

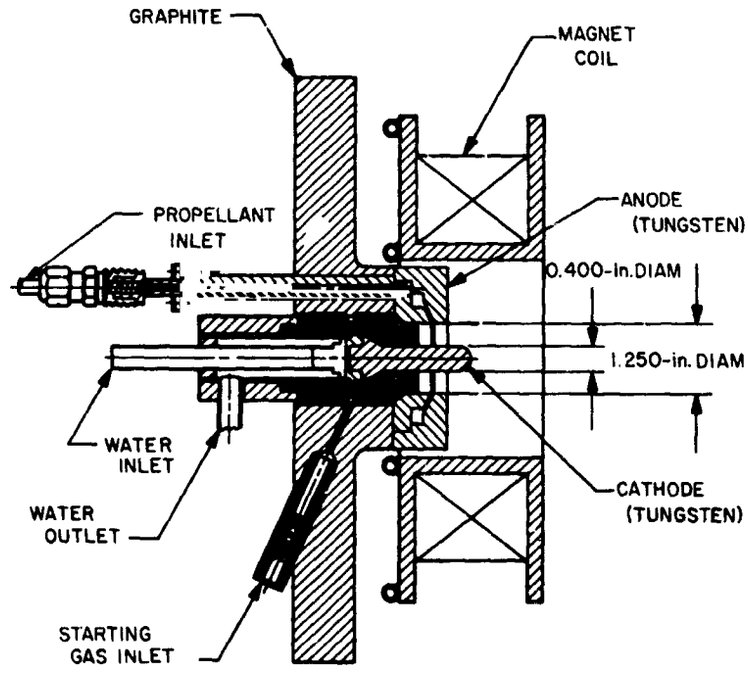

Fig. 15. EOS alkali metal Hall current accelerator. Lithium, sodium, and potassium were tested in this configuration, designated LAJ-AF-6D (Ref. 50)

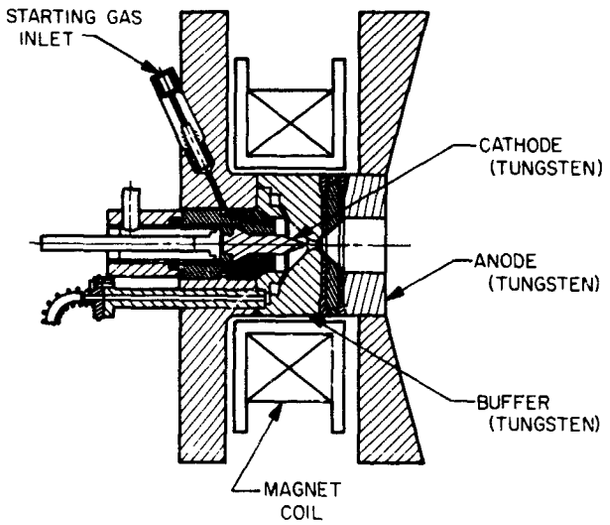

Fig. 16. EOS lithium-fed Hall current accelerator, Model LAJ-BF-1. This buffered-cathode configuration was designed to increase the pressure at the cathode tip (Ref. 50)

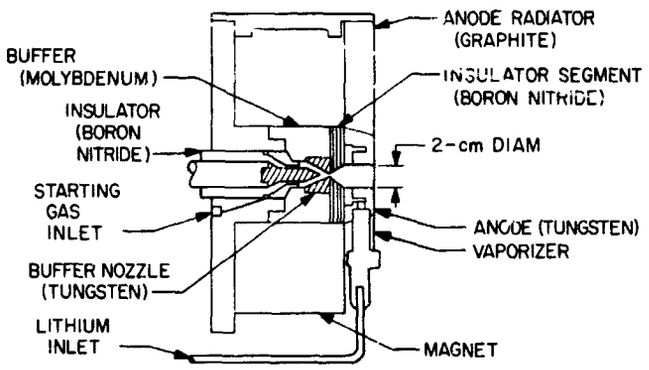

Fig. 17. EOS Hall current accelerator, Model LAJ-AF-BG-1. This configuration is one of a series designated ALPHA. Hydrogen or nitrogen is injected into the cathode region, and the alkali metal is fed through the anode (Ref. 51)

Fig. 18. Giannini lithium-fed MPD thrustor. No thrust data were obtained (Ref. 15)

the alkali metal vapor is injected through the anode, and a gaseous propellant, either hydrogen or nitrogen, is injected into the buffered-cathode region. Additional slight modifications of the design shown in Fig. 17 have been made and constitute what is now called ALPHA. Additional major modifications, such as the addition of another ionizing electrode downstream of the anode, are alluded to in Ref. 51.

The engine used at Giannini (Ref. 15) for both lithium and potassium is shown in Fig. 18. Only thermal efficiency data have been reported for this engine.

An argon-fed engine (Ref. 56), used at NASA Langley for diagnostic studies, is shown in Fig. 19. A pulsed MPD engine (Ref. 72), also operated on argon for diagnostic studies, is shown in Fig. 20.

IV. Test Facilities

A. Power Supplies

The power for the experimental MPD engine is supplied by either electric arc welding machines, usually ac rectifiers, or batteries. When batteries are used, a ballast resistor is placed in the circuit to obtain the "drooping" I–V characteristic of the power supply that is necessary for stable arc operation. The current from the welders has an inherent ripple of a few percent, but no obvious advantage has been demonstrated for the smoother battery power.

B. Vacuum Systems

The typical facility in which the gaseous propellant is tested consists of a 4- to 6-ft-diameter tank that is evacuated by a pumping system of about 5000-cfm capacity. For hydrogen feed rates of 10 to 50 mg/s, the tank pressures are in the range of 0.1 to 0.5 torr. An exception is

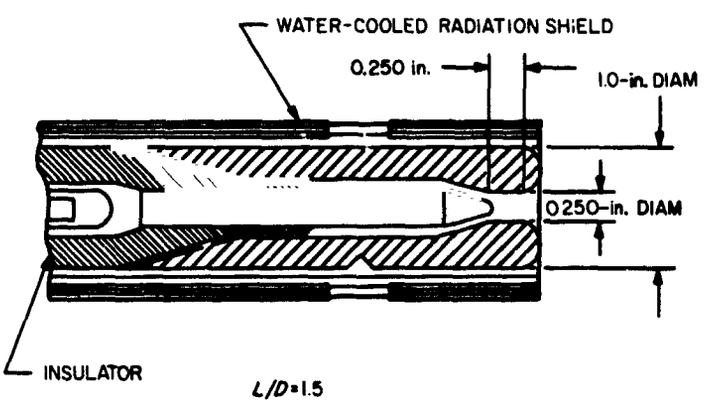

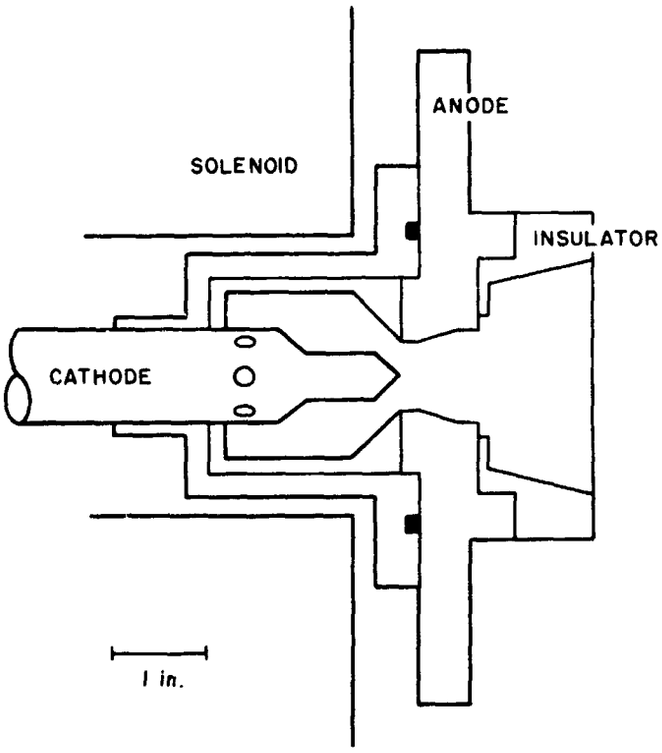

Fig. 19. Accelerator used by NASA Langley for diagnostic studies with argon (Ref. 58)

the NASA Lewis Space Environment Facility (Ref. 64) in which a pressure of 10^{-4} torr may be maintained in their 15-ft-diameter tank at a hydrogen flow rate of 10 mg/s. The tank pressure is greatly reduced, with very modest pumping capacity, when alkali metal propellants are tested. The exhaust products condense on cooled baffles (and the tank walls) and diffusion pumps are used to maintain the pressure of noncondensable leakage gas at a low level. Although pressures as low as 10^{-7} torr have been achieved during the test period (Ref. 50), the pressure at which most of the data were taken was about 10^{-5} torr.

V. Test Procedures and Performance Measurements

A. Engine Operating Variables

The performance parameters of overall efficiency and specific impulse are obtained from the measured operating parameters of propellant feed rate, input electric power, and thrust. The thermal efficiency is obtained from measured values of the input electric power and the power that is either lost to the engine electrodes or contained in the exhaust. For a given thrustor geometry and propellant type, the directly controllable operating parameters are the propellant feed rate, the arc current, and the current to the exterior magnet coil. To a limited extent, the pressure in the test tank is also controllable, but this control is seldom exercised.

The current to the magnet coil is a directly controllable variable. Correlation of the strength of the magnetic field and the current is made through a calibration, using conventional gaussmeters, that is made when the engine is not operating. Complete profiles of the field strength and direction have been made (Refs. 24 and 52), but the value of the field strength specified nearly always refers to a point, usually near the cathode tip, on the engine centerline.

Although the propellant feed rate is a controllable variable, it is not necessarily the correct value of $\dot{m}$ to use in the calculation of the specific impulse, Eq. (2), or the overall efficiency equation, Eq. (1). The mass accelerated may be different from that fed to the engine, and considerable discussion has been devoted to the correct value of $\dot{m}$ to use in the calculations. This subject is discussed in Section VI-A below and in Part IV, Section II-C.

The ambient tank pressure has been varied, independent of the propellant feed rate, by bleeding additional gas into the vacuum tank (Refs. 21 and 65). More commonly, however, a minimum tank pressure is desired, and the pressure is a function of the feed rate and is determined by the vacuum pump characteristics and the associated plumbing that connects the pump to the test tank. When alkali metal propellants are used, the tank pressure is a weaker function of the feed rate than when gaseous propellants are used, and the vacuum pump, usually a diffusion pump, serves primarily to remove noncondensable gases. This is also apparently true when alkali metals plus either hydrogen or nitrogen are used as a bipropellant, because the addition of the gaseous propellant to the accelerator does not significantly alter the test pressure. The process by which these gases are removed has been called "chemical pumping" (Ref. 51) since the gaseous exhaust products are believed to combine with the alkali metal and condense on the cool surfaces of the vacuum tank. With alkali metal propellants, independent control of the tank pressure has been achieved (Ref. 49) by bleeding in a noncondensable gas. With the gaseous propellants, the bleed gas is usually the same material as the propellant.

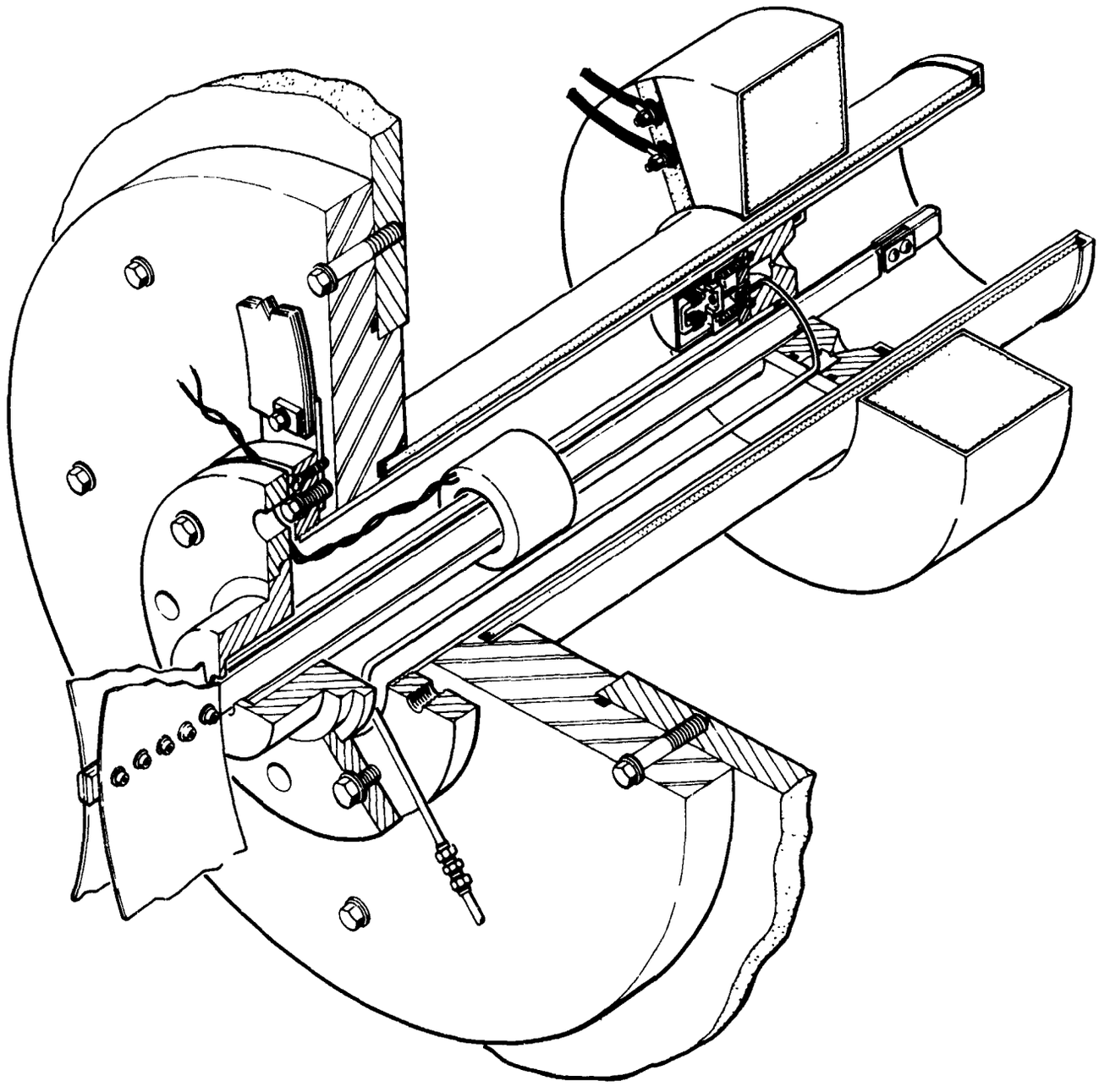

Fig. 20. Pulsed MPD accelerator investigated by Lovberg (Ref. 72)

B. Test Procedures

When independent control of the tank pressure is not attempted, the usual test procedure is to fix two of the three variables (propellant feed rate, arc current, and magnet current) and to vary the remaining variable. When the propellant feed rate and the current to the magnetic coil are fixed, the arc current may be varied to a desired thrust or a desired power level, in addition to a desired level of the current itself. In general, the arc voltage is a weak function of the arc current, and the volt-current characteristics of the engine depend unpredictably on the thrustor geometry, the propellant type and flow rate, and the strength of the magnetic field. Unexplained voltage excursions, at presumably steady-state conditions, have been frequently reported (Refs. 20 and 49). In addition, rapid changes between two distinct voltage modes at a single setting of all of the controllable variables have been noted (Refs. 36 and 65). The arc voltage increases with increasing magnetic field strength at a rate that depends, in part, on the propellant type (Refs. 36 and 40). Most of the power supplies used are suited to operation at which the current is nearly constant. At a fixed setting of the power supply, voltage changes are accompanied by a very small change in the delivered current.

The reported data are usually tabulated, at fixed values of the feed rate and field strength, for specific values of the arc current, although the tabulations have also been at fixed values of the specific impulse or total input power. The magnet power is seldom included in the performance calculations.

C. Measurement of Operating Variables

A brief description of the various measurements made to determine the performance, in terms of the overall and thermal efficiency and the specific impulse, is given in the following paragraphs. In addition to these measurements, a large number of measurements have been made to aid in the understanding of the thrustor operating mechanisms. These measurements, generally referred to as diagnostic measurements, are discussed in Section VII-C below.

1. Thrust. Thrust is determined directly by mounting the engine on a thrust stand and measuring the reactive force, or indirectly from the force exerted on a target placed in the exhaust beam. It is, of course, not possible to completely isolate the engine and thrust stand from the cooling water and the power leads, and much effort has been directed toward reducing tare forces exerted on the thrust stands to a minimum. Magnetic forces that result from currents are reduced by using concentric or twisted leads and by using nonmagnetic materials wherever possible. Current connections to the thrustor are frequently made through mercury pots with the surface of the mercury covered with an oil having a low vapor pressure. The thrust stands and supporting structures are water-cooled to minimize thermal effects.

2. Power. The input is generally calculated from the arc current and voltage, both of which are measured by conventional meters, shunts, and/or recording devices. Both the arc current and the magnet current are generally determined by measuring the voltage drop across a precision shunt.

3. Flow rate. Conventional rotometers or sonic orifice meters are used to measure the feed rate of gaseous propellants. The alkali-metal feed rate is determined from the displacement of feed, in liquid form, by a bellows or piston or by sonic meters used to measure the flow rate of the metal vapor. Conventional rotometers are also used to measure cooling water flow rates.

4. Temperature. The temperature rise of the electrode coolant is measured with conventional thermocouples or with specially designed thermistors (Ref. 40).

5. Pressure. Pressure measurements are made with conventional bourdon tube gages and McLeod gages, as well as thermocouple and ionization gages. Some difficulties in the interpretation of readings obtained for condensable vapors are experienced when ionization or thermocouple gages are used. Alkali metal vapors also have a deleterious effect on the conventional gages, and special methods (Ref. 15) have been employed to overcome this problem.

VI. Environmental Factors

Mission studies, such as those discussed in Part I, are predicated on a knowledge of the operating characteristics of the propulsion system in space. Because the only available realistic description of the MPD thrustor is empirical, it is necessary that the laboratory test conditions adequately simulate the space environment. It has become evident that at some operating conditions the calculated values of the specific impulse and overall efficiency are grossly in error because of inaccuracies of the measured quantities caused by interactions with the

test environment. One identifiable interaction is the ingestion of material (other than the metered propellant) into the discharge region where it is accelerated along with the propellant and contributes to the measured thrust. This interaction is discussed below under the heading "Entrainment." Other interactions with the test environment have also been suggested as possible sources of error, either in the measurements directly or as factors that significantly modify the operating characteristics from those that would occur in space. The interactions other than entrainment are discussed in Section VI-B below.

A. Entrainment

MPD engines have been observed to operate on either, or both, eroded electrode material or entrained ambient tank gas when the propellant feed rate was reduced to zero (Refs. 17 and 21). It is very likely that when the same engines were operated with a finite feed rate, at similar operating conditions of current, magnetic field, and tank pressure, some fraction of the measured thrust was contributed by the acceleration of eroded or entrained material. Consequently, much of the reported performance data probably are not applicable to thrustor operation in space. For a test of sufficient duration, the maximum possible contribution of eroded material to the observed thrust may be determined by a measurement of the weight loss of the engine components. Thus, while erosion poses a problem of thrustor lifetime, the performance data may be corrected to realistic values. However, the prediction of the actual performance of the engine if entrainment occurs is much more difficult because there is no way to determine the correct value of $\dot{m}$ to use in the calculations of η_a and I_s.

The most satisfactory solution to minimize the effects of entrainment appears to be to operate the engine at very low tank pressures. Pressures as low as 10^{-6} to 10^{-7} torr may be obtained if the propellant is a condensable material, such as the alkali metals, that may be cryopumped. To obtain similar pressures when gaseous propellants are used would require an immense pumping capacity. For example, a pumping speed of 20,000,000 cfm would be required to obtain 10^{-5} torr at a hydrogen flow rate of 10 mg/s. The Space Environment Facility at NASA Lewis (Ref. 64), which can maintain a pressure of 10^{-4} torr at a hydrogen flow rate of 10 mg/s, has been used to test engines designed by both AVSSD and EOS. Because entrainment appears to be associated with current loops that extend downstream of the electrodes into the exhaust jet, Ducati (Ref. 15) has suggested that a thrustor design which confines the current within the electrode region may alleviate the entrainment problem.

The existence of entrainment was conclusively demonstrated by the group at AVSSD in a series of experiments (Ref. 21) during which the engine continued to operate, with very little change in the measured thrust, when the propellant feed rate was reduced to zero. The data obtained from these experiments are reproduced in Table 3.

Table 3.[a] Comparison of MPD arc jet voltage and thrust for propellant injection through the engine and propellant injection outside the engine

Hydrogen flow rate $\dot{m}$, mg/s	Arc current I, A	Tank pressure P_{tank}, torr	Arc[b] voltage, V		Arc[c] thrust, g	
			V_{in}	V_{out}	T_{in}	T_{out}
10	500	0.10	62	58	42	42
30	500	0.20	72	55.5	45	36
50	500	0.30	78.5	61.5	55	42
10	800	0.10	60	66	70	78
30	800	0 20	70	63	75	73
30	1100	0.20	69.5	74	106	96

[a] Taken from Table II of Ref. 21.

[b] V_{in} = voltage with flow through engine.

V_{out} = voltage with flow through tank wall.

[c] T_{in} = thrust with flow through engine.

T_{out} = thrust with flow through tank wall.

The tank pressure, which was maintained constant at each feed rate by diverting the feed from the engine into the tank through the tank wall, had very little effect on the thrust over the range of 0.1 to 0.3 torr.

Because the loss of electrode material during the experiment described above was much too small to account for the observed thrust, it was concluded that the engine operated on entrained gas. Additional evidence that the engine does entrain ambient gas was obtained by lowering a thin tungsten wafer into the exhaust plume a short distance downstream of the anode. At feed rates of less than 5 mg/s of hydrogen, the wafer first moved toward the engine, and then, as it was lowered further, was swept downstream. These observations were interpreted to indicate that ambient gases were flowing into the engine around the outer edges of the exhaust jet and then being accelerated and expelled along the centerline. The backflow was not observed at mass flows greater than 5 mg/s; however, with the engine operating on nitrogen at higher feed rates, trace amounts of hydrogen were introduced through the tank wall and observed, by the appearance of hydrogen line radiation, to mix with the exhaust within 1 in. from the anode. John (Ref. 21) points out that if the acceleration region extends downstream of the anode, entrainment can influence the results even if backflow into the engine does not occur.

Using a ρu probe*, Patrick (Ref. 40) has shown that the total mass flow in the exhaust jet greatly exceeds that fed to the engine. In a series of experiments (Ref. 40), in which a quartz shroud was placed at the nozzle exit to prevent entrainment in that portion of the exhaust immediately adjacent to and for 6 in. downstream of the exit, both the mass entrained and the total thrust were reduced. The thrust was measured with a ρu^2 probe that is described in Section VII-C below.

Mixing of ambient gas with the exhaust after the propellant has been accelerated will not invalidate the experimental results. However, as noted above, the gas entrained into the acceleration volume of the thrustor, which is the region where currents exist and $\mathbf{J} \times \mathbf{B}$ forces act, will affect the performance. When entrained particles, in addition to the metered propellant, are accelerated, the calculated values of both η_0 and I_s are fictitiously high because of the use of a value of $\dot{m}$ that is too small. The occurrence of entrainment is not obvious from the data unless the calculated efficiency approaches (or exceeds) the thermal efficiency of the engine. In addition, the presence of entrained gases probably alters the operating characteristics the thrustor would have in the absence of entrainment.

The extension of the acceleration volume into the exhaust plume has been demonstrated by the measurement of axial currents far downstream of the engine (Refs. 25 and 46). The magnitude of the current and the distance the current paths extend downstream apparently vary considerably with the different engines. The variation of the extent of the acceleration volume with tank pressure is, in general, not known.

Unfortunately, there is no way to determine the quantitative effects that entrainment may have had on the performance of the experimental engine. Estimates of the maximum amount of entrainment that may occur are based on the assumption that ambient gas enters the exhaust jet by random thermal motion across an area that is estimated from the visual observation of the plume. Based on this model, the ratio of metered flow to entrained material would decrease as the tank pressure is reduced, provided, of course, that the area of the acceleration region did not increase at the same rate as the density of the background gas decreased. In one set of experiments reported by EOS (Ref. 42), the proportionality of thrust to $\dot{m}$ was interpreted to indicate that some interaction with the test pressure was occurring, because the tank pressure was also proportional to $\dot{m}$. In other results obtained at EOS (Ref. 47), the thrust was found to be independent of $\dot{m}$, and this observation was attributed to the almost entirely electromagnetic nature of the acceleration mechanisms. However, as an examination of the data published by AVSSD reveals, the absence of dependence of thrust on $\dot{m}$ does not necessarily mean the absence of entrainment.

The performance of the AVSSD X-2C engine, operating on hydrogen with a strong external field, shows a linear relationship between η_0 and I_s that is independent of the thrustor operating variables of mass flow, arc current, and magnet current. An expression relating η_0 to I_s may be obtained by combining Eqs. (2) and (3) to eliminate the mass feed rate $\dot{m}$. This expression, Eq. (8), shows that a linear dependence between η_0 and I_s requires that the ratio of thrust to power remain constant for all operating conditions:

$$\eta_0 = \left(\frac{g}{2} \cdot \frac{T}{IV}\right) I_s \qquad (8)$$

*See Fig. 42.

A consideration of the energy equation reveals that this ratio cannot remain constant for arbitrarily small values of $\dot{m}$ if energy is to be conserved. This is evident from Eq. (8), which indicates that the overall efficiency will exceed 100% at values of I_s greater than $2IV/gT$ if the thrust-to-power ratio remains constant.

The data obtained at zero feed rate obviously cannot be displayed on a plot of efficiency versus specific impulse. However, the thrust-to-power relationship obtained from experiments with zero feed rate and those with finite feed rates can be compared. This has been done here for the hydrogen performance data reported by AVSSD (Refs. 19 and 21) and is displayed in the form of thrust versus power in Fig. 21. The data obtained at zero feed rate (Ref. 21), which are indicated in Table 3 as the data obtained with flow through the tank wall, are also included in Fig. 21. Note that

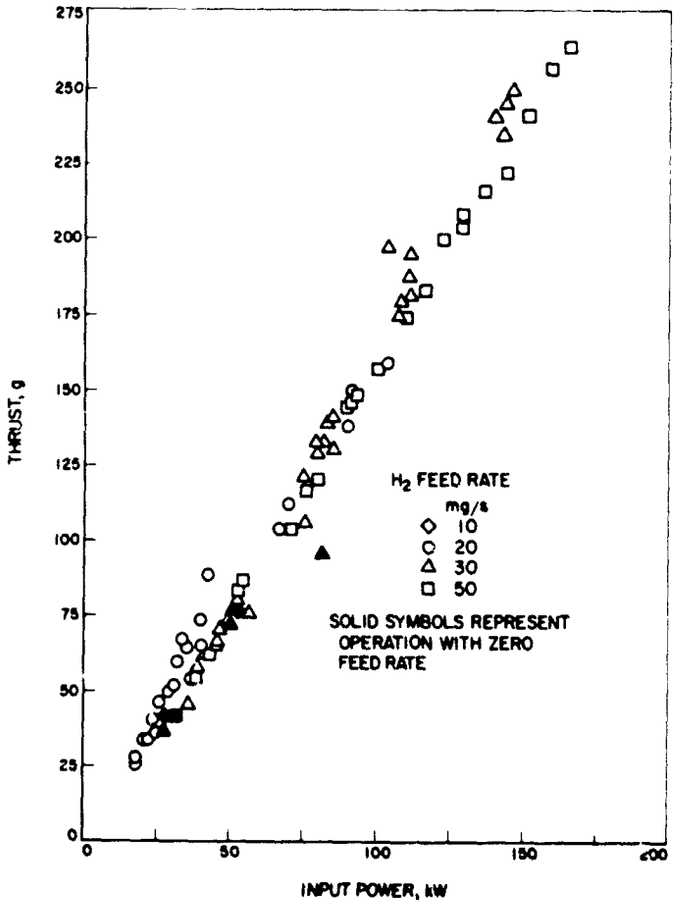

Fig. 21. Thrust vs input power of the hydrogen-fueled AVSSD X-2C engine. The data show a constant thrust-to-power ratio for all operating conditions, including zero feed rate (Ref. 21)

the points obtained from these runs fit in with the other data very closely. Because of the constant value of T/IV at all operating conditions, including zero feed rate, it must be concluded that the amount of gas that was accelerated is, in general, an unknown quantity for all runs, and, therefore, the calculated values of I_s and η_0 have no predictable relationship to the actual value.

The engine described above was also operated on both hydrogen and ammonia in the low-pressure facility at NASA Lewis (Ref. 65). The results of the tests with hydrogen are shown in Fig. 22. At pressures above 0.04 torr, the data obtained at Lewis are in very good agreement with those reported by AVSSD. It was anticipated (Ref. 65) that if entrainment had occurred at the higher pressure, the results at very low pressure would indicate lower values of both I_s and η_0 for a given operating point. However, at a pressure of 10^{-4} torr, the efficiency is surprisingly higher at the lower values of specific impulse and appears to approach the high-pressure data only at higher values of I_s. A rough extrapolation of the data indicates that the curves would cross at a specific impulse of about 4000 s. Higher values of specific impulse were not obtained, because the maximum current available was only 500 A. These data are discussed further in Part V, Section I-A.

Except at the lowest values of the external magnetic field, the tests conducted at NASA Lewis (Ref. 65) indicated that the thermal efficiency was insensitive to the pressure level and that the increased overall efficiency was the result of increased thrust as the pressure was lowered. The arc voltage at the low pressure was only a few percent higher than that at the high pressures.

The correlation of I_s with η_0 for the tests made with ammonia at NASA Lewis (Ref. 65) with the X-2C engine is complicated by the apparent existence of an optimum magnetic field and a tendency of the arc to operate in either of two distinct voltage modes. However, the same general trend of increased efficiency at very low pressures was observed. Good agreement with AVSSD's data was obtained at pressures above 0.04 torr. An error in the measurement of the ammonia flow rate reported in Ref. 65, which resulted in calculated values of the overall efficiency that exceeded the thermal efficiency, has been corrected (Refs. 67 and 68).

Because of the large increase in the size of exhaust plume, Jones (Ref. 65) concluded that the possibility of entrainment being a factor in the thrustor performance

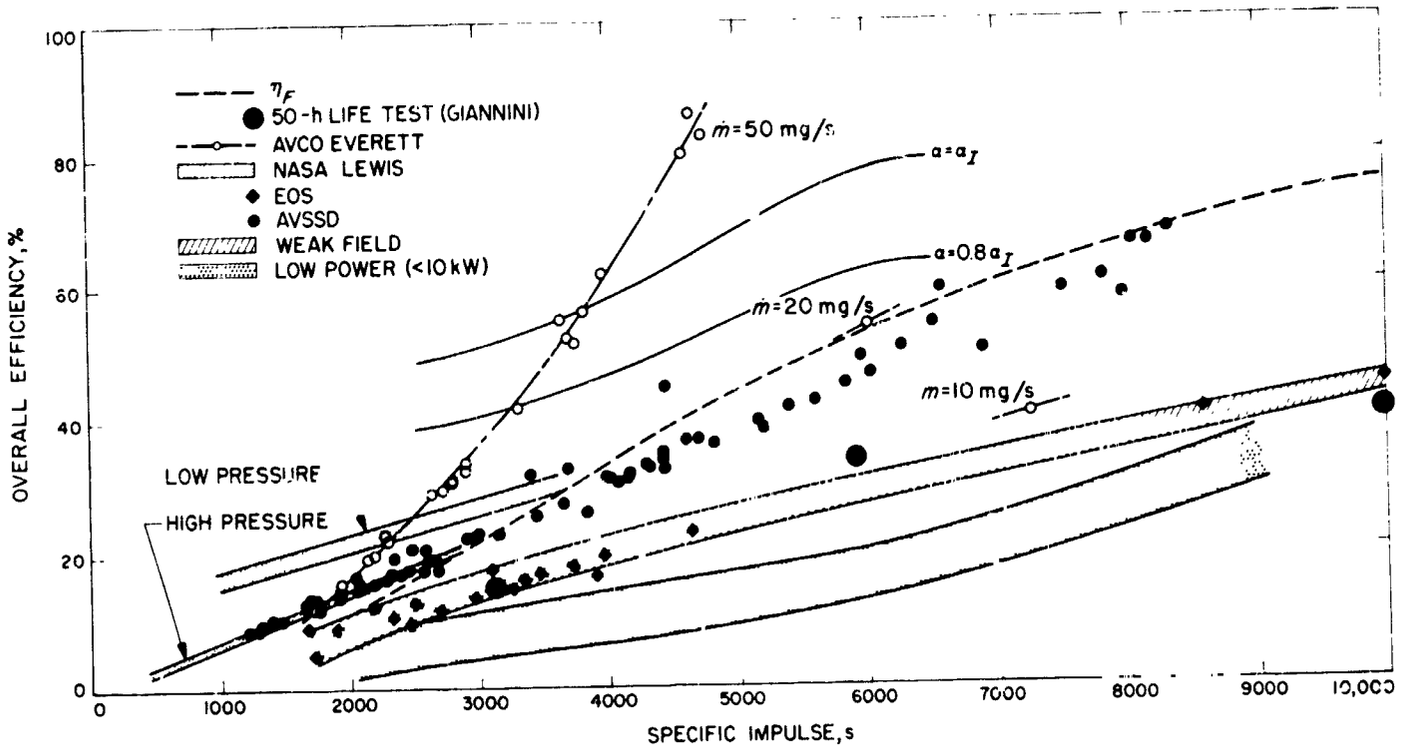

Fig. 22. Overall efficiency vs specific impulse of hydrogen-fueled engines

could not be ruled out. The expectation is that if a significant amount of entrained gas is accelerated at high pressures, a decrease in entrainment at low pressures would be indicated by a decrease in the calculated overall efficiency. An extrapolation of the low-pressure performance curve of Fig. 22 suggests that the efficiency at values of I_s greater than about 4000 s will be lower than the efficiencies reported by AVSSD. Continued testing at higher power levels is planned when a larger power supply is available.

The performance discussed above is not characteristic of all MPD engines. Patrick (Refs. 35 and 40) was unable to operate the MAARC if the feed rate was reduced to zero. He also found a very large effect of the hydrogen feed rate on the performance.

Some problems associated with the use of condensable propellants should also be noted. Ducati (Ref. 15) contends that the use of cryogenically pumped condensables does not necessarily eliminate the possibility of entrainment since an appreciable vapor pressure of the alkali metal may exist in the immediate vicinity of the exhaust plume. In addition, Cann (Ref. 51) has noted that deposition of lithium, followed by subsequent evaporation, may cause problems in the vicinity of the accelerator.

B. Interactions With Test Hardware

In Ref. 15, Ducati discusses a number of possible sources of interactions of the MPD thrustor and the test environment, in addition to entrainment, that may produce anomalies in the measurements. Some of these are postulated to occur only during operation and therefore cannot be detected by calibration procedures either before or after the test. It is suggested that the resulting errors can be minimized only by careful design of the various components. A partial listing of the possible interactions discussed in Ref. 15 is given below.

1. Thermal effects. Water-cooled parts attached either to the thrust stand or to the thrustor itself may "drift" as the result of uneven thermal expansion as the cooling water heats; this may lead to erroneous thrust readings. Because these effects are quickly "washed out" when the arc is turned off, they cannot be easily detected. Ducati recommends that the temperature differential of the coolant not exceed a few degrees of temperature. A number of devices to compensate for this effect are also discussed.

2. Mechanical effects. Any movement of the magnetic field coil, relative to the thrustor, that may be caused

either by thermal effects or by electromagnetic forces may shift the center of gravity and produce a false thrust reading.

3. Electromagnetic effects. The visual appearance of the exhaust plume at high values of the applied field strength, particularly the appearance of glow discharges on the tank wall and some portions of the engine, suggests that part of the current travels from the anode to the cathode by way of the tank wall. This condition was also accompanied by an increase in the measured thrust. When a current of a few hundred amperes was applied between the points on the tank wall where the discharge was observed, a false thrust reading resulted. Ducati recommends the use of larger, insulated tanks and the use of insulating material on all exterior surfaces, except for the electrodes, of the thrustor.

Means of deflecting the exhaust beam by 90 deg and thereby obtaining a "zero" for the thrust measuring device under actual operating conditions are also discussed by Ducati. A "thrust killer," which had proved successful when no external field was applied, could not be used when a strong field was applied because the engine operating characteristics were affected.

Cann (Ref. 49) has also investigated the effects of the proximity of the tank walls on the accelerator performance. When the exhaust plume is observed to reach the tank wall, Cann suggests that one of two types of interference may occur. Either the current path may be shortened by the existence of a cool, insulating boundary layer next to the wall, or the wall may carry part of the current between the anode and cathode.

VII. Experimental Results

Electric propulsion systems are usually defined in terms of specific impulse I_s, specific weight α, and efficiency η_0. The specific weight is not a significant factor in the development of MPD thrustors but becomes an important parameter when the capability of the MPD thrustor to perform a specific space mission is evaluated. In this survey, the reported performance of the MPD thrustor is compared with that of the ion engine for a Mars-orbiter mission for which solar panels serve as the power source. The specific impulse and efficiency are related to the thrustor operating parameters of thrust T, propellant feed rate $\dot{m}$, and input power IV by Eqs. (2) and (3):

$$I_s = \frac{T}{g\dot{m}} \tag{2}$$

$$\eta_0 = \frac{T^2}{2\dot{m}IV} \tag{3}$$

The specific weight is of little concern in the development of the MPD thrustor to date and will not be discussed further. Experimental performance data are usually presented as a plot of η_0 vs I_s. An expression relating η_0 to I_s may be obtained by combining Eqs. (2) and (3) to eliminate either the feed rate $\dot{m}$ to yield Eq. (8) or the thrust T to yield Eq. (9):

$$\eta_0 = \frac{I_s^2}{\left(\frac{2IV}{g\dot{m}}\right)} \tag{9}$$

Some of the important operating characteristics of a developmental engine – such as unexplained changes in the voltage – are masked when the data are presented in this form, but such a presentation fills the requirements of mission studies and simplifies comparison of the different propellants and thrustor geometries.

A. Performance

For the purpose of this discussion of the reported performance of MPD engines, the data are categorized by either individual propellants or certain groups of propellants and are displayed as plots of overall efficiency versus specific impulse. Separate figures are shown for hydrogen, ammonia, the alkali metals, and a miscellaneous grouping that includes helium, nitrogen, and argon. The overall efficiency is defined by Eq. (3), in which the input power includes neither the power to the external magnet nor the power used to vaporize the condensable fuels. This is the common procedure followed in the cited references and is justified, particularly for the purpose of a comparison of the performance obtained with various fuels and engine configurations, on the basis that no attempt has been made to optimize the magnet configuration, and, presumably, the power lost to the anode may be used to vaporize the incoming fuel in a flight engine. It is obvious, of course, that a final comparison of the performance of the MPD engine with that of the ion engine will require inclusion of the magnet power.

In addition to the experimental data, the frozen-flow efficiency of each propellant, as well as curves that allow

comparison with the ion engine, are displayed on each plot. The frozen-flow curves were calculated for complete single ionization and include the energy of dissociation of molecular fuels but not the energy of fusion of the alkali metals. This is discussed in more detail in Section II above. Two curves are shown for comparison with the ion engine. The first curve, labeled $\alpha = \alpha_I$, where α_I is the specific weight of the ion engine propulsion system used in the study of the Mars-orbiter mission, is the minimum performance the MPD engine must have to compete with the ion engine if the specific weights of the two propulsion plants are equal. The second curve, labeled $\alpha = 0.8\ \alpha_I$, illustrates the tradeoff between efficiency and specific weight that is possible if the specific weight of the MPD propulsion system can be reduced to 80% of that of the ion engine. The two comparison curves were taken from Ref. 1 and are discussed in Part I.

In order to achieve some degree of clarity in the graphic presentations, the performances are usually shown as shaded areas that are representative of certain definable operating conditions, propellant type, or engine configuration. These areas contain about 95% of the data reported by the referenced source. Some individual data points are plotted when the data are well correlated as η_0 versus I_s, or if the data are unusual with respect to the most commonly reported trends. In addition, the results of endurance tests are shown as individual points. Although all the data reported by the cited sources have been reviewed, not all the data have been plotted. These exceptions are generally noted in the discussion.

1. Hydrogen and deuterium. The performance data from hydrogen-fueled MPD engines are shown in Fig. 22, in which an attempt is made to classify the reported performance according to the magnitude of the externally applied magnetic field, the power level of the engine, and the ambient pressure in the test chamber. For some conditions, considerable overlap among the various areas indicated in the figure does exist; however, some important trends are apparent in the classification shown. Only a very limited amount of data has been obtained for deuterium, and these data are not plotted.

a. Weak magnetic fields. Weak fields are defined here as being less than 500 G. The stated purpose of weak fields is to prolong the life of the electrodes rather than to perform an important role in the acceleration process (Ref. 18).

Giannini. The early performance reported by Ducati (Ref. 7) for the thermo-ionic thrustor, which operated with no externally applied magnetic field, ranged from 2600 s at 14% overall efficiency to 10,000 s at 46%. Fifty-hour endurance tests of a modified design (Ref. 10), shown in Fig. 5, demonstrated that severe electrode erosion occurs at the operating conditions of the test. The probable cause of the erosion was thought to be localized arc attachment on the anode. Subsequent tests were conducted with an external coil (Refs. 10 and 11), connected in series with the arc circuit, to rotate the arc and thereby prevent the damaging effects of concentrated arc spots. The reported performance with no external field is included in the region labeled "weak fields" on Fig. 22, and the result of the endurance tests at 3000 s is shown.

AVSSD. The performance obtained by the AVSSD group (Refs. 18 and 21) with the X-2C MPD engine (Fig. 1) was in good agreement with that reported earlier by Ducati, and nearly all the data points fall in the area marked "weak field" on Fig. 22. An external field, which was less than 500 G at the cathode tip, was used to prevent local melting of the anode. Although the intended purpose of the field was to prolong the anode life, there were some indications (Ref. 19) that the weak field may have contributed to the acceleration process. The results of these experiments were used to demonstrate the electromagnetic nature of the acceleration process. This is discussed in more detail in Section IV-B-1. Additional tests, made with a pressure tap placed at the cathode tip to gain information on the mechanism of the acceleration by self-magnetic fields, yielded performance results that were about 40% lower than those made without the pressure tap. In more recent experiments performed with a very similar engine, Malliaris (Ref. 28) found that the thrust was not degraded by the presence of the pressure tap.

The operating conditions of ambient tank pressure (0.5 to 1.0 torr), power level (60 to 260 kW), and feed rate of the AVSSD engine were similar to those of the Giannini engine. No dependence of performance on the propellant feed rate from 10 to 50 mg/s was found by the AVSSD group. The data reported by Giannini were obtained with a single feed rate of 25 mg/s. One difference in the operating characteristic was that the X-2C operated at about 60 V, while the typical voltage for the Giannini engine was about 40 V.

b. Strong magnetic fields. Most of the reported performance data for hydrogen-fueled MPD engines have been obtained with strong externally applied magnetic fields. The two groups, at AVSSD and Giannini, found that strong fields increase the electrode lifetime, but only the group at AVSSD concluded that strong fields significantly increase thrustor performance. The engines at Avco-Everett and EOS were initially designed as Hall accelerators, for which the external field plays a vital role in the acceleration process. Unlike the results obtained with weak fields, the results obtained with strong fields have shown large variations in the performance of MPD engines.

Avco-Everett. The highest performance shown on Fig. 22, about 85% overall efficiency, was reported by Patrick (Ref. 40) for a feed rate of 50 mg/s. The engine developed at Avco-Everett, called the MAARC, for "magnetic annular arc," is shown in Fig. 2. A major difference in the data obtained with the MAARC and those obtained with the other engines is the marked dependence of engine performance on the hydrogen feed rate. As may be seen from Fig. 22, the performances obtained at 20 and 10 mg/s are widely separated and far below that obtained at 50 mg/s. The data points at the highest efficiency are significantly above the frozen-flow curve, and for these points a maximum ionization fraction of 0.05 was calculated (Ref. 39).

Measurements with the ρu probe (see Section VII-C) demonstrated that substantial (up to 15 times greater than the feed rate at a feed rate of 10 mg/s) (Ref. 39) entrainment of ambient tank gas into the exhaust plume occurs at all operating conditions. That part of this entrainment may contribute to the measured thrust was subsequently demonstrated in experiments in which the MAARC was operated with a quartz shroud placed at the thrustor exit. With the shroud in place, the measured thrust was reduced by 40% and the amount of entrainment was reduced by a similar amount.

All the thrust measurements at the Avco-Everett facility were made with a thrust plate, or ρu^2 probe (see Section VII-C).

AVSSD. The performance of the X-2C engine was substantially higher with a strong magnetic field than with weak fields (Ref. 19). The magnitude of the field was varied from about 700 to 1800 G for the data shown in Fig. 22. No dependence of performance on the feed rate was observed. However, that entrainment occurs at the operating conditions at which most of the data were obtained was clearly demonstrated (see Section VI-A above).

Giannini. The results (Refs. 10 and 11) of the early experiments with strong external fields that were performed at Giannini are shown in Fig. 22 as the points labeled "life test." For the 50-h test, a 4-turn coil was connected in series with the arc circuit at about 6000 s, and, at 10,000 s, the field was strengthened to about 2500 G (Ref. 11) by the addition of four more turns to the coil. The electrode configuration for the test at 10,000 s is shown in Fig. 6. As may be observed from Fig. 22, no substantial improvement in performance was achieved by the addition of the external field. However, a significant decrease in the amount of erosion was observed.

The most recently reported performance results obtained by Ducati (Refs. 15 and 16) have resulted from a systematic study of the effects of the electrode geometry and the magnitude of the magnetic field. For these tests, the field was continuously variable, independent of the arc current, up to a maximum of 20,000 G. The primary geometric variables were the anode throat diameter D, the anode throat L/D ratio, and the cathode diameter. Most of the data were obtained at a single L/D ratio of 1.5 and a fixed cathode diameter. A typical electrode geometry is shown in Fig. 7. At the lower values of specific impulse, and at constant feed rate and field strength, a noticeable increase in the performance was observed as the anode throat diameter was decreased from 1.0 to 0.125 in. At higher values of the specific impulse, a limitation on the anode energy flux density that could be tolerated without destructive effects was observed to occur at about 2 kW/mm^2. Therefore, at the feed rate tested (10 mg/s), the higher values of specific impulse were obtained with the larger throat diameters. The overall efficiency at 8000 s was found to increase significantly as the magnetic field was increased to 8000 G. Further increase in field strength, to 16,000 G, produced a slight degradation of the performance. The reported performance is shown in Fig. 23. In general, the best performance was obtained with the smallest throat diameter used at each specific impulse magnetic field strength.

From a limited amount of data, the performance with deuterium was found to be similar to that reported for hydrogen. The overall performance is stated (Ref. 15) to be about 5% higher than that of hydrogen.

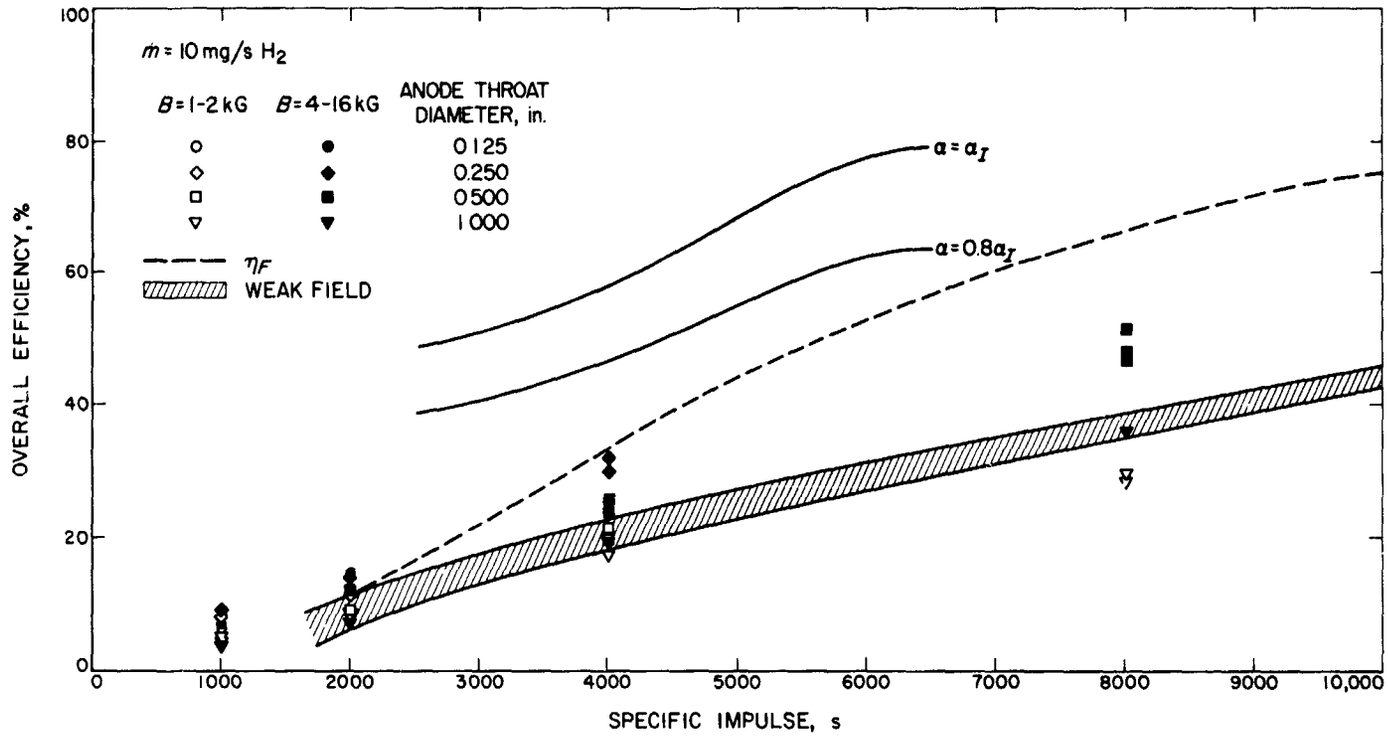

Fig 23. Overall efficiency vs specific impulse of Giannini thrustors showing the effects of variations of the anode throat diameter and very strong applied magnetic fields

EOS. The performance reported by EOS (Refs. 44 and 47) for the H_2-1 Hall current accelerator (Fig. 4) is lower than that reported by either AVSSD or Avco-Everett, and, as may be seen from Fig. 22, lies almost completely within the weak field area. Earlier results obtained at EOS (Ref. 42) with the engine configuration shown in Fig. 3 were higher than those obtained with the H_2-1 engine; however, the earlier data were obtained with a thrust target. For some later experiments (Ref. 49), the results obtained with the target were believed to be less reliable than those obtained with a thrust stand.

c. Low power. Low-power (less than 10 kW) hydrogen-fed MPD engines have been operated by EOS and by Giannini. Both groups used strong magnetic fields.

Giannini. To evaluate the effect of thrustor size on performance, the configuration shown in Fig. 8 (Refs. 12 and 15) was designed to operate at an input power level of about 5 kW. The scaling criteria used to scale from high to low power were to hold the following parameters constant:

(1) The power density in the throat.

(2) The throat L/D ratio.

(3) The magnetic field strength.

The performance of the 5-kW thrustor is described as similar (Ref. 12) to that of the high-power engines. However, only a single point, 9100 s at 39%, was published.

EOS. A number of engines designed to operate at a nominal power level of 10 kW were designed and tested (Refs. 44 and 45); the best results obtained from the configuration are shown in Fig. 9. This engine (Ref. 45), designated the H_2-4, has a radiation-cooled anode, and, to maintain a high pressure at the cathode tip (which was necessary for stable operation), has an electrically insulated tungsten buffer between the anode and cathode. The results obtained with this engine are included in the area labeled "low power" on Fig. 22.

d. Low pressure. Two of the engines described above, the X-2C (AVSSD) and the H_2-4 (EOS), have been tested at low pressure at the Space Environmental Facility (Refs. 47 and 65) at NASA Lewis. The engines were operated both at high pressure (0.04 to 0.2 torr), for comparison with the results reported by the developer, and at a lower pressure of about 10^{-4} torr to more closely simulate space operation and minimize entrainment.

Remarkably good agreement with the results reported by AVSSD was obtained at Lewis with the X-2C engine

at the higher pressures (Ref. 65). Contrary to expectations (Ref. 65), the performance at low pressure was much better than that obtained at the pressure range of 0.04 to 0.2 torr. As may be seen from Fig. 22, the low-pressure performance at 1000 s is more than twice that obtained at high pressure. The difference in the two curves decreases as the specific impulse increases, and at about 4000 s the data obtained at the low pressure nearly equal those obtained at the higher pressure. Because of power limitations at the Lewis facility, data at higher values of specific impulse, where the effect of entrainment is expected to be more pronounced, were not obtained. For this reason, the tests are inconclusive in demonstrating the effect of entrainment on the performance of the engine.

The performance obtained at Lewis with the 10-kW engine developed by EOS was much lower than that reported by EOS at comparable pressure levels (Refs. 45 and 47). At the one comparison point (a feed rate of 1.24 g/s, an arc current of 140 A, a coil current of 500 A, and a tank pressure of 10^{-2} torr), EOS obtained a specific impulse of 6900 s at 25% efficiency, whereas the value obtained at Lewis was 3850 at 7.8%. The noticeable increase in efficiency at low pressure, which was so apparent with the AVSSD engine, was not obtained with the EOS 10-kW engine.

e. Summary. A variety of engine configurations have been operated with hydrogen propellant over a wide range of operating conditions that includes power levels from less than 5 kW to more than 200 kW, magnetic field strengths from 0 to more than 16,000 G, feed rates from 0 to 50 mg/s, and tank pressures as low as 10^{-4} torr. Values of specific impulse greater than 10,000 s and overall efficiencies greater than 85% have been reported. The influence of the magnetic field in enhancing the performance, beyond a strength necessary for arc stability and long life, is presently being debated. Strong fields appear to be necessary for the operation of very-low-power thrustors. The reported results of changes of the propellant feed rate on the performance range from no effect to a very significant effect. Some engines have been demonstrated to operate, in part or in whole, on entrained or eroded materials. As a consequence, many of the data, and particularly those data obtained with strong magnetic fields that indicate the best performance, are of questionable validity.

With the exception of the data obtained by Patrick (Ref. 40), none of the reported performance data indicate that a hydrogen-fueled MPD engine is likely to be competitive with the ion engine for the missions considered in Part I.

2. Ammonia. Nearly all the reported performance data of ammonia-fueled MPD thrustors are shown in Figs. 24 and 25. The engines used to obtain the data shown in Fig. 24 were the AVSSD X-2C thrustor and the Avco-Everett MAARC; that is, the same engines as those used to obtain the hydrogen performance data discussed in the previous section. All the data shown in Fig. 25 were obtained at AVSSD with a series of engines designated X-7C (Ref. 29). This series consisted of a number of water-cooled engines (Fig. 11) with different throat diameters and a radiation-cooled engine (Fig. 10) which was designated X-7CR. The AVSSD engine, the X-2C, was tested with ammonia as well as hydrogen at the Space Environmental Facility at NASA Lewis at exhaust pressures as low as 10^{-5} torr. The X-7C engine has also been tested at NASA Lewis (Ref. 78), but the performance data were not available at the time of this writing. High-pressure data were obtained at all three laboratories in the pressure range of from 0.1 to 0.5 torr.

A limited amount of ammonia performance data was published by Giannini (Ref. 15). The overall performance, not shown in Fig. 24, was lower than that reported by either AVSSD or Avco-Everett.

a. High pressure. The operation of MPD engines at test pressures above 10^{-2} torr is classified as high-pressure operation. Most of the ammonia data were obtained at test pressures that exceeded 0.1 torr.

AVSSD. The X-2C engine was operated on ammonia at both high and low values of the external magnetic field (Refs. 18 and 19). For both conditions of external field strength, the overall efficiency was higher with ammonia than with hydrogen. The maximum specific impulse reported for ammonia was 6500 s with a weak field and 3860 s with a strong (nearly 2000 G) field. The data for high fields exhibit more scatter than do similar data for hydrogen. Two feed rates, 29 and 58 mg/s, were used with the X-2C.

The water-cooled X-7C thrustor series, Fig. 11 (Ref. 29), designated X-7C-1 through X-7C-5, included engines with anode throat diameters of 0.85, 1.25, 1.05, 0.6, and 0.4 in., respectively. The radiation-cooled anode of the X-7CR engine, Fig. 10, was constructed with a

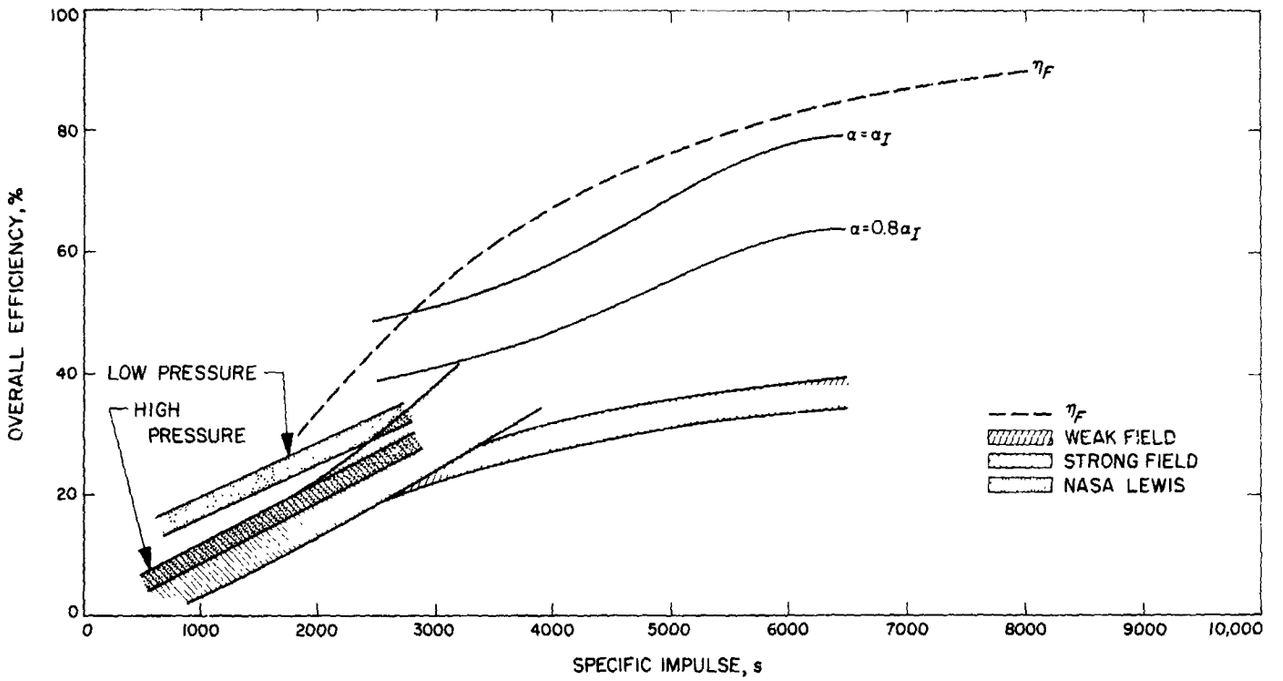

Fig. 24. Overall efficiency vs specific impulse of ammonia-fed engines. All data shown were obtained with either the AVSSD X-2C engine or the Avco-Everett MAARC. The X-2C was tested by NASA Lewis at low ambient pressures

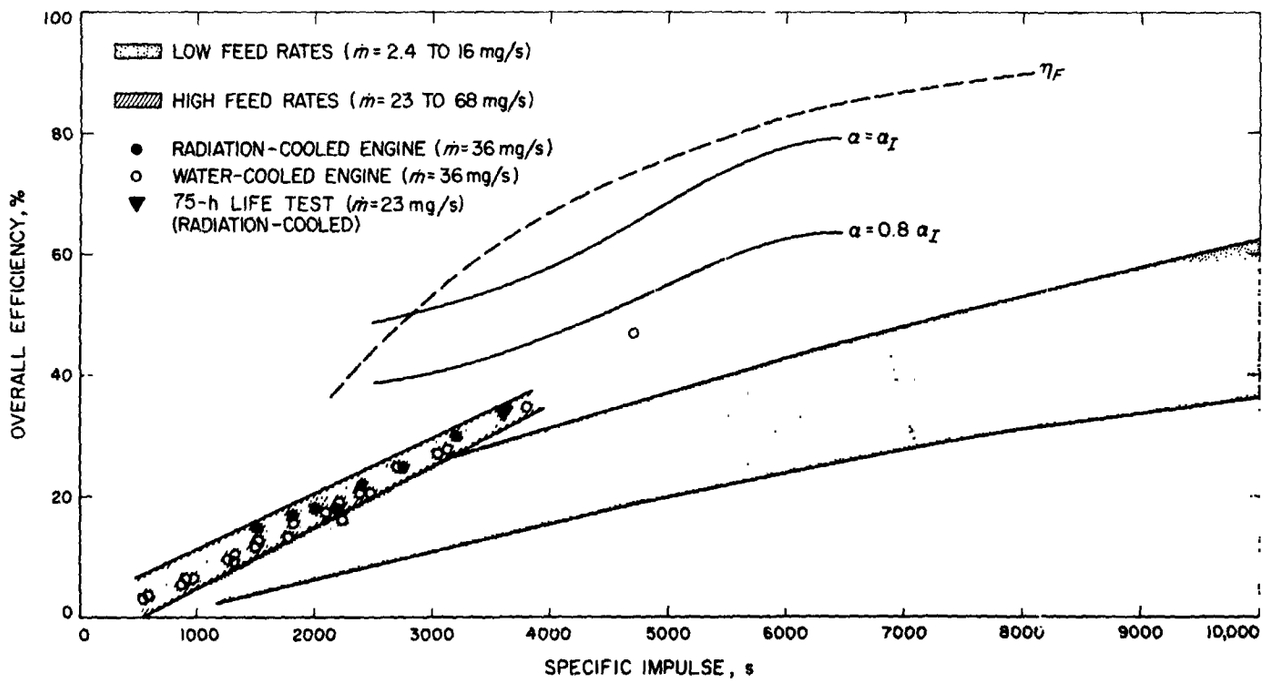

Fig. 25. A comparison of the overall performance of water-cooled and radiation-cooled ammonia-fed thrustors (data are from the AVSSD X-7C series of MPD thrustors)

throat diameter of 0.8 in. The X-7C engines were operated over a much larger range of feed rates (1.25 to 68 mg/s) than was the X-2C. At the lower feed rates (below 20 mg/s) the performance of the thrustors was generally lower than at the higher feed rates, as shown in Fig. 25. No significant differences in the overall performance of the radiation-cooled engine and the water-cooled engines were observed when the engines were operated at comparable conditions of applied magnetic field, feed rate, and power level. However, the arc voltage of the radiation-cooled engine was about 10 V less than that of the water-cooled configuration of comparable throat diameter. The arc voltage, in general, increased with increasing throat diameter.

The shaded areas of Fig. 25 include nearly all the data published in Tables I through V of Ref. 29. The individual points illustrating the comparison between the radiation-cooled and water-cooled engines were taken from Fig. 15 of the same reference. A life test of 75 h duration, which is indicated by the triangular point on Fig. 25, was obtained with a radiation-cooled engine at a specific impulse of 3600 s and overall efficiency of 34%.

Some data not included in Fig. 25, which were obtained with very small feed rates, were clearly affected by entrainment (Ref. 29), inasmuch as the calculated overall efficiency exceeded 100%.

Avco-Everett. The performance of the MAARC was generally higher with ammonia than with hydrogen (Ref. 40). However, at the maximum specific impulse reported for ammonia, about 2700 s, the efficiency obtained with a hydrogen feed rate of 50 mg/s was comparable.

The MAARC was observed to operate in either of two modes at different voltages, with the higher voltage mode the less efficient (Refs. 37 and 40). It was found that continuous stable operation in either mode could be achieved by moving the cathode either upstream or downstream of the "normal" position. When the cathode was in the downstream position, the discharge operated consistently in the low-voltage mode, and when the cathode was moved upstream, the discharge operated in the high-voltage mode. Patrick and Schneiderman (Ref. 40) report an optimum magnetic field intensity for both hydrogen and ammonia as well as an effect of the field configuration on the performance.

From the measurements with the ρu^2 probe and operation with a quartz shroud, it was concluded that entrainment was less of a problem with ammonia than with hydrogen (Ref. 40). When the MAARC was operated with ammonia on the thrust stand at the AVSSD facility, the thrust measurements were in better agreement with those determined with the thrust plate than a similar comparison, with hydrogen as the propellant, had afforded (Refs. 35 and 40).

b. Low pressure. The low-pressure operation of the AVSSD X-2C engine with ammonia at NASA Lewis produced results very similar to those obtained with hydrogen (Ref. 65). Good reproduction of the AVSSD data was obtained at tank pressures of from 0.017 to 0.40 torr, and higher efficiencies were observed at tank pressures from 2×10^{-1} to 5×10^{-5} torr. The engine was observed to operate in either a high- or low-voltage mode at all pressure and field strengths. The results also indicated the existence of an optimum field intensity, at a value of less than 1400 G when the engine was operated at the lowest tank pressure.

The results obtained with the AVSSD X-7C engine at NASA Lewis will be published at a later date (Ref. 78).

c. Summary. Two engines, the Avco-Everett MAARC and the AVSSD X-2C, have been operated both on ammonia and on hydrogen. For both, the efficiency is generally higher with ammonia than with hydrogen; however, the maximum reported value of specific impulse is less than that obtained with hydrogen. Both engines, designed initially for operation with hydrogen, were more likely to operate at different voltage modes with ammonia than with hydrogen. Stable, single-mode operation was obtained with one engine (Avco-Everett) as the result of a small change in the engine configuration.

The results obtained (Ref. 29) with the AVSSD X-7C series indicate erratic operation for engines with anode throat diameters larger than 0.85 in. and relatively poor performance for feed rates below 20 mg/s. The performances of radiation-cooled and water-cooled engines were comparable. The range of operating variables was the following: propellant feed rates from 1.25 to 68 mg/s; input power from 20 to 80 kW; external magnetic field strength from zero to 4000 G; and ambient tank pressure from 5×10^{-5} to more than 0.5 torr.

3. *Alkali metals.* The alkali metals have received attention as propellants for MPD thrustors because they are easily stored for long space flights and because the frozen-flow losses should be small. Multiple ionization of

the easily ionized material decreases the latter advantage, particularly for the heavier atoms that have low second-ionization potentials.

The alkali metals that have been tested are lithium, sodium, potassium, and cesium. The thrustors are generally of moderate power (less than 25 kW) with radiation-cooled tungsten anodes, and all have strong external fields. Because the exhaust products are condensable, the tank pressures were low, even with only modest pumping capacities, and, therefore, entrainment was less likely than with gaseous propellants. The performance of MPD thrustors operated with alkali metal is shown in Fig. 26.

a. Lithium. Because of the very high (about 65 eV) second-ionization potential of lithium, the energy invested in multiple ionization should be minimal. For this reason, most of the performance data of MPD engines operated with alkali metals have been obtained with lithium as the propellant. Giannini (Refs. 15 and 16), AVSSD (Ref. 21), and EOS (Ref. 51) have operated lithium-fueled MPD thrustors. The largest effort devoted to developing lithium-fueled engines has been expended by EOS.

EOS. A large variety of electrode configurations for the lithium engine have been tested by EOS (Refs. 48–51). In the first series of models, the propellant was injected through the cathode tip; however, better performance was obtained from configurations in which the propellant was injected through the anode. Only the data obtained with anode-fed models are included in the region on Fig. 26 labeled Li (EOS). Because of severe erosion of the insulator placed between the cathode and the anode, a number of cathode configurations were tested in an attempt to achieve stable arc attachment at the cathode tip and away from the insulator. The models shown in Fig. 14 were more efficient than the versions with extended cathodes (Fig. 15), but the erosion was more severe. The point labeled "life test" represents the average performance obtained in a 10-h endurance test of Model LAJ-AF-6D, shown in Fig. 15.

In further attempts to force arc attachment to the cathode tip, the buffered cathode configuration shown in Fig. 16 was tested. The purpose of the buffer was to increase the pressure at the cathode tip and thereby obtain arc attachment at the cathode tip. Altho . h the desired cathode tip attachment was achieved, no lithium data were obtained with the buffered-cathode engine

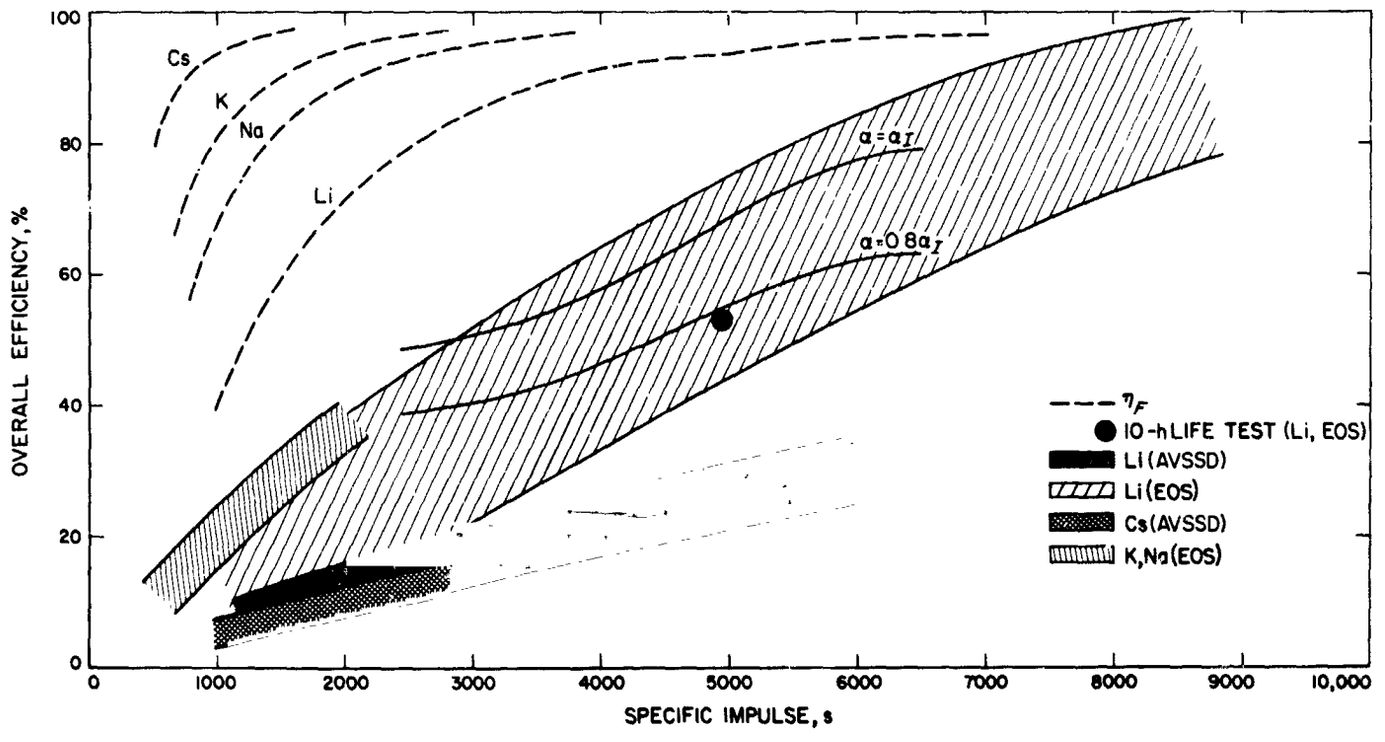

Fig. 26. Overall efficiency vs specific impulse of engines operated with alkali metal propellants

because of problems associated with the lithium feed system (Ref. 51).

Performance data were obtained with the bipropellant, buffered-cathode engine shown in Fig. 17, and with a slightly modified model in which the cathode was moved downstream a small distance. The results, obtained with either nitrogen or hydrogen injected into the cathode region, are shown in Fig. 27. (The data were published as Table II of Ref. 51.) The gaseous feed constituted roughly 10% of the total propellant for most of the tests. The best performance was obtained with total feed rates greater than 10 mg/s. Higher values of specific impulse were obtained with the hydrogen–lithium combination than with the nitrogen–lithium combination. As shown in Fig. 27, the performance obtained with feed rates of less than 10 mg/s (from 4 to 6 mg/s) was consistently lower than the performance obtained at the higher feed rate. These accelerators are now called ALPHA, for Alkali Plasma Hall Accelerator.

A scheduled endurance test was postponed because of instabilities believed to be associated with the lithium feed system (Ref. 51).

AVSSD. The experiments at AVSSD with a lithium-fueled engine were made with the thrustor shown in Fig. 12. The performance results, shown in Fig. 26, are slightly lower than the results reported by EOS (not shown in the figure) for the models in which the lithium was injected through the cathode tip.

Giannini. Only thermal efficiency data have been reported by Giannini for the lithium-fueled engines (Fig. 18) because the thrust measurements did not show sufficient reproducibility for publication (Ref. 15). The thermal efficiency varied between 30% and 40% for arc input power between 3 and 9 kW with lithium feed rates between 0.5 and 3.0 mg/s (Ref. 15).

b. Sodium and potassium. Both sodium and potassium have been tested at EOS (Refs. 47, 50, and 51) with the configuration shown in Fig. 15. With the exception that higher values of specific impulse were obtained with sodium, the performances of the two fuels were similar and the results are shown in Fig. 26 as the single area labeled "K, Na." For both propellants, the efficiency increased linearly with specific impulse and leveled off at

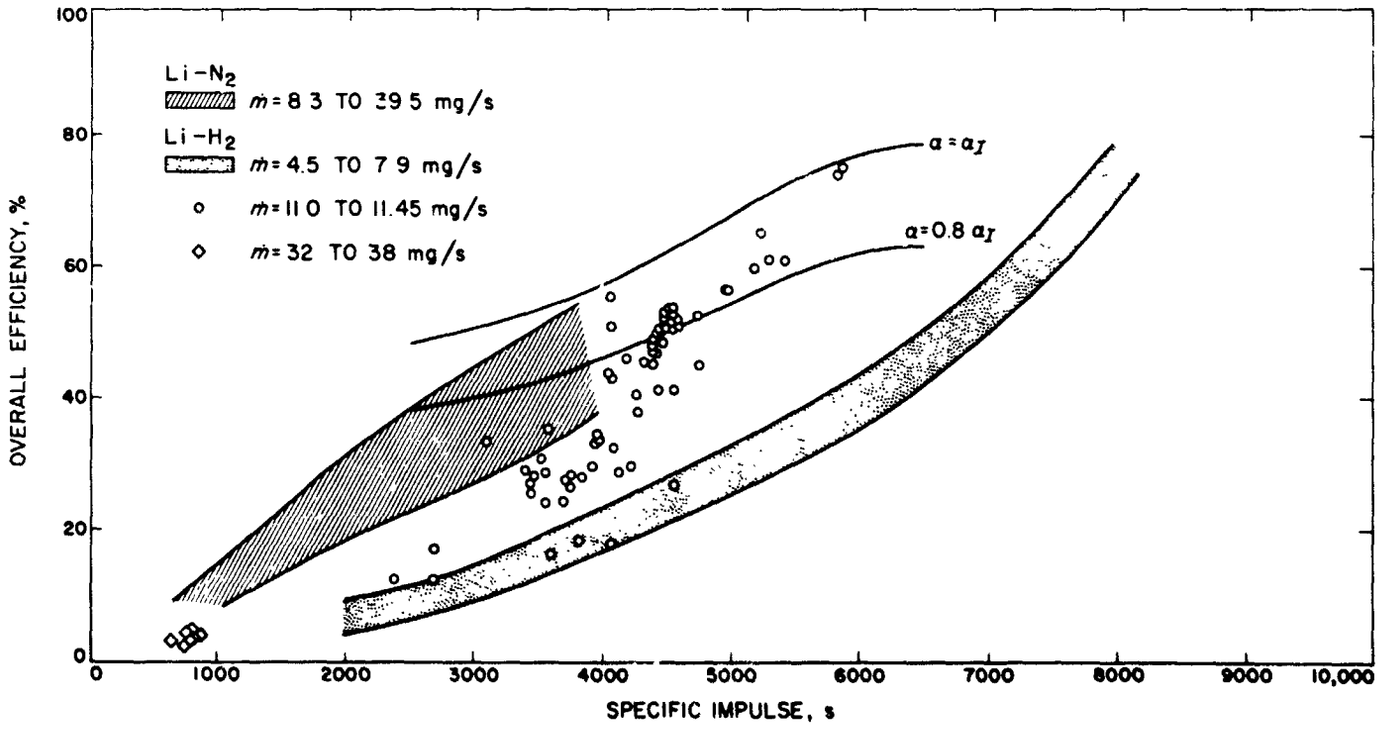

Fig. 27. Overall efficiency vs specific impulse of engines operated with Li–H_2 and Li–N_2 bipropellants. Data are from EOS ALPHA (Alkali Plasma Hall Accelerator). The lithium was fed through the anode, and the gaseous propellant through the cathode region

the higher values. The efficiency remained nearly constant at about 30% for values of specific impulse above 1200 s for potassium and at about 40% above 1800 s for sodium. The onset of second ionization was suggested (Ref. 51) as a possible reason for the leveling-off of the performance curve. Potassium was also tested at Giannini (Ref. 15); however, no performance data were reported.

c. Cesium. A cesium-fueled MPD engine was tested by AVSSD with the water-cooled engine shown in Fig. 12 (Refs. 20 and 24). An attempt to test cesium in the radiation-cooled engine (Fig. 13) was also made; however, stable operation could not be achieved and performance data were not reported (Ref. 21). The performance of cesium, which is the lowest of any obtained with alkali metal propellants, is indicated on Fig. 26.

d. Summary. The alkali metals lithium, potassium, sodium, and cesium have been tested in radiation-cooled MPD engines, all of which used externally applied magnetic fields. Cesium has also been tested in a water-cooled engine. Of these four propellants, the cesium was reported to have the lowest performance. The performance of potassium and that of sodium, which were tested in engines designed for operation with lithium, were very similar, but the performance with sodium was somewhat better. The maximum reported specific impulse for potassium and for sodium was 1200 and 1800 s, respectively. Of the four alkali metals, only lithium has been tested to obtain thrust data at more than one laboratory, and it has received, by far, the most attention. The reported performance, as well as the engine geometries and the methods of propellant injection, varies greatly among the various investigators. The maximum reported efficiency of lithium-fed engines (over 90%) was with an anode-fed, radiation-cooled engine.

The most recent investigations with alkali metals have included studies of lithium–nitrogen and lithium–hydrogen bipropellants in which the gaseous propellant was injected into the cathode region. Although somewhat lower performance was obtained with the bipropellants than with pure lithium, a number of advantages were reported for bipropellant operation. These advantages included longer life of the engine components, increased arc stability, and decreased heat losses to the cathode. Better performance was obtained with high feed rates (>10 mg/s) than with lower feed rates.

4. Miscellaneous propellants. The reported performances obtained with engines operated on nitrogen (Refs. 40 and 47), argon (Refs. 18, 40, and 47), and helium (Refs. 15, 19, and 47), are shown in Fig. 28. As

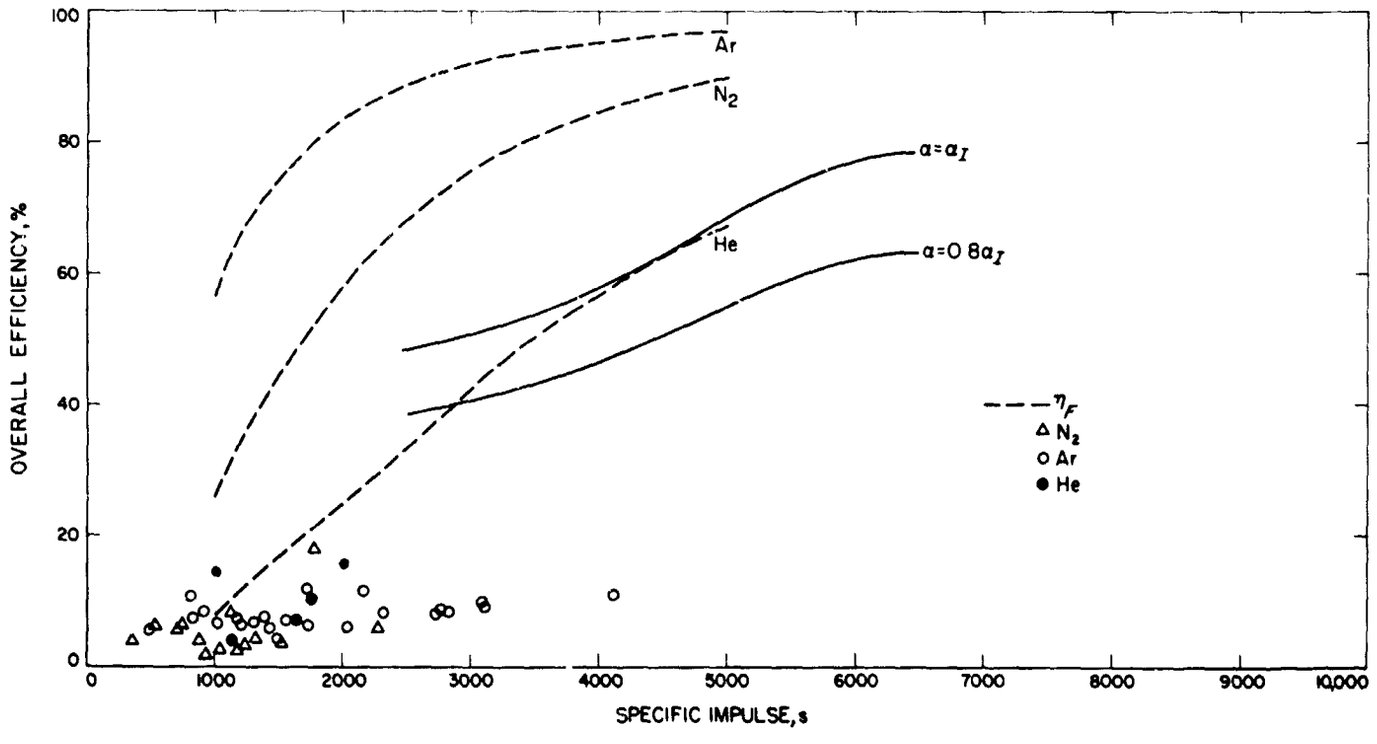

Fig. 28. Performance of miscellaneous propellants

indicated in the figure, the performance of these propellants is much lower than that obtained with the propellants discussed above.

B. Thermal Efficiencies

1. Energy loss measurements. An upper limit to the MPD thrustor's overall efficiency is obviously the thermal efficiency of the engine. Because the median range of the thermal efficiencies of many of the more technically promising engines is around 50 to 60%, reduction of the electrode losses provides one of the most potentially profitable methods of increasing the performance of MPD accelerators. The cathode loss is usually less than 10% of the total loss; therefore, experimental and analytical studies emphasize the anode loss. One exception is that Cann (Ref. 50) found the cathode loss to constitute from 30 to 45% of the total electrode losses for tests made with a potassium-fed accelerator.

The power loss to water-cooled electrodes is determined by measuring the steady-state temperature rise of a known flow rate of electrode coolant. Nearly all the accelerators operated with alkali metal propellants were radiation-cooled, and the anode losses of these engines were seldom measured. The thermal efficiency is calculated from the measured arc power and the power lost to the coolant according to

$$\eta_{th} = \frac{P - P_a}{P} = 1 - \frac{\dot{w}c_p\Delta T}{IV} \qquad (10)$$

2. Energy loss mechanisms. The different modes of energy transfer to the anode that have been discussed are the following:

(1) Radiative energy transfer from the hot plasma to the anode surface.

(2) Transfer to the anode of the kinetic energy of the electrons that carry the arc current into the anode. Also associated with the current is the potential energy, which is called the work function or the condensation energy (Ref. 44) of the free electrons relative to the conduction electrons in the anode.

(3) Heat transfer from the hot plasma through the boundary layer and into the anode. This mechanism is usually called "convective heat transfer" in keeping with the well-established nomenclature of heat transfer studies.

The term "convection" has been used by different authors to describe both of the last two mechanisms listed above. The kinetic energy carried by the electrons into the anode is energy convected across the boundary by the mass motion of the electrons. Using "heat" in a broad sense, Ducati (Ref. 16) has described the mechanism listed as item (2) above as "convective heat transfer." Heat transfer through the boundary layer is then referred to as conduction. Which meaning of "convection" is intended is usually made clear from the context of the discussion.

Of the three mechanisms listed above (primarily because of the observed correlation between anode losses and the applied arc current), the conv ction of the kinetic energy of the electrons into the anode by the current is nearly always reasoned to be the dominant energy-transfer mechanism. One method of expressing the energy of the electrons is to equate the average electron energy to $|e|\ V_a$, where V_a is an "effective" anode voltage drop that is defined by

$$V_a = \dot{w}c_p\Delta T/I \qquad (11)$$

The use of Eq. (11) implies that all other energy transfer mechanisms, such as, for example, the more familiar convective heat transfer of aerodynamic flows, are assumed to be negligible. A convenient concept that has been used (Refs. 19 and 21) is that V_a is a constant that is independent of the engine operating conditions and the propellant used. Another approximation is to somehow relate V_a to the ionization potential of the propellant (Ref. 49). The data on the anode heat transfer rates indicate that the use of a constant effective anode voltage drop is not justified for alkali metal propellants (Refs. 24 and 47). As will be discussed below, other methods have also been used to correlate the anode loss and the thermal efficiency with the engine operating parameters. Theoretical calculations of anode losses have been made by Hassan (Ref. 63).

3. Thermal efficiencies of gaseous propellants. Nearly all the MPD engines operated with gaseous propellants have been designed with water-cooled anodes. The routine tests generally included the measurement of the anode losses, and the subsequent data reduction included the calculation of the thermal efficiency. Some developmental effort has been devoted to correlating the thermal efficiency with the engine operating parameter.

a. AVSSD. John (Refs. 19 and 21) has correlated the anode cooling losses of the X-2C engine (Fig. 1) with

the arc current for a number of propellants. For hydrogen, the anode heat transfer rate was found to be independent of the feed rate and the magnetic field strength, and to increase nearly linearly with the arc current over a range of from 200 to 2000 A. The feed rate was varied from 20 to 50 mg/s, and the magnetic field strength was varied from 500 to 2000 G. A smooth curve was drawn through the hydrogen data and superimposed on a similar plot that contained the data obtained with ammonia. The line drawn to represent the hydrogen data fitted the ammonia data as well as it fitted the hydrogen data. The data obtained with helium, nitrogen, and argon were more scattered than the data for either hydrogen or ammonia; nevertheless, the line drawn to represent the hydrogen data provided an adequate fit.

John found that the data, which were plotted as the logarithm of the anode cooling loss versus the logarithm of the arc current, could be approximated by a single straight line of unit slope for all values of feed rate and field strength for all of the gaseous propellants tested. Therefore, it was concluded that a constant anode voltage drop could be used to account for the anode loss. The value of the constant anode voltage drop was found to be 26 V. Thus, since the anode cooling losses are fixed by the arc current, John concluded that the thermal efficiency is determined essentially by the arc voltage. The thermal efficiency for both hydrogen and ammonia were then plotted as a function of the field strength and shown as a family of curves with the arc current and the feed rate as parameters. The engine operated at a higher voltage with hydrogen than with ammonia; consequently, the thermal efficiencies were higher with hydrogen (up to 75%) than with ammonia (up to 50%).

If the anode loss is expressed as IV_a, with V_a equal to 26 V as determined by the method described above, Eq. (10) can be cast into the form

$$\eta_{th} = 1 - \frac{26}{V} \tag{12}$$

The most direct test of Eq. (12), which states that the thermal efficiency is a function of the arc voltage only, is to plot the thermal efficiency as a function of V. This has been done here for the data (Ref. 21) published for a hydrogen feed rate of 50 mg/s (Table C-1 of Ref. 21) and appears as Fig. 29. Superimposed on the data is the curve given by Eq. (12). It may be seen from Fig. 29 that the thermal efficiency varies with arc current as much as, or more than, it varies with arc voltage. This

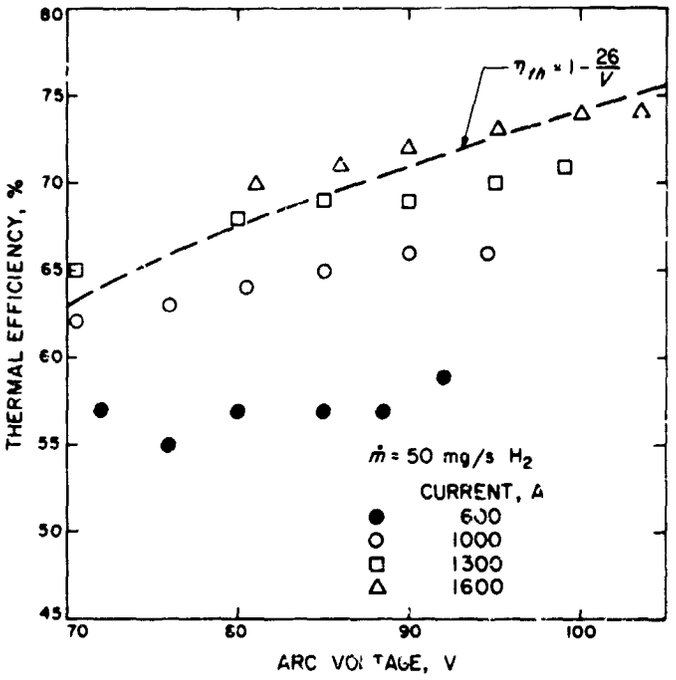

Fig. 29. Correlation of the thermal efficiency of the AVSSD hydrogen-fed X-2C engine with the arc voltage. The curve drawn on the figure is the predicted thermal efficiency if the anode loss can be represented by a constant effective voltage drop of 26 V

suggests that the use of a constant anode voltage drop to represent the anode loss is a questionable approximation. Inspection of the data obtained at 50 mg/s and at constant current levels (Table C-1 of Ref. 21) reveals a systematic increase in the power loss as the magnetic field is increased. At fixed current levels of 600, 1000, and 1300 A, the anode loss increased by about 20% as the magnet coil current was increased from 700 to 1200 A (B = 2000 G at a coil current of 1200 A). The increase in the anode power loss was less at the highest arc current, 1600 A.

The experiments (Ref. 29) conducted at AVSSD with the X-7C engines indicated that the anode voltage drop was a function of both the applied current and the applied magnetic field strength. This is shown in Fig. 30, which was taken from Ref. 29.

b. EOS. The results obtained at EOS with the H_2-1 accelerator (Ref. 44), with hydrogen as the propellant, were similar to the results obtained at AVSSD with the X-2C engine. The anode power loss P_a was found to be independent of the magnetic field strength for values of B up to 3000 G, and to depend linearly on the arc

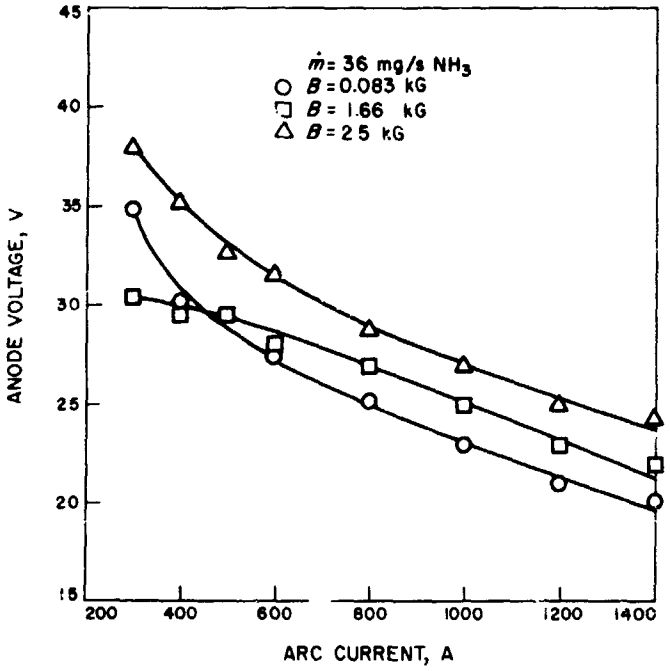

Fig. 30. Anode voltage vs arc current for the X-7C-4 engine (from Fig. 6 of Ref. 29)

current over the range of from 400 to 900 A. However, unlike the results obtained at AVSoD, the anode loss was found to depend on the inverse square root of the feed rate. The thermal efficiency varied from 0.60 to about 0.78.

These data are stated to correlate well with a convective heat transfer model similar to one used previously in arc jet technology (Ref. 44). However, the concept of this convective heat transfer model was not developed further for application to the MPD device. When the observations listed above apply to accelerators in which the arc attachment to the anode occurs on the front face of the anode, they are taken to indicate that the power transferred to the anode is primarily convected into the anode by the electrons that carry the arc current. The concept of an effective anode voltage drop, with the energy carried into the anode by the electrons, is associated with an electron temperature which has been elevated in the anode sheath. In one analysis (Ref., 49), the electron enthalpy at the anode surface is related to the ionization potential of the propellant, and the anode power loss is given by

$$P_a = I\left[n_0\left(\frac{\dot{m}_0}{\dot{m}}\right)^{1/2}\right]V_I \qquad (13)$$

where V_I is the ionization potential, $\dot{m}_0$ is an arbitrary reference feed rate, and n_0 is an empirical constant. The energy of the electrons, given by $|e|\ [n_0(\dot{m}_0/\dot{m})^{1/2}]\ V_I$, is assumed to be the same at the anode surface as in the downstream accelerated plasma stream. This restriction was relaxed in a later report (Ref. 52).

c. Avco-Everett. From the results of an experimental study of the thermal efficiency of the MAARC (Fig. 2) operated on ammonia, Schneiderman and Patrick (Refs. 37 and 40) postulate that the energy loss to the electrodes can be associated with an effective anode voltage drop V_0' that is related to the arc voltage as a constant fraction a of the quantity V_0 that appears in the empirical expression for the arc voltage given by

$$V = V_0 + U_c B\ell \qquad (14)$$

where U_c is the propellant critical velocity (see Part IV, Section II-C-2).

Thus,

$$\dot{Q} = IV_0' = aIV_0 \qquad (15)$$

where the heat transfer rate $\dot{Q}$ was determined from the temperature rise of a known flow rate of anode cooling water. Using Eqs. (10), (14), and (15), Schneiderman formulated the following expression for the thermal efficiency:

$$\eta_t = 1 - \frac{a}{1 + \dfrac{U_c B\ell}{V_0}} \qquad (16)$$

Experimental verification of the applicability of Eq. (16) was complicated by the observation that the arc was able to operate in either of two distinct voltage modes (Ref. 37). The changes in the voltage modes, which were accompanied by variations in the anode heat transfer rate, were attributed to changes in the quantity V_0. It was subsequently determined that when the cathode was moved a short distance downstream of the initial position, the arc always operated at the low-voltage mode, and, conversely, when the cathode was moved upstream of the initial position, the arc always operated in the high-voltage mode. At a fixed field strength, V_0 varied by as much as 50 V as the cathode was moved about ½ in. Although the heat transfer data appeared to scatter considerably as the voltage mode changed, the value

of the ratio V_0'/V_0, which is the constant a of Eq. (15), was between 0.5 and 0.8 for nearly all values of V_0.

The experiments were conducted by varying the strength of the magnetic field at a constant feed rate and nearly constant arc current. The results were summarized by a plot of the thermal efficiency as a function of arc power. Considerable data scatter is apparent when the results obtained from all voltage modes are included; however, correlation of the thermal efficiency with arc power was achieved (Ref. 37) for data obtained from tests in which the value of V_0 had a single fixed value. This is shown in Fig. 31, taken from Ref. 37, on which the lines are drawn to connect data points obtained during a single run in which the quantity V_0 remained constant as the field was varied. The higher values of efficiency of each curve correspond to higher field strength, and the curves of higher efficiency correspond to smaller values of V_0. No dependence of the mass feed rate, which was varied from 20 to 50 mg/s, was found.

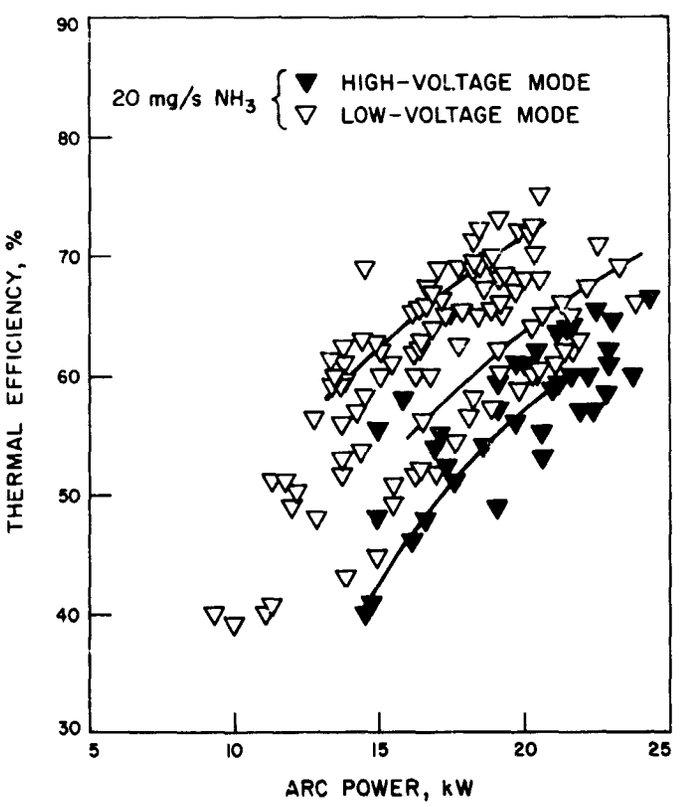

Fig. 31. Summary of the thermal efficiencies vs input power, showing the dependence on voltage modes (from Fig. 23 of Ref. 40). The curves are drawn through data for which no change in the voltage mode was observed

Table 4, which is taken from Table II of Ref. 37, was constructed to compare measured thermal efficiencies of other propellants, in addition to ammonia, with the values predicted by Eq. (16). The listed values of V_0 and the thermal efficiencies were obtained from earlier tests at Avco-Everett (Refs. 31, 32, and 39) or from the sources indicated in the table. The table shows that the maximum thermal efficiencies increase with increasing values of U_e/V_0 ratio. Schneiderman and Patrick concluded that higher values of the $B\ell$ product are necessary in order to obtain high efficiencies of propellants when lower critical speeds are used.

d. Giannini. Partial results of a systematic study of the effects of engine geometry, magnetic field strength, arc power, and propellant feed rate on the thrustor performance have been published by Ducati (Refs. 15 and 16). The general configuration of the electrodes is shown in Fig. 7. The published results are for an anode throat L/D ratio of 1.5 and a hydrogen feed rate of 10 mg/s. Anodes with four different throat diameters of 0.125, 0.25, 0.50, and 1.00 in. were used. The magnetic field was varied from 1000 to 16,000 G, and the arc power was adjusted to produce values of specific impulse of 1000, 2000, 4000, and 8000 s.

Table 4. Comparison of thermal efficiencies with predicted values[a]

Propellant	$U_r \times 10^{-4}$, m/s	V_0, V	$(U_r/V_0) \times 10^{-3}$, m/s/V	Approximate maximum observed η_{therm} near 4000 G, %
H_2	5.5	45	1.22	90
NH_3	2.6	36	0.72	75
Ar	0.87	15	0.58	70
Li[b]	1.2	22	0.55	35, 86[b, c]
N_2	1.6	30	0.53	55
Na Ref. 50)[d]	0.65	13	0.50	40 (Ref. 50)[c]
K (Ref. 47)	0.46	10	0.46	30 (Ref. 47)[c]
Cs (Ref. 24)	0.23	16	0.15	38 (Ref. 24)

[a]Taken from Table II of Ref. 37.

[b]From S. Bennett, AVSSD, private communication.

[c]Data for radiation-cooled engines where $\eta_{thermal}$ is not known. The values given are maximum $\eta_{overall}$ and hence represent the minimum possible $\eta_{thermal}$ for these cases (i.e., η_{thrust} assumed to be unity).

[d]The reference numbers conform to those used in the present report. Data not referenced were obtained at Avco-Everett.

The thermal efficiency was found (Ref. 16) to depend linearly on the throat diameter when the specific impulse and the field strength were held constant. At a specific impulse of 1000 s, the thermal efficiency obtained with the 0.125-in. throat was independent of the field strength over the full range (over which the applied field was varied), but the thermal efficiency obtained with the larger throat diameters increased significantly (from 34% to 60% for the 0.50-in. anode) as the field was increased. At 2000 s, the efficiency of the 0.125-in. throat was greater (from 48% to 55%) than at 1000 s and remained independent of the field from 4000 to 16,000 G. The smallest anode, with a 0.125-in. throat diameter, was not operated at values of specific impulse greater than 2000 s, or at field strengths less than 4000 G at 2000 s, because anode failure was likely at the excluded conditions. At values of specific impulse greater than 2000 s, the thermal efficiencies of the larger anodes were also independent of the applied field strength. The data used to correlate the engine performance were generally restricted to those obtained with the smallest throat used at each magnetic field and specific impulse. Fig. 32, taken from Ref. 16, shows the poor correlation obtained by plotting the thermal efficiency as a function of the specific impulse.

The data (Ref. 16) published by Ducati do not correlate well with a relation of the form given by Eq. (12), which makes use of a constant effective anode voltage drop. The arc voltage was observed to increase linearly with field strength up to 8000 G, but the thermal efficiency leveled off at fields of much lower strength. At fields greater than 8000 G, arc voltages greater than 200 V were measured, but the increase with field strength occurred in a very irregular manner. The voltage levels observed by Ducati were generally lower than those reported by John (Ref. 21). A possible reason for this may be that Ducati operated with a lower feed rate, and John's data, as well as those of others, indicate that the voltage increases as the feed rate is increased.

Ducati suggests that the efficiency does not depend explicitly on either the arc voltage or the arc current, and that a better correlation may be obtained by plotting the thermal efficiency as a function of the stagnation specific enthalpy of the heated propellant as shown in Fig. 33, which appeared as Fig. 53 of Ref. 16. Included in Fig. 33 are some reference data published by John (Refs. 19 and 21). These data, obtained at a feed rate of 20 mg/s, were described in Refs. 19 and 21 as showing very little systematic variation with either current or magnetic field

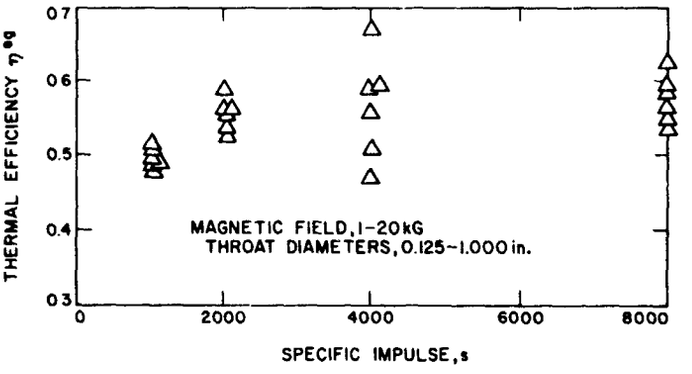

Fig. 32. Correlation of the thermal efficiency of the Giannini thrustor with the specific impulse (Ref. 16)

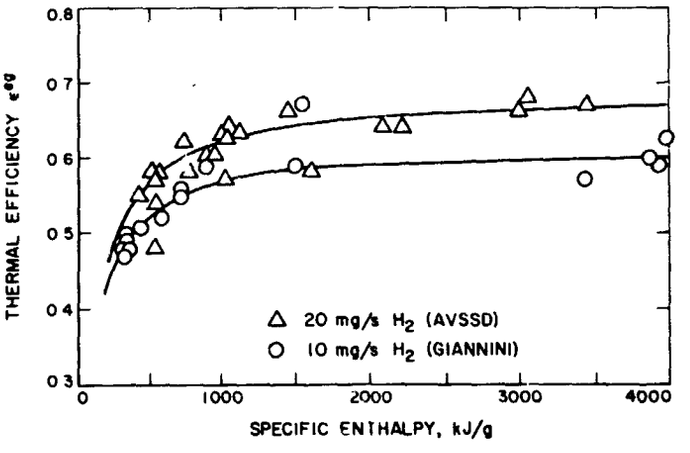

Fig. 33. Correlation of the thermal efficiency of Giannini thrustors and one set of data from the AVSSD X-2C engine with the plasma specific enthalpy. The correlating parameters are discussed in the text (from Fig. 53 of Ref. 16). The 10-mg/s data are for the smallest throat size at each specific enthalpy and magnetic field strength

strength. The two curves were drawn through the data by a curve-fitting technique that is described below.

The basis for the curves shown in Fig. 33 is the assumption that the electrode power loss could be expressed in the form

$$P_a = \lambda \dot{m} V_{ex} + \kappa \dot{m} h \qquad (17)$$

where λ and κ are constants, $\dot{m}$ is the mass flow rate, h is the specific enthalpy, including the ionization and dissociation energies, and V_{ex} is a constant associated with

the average excitation energy of the atomic hydrogen (Ref. 16).

The first term of Eq. (17), $\lambda m V_{ex}$, is identified with the radiation emitted by the atomic species and absorbed by the electrodes, and the second term is associated with convective and conductive heat transfer to the electrodes. With the electrode loss given by Eq. (17), the thermal efficiency is expressed as

$$\eta_{th} = \frac{1}{1 + \kappa + (\lambda V_{ex})/h} \tag{18}$$

The values of the constant λ and κ are adjusted to give the best fit of the data as shown in Fig. 33. Actually, λV_{ex} is adjusted instead of λ, since no criteria are given for assigning a value to V_{ex}. Because of a typographical error (Ref. 79), the value given for λV_{ex} on the figure in Ref. 16 is in error and should read 155 kJ/g. This is equivalent to 1.6 eV per particle.

Because the data can be fitted with a constant value of κ, Ducati interprets the correlation to indicate that the heat transfer is primarily due to the convection of energy across the anode surface by the electrons carrying the current. If conduction were a dominant heat transfer mechanism, the magnitude of the coefficient would be expected to be a strong function of both temperature and magnetic field.

An attempt is made by Ducati to associate the coefficient κ with physical parameters that are important in the discharge process. A simplified analytical model of the discharge, applicable only for large specific impulse and strong magnetic fields where the radiation, λV_{ex}, can be neglected, is postulated to describe the energy loss to the anode. It is assumed that the mass flow is parallel to the field lines (i.e., the electrodes are magnetically protected from the hot plasma) and that the current flows downstream along the jet centerline to some downstream position where it crosses the field lines and returns to the anode in an annular shell, called the anode jet, that is also parallel to the field lines. The voltage drop along the anode jet is called the anode voltage drop, V_a, and the power released in the annular anode jet IV_a is assumed to be divided between anode loss P_a and an increase in the enthalpy h_a of the mass flow m_a contained within the anode jet. With these assumptions, the expression for the thermal efficiency is written

$$\eta_{th} = \frac{1 - \dfrac{V_a}{V}}{1 - \dfrac{\dot{m}_a h_a}{\dot{m} h}} \tag{19}$$

where V is the total voltage drop and where $\dot{m}$ and h are the average values of the total propellant flow rate and specific enthalpy, respectively. Comparison with Eq. (18), with $\lambda V_{ex}/h << 1$, reveals that

$$\frac{V_a}{V} = \frac{\kappa + \dfrac{\dot{m}_a h_a}{\dot{m} h}}{\kappa + 1} \tag{20}$$

or

$$\kappa = \frac{\dfrac{V_a}{V} - \dfrac{\dot{m}_a h_a}{\dot{m} h}}{1 - \dfrac{V_a}{V}} \tag{21}$$

Ducati found the measured value of η_{th} to be independent of B at high I_s. Because V is observed to increase with B, Ducati concludes that if the ratio of the enthalpy flux in the anode jet to the total enthalpy flux remains constant, then V_a increases with B to keep the ratio V_a/V constant.

4. Thermal efficiencies of alkali metal propellants. The anode losses of the water-cooled cesium-fed engine (Fig. 12) operated at AVSSD (Refs. 20 and 24) were a very weak function of the arc current and could not be characterized by a constant voltage drop as were the losses associated with the gaseous propellants. The ratio of the anode loss to the arc current varied from about 75 V at 80 A to about 40 V at 180 A. The maximum thermal efficiency obtained was about 40%.

A somewhat better correlation of the anode losses of the cesium engine was obtained with the IB product than with I (Ref. 24), This is hypothesized to be a consequence of the electrothermal acceleration mechanism that was postulated to describe the operation of the cesium-fed engine. Bennett (Ref. 24) suggests that the energy gained by the electrons in falling through the voltage differential across the field of the magnetic

nozzle is sensed as anode heating. Then, since the voltage required to drive the current across the field lines is proportional to the field strength, the anode loss should be proportional to both the field strength and the current.

The accelerators operated with alkali metal propellants at EOS were radiation-cooled (Refs. 47, 49, and 51). For most tests, anode losses were not measured and therefore thermal efficiency data are not available. For tests with sodium and potassium, an oil-cooled shield was used to capture radiant energy from the anode. The ratio of the anode loss and the arc current, which is equivalent to the effective anode voltage as used by John, increased with increasing magnetic field strength for both sodium and potassium. As shown in Fig. 34 (Fig. 6-32 of Ref. 47), the dependence of the anode loss was more pronounced with potassium than with sodium. The correlation of the loss with the propellant molecular weight that is shown in Fig. 34 does not appear to be confirmed by the data plotted in Fig. 6-34 of Ref. 47. In the latter figure, the anode loss per unit current varies from about 4 to 10 V as the current is increased from 150 to 400 A at a fixed field strength.

The maximum thermal efficiency obtained with potassium was about 90%. Thermal efficiency data were not reported directly for sodium; however, from the data that were presented it appears that the maximum value was about 70 to 80% (Ref. 47). Although thermal efficiency data for lithium were not obtained, a lower limit on the thermal efficiency is the overall efficiency. The highest overall efficiency reported for lithium is 90% (Ref. 49).

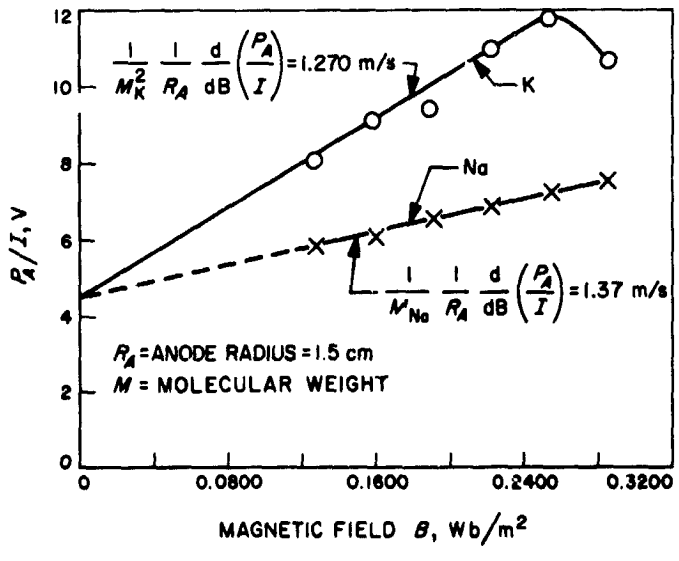

Fig. 34. Effect of magnetic field strength on anode power loss for sodium and potassium (from Fig. 6-32 of Ref. 47)

Thermal efficiencies for both potassium and lithium were obtained at Giannini with the engine shown in Fig. 16 (Ref. 15). The thermal efficiencies for both propellants were found to be independent of the magnetic field for fields above 1000 G. As the arc power was increased from 3 to 10 kW, the thermal efficiency varied from 25 to 35% for potassium and from 30 to 40% for lithium.

C. Diagnostic Measurements

Those measurements that are intended to yield detailed information on some aspect of the MPD engine operating mechanism, instead of primarily performance data, are classified here as diagnostic measurements. Within this classification, the ρu^2 probe, used at Avco-Everett (Refs. 39 and 40), serves the dual purpose of providing both detailed ρu^2 profiles and data on total thrust. Most of the measurements are made in the exhaust plume. Because each measurement is generally associated with a unique experiment at each laboratory, the major findings of the diagnostic measurements are described along with the method.

1. Visual observations. Perhaps the single diagnostic tool that has been used most extensively in the study of MPD thrustors is the visual or photographic observation of the exhaust plume. The apparent size of the exhaust plume, as judged from the extent of the luminosity of the exhaust, has been used to estimate the magnitude of entrained gas (Ref. 21). The variation of the intensity of the luminosity, across the jet diameter as well as axially, has played an important role in the development of the theoretical models that have been proposed to describe the acceleration mechanism (Ref. 50). The plume is generally described as a central, highly luminous core surrounded by an annular region of lower intensity that is separated from the core by a darker region. The outlines of the luminous regions have been correlated with the field pattern of the external magnet to demonstrate that the plasma follows the magnetic field lines (Ref. 24). A similar correlation has been made with current paths and the visual appearance (Ref. 44). Visual observation of deviations from an axially symmetric pattern have been used to indicate interactions with the test environment (Ref. 16). The visual appearance is considered to be of

sufficient importance by the group at Giannini that photographs of the plume, along with the meters registering thrust, current, etc., are obtained for each test (Ref. 16).

2. *Current densities.* Current densities in the exhaust plume have been determined by measuring the current-induced magnetic fields. These measurements have been made with both solid-state Hall-effect sensors (Fig. 35) (Ref. 25) and search coils (Fig. 36) (Ref. 40). The search coils consist of a number of turns of wire and respond to changes in the magnetic flux intercepted by the coil, whereas the Hall sensors give direct and continuous indications of the magnetic fields. The magnetic fields induced by current loops in the plasma exhaust are measured with the search coils by terminating the arc current. The use of search coils appears to be more suited to the measurement of Hall currents than the use of Hall-effect sensors because the fields induced by the Hall currents are superimposed on the much larger applied fields and are therefore difficult to detect with Hall probes. The search coil may be a short segment, or it may be made in the form of a loop called a Rogowski coil, as shown in Fig. 36. The Rogowski coil measures the total net current passing through the loop, and the measurement is independent of the distribution of the current within the loop.

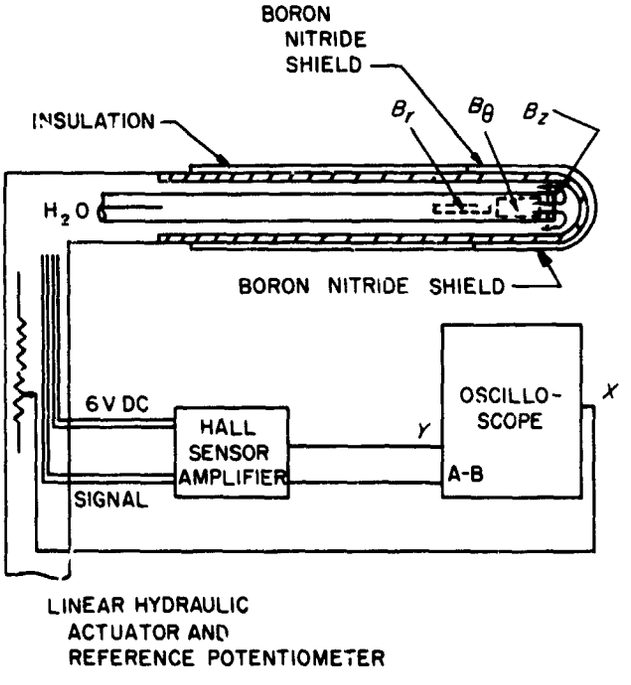

Fig. 35. Hall-effect sensor used to measure current density in exhaust plume (Ref. 25)

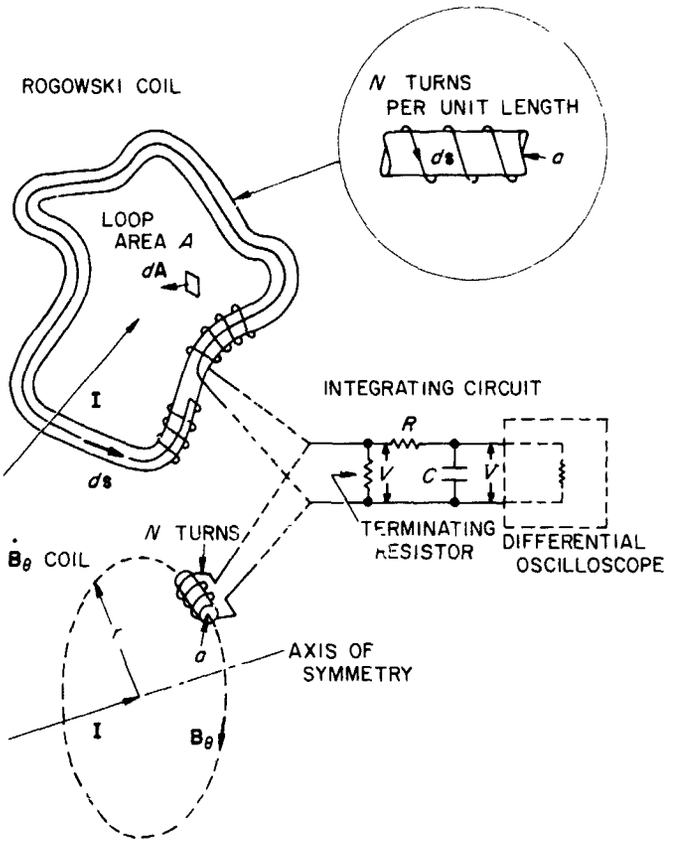

Fig. 36. Rogowski coil used by Avco-Everett to measure current loops in the exhaust of the MAARC (Ref. 40)

a. Axial and radial current. Hall-effect probes have been used by Cann (Ref. 46) to measure axial current densities in argon and by Powers (Ref. 25) to measure both axial and radial current densities in argon, ammonia, nitrogen, and hydrogen. Patrick and Schneiderman (Ref. 40) used a Rogowski coil to measure axial currents in ammonia and used a segment of a Rogowski coil, $\dot{B}_\theta$ coil, to measure axial currents in hydrogen. Nearly all measurements that have been reported indicate the existence of a central current-carrying core surrounded by an annular path that carries current in the opposite direction. The measurements (Ref. 46) also indicate that both of the two current-carrying regions closely follow the applied magnetic field lines. Large differences in the magnitude of the current are reported (Refs. 25 and 46).

Cann (Ref. 46) found nearly 100% of the arc current in the plume at 12 cm downstream of the anode and over 25% at 28 cm downstream. The current density distribution is shown in Fig. 37, which is taken from Ref. 47. Powers (Ref. 25) reports less than 15% of the arc current at 5 cm downstream for both ammonia and argon and

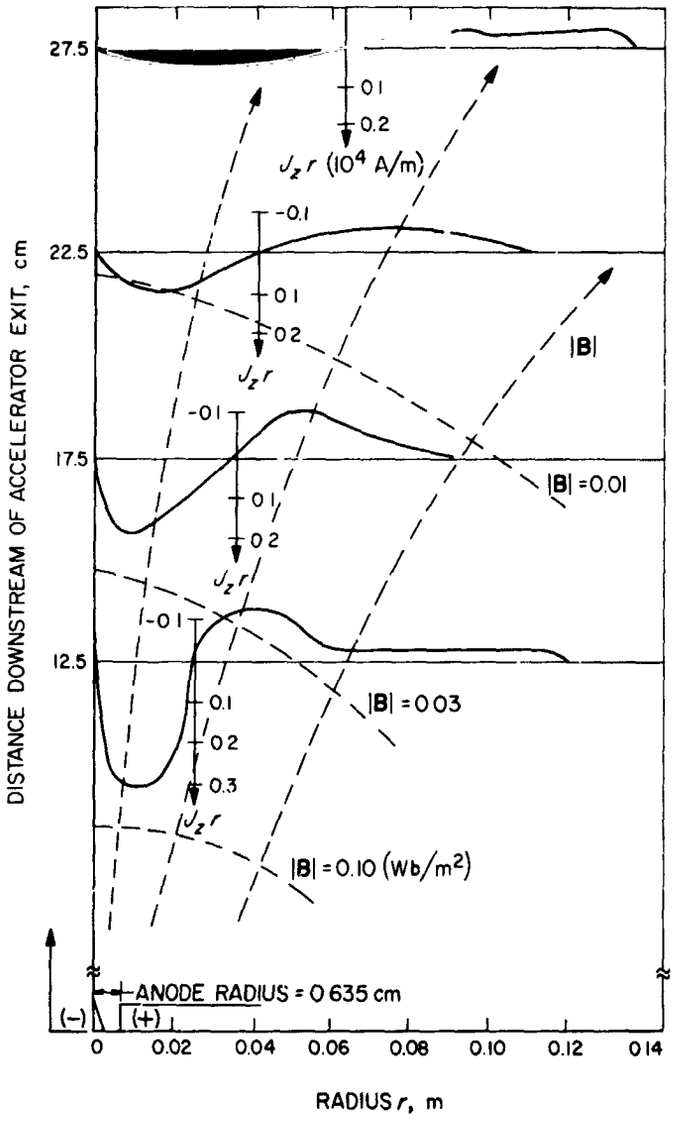

Fig. 37. Axial and radial distributions of axial current density and applied magnetic field (from Fig. 6-62 of Ref. 47). Contours of constant magnetic field strength are also shown

from 20 to 40% for nitrogen and hydrogen at the same station. The current leakage rate between the cathode and anode jets is reported to be 30 A/cm at 5 cm downstream and 10 A/cm at 17.3 cm. A sharp pinch of the cathode jet, characterized by a greatly increased current density in a smaller area, was observed when the magnetic field was increased from 750 to 1500 G. Patrick (Ref. 40) found less than 5% of the total arc current in the hydrogen exhaust at 7.5 in. downstream and only 15% of the arc current in ammonia. The results obtained in ammonia indicate no current leakage between the anode jet and cathode jet in the first 7 in. downstream.

b. Hall current. No detectable Hall currents were observed by Powers (Ref. 25), who estimated that a positive measurement would be obtained at azimuthal current densities of 1 A/cm^2. This estimate of the probe sensitivity provides an upper limit on the magnitude of the possible Hall currents and is compared with measured axial current densities of from 20 to 120 A/cm^2 on the centerline. However, search coils placed against the anode face indicate that Hall currents may exist in a gon. Similarly, Patrick (Ref. 40) found no indication of Hall currents in the exhaust plume of the hydrogen-fed engine. The sensitivity of the coils used by Patrick was estimated to be sufficient to detect a current density of 0.1 A/cm^2. Using pickup coils, Hess et al. (Refs. 56 and 57) and Hassan (Ref. 61) observed measurable Hall currents near the exit of an argon-fed MPD engine. The magnitude of the Hall current is reported to be less than 20% of the total arc current (Ref. 56).

Lovberg (Ref. 72) found the discharge of a low-pressure pulsed MPD engine, operated on argon, to consist of a current "spoke" that rotated with a frequency of about 30 kHz. No indications of Hall currents were observed. Larsen (Ref. 80) has also found indications of a rotating current "spoke" in a steady MPD engine.

The principal errors inherent in the measurements of current densities are associated with the disturbance of the plume by the probe. These errors are discussed qualitatively in the references cited above. Powers (Ref. 25) states that the measurements represent lower limits to the current densities, whereas Patrick (Ref. 40) suggests the possibility that no current flows in the undisturbed plume and that all the axial current measured may be a result of the probe.

3. Velocity measurements. Considerable effort has been devoted to velocity measurements in the MPD exhaust. Accurate velocity measurements are of particular importance in verifying the reported engine performance.

Velocity measurements in MPD engines have been made by means of $\mathbf{u} \times \mathbf{B}$ probes (Refs. 21 and 56), Langmuir probes (Refs. 56 and 58), phototracer techniques, and the measurement of doppler-shifted spectral lines (Ref. 52). The errors associated with each method are large, and, for some methods, the influence of factors known to affect the measurements is not fully evaluated at present.

Other methods are also being pursued, including the use of electrostatic probes to measure the velocity of both ion density and plasma potential fluctuations in the engine exhaust (Ref. 81). Another promising method utilizes an electronic shutter and Faraday cup arrangement to measure ion velocities directly (Ref. 80).

a. $\mathbf{u} \times \mathbf{B}$ *probes.* Plasma velocities are determined with $\mathbf{u} \times \mathbf{B}$ probes by measuring the voltage induced between two probes as plasma of velocity u crosses an applied field B. The probes and magnet coils are generally arranged so that a line between the probes and the vectors u and **B** are mutually perpendicular. To minimize the effects of noise, contact potentials, and potential gradients existing in the plasma, alternating magnetic fields are used. Measurements in the exhaust of MPD engines have been reported by John (Ref. 21) and by Brockman et al. (Ref. 56). Agreement with velocities calculated from thrust measurements with experimental scatter of up to 50% is reported. A description of the probe used at AVSSD, and its use in a more well-defined plasma, is given by Malliaris (Ref. 82).

The perturbing effects of the arc currents that may extend downstream to the probes are not known.

b. Langmuir probes. Plasma velocities have been determined by Brockman et al. (Refs. 56 and 58) from the comparisons of the saturated ion current collected by a probe aligned parallel with the flow direction and that collected by a probe, of the same area, aligned perpendicular to the flow. A further discussion of this method is given in Ref. 83. The measurements were made in the exhaust plume of an argon-fueled MPD engine. For some operating conditions, the velocity determined from the probe was in fair agreement with the velocity inferred from the thrust measurement and indicated "excess" velocities equal to about 1.25 times that expected from the arc voltage for the condition of electrostatic acceleration of the ions. The estimated uncertainty of the probe measurement is reported to be about 25%. At other operating conditions, the agreement with the thrust measurement was very poor.

The use of Langmuir probes to measure velocities requires knowledge of the electron temperature and consequently is subject to all the errors associated with the measurement of electron temperatures with Langmuir probes. The use of similar probes to measure flow velocities is also discussed by other authors (Refs. 84 and 85).

Electrostatic probes have also been used to measure the velocity of both ion density and plasma potential fluctuations in the engine exhaust (Ref. 81). For both methods, two probes are placed a known distance apart, with the line between the probes aligned parallel with the exhaust axis, and the signals from both probes are recorded as a function of time. The velocity of the ion density fluctuations is determined by recording the saturated ion currents, and the velocity of the potential fluctuations is determined by recording the probe floating potential. The "signatures" of the traces obtained from the upstream and downstream probes are similar but are displaced in time by an amount proportional to the velocity of the fluctuations and the distance between the probes. Results obtained by these methods will be published in the near future (Ref. 81).

c. Phototracer techniques. Phototracer measurements of exhaust velocities of a lithium–hydrogen bipropellant accelerator are reported by Jacobs and Cann (Refs. 52 and 53). This method consists of measuring the time of flight of local fluctuations in the plasma light intensity past two photomultiplier tubes placed a known distance apart in the axial direction. A lens is used with each tube to limit the radiation received to that emitted from a well-defined region, of about 2 cm in diameter, across the exhaust jet. The light fluctuations are associated with electron density fluctuations, which are assumed to travel at the local plasma velocity. Radial profiles were obtained by making the measurements at a number of positions off the jet centerline at a fixed axial position. To measure the velocity of individual species, optical bandpass filters were inserted into the light path to limit the radiation received by the photomultiplier tubes to the emission from a single species for each measurement.

The centerline velocity was found to increase from about 2.2×10^4 m/s at the exit plane to about 5.0×10^4 m/s at a position 118 cm from the exit plane. At the 118-cm position, the axial velocity was essentially uniform from the centerline to a radius of 5 cm and then decreased rapidly out to 10 cm. The velocities of the lithium atoms and ions were found to be nearly the same and generally greater than that of the hydrogen. Agreement with the velocities inferred from the thrust and mass flow measurements was within 20%. A special method was required to interpret the data because a large range of velocities was observed. The method used was to examine a few hundred observations and to plot the frequency of observing each velocity as a function of

the time of flight of the light fluctuation between the photomultiplier tubes. From the distribution so obtained, the average velocity and the most probable velocity were determined. The wings of the distribution curve, which has a fairly sharp peak, indicate the existence of velocities, both larger and smaller, that differ from the most probable velocity by a factor of from 4 to 5. Indications of a radial profile of the velocities were obtained by making the measurements at a number of off-centerline positions at a fixed axial position. The error associated with the velocity determination is given as about 20%. The method used to evaluate the error was not given.

The velocities obtained from the phototracer technique, the doppler shift method (see below), and the thrust and mass flow measurements are stated to agree to within a factor of 2 (Ref. 52).

d. Doppler shift of spectral line. Both axial and azimuthal velocities have been determined from doppler shifts of ionic spectral lines by the group at EOS (Ref. 52). Atomic lines were not used because the line shift was obscured by the stark broadening. The rotational velocity measurements were made on a lithium–nitrogen bipropellant accelerator and were confined to a narrow region of the cathode jet where ion lines were visible. Lithium ions were not observed, but data were obtained from N^+ and a number of impurity ions. The results indicated a rotational velocity of about 4000 m/s at a radius of 1.9 mm at an axial position 5 cm downstream of the exit. The axial velocities of lithium ions in a lithium–hydrogen accelerator were reported to be $(3\pm2) \times 10^4$ m/s. This result is compared with an average exhaust velocity of 5×10^4 m/s calculated from the thrust measurement.

The amount of shift was determined by comparison with a number of mercury lines, and the large experimental error is associated with variations in the scan rate of the monochromator used for the measurements. This source of error is expected to be largely eliminated by using a lithium hollow-cathode discharge lamp as the comparison source, instead of the mercury lamp.

4. Pressure measurements. Pressure measurements somewhere in the discharge region are generally made for those experiments designed primarily to obtain performance data. For some engine designs in which the cathode is withdrawn from the anode exit and a definable throat (usually in the anode) exists downstream of the cathode tip, the measured pressure is associated with a chamber pressure similar to that of a conventional thermal arc jet. For those designs in which the cathode tip is flush with the anode face or extends downstream of the anode, the measured pressure has a less definitive meaning. One result of these measurements is the observation that although a low pressure at the cathode (as compared with that existing in conventional arc jets) is required to apply very large currents, greater stability of the arc is afforded if the pressure is above a few torr.

Because the pinch generated by the self-magnetic fields is expected to manifest itself as an increased pressure along the jet centerline near the cathode tip, a number of experiments have been conducted with a pressure tap located at the cathode tip (Refs. 7, 18, and 28). These measurements yielded some of the earliest indications of electromagnetic interaction (Ref. 17), and the result of one such experiment is shown in Fig. 38, which is taken from Ref. 9. As the arc current was increased, with no applied magnetic field, the chamber pressure increased to a maximum value and then decreased, while the cathode tip pressure continued to increase. Fig. 39, taken from Ref. 27, shows that the tip pressure decreases when a magnetic field is applied. The results obtained from cathode tip pressure measurements are discussed further in Section IV-B-1.

5. Spectroscopic measurements. Because of the existing nonequilibrium conditions, spectroscopic measurements have not been used for quantitative studies of plasma properties in MPD devices. Rather, the spectroscopic measurements have been used chiefly to identify species. However, an estimate of the electron temperature, on the basis of the identity of highly ionized species, has been made. Thus Brockman et al. (Ref. 56) have concluded that the electron temperature ranges from 10,000 to 40,000°K in the exhaust of an argon-fueled accelerator because spectral lines from excited argon atoms and both singly and doubly ionized argon were observed. Additional discussions of the spectroscopic measurements at NASA Langley may be found in Ref. 86.

Spectroscopic observations of the exhaust plume of the AVSSD engine (Fig. 1) operated on ammonia have revealed spectral lines of H, N, NH, and N^+ as well as weak molecular bands of nitrogen. A comparison (Ref. 66) of the intensity of the different species, at the highest value of specific impulse obtained for each magnetic field strength used, indicates that the degree of ionization increases with increasing field strength. At a field

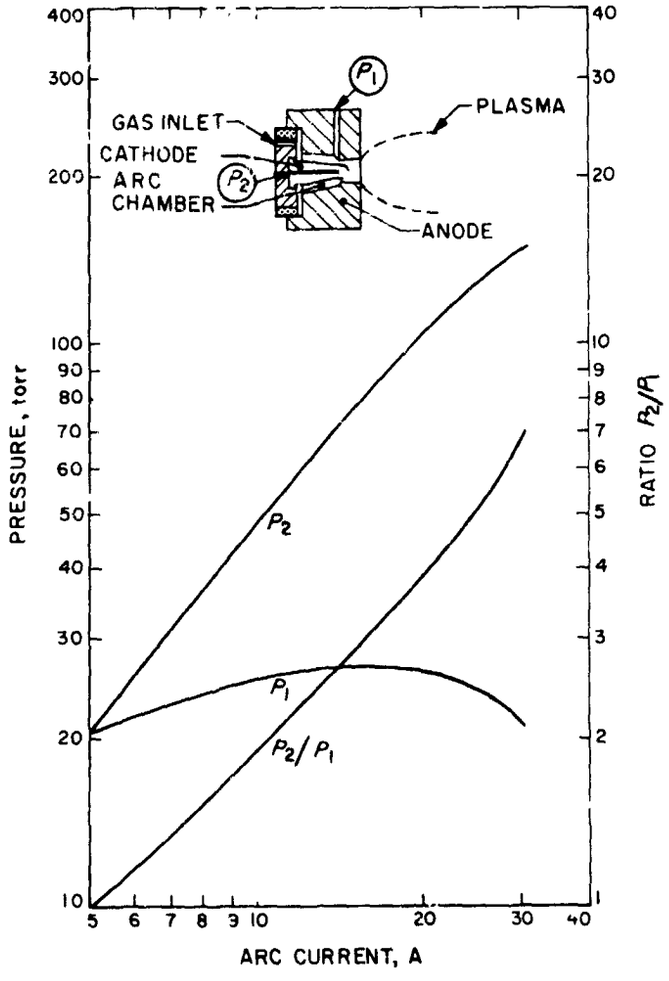

Fig. 38. Variation of the cathode tip pressure and the arc chamber pressure as a function of the applied arc current. The observed decrease in chamber pressure was one of the earliest indications of electromagnetic interactions (from Fig. 10 of Ref. 9)

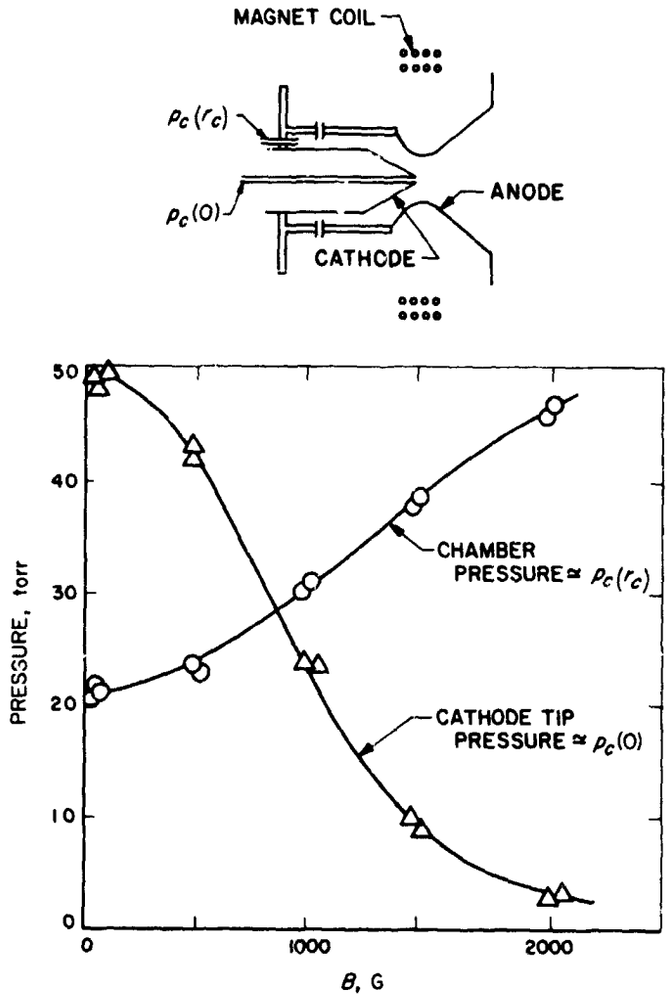

Fig. 39. Variation of the cathode tip pressure and the arc chamber pressure of the AVSSD engine with increasing applied field strength (Ref. 27)

strength of 1400 G, the spectra were dominated by very intense N^+ radiation and the hydrogen Balmer series with no indication of molecular spectra. At 1000 G N^+ and H spectra were still dominant, but the intensity of the spectra of N and NH had increased over that observed at 1400 G. The only intense lines at 600 G were the hydrogen Balmer series, and the NH lines were more intense than the N^+ lines. Although these measurements cannot be used to obtain a quantitative determination of the degree of ionization, the results demonstrate that complete ionization did not occur at the operating conditions that existed.

Spectroscopic determinations of the ion excitation temperature, using the relative intensities of argon II lines, near the exhaust plane of an argon-fed MPD device (operated without an applied magnetic field) were reported by Kelly (Ref. 87). The spectroscopic observations were made along a plume diameter and indicated a temperature of about 18,000°K. In later experiments (Ref. 88) on the same engine and at comparable operating conditions, lateral profiles of the intensities of the argon II lines were obtained and inverted through the use of Abel's transformation to obtain the radial distribution of the local emission. The results indicated a relatively flat temperature profile, over the region of strong ion line emission, of approximately 17,000 to 20,000°K. The temperature so determined was tentatively equated to the electron temperature on the basis of the apparent Boltzmann distribution of the excited levels of the argon ions. However, other measurements indicated that highly

nonequilibrium conditions existed in the plume. It is also noted that the exhaust plume was only slightly ionized (less than 10%) and therefore not comparable to the conditions that probably existed in the plume of most of the devices discussed in this survey.

6. Thrust density. Thrust density profiles in the exhaust of MPD engines have been measured both with impact-pressure tubes and with small thrust targets. A schematic of the thrust plate, or ρu^2 probe, used by Patrick (Refs. 39 and 40) to obtain the performance data reported for the MAARC is shown in Fig. 40. An example of the data obtained with the ρu^2 probe is shown in Fig. 41, taken from Ref. 40. Total thrust is obtained from each thrust density profile by integrating the expression

$$T = 2\pi \int_0^R \rho u^2 \, r \, dr \tag{22}$$

where R is the radius at which the thrust density is negligible. As may be seen from Fig. 41, the magnitude of the applied field has a pronounced influence on the ρu^2 profiles. At higher values of the applied magnetic field, the profile was found to be strongly "pinched" toward the centerline, with an accompanying decrease in total thrust. This indicates the existence of an optimum value of the applied magnetic field (Ref. 40). The measured reactive force on the engine was not directly compared with the results obtained with the ρu^2 probe. However, the MAARC was operated on a thrust stand in the AVSSD facility (see Part V, Section I-A-1).

Thrust density profiles of a nitrogen-fueled engine similar to the X-2C engine (Fig. 1) were measured by Malliaris (Ref. 28) with a blunt-tipped impact-pressure tube. The measurements were made at an axial position 0.5 in. downstream of the anode exit plane for various values of the arc current with no applied magnetic field. For the conditions of the experiment, the collision mean free path was estimated to be smaller than the probe diameter (0.5 in.), and for most operating conditions a detached bow shock was observed. The static pressure at the probe was assumed to be equal to the ambient tank pressure. The ρu^2 profiles obtained by Malliaris reveal increasing peak values at the jet centerline, relative to the average value of ρu^2, as the arc current was increased from 1000 to 2500 A. This result was interpreted to indicate increasing acceleration by self-magnetic fields. The thrustor was mounted on a thrust stand, and simultaneous measurements of the total force were made and compared with the integrated thrust density profiles. Very good agreement was obtained.

7. Mass flux. Mass flux probes were used by Patrick (Refs. 39 and 40) to measure ρu profiles in order to determine the amount of entrained gas in the accelerator exhaust and to calculate density and velocity profiles when used with the result obtained with the ρu^2 probe. A schematic of the mass flux probe is shown in Fig. 42.

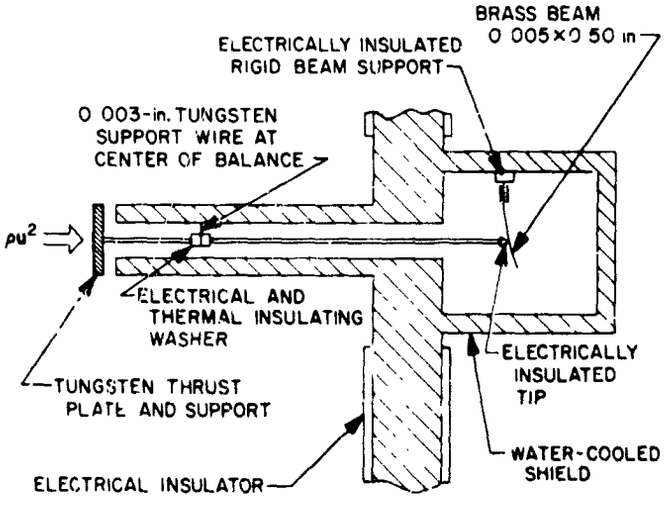

Fig. 40. Schematic drawing of the probe used to measure the thrust profiles in the MAARC experiments (from Fig. 5 of Ref. 40)

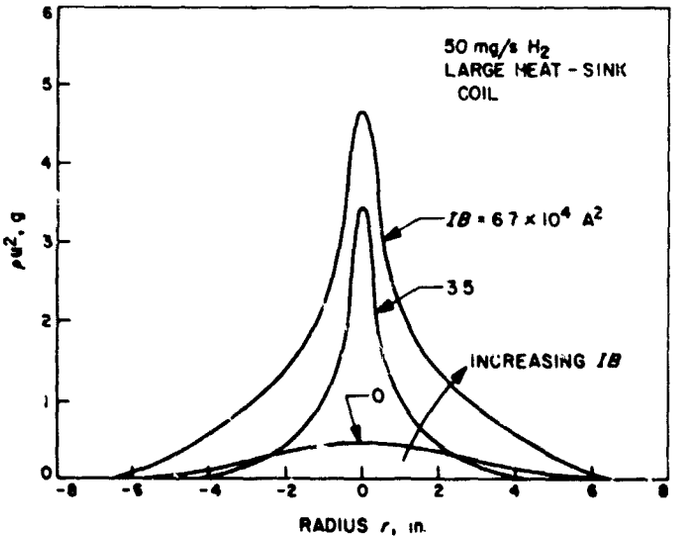

Fig. 41. Profiles obtained with the ρu^2 probe in the exhaust of the Avco-Everett MAARC operated on hydrogen (from Fig. 31 of Ref. 40)

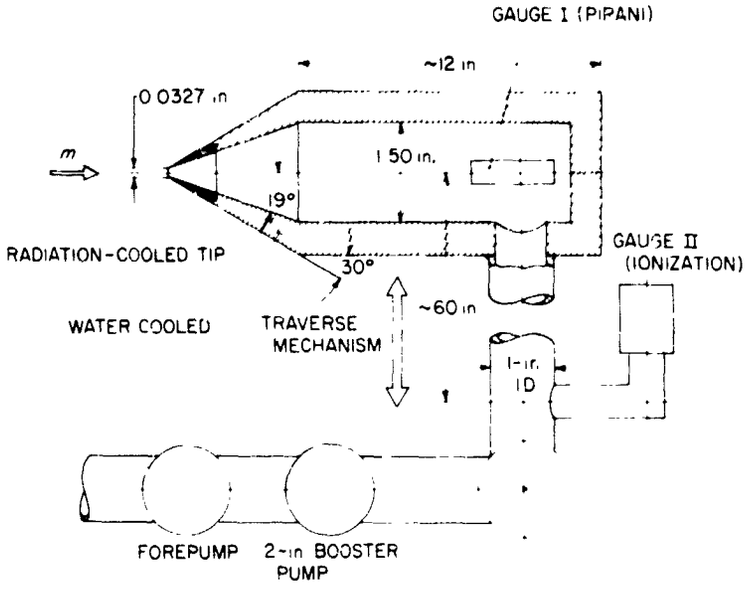

Fig. 42. Schematic diagram of the ρu probe used in the MAARC (from Fig. 9 of Ref. 40)

The results obtained with ammonia are more difficult to interpret than those that have been obtained with hydrogen, because of the generally unknown composition of the exhaust products as they recombine to form N_2, H_2, and NH_3. The possibility of relating the composition of the exhaust to the ρu probe measurements was mentioned (see Ref. 40).

A lithium-deposition probe for the determination of the local lithium mass flux in the exhaust of the alkali metal accelerator has been made by ECS (Ref. 52). The measurement is based upon the time rate of change of electrical resistance of a continuously deposited layer of lithium metal upon an insulating substrate. No data had been reported at the time of this writing.

Part IV. Theory

I. Introduction

The theory of the acceleration processes that occur in the MPD arc and the mechanism by which the energy is transferred from the electric fields to the plasma are poorly understood at the present time. A comprehensive theoretical analysis is much too difficult to accomplish because of the very complicated and nonlinear interactions of the fluidmechanic and electromagnetic forces and such rate processes as ionization and interparticle energy transfer. Unfortunately, the existing experimental data are inadequate to be used as a basis for the construction of a realistic analytical model because most of the measurements were obtained from tests designed to yield performance data. In general, the gross operating characteristics of total arc voltage, thrust, and electrode losses were obtained as a function of the controllable variables of propellant type and feed rate, arc current, and the strength of the applied magnetic field. Although an increasing emphasis on diagnostic measurements is evident, the most frequently used diagnostic tool is the visual observation of the exhaust plume. As a result, the parameters necessary for a theoretical analysis, such as particle densities and temperatures and collision frequencies and cross-sections for the various rate processes, as well as the interior electromagnetic field configurations, must be assumed or estimated.

The approach to the development of an analytical model of the acceleration process has followed one of two paths. One is to examine the trajectories of the individual particles in a postulated environment of the MPD exhaust and from this to infer the collective motion of the particles that produce the experimental observations. The other, which generally follows a macroscopic approach, is to construct a model based on one or more acceleration mechanisms that are described for idealized conditions and proposed as the dominant, although considerably modified from the idealized description, mechanism in the MPD engine. None of the proposed theories demonstrate sufficient agreement with the experimental observations to be generally accepted by the various groups actively working with the engine. This is perhaps best exemplified by the present existence of theories in which the dominant acceleration process is either electromagnetic or electrothermal, as well as the debate concerning the role (and even the existence) of Hall currents.

It should be noted that the experimental observations on which the theories are based were obtained from engines that, although similar in the general configuration, do have different geometries. It is very difficult to evaluate the significance of these differences, although the geometry apparently does affect the engine performance. This is evident, for example, from the frequently reported two-mode operation which, in at least one instance (Ref. 37), was found to depend on a factor associated with the engine geometry. Furthermore, the propellants were generally different. Thus an electrothermal model has been proposed for operation with cesium (Ref. 24) and electromagnetic models for operation with lithium (Refs. 44, 47, and 51). On the other hand, both electrothermal (Ref. 15) and electromagnetic mechanisms (Refs. 14 and 15) have been proposed as dominant processes in hydrogen accelerators. Another important complication that deters a basic understanding is the unknown degree to which interactions with the test environment modify the experimental observations. Some effort (Refs. 26 and 49) has been devoted to predicting the arc characteristics if entrainment of ambient gas into the acceleration region occurs.

Generally, the ionization process is not included in the proposed models. Rather, it is assumed that the necessary amount of ionization, usually complete first ionization, has already occurred at the point where the analysis of the acceleration process begins. However, there are analyses that are concerned primarily with the discharge region and with the arc operating characteristics. Two of these analyses (Refs. 29, 39, and 40) are described in Section II-C-2. In addition, a preliminary discussion and some initial results of an analysis, in which rate processes play a dominant role, of the discharge region is reported in Ref. 29. A more complete description of this analysis will be published in the near future (Ref. 89).

As noted above, both electromagnetic and electrothermal acceleration mechanisms have been proposed to describe the thrust production of MPD engines. The thrust in the electromagnetic mechanisms is the result of Lorentz forces that act to accelerate (or compress) the propellant, and in the electrothermal mechanism the thrust results from the expansion of thermally heated plasma. The expansion of the electrothermally heated plasma is postulated to occur through a magnetic nozzle in which electromagnetic forces act to channel the plasma flow.

One factor that determines which of the two processes is dominant is the method by which energy is transferred from the electric field to the heavy particles. In the electrothermal process, energy is gained from the field by the electrons, which carry nearly all of the current, and transferred to the heavy particles by collisions to produce a very-high-temperature plasma. Because the primary energy addition in the electromagnetic process is the result of a directed body force, the high temperatures associated with electrothermal expansion can be partially avoided.

For some high magnetic field conditions, in which the ions are postulated to carry the applied current, the ions gain kinetic energy directly from the electric field. An ion can gain a significant amount of kinetic energy directly from the electric field only if the electrons are constrained from moving along the electric field by the action of a magnetic field. In a collisionless plasma, in which there is no component of the magnetic field parallel to the electric field, the electron motion is a revolution about the magnetic field lines superimposed on a drift in the $\mathbf{E} \times \mathbf{B}$ direction (Ref. 90). The conduction current is then carried by the ions and, because of the large mass of the ions, large electric fields are required to accelerate the ions to the velocities that are necessary to conduct the applied current. The ion motion is also a rotation about the magnetic field line superimposed on a drift in the $\mathbf{E} \times \mathbf{B}$ direction; however, the ion gyro radius is much larger than that of the electron, and if the dimension across which the current is to be conducted is small compared with the ion gyro radius, the ions essentially follow the electric field lines.

For strong fields and near the collisionless limit, the electron trajectory is displaced in the direction parallel to the electric field an average of one gyro radius when an electron collides with another particle. Thus, frequent electron collisions result in an electron conduction current along the electric field, and a measure of the effectiveness of the magnetic field in preventing electron conduction current is the ratio of the electron gyro frequency to the electron collision frequency. This ratio, which is frequently expressed as $\omega\tau$, where ω is the gyro frequency and τ is the average time between collisions, is the Hall parameter. When the Hall parameter is much greater than unity, the electron motion is affected more by the magnetic field than by collisions, and the electrons drift in the $\mathbf{E} \times \mathbf{B}$ direction to produce the Hall current. If $\omega\tau$ is much less than unity, many collisions occur in the time it would take the electrons to complete one gyration and the electrons move along the potential gradient relatively unimpeded by the magnetic field.

When collisions are frequent, the energy gained by the electrons may be effectively randomized and transferred to the ions as thermal energy. Thus the magnitude of $\omega\tau$ is an indication of which process may be expected to be most important. On a macroscopic scale, the power dissipated per unit volume of plasma as thermal energy is given by J^2/σ, where σ is the plasma conductivity. The electromagnetic power per unit volume is given by $\mathbf{V}\cdot(\mathbf{J}\times\mathbf{B})$, where $\mathbf{V}$ is the plasma velocity. A comparison of these two terms would yield information as to which energy transfer process, electrothermal or electromagnetic, is dominant. The local values of the parameters needed for this calculation are not generally known.

II. Electromagnetic Acceleration Mechanisms

Electromagnetic acceleration mechanisms have been described both on a microscopic scale, in which the trajectories of the charged particles are examined, and more commonly, on a macroscopic scale, in which the collective motion of the plasma is considered. The motion of individual particles in the environment that may be expected in the discharge region of the MPD arc has been discussed by Jahn (Refs. 14 and 15). For a completely ionized hydrogen plasma, the orbits of the electrons and ions are examined as a function of the Hall parameter and of the relative magnitude of the ion gyro radius to a characteristic dimension, the interelectrode spacing of the engine. The current conduction and thrust production processes are then deduced from the expected collective motion of the particles for a postulated model of the discharge for which the particle density and temperature profiles are assumed and a simplified current density distribution is used. Because the Hall parameter and the ion gyro radius depend on the operating parameters of arc current and the externally applied magnetic field strength, the analysis can be conveniently divided into two operating conditions: operation with or without an externally applied magnetic field.

On a macroscopic scale, the orientation of the components of the $\mathbf{J}\times\mathbf{B}$ body force has been used to classify the electromagnetic acceleration process into a number of identifiable mechanisms. In principle, the total electromagnetic force exerted on the propellant can be determined by integrating this force over the volume of the discharge region. However, because of the lack of knowledge of the local plasma properties and the inability to relate, for example, the current density distribution within the plasma to the controllable arc operating parameters, the integration can be carried out for only certain special cases for which detailed descriptions of all local conditions are not required. In view of the difficulty of obtaining general analytic solutions, the various mechanisms have been examined in a qualitative manner to obtain some insight into the arc operation and, for certain idealized conditions, to predict some of the engine operating characteristics.

In a cylindrical coordinate system, the macroscopic force components are in the axial direction to produce the required thrust directly, in the radial direction to confine and compress the plasma, and in the azimuthal direction to impart rotational kinetic energy. In the discussion that follows, the unit vectors in the three directions are indicated by $\mathbf{e}_z$, $\mathbf{e}_r$, and $\mathbf{e}_\theta$, respectively. A schematic diagram of an MPD accelerator and the cylindrical coordinate system is shown in Fig. 43. The relative importance of the different components in producing the thrust depends on the relative magnitude of the applied arc current and the applied magnetic field. These components will be described (1) for arc operation with a large applied current and no external field and (2) for operation with small current and a strong applied magnetic field.

A. MPD Engine Operation With No External Magnetic Field

When the MPD engine is operated with no applied magnetic field, the electromagnetic accelerating force results from the interaction of the applied current with the self-induced magnetic field. The components of the electromagnetic force on a unit volume of plasma are $J_zB_\theta\mathbf{e}_r$ and $J_rB_\theta\mathbf{e}_z$, where J_z and J_r are the local axial and radial components of the applied arc current and B_θ is the azimuthal magnetic field induced by the applied current. The radial force component compresses the plasma and thereby increases the pressure along the centerline. Useful thrust is obtained from this component by the expansion of the propellant with the reactive force exerted on the engine as a pressure force on the cathode tip. The axial component, $J_rB_\theta\mathbf{e}_z$, produces useful thrust directly.

1. Macroscopic description. A simple analytical expression relating the thrust F_s produced by self-induced electromagnetic forces and the total arc current I has been derived for accelerator operation without an externally applied magnetic field (Refs. 21, 47, and 91). This expression, which does not depend on either the current distribution within the plasma or the local plasma

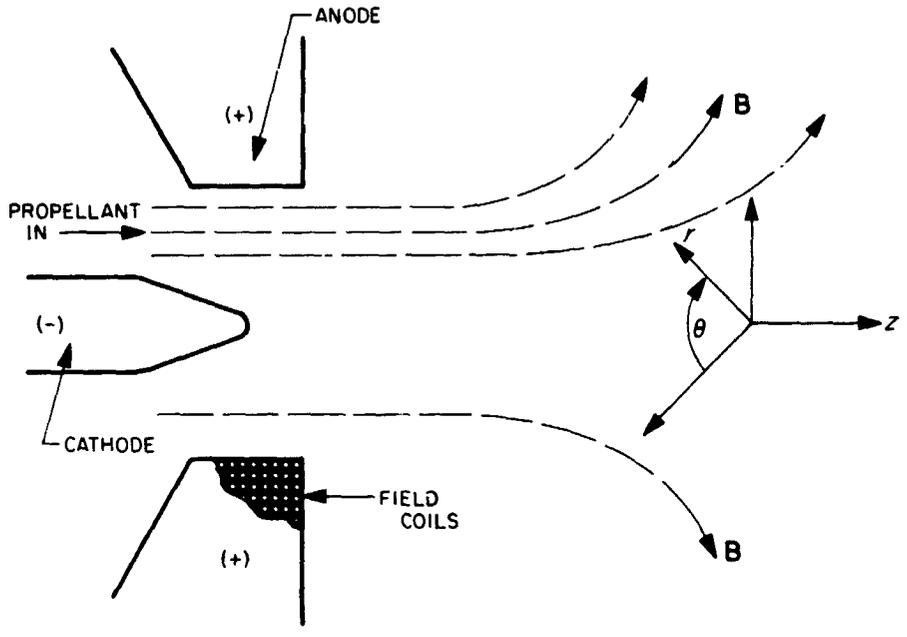

Fig. 43. Schematic of an MPD engine

properties, but does depend on the current distribution at the electrode surfaces, is given by

$$F_s = \frac{\mu_0 I^2}{4\pi}\left(0.75 + \ln\frac{r_a}{r_c}\right) \tag{23}$$

for a uniform current distribution at the cathode over an area equal to πr_c^2, and by

$$F_s = \frac{\mu_0 I^2}{4\pi}\left(0.50 + \ln\frac{r_a}{r_c}\right) \tag{24}$$

if the current enters the cathode through a thin annular ring of radius r_c. In both expressions, r_a is the anode radius at which the current enters.

This mechanism was first discussed by Maecker (Ref. 91) and has been applied to MPD thrustors by John (Ref. 18) and others (Refs. 28 and 47). It is frequently referred to as the "Maecker effect," or by the terms "pumping" and "blowing," as originally used by Maecker, to distinguish the radial and axial components, respectively.

2. *Particle viewpoint.* In the analysis presented by Jahn (Ref. 14), the electron motion throughout the discharge region is examined as a function of the local values of the Hall parameter $\omega\tau$ that are calculated for an assumed current density distribution and for assumed plasma properties. Near the cathode tip, the Hall parameter is large, and the electrons tend to spiral axially outward with little cross-field migration. Electron conduction across the induced magnetic field lines occurs at some downstream position where $\omega\tau$ is smaller and collisional effects become more important. The extent of the current protrusion into the downstream plume depends on the strength of the induced field, and, therefore, on the magnitude of the applied arc current. The trajectories of the ions also depend on the magnitude of the applied current. At low current levels, the ion gyro radius is large compared with the electrode gap, and the ions are very weakly affected by the magnetic fields. At high current levels, the ion gyro radius is reduced and there can be significant bending of the ion trajectories, particularly near the cathode tip, where the induced magnetic field is the largest. This process tends to protect the cathode from destructive ion bombardment and is suggested by Jahn as a possible reason that very high currents may be drawn from the electrodes in MPD devices. In an application discussed by Stratton (Ref. 92), it is suggested that the axial turning of the ion orbit is the mechanism by which the thrust is produced. This requires large magnetic fields, and, as a consequence, the electrons are constrained to spiral outward along the jet centerline and the current is conducted across the electrode gap by the ions. One consequence of the mechanism suggested by Stratton is that the arc voltage must be sufficient to accelerate the ions to the final exhaust velocity.

The thrust production mechanisms that are associated with the various values of $\omega\tau$ are discussed by Jahn in a qualitative manner. Jahn points out that the integrated effect of the thrust-producing interactions can be easily derived from the macroscopic approach and is given by the expression presented here as Eq. (23) or (24).

3. Experimental results. The total thrust exerted on the accelerator includes a contribution from aerodynamic forces in addition to the electromagnetic forces and is usually expressed (Ref. 18) as the sum of two terms:

$$F_T = C_F A_t P_0 + F_s \tag{25}$$

where C_F is a thrust coefficient, A_t is the anode throat cross-sectional area, and P_0 is the arc chamber pressure. The electromagnetic thrust due to self-fields, F_s, is given by Eq. (23) or Eq. (24). Direct comparison of experimental results and the predicted thrust is contingent upon separation of the electromagnetic and aerodynamic contributions to the total thrust.

Part of the thrust expressed by Eq. (23) is the result of a radial compression that produces a pressure increase on the cathode tip. An expression may be derived (Ref. 28) that relates the area across which the current enters the cathode, with the pressure at the cathode tip. This area, which is equal to πr_c^2 is referred to as the cathode spot (Ref. 18). For negligible gas flow in the radial direction, and in the absence of external fields, the radial component of the Lorentz force is balanced by a radial pressure gradient given by

$$-\frac{\partial P}{\partial r} = J_z B_\theta \tag{26}$$

For an assumed uniform distribution of J_z at the cathode tip, Eq. (26) may be integrated, after relating B_θ to J_z by Maxwell's equations, to yield

$$\Delta P = \frac{\mu_0 I^2}{4\pi^2 r_c^2} \tag{27}$$

where ΔP, the cathode overpressure, is the difference in pressure at the cathode tip and in the arc chamber. The cathode spot radius is calculated from Eq. (27) using measured values of ΔP and the arc current, and then used to compare the experimental and predicted values of the coefficient of I^2 in Eq. (23) or (24). The contribution to the thrust from this (radial) portion of the self-induced forces is independent of the distribution of J_z and is given by Eq. (28):

$$F = 2\pi \int_0^R \Delta P(r)\, r\, dr = \frac{\mu_0}{8\pi} I^2 \tag{28}$$

John (Ref. 18) and Malliaris (Ref. 28) have correlated the observed accelerator performance with Eqs. (23) and (27). The experiments were conducted in accelerators of similar geometry; however, John used a weak external field, with hydrogen as the propellant, whereas Malliaris used no external field, with nitrogen as the propellant. John assumed the thrust coefficient to be unity, but Malliaris found poor correlations between the experimental results and predicted performance if a value of unity for C_F was used. Consequently, Malliaris determined C_F experimentally from the data obtained at low current levels where the electromagnetic contributions to the total thrust were small. The empirically determined value of C_F was found to be a very weak function of current at low current and was assumed to remain constant at the higher current levels. The thrust coefficient did depend on the feed rate, and a different coefficient was used for each of the several feed rates of the experiments (see Part V, Section II-B-1).

There were some differences in the results reported by John and by Malliaris. These differences can possibly be attributed both to the presence of an external magnetic field in John's experiments and to the difference in the thrust coefficient. John found F_s to depend on the current to the 1.6 power, whereas Malliaris found that the thrust correlated with I^2 according to the predicted relation and could be expressed as $F_s = 6\ I^2$ g (force) with I expressed in kiloamperes. Malliaris found r_c to be a weak function of both $\dot{m}$ and I that varied from 4.0 to 5.7 mm. Equation (24) was evaluated using 5.0 mm for r_c and the anode throat radius, 6.2 mm, for r_a, and was found to be $F_s = 7.3\ I^2$ g (force). (For the same values of r_a and r_c, the predicted coefficient of I^2, evaluated by Eq. (23) for uniform current distribution at the cathode, is about 9.9.) At I equal to 2500 A, the electromagnetic contribution to the total thrust varied from 14% at a nitrogen feed rate of 40 mg/s to 60% at a feed rate of 10 mg/s. John reported smaller values of r_c that varied from 2.3 mm at 1000 A to 3.5 mm at 2500 A but was unable to correlate the experimental data with as simple a relation as Eq. (23). John also reported a 40% decrease in the measured thrust when the pressure tap was located at the cathode tip, whereas Malliaris found no

noticeable difference in the thrust when the engine was operated with or without the pressure tap.

The influence of an external magnetic field on the cathode tip overpressure was also investigated by Malliaris (Ref. 27). At fixed arc current and feed rate, the tip pressure was found to decrease with increasing magnetic field while the arc chamber pressure increased as shown in Fig. 39. At values of B greater than about 1500 G, the cathode overpressure was negative for all values of I and increased in magnitude as the current was increased.

Malliaris (Ref. 27) suggests that the decrease and reversal in sign of ΔP as B is increased is the result of the following mechanism: The incoming propellant is ionized upstream of the cathode tip, and, because of the geometry of the electrodes, is forced into the interelectrode region with considerable radial velocity across the axial component of the applied magnetic field. The motion of the plasma across the magnetic field lines induces an azimuthal current J_θ that is proportional to the field strength, the plasma conductivity, and the radial velocity component. The resultant Lorentz force, $\mathbf{J}_\theta \times \mathbf{B}_z$, is proportional to B^2 in the outward radial direction and is independent of the direction of the applied field. Thus, in the presence of an external magnetic field, a force exists to oppose the compression of the self-induced fields. In the experiments conducted by Malliaris, this force is sufficient to produce negative cathode overpressures at all current levels if the external field exceeds about 1500 G.

The experimental results reported by Malliaris demonstrate the difficulty of separating the various contributions to the total measured thrust. The results obtained with an applied magnetic field indicate that a simple addition of the individual contributions is evidently incorrect.

B. MPD Engine Operation With a Strong Externally Applied Magnetic Field

When the MPD engine is operated with a strong externally applied magnetic field, the arc voltage is increased and the engine is generally operated at a lower current than when no magnetic field is applied. In the limit that the magnetic field induced by the applied current is much less than the magnitude of the applied field, the acceleration is by forces that result from the interaction of the applied magnetic field and either the applied or induced current. Two thrust-producing mechanisms that result from these interactions have been identified and discussed by Hess (Ref. 54), Ellis (Ref. 93), and others (Refs. 94 and 95). Some of the high points of these discussions, plus the analysis from the particle viewpoint presented by Jahn (Ref. 14), are described in the following sections.

1. Macroscopic description. Both the applied magnetic field and the applied current have axial and radial components only. The Lorentz force associated with the applied current is in the azimuthal direction and may be expressed as the sum of the two terms $J_r B_z \mathbf{e}_\theta$ and $J_z B_r \mathbf{e}_\theta$. This force is in the same direction for both the electrons and the ions which try to move across the magnetic field lines, in opposite directions, under the influence of the local electric field. The torque exerted on the plasma as a result of this force can be evaluated (Refs. 16 and 42) because the integral involving the Lorentz force is independent of the current density distribution within the plasma as well as the local plasma properties and is given by

$$\text{Torque} = \int_v \mathbf{r} \times (\mathbf{J} \times \mathbf{B}) dv \qquad (29)$$

where r is the radius of the volume element dv on which the electromagnetic force acts. The integral depends on the current distribution at the electrode surfaces, but has a minimum value given by (Ref. 16)

$$\text{Torque}|_{min} = \frac{I \phi_{ca}}{2} \qquad (30)$$

where I is the arc current and ϕ_{ca} is the magnetic flux contained in the minimum annular area between the cathode and anode. This minimum value is obtained for the particular current distribution at the electrode surfaces in which the current enters the cathode through a thin annular ring of a radius equal to that of the cathode and leaves the anode at the anode throat. Any other current distribution, such as a uniform distribution over the cathode tip, would result in a greater quantity of flux being cut by the current and, consequently, in a greater torque.

For a nonviscous plasma, the torque can be equated to the rate of change of angular momentum of the propellant and to the reactive torque on the engine itself. The magnitude of the rotational kinetic energy of the propellant depends on the current distribution within the plasma and has been calculated for assumed distributions (Refs. 16 and 50).

To produce useful thrust, the kinetic energy of rotation must be recovered as directed kinetic energy in the axial direction. It is suggested (Ref. 50) that this occurs in the expansion through a magnetic nozzle in which the tangential velocity must decrease as the radius of the rotation increases to conserve angular momentum and that the decrease in tangential velocity must be accompanied by an increase in the velocity in the axial direction to conserve kinetic energy. The process of converting rotational kinetic energy to directed kinetic energy in a magnetic nozzle has been discussed by, for example, Rosciszewski (Ref. 96) and Treat (Ref. 15).

From a more detailed examination of this mechanism, a minimum arc voltage has been predicted (Ref. 57) for certain limiting operating conditions as a result of the "trapping" of the electrons, by the magnetic field, into circular orbits about the jet centerline. Because of their low mass, the electrons are accelerated more easily than are the ions, and the resulting azimuthal flow of electrons, relative to the ions, forms current loops that close on themselves and constitute the induced Hall current J_θ. In the limit of few collisions, i.e., large $\omega\tau$, there is little cross-field migration of the electrons, and large electric fields are required to conduct the applied arc current. Appreciable current conduction by the ions is then possible. If the ions carry all the arc current, the electrical energy is transferred directly to the ions from the electric field. In terms of the observable arc characteristics, the consequences of current conduction by the ions are, first, that the total arc voltage must be sufficient to accelerate the ions to the velocity necessary to produce the observed thrust, and, second, that the propellant feed rate and the arc current are coupled. This coupling occurs because the feed rate must be sufficient for the ionized propellant to carry the applied current.

This mechanism has also been discussed for conditions at which both the electrons and the ions conduct the applied current (Ref. 47). From the macroscopic point of view, the identity of the current carriers is of no consequence when the effects of the $\mathbf{J} \times \mathbf{B}$ body force are evaluated. However, it is of interest to examine the mechanism by which the energy gained by the electrons is transferred to the ions in the form of kinetic energy. In a linear device the electrons cannot "outrun" the ions in the flow direction because a charge separation which would result will produce local fields to pull the ions along. Cann (Ref. 50) has suggested that the mechanism by which the energy is transferred to the ions is the electron–ion drag that accompanies the flow of Hall currents. Thus, electron–ion collisions result partly in dissipation (heating) and partly in the transfer of azimuthal momentum. If a significant portion of the current is conducted by electrons, the voltage requirement to achieve a given acceleration, which is imposed when only ions conduct the applied current, is relaxed. Furthermore, the applied current and the propellant feed rate are uncoupled.

A second mechanism that has been proposed for MPD engine operation with a strong applied magnetic field is Hall acceleration. For this mechanism, the induced Hall currents discussed above interact with the applied magnetic field to produce force components $J_\theta B_r \mathbf{e}_z$ and $J_\theta B_z \mathbf{e}_r$, which yield directed thrust and containment, respectively. An accelerator in which this mechanism is dominant is called a Hall current accelerator, and a number of accelerators (Refs. 32, 42, and 57) have been designed to maximize the containment and acceleration effects of the Hall currents. Like the spinning mechanism discussed above, Hall acceleration also requires that the arc voltage be sufficient to accelerate the ions to their exhaust velocity, and the ions are the principal current carriers.

Although a rigorous calculation of the distribution of Hall currents has proved to be a very difficult task, some qualitative observations (Refs. 14, 50, and 62) on the magnitude of the induced Hall current have been made. The maximum azimuthal velocity that the electrons can attain is the drift velocity, which is equal to the local value of the ratio E/B. Because the ions drift in the same direction, the ion motion tends to decrease the Hall current. If the ion velocity also reached the maximum value, which is the same for both the ions and the electrons, Hall currents would cease to exist.

2. *Particle viewpoint.* Jahn's analysis (Ref. 14) of MPD arc operation with an external B field is, like his analysis of arc operation with no applied field, for a fully ionized hydrogen plasma with an assumed particle density and temperature profiles. The magnetic fields induced by the arc current are assumed to be small relative to the applied fields, and the local values of the Hall parameter and the ion gyro radius are calculated for a specified magnetic field pattern.

When a strong external field is applied, the Hall parameter is large near the anode as well as near the cathode tip, and the region of large $\omega\tau$ exists further

downstream than when only self-induced magnetic fields are present. As a consequence, the current loops extend a greater distance downstream before collisions become effective and the electron conduction current can cross the magnetic lines. Because the applied field has only radial and axial components, the direction of the electron drift is azimuthal, and, for a sufficiently strong field, the ion gyro radius near the electrodes is much less than the electrode gap. The ion motion is also an azimuthal drift in the same direction as that of the electrons. For a completely ionized hydrogen plasma, Jahn (Ref. 14) concludes that both the ions and the electrons can approach the limiting E/B velocity and therefore the Hall currents are negligible.

From these considerations the macroscopic description of the electron current is two rotating coaxial shells of spiraling electrons with the electron current that emanates from the cathode region flowing down the centerline cylinder, crossing the magnetic field line at some downstream position by collisional processes, and returning to the anode in the outer shell, again in a region of high $\omega\tau$. Ions also conduct current across the field lines, but for the particular conditions considered, Jahn concludes that the ion conduction would occur at approximately the same downstream position as the electron cross-field conduction, and, consequently, would not appreciably affect the distance that the current extended into the downstream region. Since the ions carry the mass of the system, the total effect is swirling motion of the gas as a whole.

In the absence of both self-field effects and any substantial Hall currents, there is no mechanism in Jahn's analysis that imparts streamwise momentum to the plasma. Thus, the analysis leaves unanswered the question of how useful thrust is obtained. To account for the observed thrust, Jahn suggests that the concentric, swirling cylinders of plasma act as extensions to the material electrodes and may provide a better environment for electrothermal or self-induced magnetic acceleration and, further, that the magnetic nozzle improves the exhaust profile and the electrothermal recovery efficiency.

The limitations of the analysis, as noted by Jahn, are that gross assumptions of the plasma properties, current distributions, and field configurations were necessary for the simplified model which was applicable only for a completely ionized plasma. Jahn suggests that before more complicated calculations are made, such as that which would result from including neutral particles and considering the magnetic field gradients, a more realistic model, such as might be deduced from more complete diagnostic measurements, should be available.

For exhaust plume conditions very similar to those postulated by Jahn, Rosciszewski (Ref. 96) reasoned that azimuthal currents result from the fact that ions, having a much larger gyroradius, fall into the region closer to the axis. Therefore they have a larger angular velocity than the electrons, and a net current in the azimuthal direction results.

3. Simplified analytical models and comparison with experimental results. A simple formula relating the thrust of the MPD engine to the controllable operating parameters when a magnetic field is applied, comparable to the formula obtained when only self-induced fields are present (Eq. 23), has not been derived. While the expression for the minimum torque exerted on the plasma, Eq. (30), is of general validity, the method and the efficiency of the conversion of the tangential velocities into axial velocity is still speculative. The effectiveness of Hall acceleration depends critically on the magnitude and distribution of the Hall currents. The lack of a convincing analytical description of the Hall currents is made obvious by the speculation of the very existence of Hall currents in anything but negligible amounts. The general applicability of the limiting conditions, discussed earlier, of ion current conduction and the subsequent voltage requirements is evidently not supported by the experimental observations.

Detailed calculations on analytical models are few and, when attempted, are greatly simplified by the numerous assumptions necessary to make the problem tractable. Three such models for the MPD engine have been examined by the group at EOS (Refs. 44, 47, and 51). Some detailed calculations on an electromagnetic model that describes primarily the ionization process and its influence on the operating characteristics have also been made by the group at Avco-Everett (Refs. 39 and 40). Before these models are discussed, some of the experimental observations pertinent to the properties of the models are listed.

a. Experimental observations. Most of the available experimental data on the MPD thrustor were obtained from tests designed to yield performance data, namely the specific impulse and overall efficiency. However, an increasing emphasis on diagnostic measurements,

which are discussed in Part III, Section VII-C, has produced some valuable information. In spite of the many differences in the performance of the various engines, using the same or different propellants, there are a number of characteristics that, to some degree, appear to be fairly common. These similarities, as well as some exceptions and reservations, are listed below.

(1) The overall efficiency increases as the specific impulse increases.

(2) The measured thrust increases with increasing arc current.

(3) The arc voltage increases with the applied magnetic field.

(4) The thrust depends on the magnitude of the applied magnetic field at low fields but is independent at some higher values. Optimum field strengths, above which the performance is degraded, have also been reported (Refs. 40 and 65).

(5) The thrust cannot be correlated with the arc voltage. In particular, velocities greater than that which would result from accelerating the ions through the available voltage drop have been inferred from the thrust measurements.

(6) Feed rates that are insufficient for singly ionized propellant to conduct all the applied current have been observed.

(7) The arc voltage (and the rate at which the voltage increases with increasing magnetic field) depends on the type of propellant.

(8) There are wide differences, ranging from no dependence (Ref. 21) to very marked dependence (Ref. 40), in the reported influence of the propellant feed rate on the thrustor performance.

(9) The general appearance of the exhaust jet is a bright central core surrounded by a luminous annular region. The boundaries of the luminous regions are closely aligned with the field lines of the externally applied magnetic field.

(10) Axial current loops extend into the downstream region of the plume. The experimental evidence of the magnitude and the extent of the penetration are conflicting (Refs. 25 and 46).

(11) Most attempts to measure the Hall current have yielded negative results. An exception (Refs. 56, 57, and 61) is the measurement of Hall currents, near the anode, in the exhaust of argon-fed engines.

(12) Evidence of swirling of the exhaust plume has been reported.

(13) The modification of many of the observations above by extraneous interactions with the test environment is suspected.

b. Analytical models. The first of the three models proposed by EOS (Ref. 44) that are discussed in this report emphasizes pure Hall acceleration as the major thrust-producing mechanism. From the visual appearance of the exhaust plume of the hydrogen-fueled engine, shown in Fig. 4, plus some diagnostic measurements indicating that current loops extend into the plume, Cann concluded that the acceleration occurs in the downstream region of the discharge, outside the engine itself. The main features of this model are given below and are sketched in Fig. 44.

One primary objective of the calculations was to obtain expressions for the local values of the Hall currents and the radial magnetic fields. Although a full set of equations was written to describe the process, an approximate solution was obtained for one special case only. The assumptions and conditions used in the model were the following:

(1) Ionization of the propellant occurs very near the electrodes by inelastic electron–neutral collisions.

(2) Current loops extend into the downstream exhaust and follow two distinct regions that coalesce at some downstream location. These regions consist of a central cylindrical luminous core, called the cathode jet, and, surrounding the cathode jet, a luminous annular region called the anode jet.

(3) The current carriers in the cathode jet are electrons. The current carriers in the anode jet are predominantly ions. The anode jet is assumed to be a cylindrical sheet with a uniform axial current.

(4) Electrons that attempt to cross the field lines are trapped and flow as azimuthal Hall currents; consequently, most of the current is conducted across the field lines by ions.

(5) The interaction of the Hall currents and the applied field produce most of the measured thrust. This interaction occurs predominantly in the anode jet.

(6) Most of the propellant flows downstream via the anode jet.

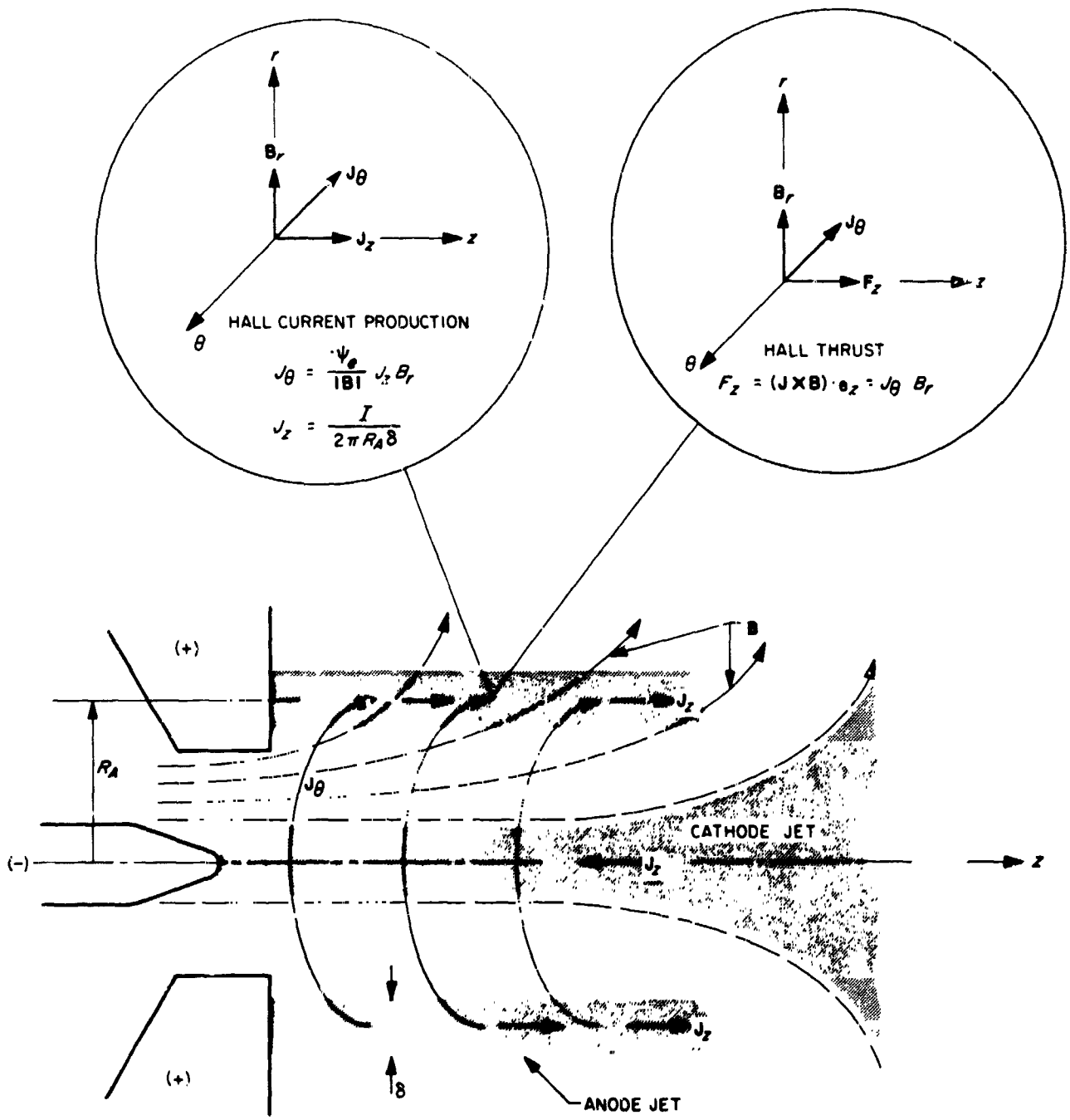

Fig. 44. A model for Hall acceleration in an MPD engine. The ions carry the current across the magnetic field lines in the anode jet and receive axial momentum directly from the electric fields

The θ complement of Ohm's law (Ref. 42) (assuming axial symmetry, $V = 0$, $B_\theta = 0$, and $\psi_e\psi_I << 1$) is used to relate the Hall current in the anode jet to the applied current and the magnetic field:

$$J_\theta = -\frac{\psi_e}{|B|}(J_z B_r - J_r B_z) \tag{31}$$

where ψ_e is the Hall coefficient. (The Hall coefficient is also expressed as $\omega\tau$; see Part V, Section I.)

Additional simplification was afforded by the assumption that J_r is zero, an assumption justified by the authors on the basis of the visual appearance of the exhaust plume. Equation (31) then becomes

$$J_\theta = -\left(\frac{\psi_e}{|B|} J_z\right) B_r \tag{32}$$

where, since $J_r = 0$, J_z is given by

$$J_z = \frac{I}{2\pi R_A \delta} \tag{33}$$

where I = total arc current

R_A = anode jet radius

δ = anode jet width

An approximate solution was obtained for a completely diamagnetic plasma. For this limiting case, the plasma conductivity is assumed to be infinite. The Hall current is confined to the outer surface of the plasma contained in the anode jet and is of sufficient magnitude to induce magnetic fields that completely cancel the applied field in the interior region. The solution was found to be

$$\text{Thrust} = K(\pi R_A^2)\left(\frac{B_z^2}{2\mu_0}\right) \tag{34}$$

where K varies between 0.681 and 0.863 depending on the assumed distribution of the Hall currents, and B_z is the magnitude of the applied field in the absence of Hall currents. This expression is believed to be an upper limit on the thrust obtainable by Hall acceleration.

Attempts were made to relax the assumption of infinite conductivity and the assumption that J_r is zero in order to obtain more realistic expression for the dependence of the Hall current on the applied magnetic field. Relations were obtained only for certain limiting conditions that could not easily be related to the operation of the device. However, the expressions that were found indicated the possibility of optimum values of the applied magnetic field.

The experimental observations were not in agreement with the predictions of the simplified model on two major points. The first was that, at some operating conditions, the measured voltages were not sufficient to accelerate singly ionized ions to the velocities inferred from the thrust measurements. Similar observations had been made at other laboratories, and the calculated velocities were called "anomalous" or "excess" (Ref. 57) in deference to the assumed Hall acceleration mechanism. At EOS (Ref. 49) "anomalous" velocities were observed with lithium at values of specific impulse above 2000 s. A related phenomenon, also "anomalous" for pure Hall acceleration, was the observation that the metered feed rates were insufficient for singly ionized propellant to conduct all the applied current. Provided all interactions with the test environment can be ruled out, both of these conditions indicate that at least part of the current is carried by the electrons and, further, that some of the energy gained by the electrons from the electromagnetic fields is transferred to the ions in a form that is eventually recovered as directed kinetic energy.

The second point of disagreement concerned the dependence of the thrust on the magnetic field. Although the B^2 dependence, predicted by the model for infinite conductivity, is believed to express only a maximum limiting thrust, most qualitative considerations for Hall acceleration suggest at least a first-order dependence of the field on the thrust. The experimental measurements indicate that there is an optimum magnetic field for a number of propellants.

Embodied in the second model proposed by Cann (Refs. 47 and 50) is a mechanism that purports to account for the "anomalous" velocities. Two of the assumptions made for this model that differ from those of the previous model are those given below, and the main features of the model are sketched in Fig. 45.

(1) The applied magnetic field is purely axial in the region of the discharge. Fringing of the field occurs downstream of the point where the anode jet and the cathode jet merge.

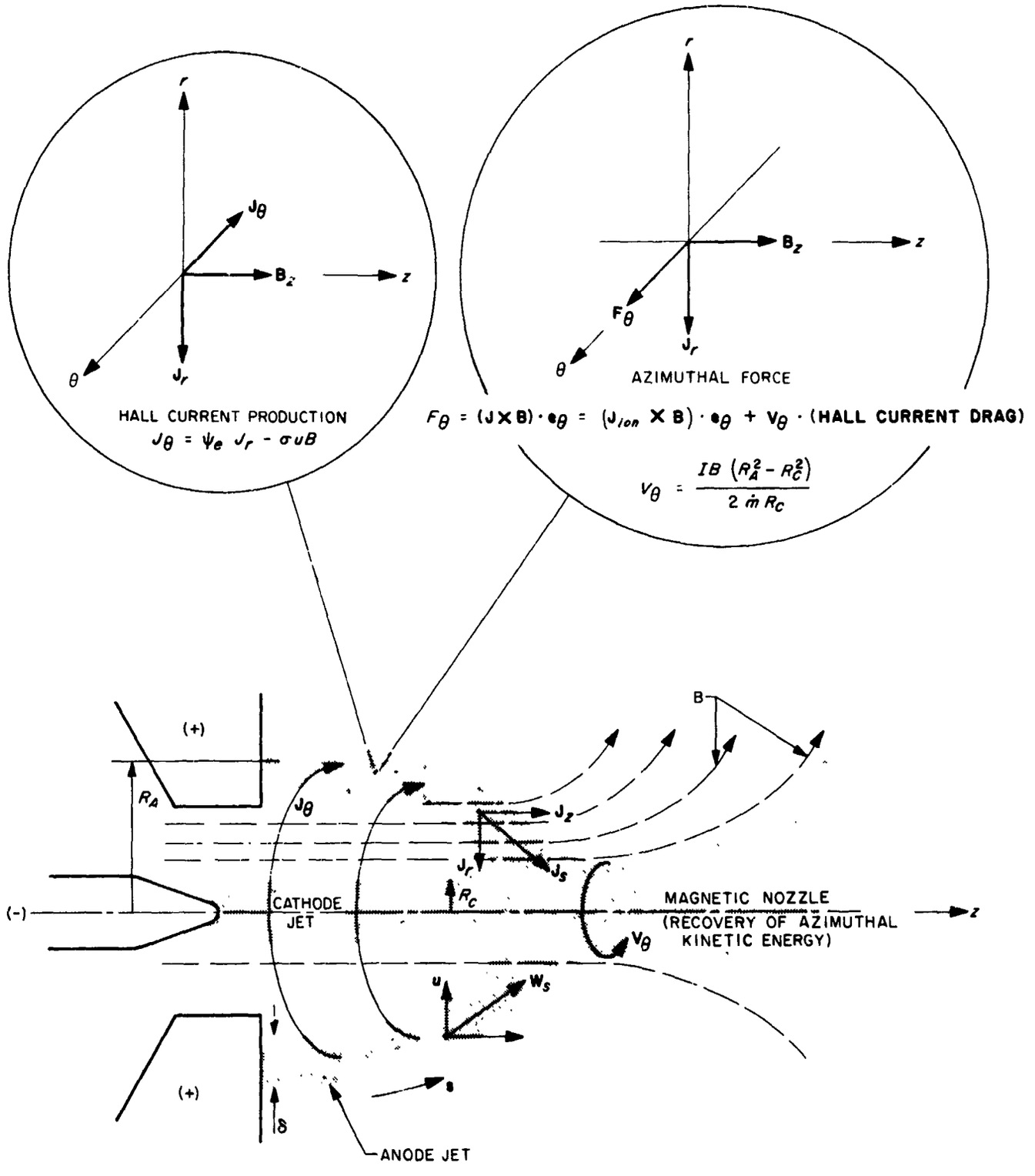

Fig. 45. An analytical model of the magnetic swirl mechanism. Electrons carry part of the current across the magnetic field lines in the anode jet and aid in "spinning up" the ions by collisions. The rotational kinetic energy is recovered in the magnetic nozzle

(2) The anode jet diameter decreases, instead of remaining constant as in the previous model, with distance downstream.

(3) The electrons are not assumed to be "trapped" by the magnetic fields and may therefore conduct current in the anode sheath.

(4) Acceleration by the interaction of the Hall currents and the applied field is not assumed to produce most of the thrust.

One important consequence of the first assumption is that although Hall currents may exist, there is no Hall acceleration, because the radial component of the applied field, B_r, is assumed to be zero. In the previous model, B_r, and not B_z, was important in determining J_θ (see Eqs. 31 and 32). In the revised analysis, J_r is necessarily finite as a consequence of the assumption that the anode jet diameter decreases in the downstream direction, and B_r is zero as a consequence of the first assumption above. Thus, J_θ results from the interaction of J_r and B_z.

The electromagnetic forces on the plasma in this model, in addition to the self-field effects, which are assumed to be small, are in the radial direction, given by $J_\theta B_z \mathbf{e}_r$, and in the azimuthal direction, given by $J_r B_z \mathbf{e}$. Thus, the electromagnetic force imparts rotational kinetic energy to the ions instead of axial kinetic energy as postulated in the previous model. In contrast to the views expressed by others (Refs. 14 and 21) that the Hall currents are near zero for a fully ionized plasma in the MPD engine, Cann believes that the ions cannot reach as high an azimuthal velocity as do the electrons and so Hall currents will always flow and are necessary to balance the centrifugal force on the rotating ions. For $B_\theta = 0$, and assumed zero net radial force on the anode sheath, Cann (Ref. 47) obtained the following expression from the radial momentum equation:

$$\Delta P = \int J_\theta B_z dr \tag{35}$$

where ΔP is the pressure difference across the anode sheath and J_θ is given by

$$J_\theta = \psi_e J_r - \sigma u B \tag{36}$$

where σ is the plasma electrical conductivity and u is the radial component of the plasma velocity. From Fig. 45, it may be seen that both J_r and u are related to the streamwise quantities of current density and mass velocity, J_s and w_s, respectively, along the anode jet, by geometric relations.

Application of the azimuthal momentum equation yields the total torque exerted on the plasma as given by Eq. (29). The torque is then equated to the rate at which angular momentum is imparted to the propellant, and the azimuthal velocity V_θ of the fluid leaving the discharge region through a thin annular region of radius R_c is determined as

$$V_\theta = \frac{BI\,(R_A^2 - R_c^2)}{2\,\dot{m}\,R_c} \tag{37}$$

where $\dot{m}$ is the propellant feed rate.

The arc voltage is determined, in part, by the fraction of the total current that is carried by the electrons. If all the current is carried by the ions, sufficient voltage is required for electrostatic acceleration of the ions to the final velocity. On the other hand, if part of the current is carried by the electrons, some of the energy gained by the electrons is transferred to the ions and the arc voltage may therefore be smaller. In this way the anomalous velocities may be explained.

Cann proposes that the mechanism by which energy is transferred from the electrons to the ions is by the electron–ion drag resulting from the flow of electrons that constitutes the Hall current. The calculations are made with the aid of several assumptions of plasma properties and the assumption that the currents will adjust to minimize dissipation and, further, that the discharge will operate at a minimum voltage. In this model, the energy gained by the electrons in the electric field is partly randomized and the rest is transferred, by collision, to the ions as rotational kinetic energy. By this process the electrons are strongly heated, and by the time they reach the anode they have sufficient energy to ionize the propellant easily. Much of the electron energy is lost to the anode as anode heating.

Some results of the calculations are the following:

(1) As a result of the requirement that the dissipation in the anode jet (energy lost to electron heating) be a minimum, the product of the thickness and the conductivity of the anode jet adjusts so that J_θ is equal to J_s, the current density along the anode jet.

(2) The electrons carry from 70 to 90% of the applied current.

(3) The thrust depends linearly on the arc current and is nearly independent of the magnetic field strength.

In the most recent model (Ref. 51), which is roughly illustrated in Fig. 46, the anode jet (or anode sheath) is assumed to be of very low density and the cathode jet of relatively high density, in which collisional effects dominate. The analysis was initially made for another device (the X-ATRON, an EOS proprietary item) that is designed to strongly heat a plasma. The heating that occurs in the cathode jet of this device is believed to be similar to the heating mechanism of the Alkali Metal Plasma Hall Accelerator (ALPHA), which is the present designation of the EOS accelerator. The analysis of these jets is presented below.

(1) Anode Jet. Cann states that the collisionless anode sheath is theoretically possible, but it is not believed to be typical of the actual operation of Hall

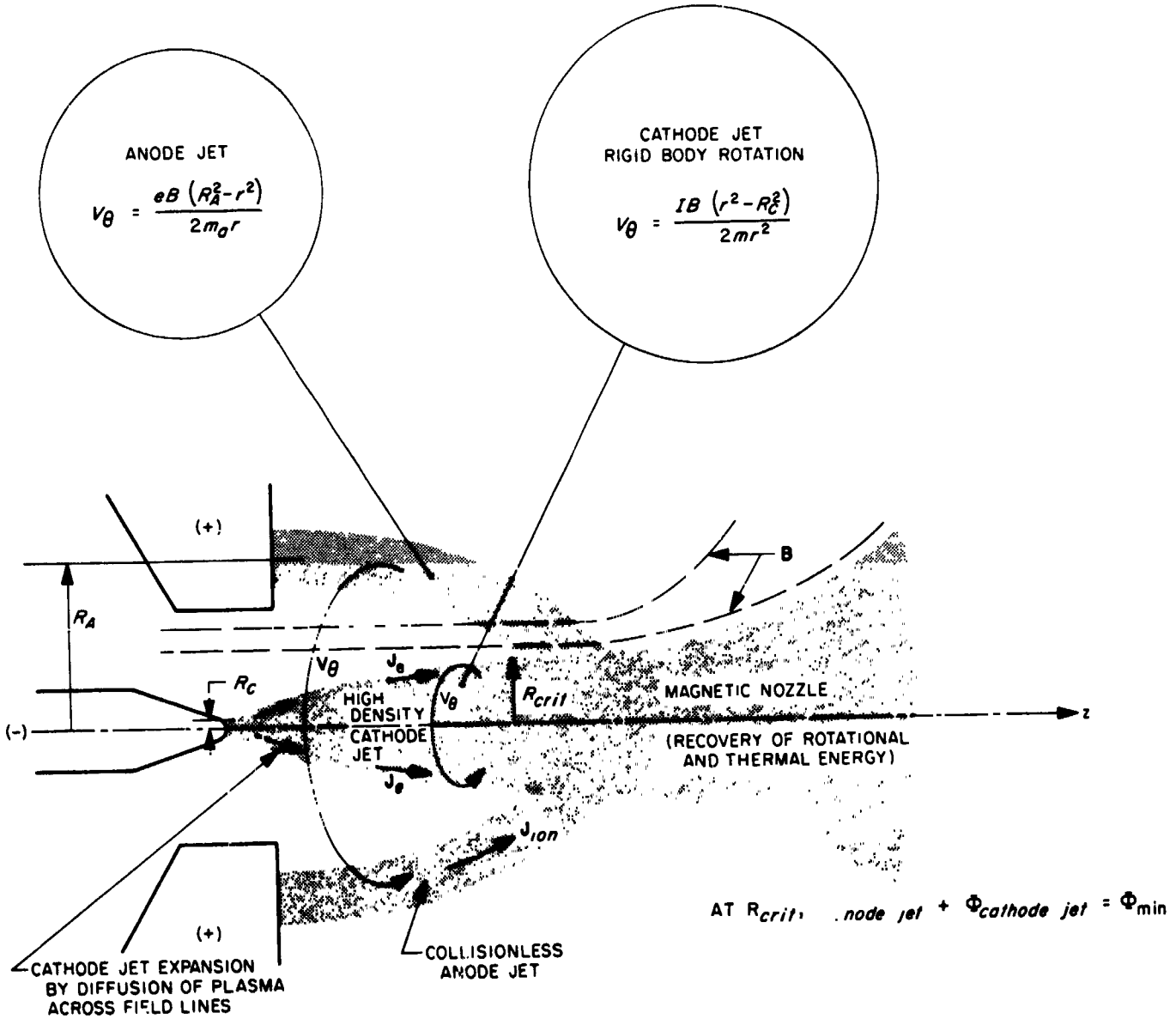

Fig. 46. One model of the mechanisms proposed for the EOS ALPHA. Ions receive rotational kinetic energy in a collisionless anode jet and receive thermal energy in the high-density cathode jet. The energy contained in both the cathode jet and the anode jet is recovered in the magnetic nozzle as directed kinetic energy

current accelerators. It is not clear from Ref. 51 whether this observation is for the laboratory tests only or whether it also includes the expected operation in space. Nonetheless, the analytical model of the acceleration process is based on a collisionless anode sheath.

The analysis of the anode sheath proceeds by first deriving an expression for the azimuthal velocity of the ions and then determining the potential required to electrostatically accelerate the ions to the final velocity. The assumptions for this model that are similar to those used for the second model discussed above are that the applied magnetic field has only axial components in the interaction region, that the propellant that flows in the anode jet is fully ionized and is introduced through the anode at the maximum radius of the anode jet, and that the rotational kinetic energy is recovered in a magnetic nozzle. The major differences are that the plasma in the anode sheath of this model is collisionless and that the ions conduct all the applied current in the anode sheath.

The azimuthal velocity of the ions in the anode sheath is found from the angular momentum integral and is given by

$$V_\theta = r\dot{\theta} = \frac{eB\,(R_A^2 - r^2)}{2\,m_a r} \tag{38}$$

Equation (38) is identical to Eq. (37), which was derived for the ion spin model, in which electrons conduct most of the current, in the limit that singly ionized particles conduct all the current. This may be seen by replacing the current I of Eq. (37) with the expression for ion current, $I = \dot{m}e/m_a$.

Because the electrical energy is transferred directly to the ions as azimuthal kinetic energy in the collisionless anode sheath, the potential drop required to produce any given velocity may be calculated directly. For the condition that both the axial and radial velocities are zero at radius r, and that the particles are introduced at rest from the anode at potential ϕ_A, the potential drop is given by

$$\phi_A - \phi = \frac{1}{2} m_a V_\theta^2 = \frac{eB\,(R_A^2 - r^2)^2}{8 m_a r^2} \tag{39}$$

The total accelerator potential drop (exclusive of the electrode sheath drops) is found by determining the value of r, where the cathode and anode jets coalesce, at which the sum of the anode and cathode potential drops is a minimum.

(2) Cathode Jet. The cathode jet of this model is composed of a high density, fully ionized plasma in which the applied current is carried by the electrons. The plasma, which is confined by the interaction of the applied magnetic field and the induced azimuthal currents, expands in the radial direction as the result of diffusion across the field lines. Because of the frequent collisions within the cathode jet, all species within the cathode jet are heated. As a result of the expansion of the plasma across the field lines, the current has a radial component that interacts with the applied field to cause the cathode jet to rotate. Both the rotational kinetic energy and the thermal energy are recovered in the magnetic nozzle.

The analysis of the cathode jet is presented for a simplified model for which it is assumed that the flow is quasi-one-dimensional with uniform current and mass flow distributions across the jet cross-section. The rotation, at a fixed axial position, is assumed to have a constant angular velocity, i.e., a rigid-body rotation. These assumptions are formulated as shown in Eqs. 40:

$$\rho w = \dot{m}/\pi R^2 \tag{40a}$$

$$j_z = I/\pi R^2 \tag{40b}$$

$$B = B_z = \text{constant} \tag{40c}$$

$$V_\theta = \omega(z) \cdot r \tag{40d}$$

where R is the radius of the cathode jet and r is any radial position within the cathode jet.

The angular velocity $\omega(z)$ is determined from the angular momentum equation given by Eq. (41):

$$\frac{d}{dz}\left[\int_0^R \rho w(rV) 2\pi r\,dr + \int_0^R j_z \left(B\frac{r^2}{2}\right) 2\pi r\,dr\right] = 0 \tag{41}$$

Equation (41) is integrated with the aid of Eqs. (40) to yield the angular velocity:

$$\omega(z) = \frac{BI\,(R^2 - R_c^2)}{2\dot{m}R^2} \tag{42}$$

where $\omega = 0$ when $R = R_c$, the radius of the cathode attachment zone.

The radial potential gradient is determined from the ion radial momentum equation, in which the radial electric field is equated to the centrifugal force on the ion plus the Lorentz force resulting from the rotation in the applied field, and, finally, the radial pressure gradient. For the analysis, the pressure gradient is assumed to be negligible. Thus,

$$\frac{\partial \phi}{\partial r} = BV + \frac{m_a V^2}{er} \tag{43}$$

and, with $V = \omega \cdot r$,

$$\phi(r) = \frac{\omega B r^2}{2} + \frac{m_a \omega^2 r^2}{2e} = \frac{B^2 I (r^2 - R_c^2)}{4\dot{m}}\left[1 + \frac{m_a I}{2em}\left(\frac{r^2 - R_c^2}{r^2}\right)\right] \tag{44}$$

The electrical conductivity is assumed to be large and, therefore, the axial potential gradient is negligible. Because of this assumption, the magnetic field lines represent equipotential surfaces, and the total potential drop is the sum of the anode and cathode jet potential drops, as given by Eqs. (39) and (44), respectively. The value of r at which the cathode jet and the anode sheath coalesce is taken as the value of r, which is called R_{crit}, that makes the total potential drop a minimum.

The amount of energy added to the cathode jet as thermal energy is found from the energy equation, Eq. (45). The axial and radial velocities are assumed to be negligible. Thus

$$\frac{d}{dz}\left[\frac{2\gamma - 1}{\gamma}\frac{kT}{m_a}\right] = (\text{energy input}) - (\text{change of azimuthal kinetic energy}) \tag{45}$$

The electrical energy input is determined with the aid of Eq. (44) and is given by

$$\text{Energy input} = -\frac{d}{dz}\int j_z \cdot \phi\, dA = \frac{d}{dz}\left[\frac{I\omega B R^2}{4} + \frac{m_a I \omega^2 R^2}{4e}\right] \tag{46}$$

The change of azimuthal kinetic energy is found with the aid of Eqs. (40) and is given by

$$\text{Change of azimuthal kinetic energy} = \frac{d}{dz}\int \rho\, w \frac{V^2}{2}\, dA = \frac{d}{dz}\left[\frac{\dot{m}\,\omega^2 R^2}{4}\right] \tag{47}$$

The result of the integration is shown in Eq. (48):

$$\frac{2\gamma}{\gamma - 1}\frac{kT}{m_a} = \left(\frac{2\gamma}{\gamma - 1}\frac{kT}{m_a}\right)_{inlet} + \left(\frac{BI}{4m}\right)^2 (R^2 - R_c^2)\left[\frac{R^2 - R_c^2}{r^2} + \left(\frac{m_a I}{e\dot{m}}\right)\left(\frac{R^2 - R_c^2}{r^2}\right)\right] \tag{48}$$

In addition to the quasi-one-dimensional analysis described above, Cann has initiated an analysis, based on the principles of the one-dimensional model, to determine the radial distributions of the variables.

c. Correlation of experimental data. The correlation of experimental data with the controllable operating variables in a way that would verify the existence of a particular electromagnetic acceleration mechanism has not been accomplished. The method used most frequently to correlate the thrust is to plot the thrust as a function of the product of the magnetic field and the arc current. This method would appear reasonable for the ion-swirling mechanism since the torque exerted on the plasma has been shown to depend on the amount

of magnetic flux that is crossed by the applied current. As demonstrated by the analytical studies reported by Cann, the dependence of the currents, including the Hall current, can be a very complicated function of the magnetic field and it is not unreasonable to suppose that, at least for some limited range, Hall acceleration would depend on the *IB* product. One example of correlating thrust with *IB* is described very briefly in the following paragraph.

In an attempt to separate the thrust that may be attributed to interactions with the applied magnetic field from the total thrust, John (Ref. 19) has assumed that the measured thrust F_T could be expressed as the sum of three terms:

$$F_T = C_F P_0 A_t + F_s + F_H \qquad (49)$$

where the first two terms on the right-hand side represent the contributions from aerodynamic forces and the self-induced fields, respectively. The third term represents the contribution associated with the applied field which was, tentatively, identified as Hall acceleration. The magnitude of the first two terms was estimated from the results obtained when no external field was applied, as described in Section II-A-3 above. The quantity F_H was then plotted versus the *IB* product, which was the assumed form of the dependence of the Hall thrust on the applied current and magnetic field. A reasonable straight-line correlation of F_H with *IB* was found with hydrogen for field strengths up to 2 kG and arc current to 1600 A. The correlation with ammonia was less satisfactory, and, in addition, the value of F_H obtained with ammonia was lower, by a factor of nearly 4, than that obtained with hydrogen at identical values of the *IB* product. John concluded that the magnetic field plays a much smaller role in the acceleration of ammonia than in the acceleration of hydrogen.

4. Another analysis. In the analyses described above, rate processes play a very minor role in the theoretical analysis of the MPD thrustor. It is generally assumed that the required rates are sufficient to produce the postulated conditions of the proposed mechanisms. A third approach, in which rate processes do play an important role, has been initiated at Avco-Everett (Ref. 29). This analysis is for thrustor operation with an applied magnetic field and with hydrogen as the propellant. Preliminary results have been published, but only a qualitative description of the analysis was available at the time of this writing. The method is described as a quasi-one-dimensional analysis that requires only the voltage characteristics as an empirical input. Changes in the area of the flow channel are considered, but radial variations are neglected. The analysis proceeds by writing the conservation equations of mass, momentum, and energy for each of four species considered (H_2, H, H^+, and e) and the appropriate Maxwell equations. Transport coefficients and reaction rates are deduced from the available experimentally determined cross sections. The applied boundary conditions are the cold incoming gas and the requirement that the flow of each species in the exhaust proceed through its sonic point in a regular manner. The preliminary results indicate that the discharge is largely confined to a region very near the electrodes and does not extend significantly into the downstream exhaust stream. The strong expansion in the supersonic region, immediately downstream of the nozzle throat, results in a rapid increase in the value of $\omega\tau$ for the electrons and quickly terminates the discharge.

The processes that occur in the supersonic region have yet to be analyzed.

C. Thrustor Operating Characteristics

1. The effects of entrainment and the minimum-energy principle. In an analysis of the MPD arc characteristics, Cann (Ref. 49) has proposed that the discharge will attempt to operate at a minimum voltage by adjustment of the mass of propellant that is accelerated. The mass flow rate accelerated, which is called the effective mass flow rate $\dot{m}_e$, is thus distinguished from the mass flow rate $\dot{m}$ that is actually fed to the engine. One key assumption made by Cann to determine the effective mass flow rate is that the mass ionized is equal to the mass accelerated.

In the discussion that follows, the analysis presented by Bennett (Ref. 26) is followed more closely than that presented by Cann. The energy balance on the discharge, written in a simplified form that nevertheless illustrates the principle involved, is given by

$$IV = P_a + \frac{\dot{m}_e}{m_a} eV_I + \frac{T^2}{2\dot{m}_e} \qquad (50)$$

where the first term, P_a, is the power loss to the anode, the second term represents the power expended in ionization, and the third term is the kinetic energy flux. If both P_a and the thrust T are independent of $\dot{m}_e$, the value of $\dot{m}_e$ at which the power to the engine, IV, is a minimum

is found from the condition $d(IV)/d\dot{m}_e = 0$ to be

$$\dot{m}_e|_{min} = T\left(\frac{\dot{m}_a}{2eV_I}\right)^{1/2} \tag{51}$$

When the value of $\dot{m}_e$ given by Eq. (51) is substituted into Eq. (50), the last two terms on the right-hand side are found to be equal:

$$\frac{\dot{m}_e}{\dot{m}_a}\, eV_I = \frac{T^2}{2\dot{m}_e} = \frac{T}{2}\left(\frac{2eV_I}{\dot{m}_a}\right)^{1/2} \tag{52}$$

Thus, at the condition of minimum power, the electrical energy transferred to the propellant is equally divided between kinetic energy and that required to ionize the propellant. The maximum thrust efficiency at this operating point is limited to 50%.

In Cann's analysis (Ref. 49), the internal energy of the electrons is included in the energy equation and the anode loss is given by a term that is a function of $\dot{m}$. Cann relates both the thrust and the anode loss to the arc current and formulates an expression for the arc voltage. The minimum voltage (and the value of $\dot{m}_e$ at minimum voltage) is found by differentiating the expression for the arc voltage, at const $\dot{m}_e$, with respect to I. Because the internal energy of the electrons is included in the energy balance, the expression for $\dot{m}_e$ at the current level that yields the minimum voltage is slightly different from Eq. (51) and is given by

$$\dot{m}_e|_{min} = T\left\{\frac{\dot{m}_a}{2eV_I\left[1 + n_0\left(\frac{\dot{m}_0}{\dot{m}}\right)^{1/2}\right]}\right\}^{1/2} \tag{53}$$

where the term $n_0\,(\dot{m}_0/\dot{m})^{1/2}$ is the ratio of the electron internal energy to the ionization energy. The expression obtained by Cann that is equivalent to Eq. (52) shows that the energy transferred to the gas is equipartitioned between (1) kinetic energy and (2) the sum of the electron internal energy and that required to ionize the propellant. In a later report (Ref. 52) the value of $\dot{m}_e$ given by Eq. (53) is called the critical mass flow rate $\dot{m}_{cr}$. This nomenclature will be followed in the subsequent discussion.

Cann postulates that the manner by which the mass flow is adjusted to the value by Eq. (53) is the following: If $\dot{m} > \dot{m}_{cr}$, the discharge bypasses the excess and continues to operate at the minimum voltage. Thus, the overall efficiency is always less than 50%, and the mass utilization of the propellant is poor when the injected feed rate exceeds the critical mass flow rate. If $\dot{m} < \dot{m}_{cr}$, the discharge will still attempt to ionize and accelerate an amount equal to $\dot{m}_{cr}$ by entraining ambient gas or by utilizing electrode material, or both, if these sources of potential propellant exist. If the possibility of entrainment does not exist, i.e., if the engine exhausts to zero pressure surroundings, and if the electrodes are not eroded, the discharge cannot operate at the minimum voltage. Then, $\dot{m} = \dot{m}_e$, and the power transferred as kinetic energy, $T^2/2\dot{m}_e$, exceeds the frozen-flow loss, $(\dot{m}_e/\dot{m}_a)eV_I$; the overall efficiency may exceed 50%.

It is clear that if Eq. (50) is applicable, and if the discharge bypasses all excess propellant, the arc voltage will remain constant as the propellant feed rate is increased to a value greater than $\dot{m}_{cr}$ (as given by Eq. 51). Furthermore, the arc voltage will remain constant as $\dot{m}$ is decreased below $\dot{m}_{cr}$ if the discharge entrains the necessary amount of gas to make $\dot{m}_e$ equal to that necessary for minimum power operation. As a consequence of the assumption that both P_a and T are independent of $\dot{m}_e$, the observed arc voltage must increase, if no ambient gas or electrode material is available, as $\dot{m}$ is decreased. It follows that a necessary condition to indicate elimination of entrainment is an increase in the arc voltage at very low feed rates. Bennett (Ref. 26) did not make any assumption concerning P_a because the energy balance was written exclusive of the electrode losses. Cann used an empirical expression relating P_a to $\dot{m}$ and, further, did not make an explicit assumption concerning the dependence of T on $\dot{m}_e$. (T was assumed to be a linear function of the current I.) Nonetheless, both authors conclude that the arc voltage will increase at low feed rates if no entrainment occurs.

From a general consideration of the energy equation, it may be concluded that either the observed thrust must decrease or the arc voltage must increase when the feed rate is reduced to very small values, at constant current, in order to conserve energy. This may be seen by inspection of Eq. (50) for an assumed condition of constant thrust-to-power ratio for arbitrarily small values of $\dot{m}_e$.

Both Cann and Bennett continue the analysis to predict some of the operating characteristics of the thrustor. Thus Cann assumes that the engine operates in a regime where thrust is independent of the magnetic field, that is, that the thrust may be expressed by $T = KI$, where I is the arc current and K is not a function of B. Consequently, in the expression derived from the energy equation, the arc voltage is independent of the magnitude of the magnetic

field. Furthermore, Cann assumes that all of the current is carried by ions instead of electrons. These assumptions do not alter the primary conclusions of the critical mass flow model, namely, that there exists a critical mass flow rate, as given by Eq. (51) (or Eq. 53) and that at this flow rate the power will be equally divided between the ionization energy and the beam kinetic energy.

From experimental observations, Bennett concludes that the arc voltage and the thrust may be expressed by the empirical relations given by Eqs. (54) and (55) respectively:

$$V = C_1 + C_2 B \tag{54}$$

$$T = C_3 IB \tag{55}$$

As a result of the analysis of the critical mass model discussed above, the minimum power, exclusive of the electrode loss, is given by

$$(IV)_{min} = T\left(\frac{2eV_i}{m_a}\right)^{1/2} \tag{56}$$

The minimum voltage may be found by combining the empirical relation for thrust, Eq. (55), and Eq. (56) with the result

$$V = C_3 B\left(\frac{2eV_i}{m_a}\right)^{1/2} \tag{57}$$

Thus, the slope of the V–B characteristic, dV/dB, is observed experimentally to be C_2 of Eq. (54) and predicted by the minimum energy principle to be

$$C_3\left(\frac{2eV_i}{m_a}\right)^{1/2}$$

where C_3 is the empirical constant relating T to the IB product, Eq. (55). A comparison of the predicted

$$C_3\left(\frac{2eV_i}{m_a}\right)^{1/2}$$

and the measured slope, dV/dB, is presented as Table II of Ref. 26, which is given here as Table 5.

Evidently, the data for which the voltage can be represented by Eq. (54) were obtained either at mass flows greater than that required for minimum power operation, Eq. (51), or for conditions at which entrainment occurred because, from the analysis presented, the voltage becomes a function of m when the mass accelerated is less than that given by Eq. (51).

Hassan (Ref. 59) suggests that it is not necessary to invoke the concept of the minimum energy principle to explain the operating characteristics of the MPD engine. Hassan's analysis also includes a "critical mass flow rate," but in an entirely different concept. A major difference in Hassan's analysis and the analyses described above is that the thrust is assumed to be a strong function of the feed rate. The feed rate at which the engine thrust is a maximum, at fixed power input, is defined as the "critical mass flow rate."

2. The influence of the ionization process on the arc voltage. On the basis of the experimental observations, Patrick and Schneiderman (Ref. 40) suggest that two basic acceleration modes are possible. One is an electrothermal process in which Hall currents flow to give body forces directed radially inward to reduce anode losses. The other mode is the interaction of the azimuthal Hall currents with the radial component of the applied field to produce thrust in the axial direction. The ion-swirling mechanism, as well as supersonic heating,

Table 5. Comparison of the observed and predicted slopes of the voltage–magnetic field characteristics[a]

Propellant	$\left(\frac{2eV_i}{m_a}\right)^{1/2}$, m/s	C_3, $\frac{\text{newtons} \cdot \dot{m}^2}{\text{A weber}}$	Predicted $(dv/dB)_{pred}$, $\frac{V \cdot \dot{m}^2}{\text{weber}}$	Measured $(dV/dB)_{meas}$, $\frac{V \cdot \dot{m}^2}{\text{weber}}$
Hydrogen	5.5×10^4	4.8×10^{-3}	260	230
Ammonia	2.6×10^4	4.7×10^{-3}	120	130
Lithium	1.24×10^4	1.9×10^{-3}	24	50

[a]Taken from Table II of Ref. 26.

followed by expansion, is also considered. The Hall acceleration mode is characterized by a higher voltage than the electrothermal acceleration mechanism.

An interesting aspect of the theory advanced by Patrick is the mechanism by which the arc voltage is fixed in the Hall acceleration mode. Patrick proposes that the ionization mechanism is by ion–atom collisions for which the ions have gained the necessary energy by acceleration through the potential drop in the region where the crossed electric and magnetic fields produce azimuthal motion, i.e., the ion-swirling mechanism described in Section II-B-1 above. After the ion is accelerated to the velocity at which the ion kinetic energy is equal to the ionization energy, which is called the critical speed U_c, an ion–atom collision will produce ionization. One assumption in the derivation, which includes combining the energy equation and the azimuthal momentum equation, is that the ions easily slip past the neutrals and therefore may attain the local E/B drift velocity. The expression $E/B = U_c$ is then integrated to give the total arc voltage as

$$V = V_a + (U_c B)\ell \tag{58}$$

where V_a is a constant that represents, in part, the voltage drop associated with the electrodes, and ℓ is a characteristic length of the order of the electrode radius. This concept of the ionization process is attributed (Ref. 40) to a suggestion made by Petschek to explain the "burning velocity"–"critical speed" relationship observed by Alfvén (Ref. 97) and others (Refs. 98 and 99) in an ionizing plasma in the presence of a strong magnetic field (homopolar devices). The ion kinetic energy equals the ionization energy at the velocity given by the relation

$$U_c = \left(\frac{2eV_i}{m_a}\right)^{1/2} \tag{59}$$

Patrick postulates that part of the current applied to the MPD engine flows in the interelectrode region where ionization occurs. The arc voltage is determined by the ion–atom collision process of ionization. The rest of the current then flows in the downstream region, where Hall acceleration can occur. Patrick concludes that to produce high exhaust velocities, a propellant with a large ionization energy is required, i.e., U_c must be large, to produce high arc voltages so that the radial electric fields in the downstream acceleration region can be as large as possible for a given magnetic field intensity.

Another feature of the model proposed by Patrick is the prominence given to the ion–neutral charge exchange mechanism by which neutral particles are accelerated. On the basis of the measured thrust, input power, and metered feed rate, Patrick has concluded that, to conserve energy, the accelerated gas can be as little as 5% ionized. The charge-exchange mechanism is postulated as the method by which the neutrals are accelerated.

The results obtained by Patrick (Ref. 40) are similar to the results obtained by Bennett (Ref. (26) and Cann (Ref. 49) from the minimum energy principle. From Eq. (51) and the relation for thrust, $T = \dot{m}U$, Bennett found the velocity of the exhaust at the minimum power condition to be

$$U = \left(\frac{2eV_i}{m_a}\right)^{1/2} \tag{60}$$

Thus, the plasma velocity at minimum power is identical with the critical velocity, Eq. (59). It may be noted that the energy equation as written in Eq. (50) cannot be applied to the mechanism proposed by Patrick because Patrick postulates that appreciable quantities of atoms may be accelerated. Bennett (Ref. 26) points out that more detailed diagnostic measurements, at conditions with no entrainment, are necessary to distinguish between the possible modes of operation.

A derivation of a linear relationship between the arc voltage and the applied magnetic field, which does not invoke the ion–atom ionization process, has been published by Hassan (Ref. 57) for a quasi-one-dimensional model of the discharge region. The analysis, which was made for a constant-area duct with a uniform axial applied magnetic field, is based on the conservation equations of the plasma species and relates the ionization fraction to the electron temperature by means of the Saha equation. Ion slip terms are considered through the use of a generalized Ohm's law. Some of the assumptions and approximations made for the model are the following:

(1) The plasma pressure, density, and axial velocity are all constant over the region of the discharge.

(2) The radial current density is given by the following expression:

$$j_r = \frac{I}{2\pi r \ell}$$

where I = total current

r = radial position

ℓ = length of the discharge in the flow direction

(3) There are no axial components of the current.

(4) The electric field is purely radial.

III. Electrothermal Acceleration Processes

A. Introduction

As discussed in Section I above, electrothermal acceleration depends on both effective randomization of the electrical energy by electron–ion collisions and effective containment of the plasma during the expansion process. The expansion is proposed to occur through the so-called magnetic nozzle formed by the applied magnetic field. The properties of a magnetic nozzle, particularly where collisions are frequent, are ill-defined at present. One measure of the effectiveness of a static magnetic field to contain a fully ionized gas is the ratio of the magnetic pressure, $B^2/(2\,\mu_0)$, to the plasma kinetic pressure P. The condition

$$\frac{B^2}{2\,\mu_0} + P = \text{constant}$$

where P is the plasma pressure, has been derived (Ref. 90) for a collisionless plasma of infinite conductivity. This condition cannot be approached in the electrothermal model of the MPD thrustor, particularly in the region where energy is effectively transferred by collisional processes. Consequently, the condition $B^2/(2\,\mu_0) > P$ is necessary but not sufficient for containment. Another assessment of the containment is to compare the rate of particle diffusion across the field lines with the estimated axial flow velocity (Ref. 16). If the axial velocity is much greater than the cross-field diffusion velocity, effective containment is indicated.

B. An Electrothermal Model for a Cesium-Fed Engine

The hypothesis that the plasma acceleration in MPD arcs is the result of thermal expansion of heated plasma has received renewed interest because of the inability of the more complicated electromagnetic mechanisms to correlate the observed engine characteristics with the controllable parameters in a satisfactory manner. John (Ref. 20) has proposed an electrothermal model to describe the operation of a cesium-fueled MPD arc jet, and Treat (Ref. 15) has suggested that the electrothermal process is also applicable to operation with hydrogen. The visual appearance of the cesium jet was the typical central, luminous core surrounded by an outer luminous core. The main features of the model proposed by John are the following:

(1) The propellant, injected through the cathode tip, is ionized almost immediately.

(2) Magnetic pressure prevents radial expansion of the cathode jet.

(3) The current is carried everywhere by electrons. In some downstream regions the electrons cross the field lines and return to the anode along a magnetic field line.

(4) The luminosity of the outer zone (anode jet) is the radiation from ambient cesium atoms that are excited by collisions with electrons returning to the anode. The anode jet is not involved in the acceleration process.

(5) The cathode jet contains all the cesium, which is heated to a very high temperature and expands thermally through the magnetic nozzle.

(6) The energy is transferred to the plasma by ohmic dissipation.

The arguments advanced to support the mechanism above are that the experimental observations are not satisfactorily explained by the electromagnetic processes, whereas the observed characteristics are compatible with an electrothermal process. These observations are the following:

(1) The cesium feed rate is much too low for singly ionized particles to carry the applied arc current. Because the necessary multiple ionization required if ions conduct all of the current (30- to 40-fold) is unlikely to occur, it is concluded that electrons, not ions, carry the current. Furthermore, because the ions are not strongly tied to the field lines, the anode current would not be expected to follow the applied field lines as other measurements (Ref. 46) have indicated. In the electrothermal model, the electrons carry the current; therefore, the feed rate and the applied arc current are not coupled.

(2) There is insufficient voltage drop in the plasma to accelerate the ions by the electric field to the indicated velocities; furthermore, the arc voltage is not a function of the specific impulse. If electrons carry the current, and many electrons flow for each ion accelerated, there is no limit on the specific impulse imposed by the arc voltage.

(3) The measured thrust is insensitive to the applied magnetic field strength. In the electrothermal model, the function of the exterior magnetic field is to establish the nozzle. After the nozzle is formed, the nozzle shape, and therefore the expansion process, should be relatively insensitive to changes in the field strength; consequently, the thrust should be independent of the magnitude of the applied field beyond a minimum value necessary to form the nozzle.

(4) The experimental observation that the arc voltage increases as the field strength is increased is compatible with the electrothermal model because the voltage required to force the electrons across the field line is expected to be a function of the field strength.

John concludes that magnetic confinement is possible by showing that the magnetic pressure greatly exceeds the expected aerodynamic pressure, and that the magnetic Reynolds number, calculated using estimated plasma properties and flow conditions, is much larger than unity. John also concludes that because of the magnetic effects of increasing the pressure, there will be numerous collisions to transfer energy to the ions. To obtain the predicted thrustor performance as a function of engine operating parameters, calculations were made on a simple model for which many assumptions and approximations were used.

C. An Electrothermal Model for Hydrogen

A number of the arguments used in the discussion above to demonstrate that electromagnetic processes were not dominant apply also to observations made on engines operating with propellants other than cesium. One of the major points of the discussion above is that electrons, and not ions, carry the current because of the low number density flux of the ions. Although this argument is not generally applicable to operation with hydrogen, Treat (Ref. 15) has proposed that electrothermal process as the dominant acceleration process for operation with hydrogen.

Following the derivation given by Allis (Ref. 100), Treat has used the Langevin equation, which describes the motion of a single electron, to obtain an expression for the average electron energy, relative to the average proton energy, in a fully dissociated and ionized hydrogen plasma. This expression, derived for a uniform and constant electric and magnetic field, is given by Eq. (61):

$$\frac{u_e - u_p}{u_e} = \frac{m_p}{4\, m_e}\left(\frac{e\lambda}{u_e}\right)^2 \left(\frac{E_\perp^2}{1 + \omega\tau^2} + E_\parallel^2\right) \qquad (61)$$

where u_e and u_p are the average proton and electron energy, respectively, m_p and m_e are the proton and electron masses, and λ is the mean free path for momentum transfer. The radial electric field is taken to be $E_\perp$, the field component perpendicular to the magnetic field, and the axial electric field as the parallel component.

In the region away from the jet centerline, where the axial field is expected to be small, for the assumed conditions of

$$E_\perp = 20 \text{ V/cm}$$

$$n_e = 10^{14} \text{ cm}^{-3}$$

$$T_e = 2 \times 10^4 \text{ °K}$$

$$B = 2500 \text{ G}$$

Treat obtained

$$\lambda = 0.07 \text{ cm}$$

$$\frac{eE_\perp \lambda}{u_e} = 0.7$$

$$\omega\tau = 43$$

and, from Eq. (61),

$$\frac{u_e - u_p}{u_e} = 0.2$$

In the region near the centerline, where the dominant term in Eq. (61) may be $E_\parallel$ instead of $E_\perp$, Treat concludes that the electrons are likely to continue to gain energy from the field faster than they lose energy by collision until they leave the region of strong parallel electric field. Therefore the condition $du_e/dt = 0$, which was used to obtain Eq. (61), does not apply in this region, and thermalization must occur downstream of the discharge. For $T_e = 2 \times 10^4$ and $n_e = 10^{14}$ cm^{-3}, Treat obtained

$$t_{eq} = 7.7 \times 10^{-7} \text{ s}$$

where t_{eq} is the characteristic time of equipartition of energy as used by Spitzer (Ref. 90). Then, assuming the mass velocity equal to the sonic velocity in a proton gas, Treat calculates a characteristic length for equipartition of 0.9 cm. Thus, equipartition of the proton and electron energy should be obtained in several equipartition times,

or within about 3 cm downstream of the region of energy addition even if a very strong nonequilibrium state is produced by the discharge. For an electron temperature of 10^5 °K and a density of 10^{14} cm^{-3}, the calculated equipartition length is 10 cm, and a nozzle of about 30 cm would be required to complete the transfer of excess electron energy to the ions. Lower electron densities would also require greater length for equipartition.

The effectiveness of the containment of the plasma by the magnetic field is estimated by calculating the diffusion velocity perpendicular to the magnetic field using the classical diffusion equation given by Spitzer (Ref. 90):

$$v_D = \frac{\eta_\perp (\text{grad } p)_\perp}{B^2} \tag{62}$$

where $\eta_\perp$ is the plasma resistivity perpendicular to the magnetic field and p is the pressure. For assumed conditions the same as those used to calculate the equipartition times, and with $r = 1$ cm, Treat calculated

$$v_D/v_z = 2 \times 10^{-3}$$

where v_z is the axial velocity taken equal to the speed of sound at 2×10^4 °K.

The analysis described above is primarily concerned with the equipartition of the energy added to the plasma by ohmic dissipation, and it is for this reason that the mechanism is described as electrothermal. Because of the relatively small value for the diffusion velocity across the magnetic field lines, as well as the visual observation that the exhaust plume appears to follow the field lines, Treat concludes that the containment of the plasma by the magnetic field is effective, and, in his subsequent analysis of the acceleration process, the assumption of zero plasma flow across the magnetic field lines is made. In addition to adding thermal energy, the discharge produces a torque on the plasma as it crosses the field lines. For an electrically neutral, nonviscous flow, Treat shows that the torque, as given by Eq. (29), is equal to the rate at which angular momentum is imparted to the flow. In the region downstream of the discharge, the rate of change of angular momentum is zero; consequently, in the expansion that occurs in the divergent magnetic nozzle, not only the thermal energy but also the rotational kinetic energy is converted into useful thrust. Under-expansion, or plasma leakage across the field lines, would result in the loss of both thermal and rotational energy.

IV. Summary

The electromagnetic acceleration mechanism of an MPD thrustor operated at large applied currents and no externally applied magnetic field has been described in terms of the Lorentz force that results from the interaction of the applied arc current and its self-induced magnetic field. Simple analytic expressions for the electromagnetic thrust, which has been shown to be independent of the current density distribution within the plasma but to depend on the current distribution at the electrode surfaces, have been derived as shown by Eq. (23) for a uniform current distribution at the cathode.

Additional insight into the details of the acceleration mechanism, such as voltage characteristics, current paths, and the identity of the current carriers, is afforded by the microscopic description of the motion of individual particles. The results of experiments designed to verify this mechanism have been published. In the experimental studies, the measured thrust includes a contribution from aerodynamic forces that is treated through the use of a thrust coefficient which is either assumed to be unity or determined empirically.

The mode of operation with an applied field is more attractive for space missions for two important reasons: first, prolonged operation appears to be feasible only if a field is applied to prevent localized, high-current-density regions on the anode surface; second, high performance at the low power levels available from solar power panels is possible only if external magnetic fields are applied. Most of the developmental effort has been devoted to thrustor operation with an applied field.

No simple expression has been derived to relate the thrustor operating variables to the thrust when a strong external field is used. A variety of simplified models that emphasize either electromagnetic or electrothermal processes have been proposed to describe the acceleration process. In the electromagnetic models, the predominant energy addition process is through $\mathbf{J} \times \mathbf{B}$ forces that impart directed velocity to the propellant without heating it to high temperatures. The proposed models are similar in some respects and very different in others. Some features common to most of the models are the following:

(1) Directed thrust is obtained by expansion of the propellant in a magnetic nozzle. The only thrust-producing mechanism that does not make use of the external field in this manner is the pure Hall acceleration.

(2) At sufficiently high magnetic fields, current loops extend into the exhaust plume. The current flows in the downstream region via two distinct zones and crosses the magnetic field lines in some downstream region. The current carriers in one zone, the central core, are electrons.

(3) The energy used to dissociate and ionize the propellant is not recovered.

It is generally accepted that all the known mechanisms contribute, to some degree, to the thrust of a real engine. Each model, then, emphasizes one or more mechanisms as being dominant. Some major differences, and the consequences thereof, are the following:

(1) Identity of the current carriers. In the electrothermal process the current is carried everywhere almost exclusively by the electrons. In the pure Hall acceleration and two versions of the ion-swirl mechanism, the current is carried across the field lines by the ions. When the current is carried by ions, the arc current is coupled to the mass feed rate, and a minimum thrustor voltage, which is that required to achieve a given velocity of the propellant, by electrostatic acceleration, is fixed. In one description of the ion-swirl mechanism, part of the rotational kinetic energy imparted by the tangential Lorentz force to the ions results from electrons that conduct current across the magnetic field. Because a number of electrons can flow as current for each ion accelerated, the feed rate and the applied current are uncoupled, and the voltage requirement is relaxed.

(2) Distribution of mass in the exhaust and the spatial location of the thrust production. In the electrothermal process, nearly all the mass is located in the cathode jet, and the thrust is produced in the cathode jet and the subsequent expansion in the magnetic nozzle. In most of the electromagnetic models, the plasma is located in and accelerated in the anode jet, and the cathode jet serves primarily as a current path only. The method of propellant injection is sometimes predicated on the process that is believed to be dominant.

(3) The role and identification of the ionization processes. No particular difference in the ionization process is inherent in the acceleration mechanisms, since, in general, the models begin with the assumption that sufficient ionization has occurred prior to the position where the acceleration process starts. The ionization processes are discussed, however, and generally stated to be the result of electron–atom collisions. The exception is the suggestion of Patrick (Ref. 40) that ion–atom collisions are responsible for the ionization of the propellant. This mechanism is proposed to explain the observed dependence of arc voltage on applied field strength and is postulated to be the mechanism by which the voltage drop in the acceleration region is determined.

The ionization and other rate processes do play an important role in the analysis reported by AVSSD (Ref. 29). Only very preliminary results have been reported at this time.

Part V. Discussion

The primary problems associated with the development of the MPD thrustor pertain to the question of the reliability and validity of the experimental data. Of these problems, the existence of entrainment and other interactions with the test environment has received the most attention. Entrainment not only invalidates the performance data but also alters many of the observable parameters that play an important part in a theoretical description of the thrustor. Other factors affecting both the performance data and the theory are the large amount of data scatter that is frequently present and the variation in the operating voltage, both fast "jumps" from one voltage to another and slow variations over a significant range of voltages. Part of the difficulty of attacking and solving these problems directly may be attributed to the difficulty of making the diagnostic measurements needed to verify the performance and identify the acceleration mechanisms.

I. Reliability of Performance Data

A. Entrainment

A number of laboratories (for example, Refs. 17 and 21) have reported operation of the MPD thrustor at zero feed rate and have identified the plasma accelerated at this condition as either electrode material or the ambient gas contained in the vacuum chamber in which the tests were conducted. The likelihood of entrainment in devices that could not be operated at zero feed rate has also been reported (Ref. 40). One of the conclusions reached in this survey is that much of the reported data is questionable because of the probability of entrainment at the operating conditions of the experiments, and, further, that the probability of entrainment is increased as the strength of the applied magnetic field is increased and as the power-to-feed ratio is increased. These conclusions are particularly applicable to those results obtained with gaseous propellants at "average" vacuum tank pressures of from 0.1 to 0.5 torr. It is also concluded that the available evidence concerning entrainment at very low pressures is inconclusive but is nevertheless not inconsistent with the argument that the effects of entrainment are reduced at the lowest pressures presently attainable in the laboratory. Finally, it is concluded that a greater degree of redundancy in the measurement of the critical parameters than presently exists is necessary to establish confidence in the validity of the performance data. The reasons for these conclusions are discussed below.

1. Gaseous propellants. The most comprehensive data concerning entrainment that have been reported for a single engine configuration are the data that were obtained with the hydrogen-fed X-2C engine designed by AVSSD. These data include the very convincing evidence of the existence of entrainment (Part III, Section VI-A), the results obtained at very low tank pressure at the Space Environmental Facility of the NASA Lewis Research Center (Part III, Sections VI-A and VI-B), and finally, the current density measurements reported by Powers (Ref. 25). The results obtained at AVSSD that demonstrated the existence of entrainment can be briefly summarized as follows:

(1) The X-2C engine can operate on entrained gases only.

(2) No detectable changes occur in the usually observed parameters as the feed rate is decreased to zero if the tank pressure is held constant.

(3) Reverse flow of the tank gases into the engine occurs by way of the peripheral region of the exhaust jet at very low feed rates.

From these results, it may be concluded that, at the particular test conditions and for the engine configuration involved, neither the onset nor the amount of entrainment can be detected from the parameters that are usually observed when the thrustor performance is determined. Indisputable evidence of invalid results is obtained only when the calculated overall efficiency exceeds the thermal efficiency.

In order to determine whether the observations of flow reversal into the engine, which are described in Part III, Section VI-A, can be associated with the onset of a significant amount of entrainment, it is necessary to know where the acceleration takes place. For those experimental conditions at which no back-flow occurs, and provided that all the acceleration occurs within the interelectrode region, the correct value of $\dot{m}$ to use in the calculation of the performance parameters would be the metered value of the feed rate. For these conditions, the mixing of tank gases with the exhaust downstream of the acceleration region would not affect the thrust measurement. On the other hand, if the acceleration region extends into the downstream plume, any gas that is entrained into this region and is accelerated as though it were part of the feed would produce misleading results.

The experimental results reported by Powers (Part III, Section VII-C) show that about 20% of the total arc current extended to an axial position greater than about 7 in. downstream of the anode exit plane when the X-2C engine was operated on hydrogen at conditions similar to those at which the data discussed above were obtained. The current density measurements demonstrated that although an increase in the magnetic field strength caused a compression of the area through which the current flowed and, consequently, an increased current density along the centerline, there was no change in the total axial current. No measurements were reported for hydrogen at zero applied field; however, in a nitrogen plume, for which the results were otherwise similar to those obtained with hydrogen, Powers found that the current flowing downstream of the engine decreased to zero at zero applied field. Assuming that the current flowing in the upstream region and the current flowing in the plume are equally effective in accelerating the propellant, Powers concluded that only about 10% of the thrust is added in the plume. It is noted here that if all the ionization occurs in the upstream region, the power utilized to ionize and dissociate the hydrogen would not be available to accelerate the plasma.

Powers' results were obtained at a fixed hydrogen feed rate of 10 mg/s and at a single arc current of 1000 A and therefore do not relate to current penetration as a function of the magnitude of the applied current, the feed rate, or the total tank pressure. Results obtained with nitrogen, however, indicate that the magnitude of the current is a very weak function of the feed rate.

The theoretical analysis presented by Jahn (Ref. 14), described in Part IV, Section II-B, predicts that, for a completely ionized hydrogen plasma, the current penetration will increase as the field is increased and that radial electron flow between the anode and the cathode jet will occur, by collisional processes, at some downstream region where the Hall parameter becomes smaller. No division of the current between the upstream and the plume region, as observed by Powers, can be inferred from Jahn's analysis; however, as mentioned previously, the analysis is not concerned with the ionization process. Powers' experimental observation that the total current at the 7-in. position is independent of the magnitude (from 750 to 1500 G) of the applied field would seem to be inconsistent with the theoretical prediction of increased current penetration; however, the extent of the current loops was not measured at positions

further downstream, and therefore the extent of the current penetration cannot be determined from the reported measurements. One result of increasing the field was a pinching of the discharge. This effect was more pronounced on the cathode jet than the anode jet as evidenced by the small decrease, about 15%, of the anode jet's outer diameter as the field was doubled from 750 to 1500 G. Thus, although the experimental evidence indicates no increase in the total current flowing downstream as the field is increased, the possibility of increased current penetration, and therefore increased anode jet area, still exists.

Another theoretical analysis that concerns itself with the question of current loops extending into the plasma was presented by Treat (Ref. 16). For certain experimental conditions, Treat shows that if energy is to be conserved, part of the current must flow in the downstream region. This conclusion, which is independent of the degree of ionization, follows from an examination of the torque exerted on the plasma as a result of the arc current crossing the applied field lines. In the interelectrode region, the kinetic energy transfer is a minimum when the torque is applied at the maximum possible radius, that is, the anode radius. It follows that for certain values of the power transferred to the gas, arc current, and applied field strength, the production of rotational kinetic energy flux greater than the electrical power transferred to the propellant would result unless part of the current extends into the exhaust and crosses the field lines at a larger radius.

An argument given (Ref. 21) for operating MPD thrustors at very low pressure is that less of the tank gas will cross a unit area of the exhaust by random thermal motion because of the decrease in the gas density. A smaller amount of total entrainment will thus occur at low pressure provided the area of the acceleration region does not increase as fast as the density decreases as the pressure is lowered. The AVSSD X-2C engine was operated at the low-pressure Space Environmental Facility at the NASA Lewis Research Center to test this hypothesis and to simulate space conditions more closely. The results obtained at Lewis (Ref. 65) with hydrogen propellant, which are included in Fig. 22 and indicate a large increase in the overall efficiency at low pressures, may be summarized as follows:

(1) The measured thrust increases significantly as the pressure is lowered from 6×10^{-2} to 10^{-4} torr.

(2) The arc voltage increases only a few percent as the pressure is lowered.

(3) The thermal efficiency is not affected by the change in pressure.

(4) The size of the exhaust plume, as determined by the visual observation of the luminous portion, increases greatly as the pressure is lowered.

(5) The data obtained at pressures greater than 6×10^{-2} torr are in excellent agreement with the data reported by AVSSD.

Provided the measurements are correct, the results indicate that the increased thrust at low pressures (which, incidentally, had not been anticipated, Ref. 65) may be attributed to more efficient conversion of the electrical energy (that is, energy transferred to the hydrogen) to useful thrust. Because of the increased size of the luminous plume, Jones (Ref. 65) concluded that the possibility of entrainment as a significant factor could not be ruled out. As mentioned above, the size of the acceleration region, rather than that of the luminous region, is the important factor. No directly applicable experimental results concerning the relation of the size of the acceleration region to the tank pressure are available. On the other hand, Jahn's theoretical analysis suggests a greater current penetration at low pressures because of the increased value of $\omega\tau$ to be expected at low pressures. However, as noted previously, this analysis was limited to a completely ionized plasma, and, as discussed below, the condition of complete ionization of the hydrogen was not realized at the operating conditions used for the experiments at Lewis.

Another useful comparison of the results published by Lewis is the maximum degree of ionization, at the two pressure levels, that is consistent with the reported performance data. The values obtained from performance data are average values. It is expected that the values so obtained are lower than the ionization in the core and greater than that in the outer edges of the exhaust jet. From an energy balance, and using the efficiency values reported, the maximum fraction of the gas ionized can be found by assuming that all the energy transferred to the gas resides in either directed kinetic energy or ionization and dissociation energy. This is equivalent to equating the thrust efficiency defined by Eq. (6) to an expression for a frozen-flow efficiency that is similar to that given by Eq. (7), but includes the degree of ionization α. For hydrogen, and assuming that the degree of dissociation is identical with the degree of ionization,

this expression is

$$\eta_T = \eta'_F = \frac{\frac{1}{2}\dot{m}v^2}{\frac{1}{2}\dot{m}v^2 + \alpha\,(\text{ion.} + \text{dissoc.})}$$

$$= \frac{1}{1 + \alpha\,\dfrac{31.72}{I_s^2 \times 10^{-6}}} \qquad (63)$$

If the calculated value of α is large, little error is introduced by equating both the dissociation and ionization degree to a single value even though the hydrogen may be completely dissociated. On the other hand, if α is small and the gas is completely dissociated, considerable error is introduced by the use of Eq. (63). In the limit that the hydrogen is only partly ionized but completely dissociated, the expression equivalent to Eq. (63) becomes

$$\eta_T = \eta''_F = \frac{\frac{1}{2}\dot{m}v^2}{\frac{1}{2}\dot{m}v^2 + \text{dissoc.} + \alpha\,(\text{ion.})}$$

$$= \frac{1}{1 + \dfrac{4.52 + 27.2\,\alpha}{I_s^2 \times 10^{-6}}} \qquad (64)$$

The results of calculations using both Eqs. (63) and (64) are shown in Table 6 for 1000 s and the maximum values of the specific impulse obtained at NASA Lewis for the two pressure levels. Also included in Table 6 are values of the ionization fraction calculated according to Eqs. (63) and (64) from the data published by AVSSD at 6000 and 8000 s (Ref. 21). The values of the overall efficiency and thermal efficiency, listed in the table for the AVSSD results, are not from individual runs but are believed to be reasonably accurate average results based on the reported data. Note that the thermal efficiency was found to increase at the higher values of the specific impulse.

It may be seen from Table 6 that the degree of ionization calculated from Eq. (63) for the low-pressure data increases from about 8% at 1000 s to about 40% at 3500 s. However, if complete dissociation is assumed and Eq. (64) is used, the calculated value of α is negative at 1000 s. This demonstrates that there is insufficient energy transferred to the hydrogen to completely dissociate it, even at zero ionization, and yet produce the reported thrust. The reported spectroscopic observation (Refs. 65 and 66) of very weak molecular spectra and abundant atomic spectra supports the use of Eq. (64) instead of Eq. (63) for the low-power conditions. It is possible that a more realistic approach would be to assume equilibrium. This has not been done here, other than to note that the overall efficiency at 1000 s, assuming a thermal efficiency of 60%, would be greater than 50% for frozen-flow expansion of hydrogen.

One may intuitively expect the degree of ionization to increase as the power is increased. The results shown in Table 6 for the data obtained at NASA Lewis with the AVSSD X-2C engine indicate that this trend is followed

Table 6. Ionization fraction in the exhaust of the hydrogen-fed X-2C MPD engine

Pressure P torr	Specific impulse I_s, s	Efficiency				Calculated degree of ionization	
		η_0	η_{th}	η_T[a]	η_F (Eq. 7)	Ion. = dissoc. = α (Eq. 63)	Dissoc. = 100% (Eq. 64)
NASA Lewis							
1×10^{-4}	1000	0.17	0.60	0.288	0.03	0.078	−0.075
	3500	0.30	0.60	0.50	0.28	0.40	0.28
6×10^{-3}	1000	0.064	0.60	0.11	0.03	0.26	0.13
	2900	0.21	0.60	0.35	0.21	0.49	0.41
AVSSD							
≈ 0.5	6000	0.46	0.68	0.68	0.53	0.55	0.48
	8000	0.62	0.72	0.86	0.67	0.33	0.22

[a] $\eta_T = \eta_0/\eta_{th}$

at the low pressure and is also followed at the higher pressure but at a slower rate. When the data reported by AVSSD for the same engine are considered, it is seen that the trend of increasing degree of ionization with increasing specific impulse is followed up to 6000 s, but that the degree of ionization decreases to a relatively low value at 8000 s. The reasoning that the degree of ionization will increase as the power is increased, as well as the lack of any concrete experimental evidence of the existence of a low degree of ionization at the high-power conditions, supports the argument that the reported performance at the highest values of specific impulse is of questionable validity and unreasonably high.

The experiments reported by Powers (Ref. 25), for which hydrogen was used as the propellant, were all conducted at an arc current of 1000 A; therefore, direct experimental evidence of current penetration as a function of the magnitude of the applied arc current is not available. However, because current penetration appears to be associated with the effects of the applied magnetic field, and since the effects of the field should be greater at the higher degree of ionization, it is not unreasonable to suppose that the acceleration region in the downstream plume becomes larger as the power, at a constant value of the applied field, is increased. This line of reasoning also supports the argument that the data indicating high values of the specific impulse are the most likely to be affected by entrainment.

Although extrapolation of experimental results is admittedly of questionable merit, the conclusion one would draw from an extrapolation of the low-pressure data reported by NASA Lewis is that the curve for overall efficiency versus specific impulse would cross the data reported by AVSSD at about 4000 s (see Fig. 22). A continuation of this extrapolation to higher values of specific impulse suggests that the calculated efficiency of the thrustor operated at very low pressures would be lower than the values reported by AVSSD at values of specific impulse greater than 4000 s. If the data reported by AVSSD are indeed affected by entrainment, lower performance would be expected if entrainment were significantly reduced at low pressure. The data obtained at NASA Lewis are inconclusive in demonstrating the absence of entrainment at low pressure, partly because of the limited range of the operating variables that were investigated; nevertheless, the data are not inconsistent with the contention that entrainment is reduced at very low tank pressures.

The highest overall efficiency to be obtained with a hydrogen-fed MPD thrustor (the MAARC) is that reported by Patrick (Ref. 40) for a feed rate of 0.05 g/s. Because of the difference in the geometry of the electrodes, much of the data obtained with the X-2C engine, discussed above, does not necessarily apply to the MAARC. Some significant differences in the operating characteristics of the two engines have been reported. For example, unlike the X-2C engine, the MAARC could not be operated at zero feed rate; furthermore, the performance of the MAARC was found to be very sensitive to the feed rate, as may be seen from Fig. 22. The calculated efficiency dropped sharply as the feed rate was reduced from 50 mg/s to 10 mg/s.

To determine the effect of entrainment, Patrick placed a quartz shroud 6¼ in. in diameter and 6 in. long at the exit plane of the MAARC. The shroud reduced the measured thrust, at a feed rate of 50 mg/s, by almost 40%. Using a $\dot{B}_\theta$ probe, which is described in Part III, Sec. VII-C, Patrick found that less than 5% of the applied current flowed downstream of the shroud. The magnitude of the current at a fixed axial position did not change when the shroud was removed. Because of the small amount of current flowing in the plume at the exit plane of the shroud, Patrick concluded that very little entrainment (of the type that could influence thrust measurements) could occur with the shroud in place.

The amount of thrust reduction as a result of viscous drag on the quartz shroud was not measured and, therefore, no meaningful assessment of the amount of thrust reduction attributable to reduced entrainment can be made. However, if it is assumed that the reduction of the thrust is the result of reduced entrainment only, the data may be adjusted on the basis of this assumption. By way of illustration, replacing T by $0.6T$ in both the expression for the specific impulse, Eq. (2), and the expression for the overall efficiency, Eq. (3), changes the point representing the highest performance reported by Avco-Everett from approximately 85% at 4600 s to 31% at 2700 s. This adjusted point lies very close to the line drawn through the data for 50 mg/s. In fact, the adjustment of any point on the curve, by the procedure above, for any fractional decrease in the thrust, will move that point on a path that very nearly coincides with the curve drawn through the data, towards the origin of the plot.

All the thrust measurements at the Avco-Everett facility were made with a thrust plate, or ρu^2 probe (see Part III, Section VII-C). The MAARC was also operated on a thrust stand at the AVSSD facility. Some results of the tests made on the test stand are shown in Fig. 47, taken

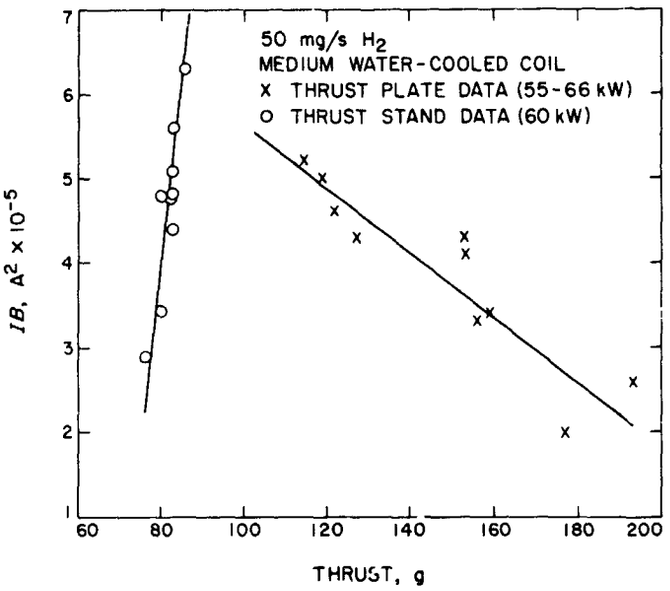

Fig. 47. Comparison of thrusts obtained from thrust stand measurements and thrust density profiles (from Fig. 34 of Ref. 40)

from Ref. 40, in which the thrust measured with the thrust plate is compared with that measured with the thrust stand; the comparison is a plot of thrust versus the *IB* product. Identical values of the *IB* product correspond to identical values of both *I* and *B*. As pointed out by Patrick (Ref. 40), a large discrepancy exists not only in the magnitude but also in the functional dependence of the measured thrust on the *IB* product. For the data shown in Fig. 47, the performance obtained from the thrust stand was about 1630 ±100 s (which is very close to the data reported for the X-2C engine operated with large external fields) whereas the performance obtained from thrust profile measurements with the ρu^2 probe appears to be well correlated with the *IB* product and varies from about 2300 s at 20% to about 3900 s at 60%. The operating conditions for the tests on the thrust stand were identical with those for which the thrust target was used. Although the reasons for the discrepancies are not known, it is suggested (Ref. 40) that the difference is most likely due to difference in the mode of operation of the MAARC at the two facilities.

The ionization levels present in the exhaust of the MAARC, which were calculated for a number of typical experimental points and listed in Table 3 of Ref. 39, varied from 5.6% at the higher thrust efficiencies to 75% at low thrust efficiency. Neither the ionization fraction nor the thermal efficiency for the highest performance point reported, which was better than 85% overall efficiency at 4600 s, was given in Ref. 40. However, using the maximum value of the thermal efficiency that was mentioned (Ref. 39), which was 87%, and using the performance figures given above (85% at 4600 s), an estimate of the degree of ionization of less than 2% may be obtained from Eq. (63). Since the dissociation energy represents about 14% of the total frozen-flow loss, most of the hydrogen must have been accelerated as molecular hydrogen to produce the measured thrust if the thermal efficiency was not greater than 87%.

The solid line drawn through the Avco-Everett data (Fig. 22) connects points that were obtained at constant power and constant feed rate (Ref. 40). The thermal efficiency was observed (Ref. 40) to be relatively constant at a fixed power level as the magnetic field was increased to produce the higher values of the thrust; therefore, the increased overall efficiency was the result of increased thrust efficiency. With the total power in the propellant constant, the increased thrust must be accompanied by a decrease in the maximum possible average ionization fraction as calculated by Eq. (47). Thus, if no experimental anomalies were present, the reported data indicate that increasing the magnetic field resulted in decreasing the ionization level to almost vanishingly small amounts. This trend clearly conflicts with the spectroscopic observations of the exhaust of the AVSSD X-2C engine operated on ammonia. Connolly (Ref. 66) found the intensity of the N^+ spectra to increase and the intensity of the N spectra to decrease with increasing applied magnetic field (see Part III, Section VII-C-5).

With the exception that the X-2C engine was not operated at zero feed rate with ammonia, the series of experiments that were conducted with hydrogen were also conducted with ammonia. Axial current loops in the plume were observed at AVSSD and the overall efficiency obtained by NASA Lewis generally increased as the tank pressure was lowered. The thermal efficiency was insensitive to the pressure level. Two exceptions to the similarities with hydrogen were that (1) the performance obtained with a field of 1400 G did not increase at low pressure, and (2) an unpredictable tendency of the discharge to undergo a transition between two distinct voltage modes was observed for all operating conditions at the Lewis facility.

The data published in Ref. 65 included some for which the calculated overall efficiency exceeded the thermal efficiency. However, all the ammonia data were too large because of an error in the measured feed rate and were corrected in Ref. 68. The feed rate initially reported was

too small by a factor of 2.04 (Ref. 68); consequently, the values of both the specific impulse and the overall efficiencies were too large by the same factor. This correction removed the discrepancy of the overall efficiency exceeding the thermal efficiency. It is apparent that the consequences of the error in the measured feed rate are very similar to an error that would result from entrainment into the acceleration region. The fact that the error could escape immediate detection, as witnessed by the initial publication of the data, illustrates again the difficulty of detecting entrainment from the usually observed parameters.

By the method discussed above for hydrogen, some additional information may be obtained from a calculation of the maximum possible degree of ionization that is consistent with the performance data. The equation equivalent to Eq. (64), for which 100% dissociation is assumed, is given by Eq. (65), for which the values of the dissociation and ionization energies given in Table 1 for ammonia are used.

$$\eta_T = \eta_F'' = \frac{1}{1 + \dfrac{(1.48 + 6.52\alpha)}{I_s^2 \times 10^{-6}}} \qquad (65)$$

The calculated values of the ionization fraction for some representative conditions, at both the high and low voltage modes, and at the two pressure ranges, are included in Table 7. The test conditions at high pressure that existed for the experiments at AVSSD could not be exactly duplicated at the Lewis facility because the maximum current available at Lewis was about 500 A, whereas the minimum value used at Avco was 600 A. The two voltage modes were not observed at AVSSD; consequently, the placement of the data in the column of Table 7 labeled "low-voltage mode" is arbitrary.

From the table it may be seen that, if the performance data are correct, the ammonia could not have been fully dissociated at the low tank pressure when the accelerator was operated at 1000 s in the low-voltage mode. Spectroscopic observations of the atomic spectra of both nitrogen and hydrogen support the calculation of low ionization at nearly all conditions.

The values of the thrust efficiency listed in Table 7 for the AVSSD data were taken from a smooth curve drawn through a plot of thrust efficiency versus the specific impulse. The thrust efficiencies were calculated according to Eq. (6) from the published data (Ref. 19). For a feed rate of 58 mg/s these data indicate that the ionization fraction decreases as the specific impulse increases. The single entry at a feed rate of 29 mg/s represents the data obtained at the maximum reported specific impulse. The calculated ionization fraction was generally higher at the lower feed rate; however, there were considerable differences in the values of the thrust efficiency at the different arc current levels. For example, at 2400 s, the

Table 7. Ionization fraction in the exhaust of the ammonia-fed X-2C MPD engine

Test condition	I_s, s	High-voltage mode				Low-voltage mode			
		η_0	η_{IA}	η_T[a]	α (Eq. 65)	η_0	η_{IA}	η_T[a]	α
NASA Lewis[b]									
$P = 2 \times 10^{-4}$ to 5×10^{-5} torr	1000	0.16	0.48	0.33	0.08	0.18	0.42	0.43	−0.024
	2000	0.34	0.48	0.71	0.26	0.34	0.42	0.81	0.056
P = 0.40 to 0.017 torr	1000	0.10	0.48	0.21	0.36	0.10	0.42	0.24	0.26
	2800	0.28	0.48	0.58	0.63	0.28	0.42	0.67	0.38
AVSSD[c]									
m = 58 mg/s	1000							0.20	0.38
	2000							0.50	0.39
	3000							0.78	0.16
	3200							0.84	0.07
m = 29 mg/s	3800[d]							0.78	0.40

[a] $\eta_T = \eta_0 \eta_{IA}$

[b] The values used are the corrected data published in Ref. 68.

[c] Average values of η_T taken from a smooth curve drawn through a plot of η_T, calculated from published data, versus I_s.

[d] Highest reported I_s obtained at 1400 A.

thrust efficiency for the 29-mg/s data varied from less than 0.45 at 1400 A to more than 0.65 at 800 A. This variation in the thrust efficiency corresponds to a variation in the value of α of from 0.86 to 0.25. The values of the thrust efficiency calculated from the data obtained at a feed rate of 58 mg/s were less sensitive to the arc current level.

The data obtained with the X-2C engine at NASA Lewis indicate a very definite correlation of the degree of ionization of ammonia with the strength of the applied magnetic field for fixed values of specific impulse. These data (Fig. 4, Ref. 66) show that the highest thrust efficiency was obtained with the lowest field strength, in agreement with the qualitative spectroscopic observations (see Part III, Section VII-C-5). Precisely the opposite trend is indicated by the data reported by AVSSD. This is shown in Fig. 48, where the data for the ammonia feed rate of 29 mg/s (Table A-5 of Ref. 19) is displayed as a plot of thrust efficiency versus the specific impulse, with the strength of the applied magnetic field as a parameter. From this figure it is seen that, unlike the low-pressure data obtained at NASA Lewis, the highest thrust efficiency, corresponding to the lowest ionization

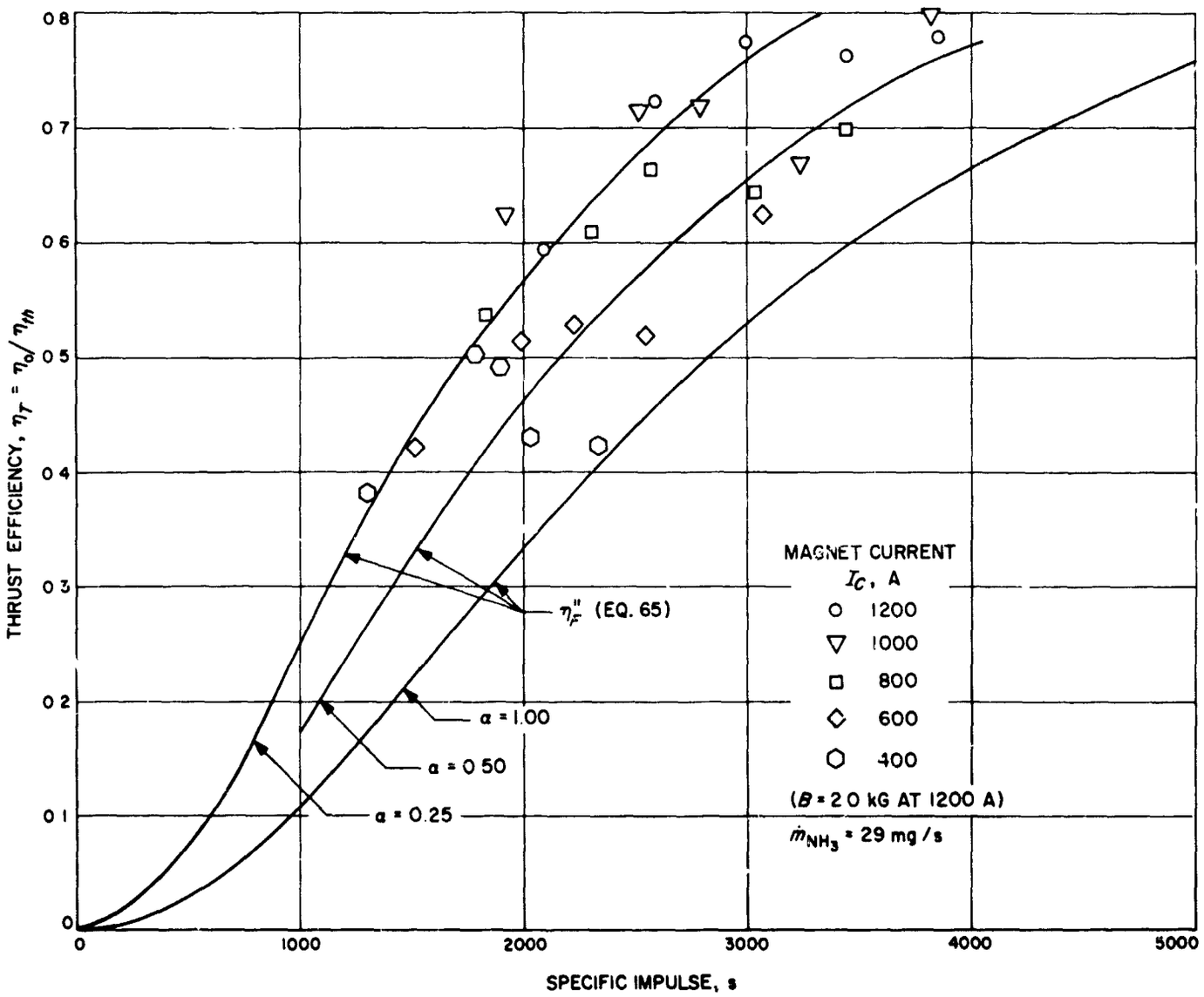

Figure 48. Thrust efficiency vs specific impulse for the AVSSD ammonia-fed X-2C engine for a number of applied magnetic field strengths. These data indicate that both high thrust efficiencies and low ionization fractions are obtained at high field strength

fraction, was obtained with strong applied fields. The superimposed curves of the frozen-flow efficiency were calculated from Eq. (65).

In a comparison of the data obtained with hydrogen and that obtained with ammonia, John (Ref. 19) has shown that there is reasonable agreement between the ratios of the calculated frozen-flow efficiencies and the measured thrust efficiency of the two propellants. The comparison was made for values of the specific impulse that varied from 2000 to 5000 s. The values used for the performance of ammonia at 4000 and 5000 s were, presumably, extrapolated from the measured data. On the basis of this comparison, John concluded that, at least to first order, the difference in the overall efficiency of the two propellants can be attributed to the differences in the thermal and frozen-flow efficiencies. This conclusion was based on the assumption that the expansion efficiency is essentially the same for the two propellants. It is noted here that if entrainment was indeed a factor in determining the thrust of either, then the comparison would require that it too was essentially the same for the two propellants.

The recent data obtained at AVSSD with the X-7C engine were used to produce Fig. 49, in which the thrust

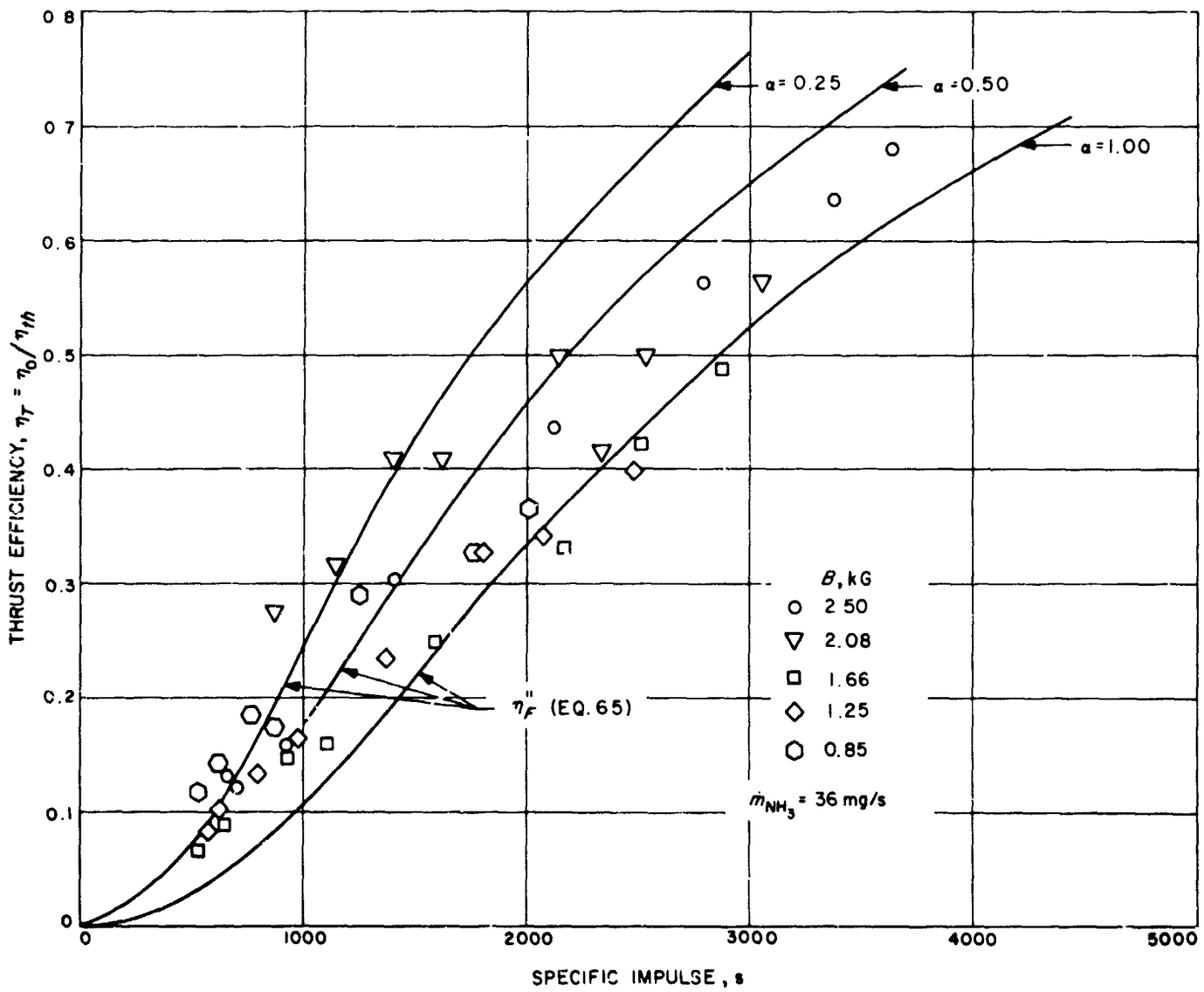

Fig. 49. Thrust efficiency vs specific impulse for the AVSSD ammonia-fed X-7 engine. The obvious correlation between the field strength and the thrust efficiency ionization fraction shown in Fig. 48 is not apparent from the data shown here

efficiency is plotted as a function of specific impulse. Only the results reported for an ammonia feed rate of 36 mg/s, for which most of the comparisons in Ref. 29 are made, are included in Fig. 49.

Most of the discussions contained in Ref. 29 were limited to the fixed feed rate of 36 mg/s because of the unknown effects of the test environment and the belief that the observed trends in the voltage and thrust would be maintained at a lower back pressure. The flow rate of 36 mg/s was chosen for the comparisons and discussions because this flow rate appeared to be a reasonable compromise between avoiding the interactions with the test environment that were observed or suspected for the lower feed rates and not requiring excessively high input power to achieve a desired specific impulse at the higher feed rates. It was stated (Ref. 29) that the absolute values of the specific impulse and thrust for the 36 mg/s feed rate may be in error because of possible interactions with the test environment.

The correlation of the thrust efficiency with the magnetic field, displayed by the data obtained with the X-2C engine (Fig. 48) is not apparent in Fig. 49. A much higher ionization fraction is indicated for nearly all of the data obtained with the X-7C engine than with the X-2C engine, and the tendency of decreasing ionization fraction with increasing specific impulse (Table 7) is not apparent. When lower feed rates were used, however, the effects of experimental anomalies became indisputable when calculated overall efficiency exceeded 100%; e.g., 210% at 36,000 s (Ref. 29).

The results obtained with ammonia at Avco-Everett were similar to the results obtained with hydrogen (Ref. 40). Axial current loops were measured in the exhaust plume, and the thrust was reduced by about 40% when the quartz shroud was used. One difference was that when the MAARC was operated on the thrust stand at AVSSD with ammonia as the propellant, agreement of the results at the two facilities was obtained for some operating conditions.

On the basis of the factors considered in the foregoing discussion, it is concluded that entrainment cannot be ruled out as a factor in the operation of ammonia-fed MPD thrustors. Although the available data and the range of operating conditions covered are less than for hydrogen, there are similarities in the data obtained with the two propellants. Thus, at high pressures, the highest overall efficiency (which corresponds to the lowest value of the calculated ionization fraction) that was obtained with the ammonia-fed X-2C engine was obtained from tests conducted with the highest values of both the applied magnetic field and arc current. The curve of overall efficiency versus the specific impulse obtained at low pressure at the NASA Lewis facility tends to cross the data reported by AVSSD for thrustor operation at 58 mg/s. However, this tendency is less obvious when the data obtained at Lewis are compared with the data obtained at 29 mg/s.

The data obtained at low test pressures indicate increasing ionization fraction with increasing specific impulse as one might intuitively expect. The data obtained at high pressure do not follow this trend, and some display the reverse trend of decreasing ionization with increasing specific impulse. It is concluded that these trends support the contention that entrainment is less likely to affect the thrust measurements in the low-pressure test facilities.

2. *Condensable propellants.* There are fewer experimental data concerning entrainment in the exhaust of MPD thrustors operated on alkali metal than for either hydrogen or ammonia. The series of Hall current accelerators designed by EOS has been tested at different pressure levels with lithium, potassium, and sodium. However, because it was not possible to vary the tank pressure systematically by increasing the density of the alkali metal vapors, the variation in the pressure was accomplished by bleeding a noncondensable gas, usually argon (Ref. 49), into the tank. The results with all three propellants indicated that there was no change in the thrust as the tank pressure was varied from 10^{-4} to 10^{-3} torr (Refs. 47 and 49). As the pressure was increased above about 5×10^{-3} torr there was a very substantial decrease in the thrust, with a minimum at about 2×10^{-2} torr, followed by an increase to a maximum at about 0.1 torr. It was also noted that the voltage of the accelerator was strongly affected by the addition of the noncondensable bleed material (Ref. 49).

One of the accelerators, Model LAJ-AF-6D (Fig. 15) was operated on lithium in the ion engine chamber at EOS at a pressure of 10^{-7} torr (Ref. 50). Compared with the results obtained at the more normal operating pressure of about 10^{-4} torr, the low-pressure results indicated no significant change. Because of a possible increase in the size of the interaction region, Cann has noted that the results are not conclusive.

The possibility of entrainment in the plume of alkali metal acceleration, even at very low pressures, has been

discussed by Cann (Ref. 51). This observation is based on the possibility that, once condensed on a surface, the condensed phase may be released as a vapor, either because of thermal effects or as the result of continued bombardment by the high-velocity exhaust beam.

The buffered cathode models, operated with a lithium–nitrogen bipropellant, were also operated at different tank pressures (Ref. 51). As before, the tank pressure was varied by bleeding argon into the tank. When the pressure was varied in a transient manner, the results were similar to those described above; however, when the bleed was controlled to produce similar steady-state pressure conditions, radical departures from the above results were observed. Instead of remaining constant, the thrust decreased to a low asymptotic value as the pressure was lowered from 10^{-3} to 10^{-4} torr. Models of slightly different geometries were used in the transient and steady-state tests; consequently, the results are considered tentative and not conclusive of either a difference in the operating characteristics of the two engines or a difference because of the different methods employed to vary the pressure.

No current density measurements have been performed in the exhaust of thrustors operated on alkali metals; however, these measurements are planned (Ref. 52). From other observations, Cann (Ref. 49) has concluded that current loops do exist in the plume of the Hall current accelerators and extend far downstream of the accelerator exit.

3. Summary. Conclusive evidence that entrainment can cause experimental data to be completely invalid has been reported by AVSSD at zero and near-zero feed rates in hydrogen-fed engines. Other observations, although not conclusive, indicate strongly that entrainment has affected much of the reported performance data. Thus, although the acceleration of a very weakly ionized gas to very high exhaust velocities has not been proved impossible, it is reasoned here that until unambiguous evidence supporting the performance data is available, and/or until a reliable theory (which, it appears, will await the appearance of the unambiguous evidence) indicates that the necessary neutral-acceleration mechanism is feasible, the data should be considered questionable. Since, except for specific impulse values of less than about 2000 s, the hydrogen data indicating the highest performance and the highest efficiency also indicate the lowest ionization fraction, it appears that the "best" data are the most suspect. Furthermore, since these data were obtained with strong applied magnetic fields and at high current levels, support for this argument is afforded by the (qualitative) theoretical considerations that the danger of entrainment is increased because of the increased penetration of the current loops into the plume.

A reliable definition of the proper test environment does not exist. However, in spite of the fact that the tests at low pressures are inconclusive, the data obtained at low pressure are probably more reliable than those obtained at higher pressure. None of the data obtained at low pressure are inconsistent with this argument.

B. Interactions With the Vacuum Tank Walls

The possibility of interactions between the electromagnetic fields and the vacuum tank walls and of subsequent errors in the thrust measurements has been discussed by a number of authors (Refs. 15, 49, and 51). Because of the strong, easily observable effects of the applied magnetic field on the measured thrust when the vacuum tank, or thrustor component parts, are constructed of magnetic materials, the tanks are usually made of aluminum or stainless steel. Less obvious, however, are the effects of interactions of an electrically conducting tank wall with the current loops in the engine exhaust plume.

Ducati (Ref. 15) has observed arcing to the walls at positions that could be correlated with the visual boundaries of the exhaust plume. Ducati has also observed a deflection of the jet and has associated this phenomenon with interactions with the wall as well.

Cann (Ref. 51) has also observed arcing to the tank walls and views this occurrence as a manifestation of a mechanism by which the wall acts as a short circuit for the current flowing in the anode and cathode jets. The solution suggested by Cann is to increase the length of the tank so that the current loops do not extend to the tank walls.

The use of insulating tank walls, or insulating coatings on the walls, has been suggested as a means of minimizing the interactions (Ref. 15).

C. Voltage Mode Variations

In addition to entrainment and other interactions of the thrustors with the test environment, the observation that a number of accelerators can operate in more than one voltage mode and, further, that the transition from

one mode to the other can occur in an unpredictable manner detracts from the confidence one can safely assign to the reported performance.

The overall efficiency of the AVSSD X-2C engine operating on ammonia apparently was not strongly affected by the voltage mode at which the thrustor operated (Ref. 65). This is not true (Ref. 49) of the lithium-fed accelerators designed by EOS, which have been observed to operate over a wide range of voltages with accompanying large variations in the thrust and the overall efficiency. This is illustrated in Fig. 50, on which some of the data obtained with two of the EOS engines are plotted. Figure 50, on which the reported data obtained at a single operating condition for each of two of the engines are plotted, also illustrates the reason for the wide area shown on the performance plot of Fig. 26. The data at the left of the figure were obtained with Model LAJ-AF-2 (Fig. 14) at the operating conditions noted on the figure. For the points shown, all the controllable operating variables were held constant, but the arc voltage was observed to vary from 36 to 58 V and the measured thrust from 23.4 to 39.4 gf. The second set of points was obtained with Model LAJ-AF-4 (Fig. 14) at the operating conditions noted on the figure. During the endurance tests, which were conducted at a constant setting of all controllable parameters, the arc voltage, as well as the thrust, varied slowly over a wide range.

A very large variation in the thrustor voltage at a fixed value of the magnetic field was reported by John (Ref. 21) for a cesium-fed engine. Individual data points were not published, although the current and feed rate ranges were reported to be from 70 to 180 A and 3.5 to 6.0 mg/s, respectively. Since John attributes the variation to data scatter, there apparently was no correlation between these variables and the arc voltage.

II. The Effect of Feed Rate on Thrustor Performance

In many of the earliest experiments with MPD thrustors, the observed invariance of the performance with the propellant feed rate was cited as evidence of the predominantly electromagnetic nature of the acceleration process (Refs. 19 and 47). This conclusion was consistent with the argument that the thrust was derived from $\mathbf{J} \times \mathbf{B}$ forces and that these forces are independent of the propellant feed rate. Some exceptions are to be noted.

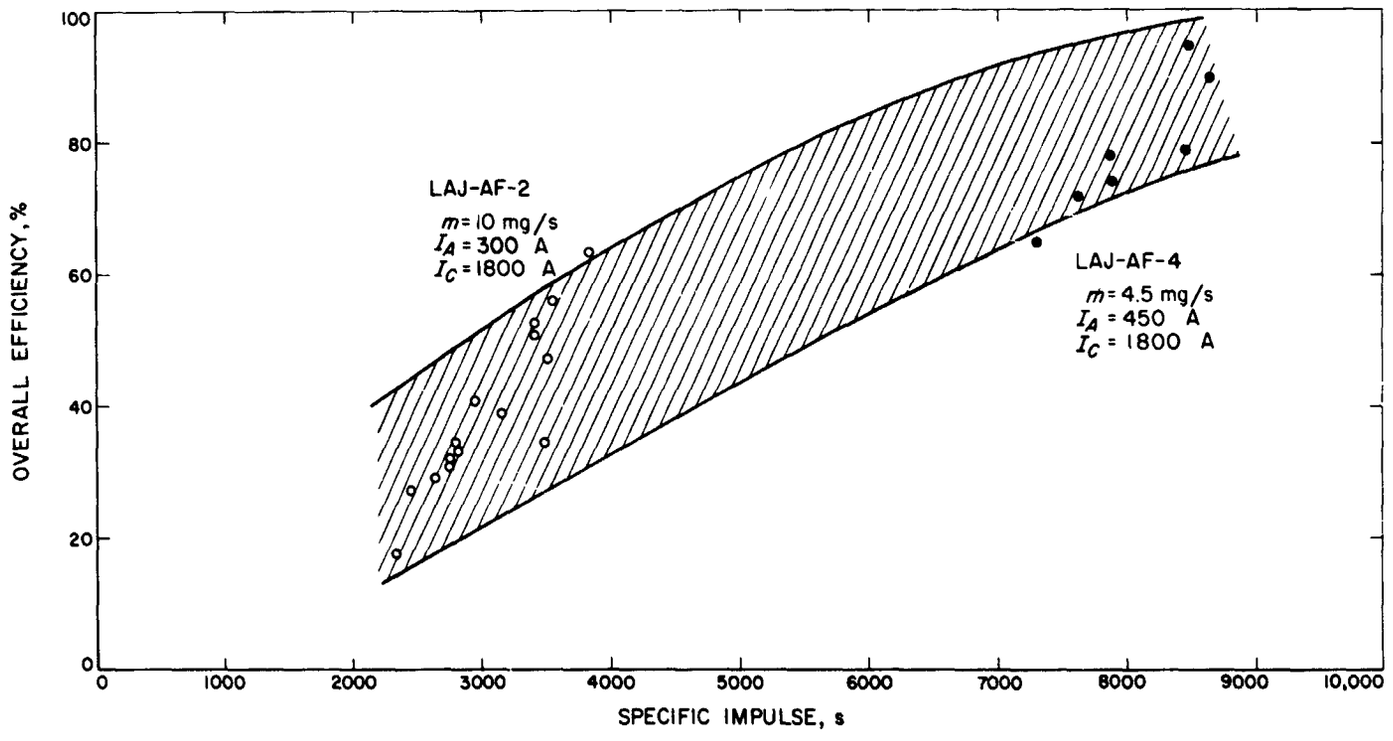

Fig. 50. Two examples of the variation in the performance of the EOS lithium-fed accelerators at fixed settings of the operating parameters. The shaded area is identical to that shown in Fig. 26

The results obtained by Patrick (Ref. 40) with the MAARC operated with hydrogen showed a very pronounced dependence of the specific impulse and the overall efficiency on the feed rate (see Fig. 22). Brockman (Ref. 56) has also reported data that show a strong dependence of thrust on the feed rate.

The results obtained at AVSSD with the ammonia-fed X-2C engine were for only two feed rates, 29 and 58 mg/s, and indicated no dependence of the observed performance on the feed rate. The AVSSD X-7C engines, on the other hand, have been operated over a much larger range of feed rates that varied from 0.7 to 68 mg/s of ammonia (Ref. 29). At the higher feed rates, from 36 to 68 mg/s, no dependence on the feed rate was observed, in agreement with the earlier results. However, at the lower feed rates, a very strong dependence of efficiency on the feed rate was observed. The discussion of the effects of the feed rate presented in Ref. 29 was directed toward a comparison of the results obtained at (nearly) constant input power with the X-7C-4 engine, which has a 0.6-in. anode. This comparison, Table XI of Ref. 29, shows that both the arc voltage and the measured thrust are at a minimum at a feed rate of 16 mg/s and that obviously anomalous results were obtained at the lowest feed rates where the indicated overall efficiency exceeded 100%. If the comparison is made at a constant value of the specific impulse, the observed performance is consistently lower for the lower feed rates. This trend is clearly evident in Fig. 10 of Ref. 29, and may be seen from Fig. 25 of the present report.

Recognizing that the reported results may not be representative of the performance in a hard vacuum, John (Ref. 29) concluded that there appears to be a minimum mass flow for efficient MPD operation and that there is also a minimum power which must be used to obtain a given specific impulse at the maximum efficiency. To explain the observed dependence of the feed rate, John hypothesized that at high mass flows the interaction with the test environment is negligible, and that at very low flow rates these interactions will dominate the observed results completely.

Somewhat similar results were published by Cann (Ref. 51) for the bipropellant ALPHA operation (Fig. 27). The results concerning the feed rate are somewhat obscured because a number of different electrode configurations were used to obtain the data shown in Fig. 27. However, it is apparent that the results obtained with a feed rate greater than about 10 mg/s indicate higher efficiencies than do the results obtained at feed rates in the 4- to 8-mg/s range.

III. Status of Theoretical Studies

A. Summary of Theoretical Problems

Because of the complexity of the processes that occur and the coupling between these different processes to produce thrust, a comprehensive theory describing the mechanisms and defining the performance capability of MPD thrustors has not been achieved. The analyses that have been made are devoted to one or more isolated features, generally uncoupled from other processes to simplify the analysis, that are thought to be important in determining the overall performance. Some of the processes that have been investigated are the ionization process, fluid dynamic interactions, electrode phenomena, the effect of magnetic field configuration, and finally and probably most important, the energy addition and acceleration mechanisms and the attainment of axial ion velocities. The relative effectiveness of the different acceleration mechanisms that have been identified is a strong function of the local plasma conditions, the electromagnetic field configurations, and the distribution of the current densities. These factors are poorly defined at present, and the existing theoretical descriptions depend heavily on numerous assumptions.

At the present time, the level of understanding of the basic phenomena is not sufficient to allow a critical evaluation of the reported performance data, to extrapolate the performance obtained in the laboratory to that which may be expected in space, or to aid appreciably in the design of an "optimum" engine. Thus, the full potential and the limitations of the MPD thrustor are not known at the present time. The difficulties that have prevented the evolution of a realistic theory may be traced to the complexity of the different physical processes that take place, the questionable validity of much of the performance data and, finally, the difficulty of making the necessary diagnostic measurements with sufficient accuracy to verify the more critical assumptions that form the basis of the simplified models of the acceleration mechanisms.

It is concluded here that little additional progress in the development of a realistic theory is likely until the ambiguities caused by the interactions with the test environment are either removed or adequately understood and, in addition, until those measurements that are necessary to confirm the assumptions concerning the local

conditions are made with sufficient accuracy to be useful for the intended purpose.

B. Acceleration Mechanisms and Energy Addition Processes

The acceleration mechanisms that have been discussed involve the heating and thermal expansion of the propellant plasma and the effects of the interactions of current, either applied or induced, with the magnetic fields, which are also either applied or induced. Although all the possible mechanisms are generally considered to contribute to some extent to the observed thrust, the analytical models that have been proposed generally emphasize one mechanism as being most likely to be responsible for a preponderance of the thrust.

1. Electrothermal processes. The heating of the propellant is usually referred to as an electrothermal process and the expansion is described as an aerodynamic process even though electromagnetic effects, such as the distribution of the arc attachment region at the electrode surfaces and plasma containment during the expansion and possibly some of the heating processes, may contribute significantly to the performance. A common method of handling the data is based on the proposed similarity with the more conventional thermal expansion processes in which it is assumed that the thrust can be related to the arc chamber pressure through a thrust coefficient C_F.

An initial attempt (Ref. 18) to correlate part of the observed thrust of an engine operated with a very weak applied magnetic field with an expansion process was made by assuming a thrust coefficient equal to unity. Later experiments, by both Malliaris (Ref. 28) and Hügel (Ref. 101) demonstrated that a value of unity was a poor approximation for the thrust coefficient. Although the thrust coefficient of more conventional flows is greater than unity for adiabatic supersonic expansions, Malliaris (Ref. 28) found that the use of a coefficient equal to unity resulted in a calculated aerodynamic thrust that exceeded the total observed thrust for a number of experiments and, therefore, that the thrust coefficient must have a value of less than unity. Hügel (Ref. 101) reported C_F to vary from 0.4 to 0.8 for argon and from 0.9 to 1.15 for hydrogen. The effect of supersonic heating (which would be to increase the apparent value of C_F) on the performance of an MPD thrustor operated with no applied magnetic field was discussed by Hügel for an isothermal expansion.

As indicated above, some limited success was obtained through the use of a thrust coefficient to relate part of the thrust to aerodynamic effects when no (or a very weak) external magnetic field was applied. For thrustor operation with a strong applied magnetic field, Malliaris (Ref. 27) found that the concept of a thrust coefficient could not be used in the customary way. The pressure distribution in the interelectrode region, as determined by measurements of the cathode tip pressure and the expansion nozzle, appeared to be determined more by the interaction of the flow pattern and the applied field than by the fluid dynamic effects alone. However, many of the experimental data (Refs. 19, 40, 65, and 66), and particularly those obtained at low specific impulse, for which the performance parameters indicate a low ionization fraction, suggest the possibility that a significant portion of the measured thrust may be aerodynamic, even when strong external magnetic fields are applied.

Energy addition by Joule heating and the subsequent randomization of the energy in a fully ionized hydrogen exhaust was discussed by Treat (Ref. 15). For assumed values of the electron density, electron temperature, and the local values of the electric field, Treat has calculated the length of the magnetic nozzle, downstream of the region of strong electric fields, that is required to allow randomization of the energy. The conclusion (Ref. 21) that the energy addition process of the AVSSD cesium-fed engine was electrothermal was based on the observed operating characteristics of the cesium engine.

2. Acceleration by self-induced magnetic fields. The principle of plasma acceleration by the electromagnetic forces that result from the interaction of an applied current and its self-induced magnetic fields has been known since 1955 when Maecker (Ref. 91) described and demonstrated the effect for a free-burning atmospheric arc. It was quickly recognized that a large part of the thrust of a high-current MPD thrustor operated without an externally applied magnetic field could result from this mechanism, and experiments were designed to demonstrate the applicability of the mechanism.

The most common derivation (see Part IV, Section II-A) of the relation between the current and the force exerted on the plasma is from a macroscopic approach in which it is shown that the thrust produced is not dependent on the local plasma conditions. The source of uncertainty in this development of a quantitative expression for the thrust lies in the dependence of the electromagnetic force on the current distributions at the electrode surfaces. Nonetheless, considerable confidence is expressed in the correctness of the solutions obtained. This is perhaps best exemplified by the practice of defining

the aerodynamic thrust as the difference between the total measured thrust and the calculated electromagnetic contribution.

Although the macroscopic approach has been used successfully to relate the electromagnetic thrust to the applied current, it cannot be used to predict the voltage characteristics. The voltage–current characteristic does depend on the local plasma conditions and has not been treated quantitatively. However, the qualitative relation between the voltage and the identity of the current carrier throughout the discharge, which is a strong function of the local conditions, has been discussed by Jahn (Ref. 14). Stratton (Ref. 92) has discussed the limiting condition in which ions conduct all the current across the induced magnetic field and for which the voltage must be sufficient to accelerate the ions to the final velocity electrostatically.

3. Acceleration in the presence of an applied field. The number of possible interactions when a strong field is applied is greater and the interactions are much more complicated than when no field is applied. There are no general relations between the thrust and the engine operating parameters similar to that obtained for operation with no field. Because of the complexity of the processes involved, the thrustor characteristics for each of a number of possible mechanisms have been described for limiting conditions and compared with the experimental observations. The postulated limiting conditions usually specify that the proposed acceleration mechanism was dominant and that it could be uncoupled from all other processes that take place.

The initial emphasis placed on the pure electromagnetic acceleration mechanisms has lessened during the last two years largely because of the inability to correlate the predicted engine performance with the experimental observations. As one example, the inability to relate the measured thrust with the arc voltage (Ref. 47), as well as the negative results obtained from experiments designed to measure Hall currents (Ref. 25), has caused a reevaluation of the role of Hall currents in Hall current accelerators. In addition, some theoretical studies, such as the particle analysis presented by Jahn (Ref. 14), have cast doubts on the possibility of significant Hall acceleration in devices with the geometry of the MPD thrustor.

Although the role of the Hall currents is questionable, there appears to be general agreement that a large fraction of the electrical energy may be transferred to the propellant as rotational kinetic energy when an external field is applied. The torque exerted on the plasma as a result of the arc current crossing the applied magnetic fields has been calculated (Refs. 16, 42, and 47) in a general way and shown to be dependent only on the current distribution at the electrode surfaces. The rate at which the torque is converted to angular momentum depends on some of the plasma properties, and has been calculated for a nonviscous, neutral plasma (Ref. 16). Finally, the production of useful thrust by this mechanism by the conversion of the rotational kinetic energy to axial kinetic energy depends on the effectiveness of the "magnetic nozzle" in containing the plasma. This mechanism is referred to as the ion-swirl mechanism. Although relatively small azimuthal velocities have been measured (Ref. 52) very near the exhaust centerline, these measurements are not conclusive in demonstrating the effectiveness of the mechanism.

The role of the magnetic nozzle in transforming rotational motion to axial motion was not invoked by Jahn (Ref. 14) in his particle viewpoint analysis. Consequently, the analysis was unable to reveal any thrust-producing mechanism for thrustor operation with a strong applied field and small applied currents.

The arc voltage of the swirl mechanism depends strongly on the identity of the current carriers which, in turn, depends on the local plasma conditions. If collisions are infrequent, and the electrons are "trapped" by the magnetic field, the ions carry most of the current and the voltage is high. If electrons carry the current, the torque exerted on the plasma remains unchanged but the voltage drop may be smaller. A detailed analytical model, in which electrons carry most of the current and therefore are responsible for most of the torque, has been described by Cann (Ref. 47).

4. Analytical models. The theoretical analyses of the electromagnetic acceleration mechanisms of the MPD thrustor have followed a number of approaches with varying degrees of thoroughness. The acceleration mechanisms, when analyzed in some detail, are invariably uncoupled from all other processes. This procedure necessitates the assumptions of the local conditions at the point in the discharge where the acceleration process is assumed to begin. The description of the acceleration mechanisms are generally qualitative and few attempts have been made to obtain solutions that relate the thrustor operating characteristics to the controllable operating parameters, except for very idealized conditions.

The group of workers at EOS have followed a course of attempting to calculate, among other parameters, the current density distributions within the exhaust plume, the accelerator voltage characteristics, and the dependence of the thrust on the applied magnetic field. The difficulty of a comprehensive analytical solution and the sensitivity of approximate solutions to both the assumptions that are made and the processes that are considered can be appreciated from a review of the evolution of the different analytical models that have been proposed by EOS. The assumptions common to all of the models are the following:

(1) Ionization is complete.

(2) Ionization occurs by electron–atom collision. (Although this assumption is made, it has no direct bearing on the acceleration mechanisms per se, inasmuch as the ionization is assumed to occur upstream of the acceleration region.)

(3) Current loops extend downstream via two zones: a central cathode jet and a thin annular anode jet, which coalesce at some downstream position.

(4) The current carriers in the cathode jet are electrons.

No direct assumptions of the particle densities or temperatures were made, but the effectiveness of different processes, which depends on the plasma properties, was assumed. In the first model, which emphasized Hall acceleration, the ions carried most of the current across the magnetic field lines because the electrons were assumed to be trapped by the field and, therefore, flowed only as Hall currents. The model was based on the assumption that most of the thrust was the result of Hall acceleration, and the analysis was devoted to the determination of the Hall currents and the effects of the Hall current interactions. Attempts to solve the set of equations that was written to describe the interactions were largely unsuccessful, and for this model an approximate solution was obtained for a completely diamagnetic plasma for a region of the discharge in which the radial current distribution was everywhere zero.

In the second model, azimuthal acceleration of the ions was considered to produce most of the thrust, and the Hall acceleration was assumed to be zero. The analysis was restricted to a region in which the applied magnetic field was purely axial. The absence of any Hall acceleration followed from the assumption that the radial component of the applied magnetic field was zero and, consequently, there existed no component with which the Hall currents could interact to produce axial acceleration. In this model the electrons remained trapped in the cathode jet, but the anode jet was assumed to be sufficiently dense to permit electron conduction across the magnetic field by collisional effects. Because the electrons could conduct part of the current, the voltage requirement imposed by the assumption that only ions carried current across the field was related. The geometric configuration of the anode and cathode jet, sketched in Fig. 45, consisted of an anode jet of decreasing diameter and a low-density cathode jet, in which little energy was released and virtually no thrust produced, of uniform diameter.

In the most recent model, the role and appearance of both the anode jet and the cathode jet have changed considerably. The cathode jet is assumed to be a relatively high-density region in which there is considerable energy addition, part of which is by electrothermal effects. Because of the high density in the cathode jet, the plasma diffuses across the magnetic field lines, and, as a result, the cathode jet rotates and increases in diameter. The rate of increase of the cathode jet is determined by the rate of diffusion across the field lines. The anode jet, on the other hand, is assumed to be a very low-density, collisionless region of uniform diameter. Thrust is produced by the recovery of both the rotational and internal energy of the cathode jet in the magnetic nozzle and from the electrostatic acceleration of the ions in the collisionless anode jet.

The analysis proceeds by finding the condition at which the sum of the voltage drops through the collisionless anode jet and the high-density cathode jet is a minimum. The assumed conditions of the cathode jet are stated to be based on experimental investigations which, however, are not identified further. The statement is made that the low-density anode jet is not expected to exist in the working MPD arcs.

C. Common Assumptions

Numerous assumptions have necessarily been made to formulate the mechanisms that have been proposed. Some of these have been assumptions of local conditions, such as the electron densities and temperatures, and the effectiveness of well-known processes are then evaluated for the postulated conditions. The effectiveness of the processes themselves, such as ion–neutral ionization processes and charge-exchange mechanisms, are also sometimes assumed. Other examples of the assumption of

effectiveness of processes include (1) the ability of a magnetic nozzle to contain the exhaust products and (2) the existence of large azimuthal Hall currents at specified locations in the discharge region.

Few of the assumptions are adequately verified by experimental data. However, even with more detailed and accurate diagnostic measurements than now exist, some questions will be likely to remain if the test conditions do not adequately simulate the thrustor operation in space.

In the following discussion, some of the more critical assumptions are compared, and an attempt is made to relate the available experimental data to the validity of the assumptions for the experimental engines.

1. Degree of ionization and acceleration of neutrals. One of the assumptions that is made most frequently is that the accelerating plasma is fully ionized. This assumption appears to be justified for the heavier propellants that have been tested, such as cesium and argon, for example, but is a very doubtful assumption for much of the data obtained with hydrogen and ammonia at the lower values of specific impulse. As mentioned earlier, the experimental evidence of the degree of ionization is frequently restricted to calculations of the average value based on the measured performance parameters. In keeping with the conclusion that entrainment is more likely to falsify data indicating high specific impulse (and obtained with a strong applied field), we suggest that calculations of the degree of ionization are also more likely to be incorrect at the same conditions. However, low degrees of ionization appear to be well substantiated at some operating conditions. In particular, the performance data obtained at very low tank pressure by NASA Lewis with a hydrogen-fed engine indicates not only low ionization but also incomplete dissociation of the propellant at a specific impulse of 1000 s (Ref. 65) These data are at least qualitatively substantiated by the spectroscopic observations of large amounts of atomic line radiation as well as faint molecular spectra. Similar data were also reported for ammonia (Ref. 66).

The question of the acceleration of neutral particles does not enter into those theories for which complete ionization is assumed. These include the description of the pure Hall acceleration (Ref. 44), the ion-spin mechanism (Ref. 47),[5] and Jahn's analysis based on the particle viewpoint (Ref. 14). The effectiveness of the magnetic nozzle and the energy randomization process of the electrothermal mechanism discussed by Treat (Ref. 15) were also analyzed for a completely ionized plasma. On the other hand, the critical mass flow theory proposed by Cann (Ref. 49) and discussed further by Bennett (Ref. 26) to explain the thrustor operating characteristics in the presence of entrainment (see Section IV-B-3) is critically dependent on the assumption that neutral particles are not accelerated and that they do not in any way absorb energy from the discharge. This assumption clearly conflicts with the assumption made by Patrick that neutral particles are very effectively accelerated by a charge-exchange mechanism. The experimental data reported by AVSSD for hydrogen are in substantial agreement with the predictions of the critical mass flow theory; however, the low-pressure data (Ref. 65) obtained at NASA Lewis with the same engine and propellant do not agree with this theory. All the tests conducted at Lewis were operated at a feed rate below the critical mass flow rate defined by the theory. The critical mass flow model predicts that a thrust efficiency of 50% is attained at the critical specific impulse (the specific impulse at which the kinetic energy is equal to the ionization energy) and that the ratio of the thrust efficiency to the specific impulse is a constant at all values of the specific impulse less than the critical specific impulse. This constant for hydrogen, which has a critical specific impulse of 5600 s, is therefore $0.5/5600\ s^{-1}$. The results obtained at Lewis at high pressure are in agreement with those reported by AVSSD, but the data obtained at low pressure are in marked disagreement with the predictions of the theory, particularly at low values of the specific impulse where the observed efficiency exceeds the predicted value by nearly a factor of 3 at low specific impulse. (See Table 6.) That at least part of this thrust derives from the expansion through the anode nozzle is possible. However, there is no known way to separate the aerodynamic thrust from the electromagnetic thrust for an engine operated with a strong applied magnetic field.

2. Ionization mechanisms. The ionization process in MPD engines is usually attributed to electron–atom collisions; however, the ionization mechanism is generally tacitly assumed to have little or no influence on the acceleration process. Cann (Ref. 47) has discussed the heating of Hall current electrons to temperatures that are high enough to effect ionization of lithium by thermal electrons. Those theories describing acceleration processes in fully ionized plasmas attempt to relate the

[5]This mechanism is also referred to as the "ion swirling" mechanism by other investigators.

operating parameters, exclusive of the effect of the voltage drop through the electrode sheaths, to the acceleration mechanisms and not to the ionization processes.

A notable exception is the ionization mechanism by ion–atom collision that has been postulated by Patrick (Ref. 40). The experimental basis for Patrick's model is the empirical relation of the arc voltage and the magnetic field strength, which indicates that the slope of the V–B curves can be associated with the propellant ionization potential. The similarity of the voltage dependence on the field strength of the MAARC to that of engines in other experiments (Ref. 98) in which a "critical velocity" of the ions has been observed is used to justify the proposed mechanism in the MPD thrustor. This model suggests that a propellant with a high ionization potential should be used to achieve the highest possible efficiency because the ionization process determines the arc voltage and, therefore, the voltage available for the acceleration process. Since the ion velocity is limited by the ionization process, the proposed mechanism is applicable only to thrustor operating conditions for which ionization is incomplete.

Detailed measurements that are needed to verify the mechanism postulated by Patrick have not been made. The physical process of very rapid ion–atom ionizing collisions is as yet poorly understood, and the application of the limiting velocity concept to the conditions that exist in the MPD engine remains questionable.

It may also be noted that the conclusions reached by Patrick are not strongly supported by the data that were used to obtain the empirical relation between the voltage and the field strength. Although the relation given by Eq. (58), $V = V_0 + U_c B\ell$, is stated to be independent of the current, Fig. 4 of Ref. 39 shows that the voltage is a strong function of the current at zero applied field strength and a weaker function of the current at finite field strengths. The variation in arc voltage with applied current would affect not only the value of V_0 in Eq. (58) but also the slope of the V–B curve. The figure cited

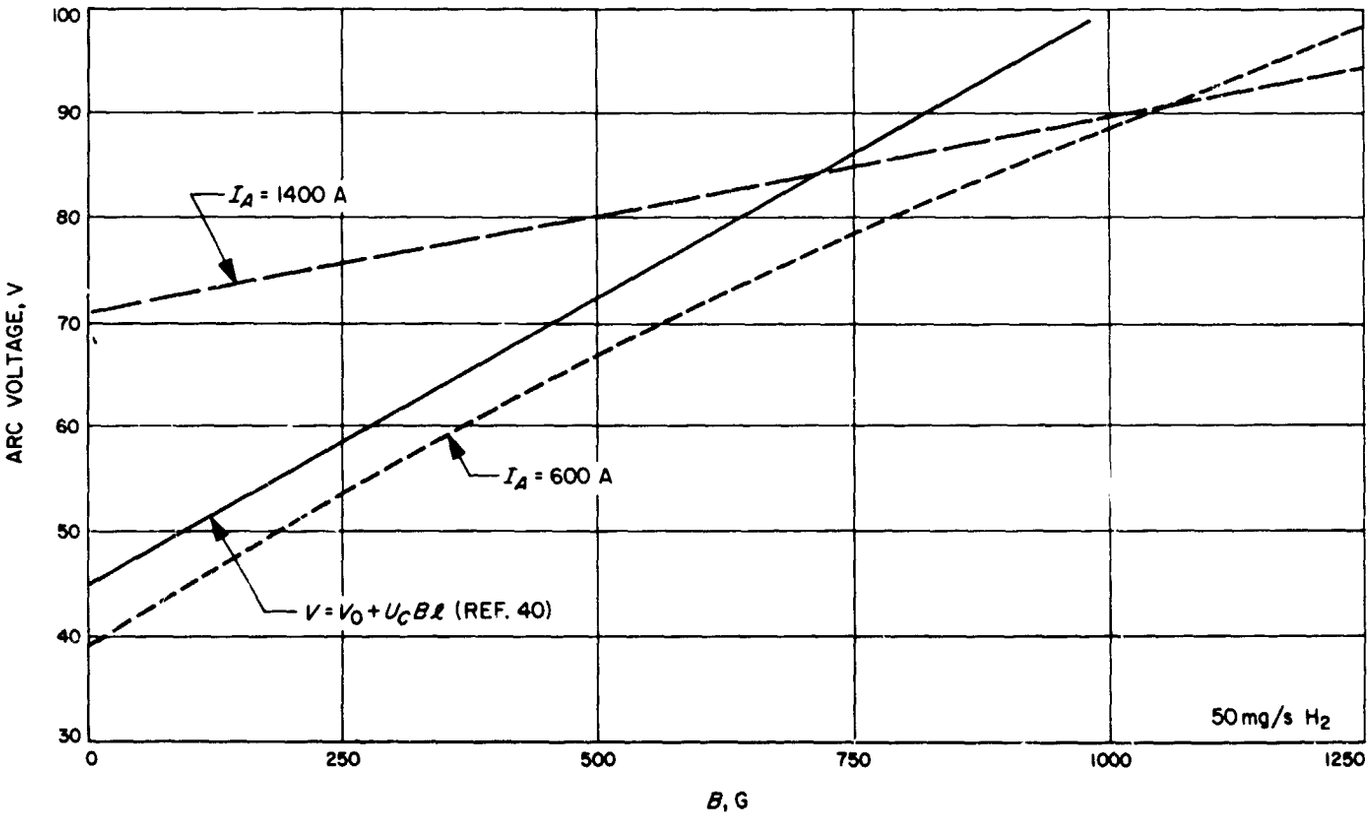

Fig. 51. Correlation of the arc voltage of the Avco-Everett MAARC with the applied magnetic field strength at two values of the applied current (data from Ref. 40)

above contains smooth curves that are drawn through the data obtained at each of five field strengths that varied from zero to 1250 G. The data were obtained at a single feed rate of 50 mg/s. If the voltage represented by the smooth curves is used to determine the V–B curves, the relations obtained depend on the value of the arc current. This is shown in Fig. 51, in which the arc voltage, taken from the smooth curves, is plotted as a function of the applied magnetic field for two different values of the applied arc current. Also included on the figure is Eq. (58) with V_0 equal to 45 V, U_e equal to 5.6×10^4 cm/s, and l equal to 1 cm, as given by Patrick (Ref. 39). The slope of the line drawn through the data for 1400 A yields a value of U_i of less than 2×10^4 cm/s when l is set equal to 1 cm.

As discussed in Part IV, Section II-C, other analyses, which used assumptions very different from those used by Patrick, have also predicted a linear V–B relationship as well as a "critical velocity" that is related to the ionization potential of the propellant. Additional criticism (Ref. 102) and further discussion (Ref. 103) of the mechanism proposed by Patrick have been published recently. Reference 103 contains a number of references related to this subject.

3. Plasma containment by a magnetic nozzle. Channeling of the plasma flow through a magnetic nozzle is proposed as the method by which the thermal and rotational energy is recovered as axial kinetic energy. The effectiveness of a magnetic nozzle in containing the plasma has been assessed by showing that the magnetic pressure exceeds the kinetic pressure (Ref. 21) and by calculating the rate of diffusion of charged particles across the magnetic field lines and comparing this value with the anticipated axial velocities (Ref. 15). The portion of the applied field that acts as a magnetic nozzle is generally assigned to the region downstream of the region of large axial current loops.

Very few experimental data pertain directly to verification of the effectiveness of the magnetic nozzle. These data include the alignment of the luminous contours of the exhaust with the undisturbed field lines of the applied magnetic field (Ref. 24) and the results of the measurements of the momentum profiles in the exhaust. The latter measurements indicate an increased "pinching" of the plasma along the exhaust centerlines as the magnetic field is increased. In particular, no direct measurements of the required azimuthal current J_θ have been reported.

The concept of a magnetic nozzle is a problem that requires much additional study to determine its actual role in the MPD accelerator. The existing concept is very qualitative, and few of the properties of the flow, such as the location of a sonic point (if one exists) or the velocity profile, can be predicted. In addition, the behavior of the nozzle "wall" in the presence of a swirling plasma has not been investigated. The influence of neutral particles, discharge instabilities, and the coupling with the region of high current densities needs additional study.

A review of the analyses of magnetic nozzles, in more well-defined flow patterns, has been published by Hernbegger (Ref. 104)

D. Experimental Verification of Theories

1. Performance data. The experimental evidence that is used most extensively to assess the validity of theoretical descriptions of MPD thrustor operation are the observed gross operating characteristics and the overall performance. These parameters include the dependence of the thrust, the arc voltage, and the electrode losses on the independent variables of applied arc current, applied magnetic field strength, propellant feed rate, and the propellant type. Effects of engine geometry can be expected and are frequently discussed; however, theoretical justification for the magnetic field and the electrode configurations that are used are largely qualitative observations.

If the comparison of the observed and predicted performance is to constitute a valid test of a theory, it is obvious that the data used for the comparison must be obtained from tests that adequately simulate the conditions for which the theoretical model was proposed. The questionable validity of much of the performance data was discussed in the previous section. It is evident that conclusions inferred from the operating characteristics can be misleading if part of the measured thrust is a result of the acceleration of entrained or eroded material. An example of the general awareness of this problem is the emergence of an additional theory, the critical mass flow model that pertains specifically to the effect of entrainment on the thrustor operation.

Certain features of MPD thrustor operation are common to nearly all engines tested. For example, as the magnetic field strength is increased, an increase in the arc voltage has been observed for all propellants tested and at all levels of the vacuum tank pressures

used. Some other features, which are listed in Part IV, Section II-B, are also commonly reported for most of the engines tested. Because of the wide range of operating parameters, engine configurations, and test facilities and conditions used at the different laboratories, these common trends are probably valid indications of the true thrustor operation.

Because of the complexity of the processes that occur, it is not likely that sufficient information to distinguish mechanisms can be acquired from observations of the gross operating parameters alone, even if the absence of all anomalies in the performance measurements could be assured.

By way of illustration, the operating characteristics of the model proposed by Treat (Ref. 15), which is described here as an electrothermal mechanism, and one of the models proposed by Cann (Ref. 47), in which Hall currents aid in "spinning up" the ions, could be very similar. Both models describe a swirling, fully ionized plasma that is contained by the interactions of azimuthal currents and the applied field and accelerates as it flows through a magnetic nozzle. In both processes, the electrons carry either all or nearly all the applied current, are strongly heated by the electric field, and transfer a significant amount of momentum, gained from the electric field, to the ions. Because the electrons carry current, the voltage requirements of both processes are less than that which would result if the energy were transferred directly to the ions. The most significant difference in the two models is the emphasis placed on the randomization of the energy among the different species and the subsequent recovery by thermal expansion for the one and the emphasis placed on the role played by the Hall currents for the other.

2. *Diagnostic measurements.* Diagnostic measurements are used in attempts to verify the performance data, to determine the validity of the assumptions that have been made, and to provide reliable data for the construction of realistic models of the acceleration mechanisms. The different diagnostic tools that have been used are described in Part III, Section VII-C. Here we attempt to assess the usefulness of the measurements in accomplishing their intended purpose of verifying performance data and the assumptions of local plasma conditions.

The diagnostic measurements that have been made include determinations of current densities, plasma velocities, and mass and momentum distributions in the exhaust plume and of pressure measurements within the engine itself. In addition, spectroscopic observations of the plume radiation have been used to identify species present and thereby gain a very qualitative indication of the degree of ionization and the electron temperature. Spectroscopic temperature determinations, using the Relative Line Intensity method, have been reported for a weakly ionized exhaust plume (see Section III-3-e); however, the reported values remain questionable because of the nonequilibrium conditions. Some of the reasons for the lack of data on the electron properties are (1) the MPD exhaust is in a highly nonequilibrium state with significant pressure, density, and temperature gradients, (2) the presence of strong magnetic fields hampers the use of the Langmuir probe, and (3) the discharge of the hig' -powered engines presents a very hostile environment for physical probes.

The properties of some of the propellants, such as lithium, also pose special problems that are not generally encountered in diagnostic measurements. Because the exhaust products condense on any cool surface, the techniques required for most of the measurements on the alkali metal plasmas are different from those for the gaseous propellant plasmas. As a result, fewer diagnostic data have been reported for MPD engine operation with the alkali metals than with, say, hydrogen or argon. However, a very ambitious program of diagnostic measurements on the lithium-fed engine has been outlined by Jacobs and Cann (Refs. 52 and 53). This study includes measurements of the total beam power, total beam angular momentum, mass flux and energy flux distributions, and magnetic field and current density distributions. Velocity measurements, both by the doppler-shift method and by phototracer technique, have already been reported (Ref. 52).

It should be noted that the application of the results obtained with one particular engine configuration and propellant type to the general class of MPD engines is a very questionable procedure. From the published data, it may be concluded that very significant differences can exist for the different engines and for the different operating conditions. However, some general trends have been observed and are worth noting. Some of these are summarized below:

(1) An increase in the applied magnetic field strength tends to pinch the discharge and may increase the centerline velocity. This tendency has been observed from measurements made with impact probes (Refs. 28 and 40) and current density measurements (Ref. 25).

(2) Two definable areas, which have been called the cathode jet and the anode jet, are generally observed visually. These areas are usually associated with current paths.

(3) Some current flows downstream of the engine itself. The magnitude of this current has been reported to vary from a few percent to nearly 100% of the applied current. It has been suggested (Ref. 40) that some of the measured current may be due to the presence of the measuring device itself.

(4) No detectable Hall currents have been observed in the high-specific-impulse devices. The only engines in which detectable Hall currents have been measured have been operated with argon (Ref. 56).

With the exception of the lack of Hall currents, these observations are generally compatible with all the acceleration mechanisms that have been proposed.

Except for the possibility of a disturbance of the discharge by the presence of probes, the reported estimated accuracies of the techniques used for current density measurements are relatively high. However, a comparison of the results obtained at the individual laboratories reveals a number of differences in the magnitude of the measured current. The reported differences are not easily traced to the engine geometry, field strength, or other operating conditions, or to the propellant type. The integrated current densities reported by Cann and Lenn (Ref. 46) for an argon-fed engine constituted a large fraction of the total current, whereas the measurements reported by Powers (Ref. 25) indicate that a very small fraction of the total current extends into the plume of an argon-fed engine. Also, with both engines operated on hydrogen, less current was found in the exhaust of the Avco-Everett engine than in the AVSSD engine. Because of the more "open" electrode geometry of the Avco-Everett engine, one would expect the current loops to be greater in that engine.

Negative results were obtained by both Patrick and Powers in their attempts to measure Hall currents in hydrogen- and ammonia-fed engines. The only measurements of Hall currents in significant amounts were reported by the group at NASA Langley for argon-fed engines (Refs. 55, 56, and 61).

Velocity measurements constitute one of the most useful methods of verifying the thrust measurements as well as some critical aspects of the proposed theories. Much effort has been devoted to the velocity measurements and a number of techniques have been used. Unfortunately, the accuracy of none of the techniques is sufficient to accomplish either purpose.

Those techniques in which the radiation from the plasma is utilized to determine the velocity have the obvious advantage over the use of physical probes of not disturbing the discharge. Preliminary doppler-shift measurements of the rotation of the exhaust of an engine operated with a nitrogen–lithium bipropellant (Ref. 52) indicated relatively low (4000 m/s) azimuthal velocities at a radial position of 0.19 cm. Axial velocities (Ref. 52) of $(3 \pm 2) \times 10^4$ m/s, also measured by the doppler-shift method, were reported for an engine operated with a hydrogen–lithium bipropellant at a specific impulse of 5000 s. Because of the large error associated with the velocity measurement, which indicates that the specific impulse is somewhere in the range of from 1000 to 5000 s, it is apparent that considerable refinement in the method is needed if the measurements are to be useful to either confirm the performance measurements or verify an acceleration mechanism.

The velocity measurements by the phototracer technique (Ref. 52) indicate that the exhaust velocity increases by a factor of two between the axial positions of 5 and 118 cm downstream of the exit plane of the EOS accelerator. These data, which indicate that the acceleration region extends into the downstream region of the plume, are in agreement, in this respect, with most of the theories that have been proposed. The assigned error, about 20%, is less than for the doppler-shift method, and agreement with the velocities inferred from the thrust and mass flow measurements is stated to be within a factor of 2. Refinement of the technique is planned.

The estimated accuracy (Ref. 56) of the velocity measurements in an argon engine by the Langmuir probe technique is 25%. Another method (Refs. 28, 55, and 82), which also involves a physical probe, is the use of $\mathbf{u} \times \mathbf{B}$ probes. Although the technique has been improved by applying an alternating magnetic field and thereby eliminating much of the "noise" and the need for a large field, the behavior of the probe in the presence of strong external fields of the MPD thrustor needs additional study.

In equilibrium plasmas, spectroscopic measurements can be used to determine the electron temperature, the electron density, and the degree of ionization; however, the application of the commonly used spectroscopic

techniques to nonequilibrium plasmas remains a questionable procedure. A determination of the degree of ionization, by the comparison of the intensities of an ion line to that of an atom line, is particularly sensitive to the requirement for equilibrium. Because of this, the reported spectroscopic data obtained on MPD engines are only qualitative and cannot be used for quantitative calculations. For example, the relative intensities of, say, the strong lines of AI and AII spectra can be used to infer that the degree of ionization is small, moderate, or large.

One advantage of spectroscopic observations over the calculations of the average ionization fraction based on the performance parameters is that some indication of the variation of the ionization fraction over the plume cross-section may be obtained. Thus, Cann (Ref. 50) has observed strong emission from the potassium ions in the core of the jet, but weak ion lines and strong atomic lines in the jet periphery.

For many of the engines operated with radiation-cooled engines, spectroscopic observations are the only available data concerning the degree of ionization. Spectroscopic data concerning the degree of ionization in lithium engines, reported by Jacobs (Ref. 52), indicate that the ion lines are emitted almost exclusively from the cathode jet and the atomic line radiation from outside the exhaust beam.

E. The Role of Hall Currents in MPD Thrustors

One of the most perplexing aspects of this study has been the evaluation of the role of azimuthal Hall currents, both from a theoretical viewpoint and on the basis of the reported experimental data, in the operation of MPD accelerators. Although a number of the acceleration models require the existence of azimuthal currents for thrust production, the direct experimental evidence of Hall currents is meager and somewhat confusing. Comparatively large Hall currents have been measured by Hess and his co-workers for argon-fed engines, whereas negative results have been reported by Powers (Ref. 25) and by Patrick (Ref. 40) in their attempts to measure Hall currents in the exhaust of accelerators operated on hydrogen and on ammonia. Powers found a noticeable effect, but of very low order, in argon when the search coil was placed against the nozzle. This was interpreted (Ref. 25) as suggesting possible Hall currents within the nozzle. Indications of possible Hall currents were also obtained with nitrogen; however, the signals were weaker than those obtained with argon. The measurements reported by both Brockman (Ref. 56) and Powers (Ref. 25) were obtained with the search coil located very near the thrustor anode. The search coils employed by Brockman were embedded in a boron nitride sleeve located at the exit plane of the anode. The coil nearest the anode was located 0.5 in. from the anode exit plane. The coil used by Powers was placed against the nozzle to obtain the reported indications of Hall currents. Patrick used a rectangular Rogowski coil aligned in a meridian plane of the exhaust. No signals were obtained at any location within the exhaust of the MAARC. In the earlier magnetic annular arc (Fig. 3a) investigated at Avco-Everett, very large Hall currents were measured for operation with both argon and helium.

No particular correlation between the magnitude of the measured Hall currents and the engine geometries is readily apparent. Both the Langley (Fig. 19) and the AVSSD (Fig. 1) engines have a definite anode throat, whereas the Avco-Everett engine (Fig. 3b) has a more open electrode configuration.

The available evidence from the engines discussed above suggests that the discharge occurs very near the anode and therefore that the acceleration occurred within, at most, one or two anode diameters downstream of the engine exit plane. This description is at variance with the analytical models proposed by Cann (Refs. 44, 50, and 51) in which the acceleration occurs much farther downstream. No attempt to measure azimuthal current in the exhaust of the EOS engine has been reported.

Another experimental measurement is of interest. Using a pulsed engine, for which very low discharge pressures were possible, Lovberg (Ref. 72) found no indication of Hall currents. These measurements, which were made within the interelectrode region, indicate that the discharge consisted of a current "spoke" that rotated at about 30 kHz. Lovberg concluded that, because of the lack of appreciable azimuthal current necessary for containment, there would be significant losses to the walls. Although the engine investigated by Lovberg is designed as an MPD accelerator, there are some differences between it and all the other engines discussed in this report. Because the engine operates in a transient mode, it was necessary to heat the cathode prior to the discharge to insure thermionic emission. This requirement dictated the shape of the cathode, which consists of a hairpin turn of a tungsten strip, as shown in Fig. 20. To simplify the

measurements in the interelectrode region, the gap between the cathode and the anode was made much larger, about 3.75 in., than that used for most MPD engines. It is noted that John (Ref. 29) found the X-7C engine to operate in a very erratic manner when the anode diameter was increased to 1.25 in. This comparison is not meant as an evaluation of the ability of the pulsed engine used by Lovberg to simulate the continuous MPD engines, but rather as an observation of some of the major differences between it and those for which performance data are available.

In recent experiments with a segmented anode, Larson has obtained some very convincing evidence of a current "spoke" in a steady-state MPD accelerator. The accelerator geometry is very similar to that of the engines designed at AVSSD, and the exhaust plume appears to have the typical shape associated with MPD thrustors. Larson found the current "spoke" to consist of a fan shape comprising approximately 90 deg and to rotate at a frequency that was greater than 50 kHz and that depended on the thrustor operating parameters of applied arc current, applied field strength, and the feed rate. One of the objectives of Larson's study was to determine whether the observations made by Lovberg were typical of steady-state operation.

The published theoretical considerations concerning Hall currents are conflicting, particularly for a fully ionized plasma. Jahn (Ref. 14) concluded that the ions and electrons will rotate at very nearly the local E/B velocity in a fully ionized hydrogen plasma and therefore there will be negligible Hall currents. The force required to balance the centrifugal force on the particles was not discussed. A similar conclusion was reached by John (Ref. 21). However, for very similar conditions, Rosciszewski (Ref. 96) concluded that Hall currents would flow (see Part IV, Section II-B-2).

From a consideration of the generalized Ohm's law, Hassan (Ref. 61) has concluded that Hall currents flow in the exhaust of the engines operated at Langley. Cann (Ref. 47) argues that there must be Hall currents to provide the necessary containing force to counteract the centrifugal force on the rotating ions as well as to contain the pressure forces. This argument is based on a consideration of the radial momentum equation and also applies to the existence of azimuthal currents in the magnetic nozzle, where recovery of the thermal and rotational energies is postulated to occur. In the absence of any appreciable induced azimuthal magnetic fields, the only containing force that is available is that which results from interactions of an azimuthal current with the applied magnetic field. As discussed previously, there have been no measurements of azimuthal currents in the downstream region that has been identified as a magnetic nozzle.

IV. MPD Magnet Systems

A. Magnet Systems Used With Experimental Engines

A realistic comparison of the MPD thrustor and the ion engine for use on space missions requires that the magnet used with the MPD thrustor be included in the comparison. One method of assessing the magnet requirements is to include the magnet power in the calculation of the overall efficiency. The "cost" of the magnet, in terms of the reduction of the overall efficiency, depends on the strength of the field required and the thrustor power level as well as on the magnet configuration. At a field strength of about 2500 G (Ref. 15), Ducati found that the coil consumed about 4% of the total power of 168 kW and therefore reduced the efficiency by about 2 percentage points at an overall efficiency of about 40% (Ref. 11). For lower power levels and larger magnetic fields, the cost is greater. For example, at an arc power of 20 kW and a field strength of 5000 G, Cann (Ref. 50) reported that the magnet consumed more than 50% of the total input power.

The magnets used in the MPD experimental studies are generally coils of water-cooled copper tubing. This configuration was used because of the economy and ease of fabrication as well as the ease with which the magnet could be operated over a large range of field strengths. Because none of the magnets were designed for use on a space mission, it would not be realistic to use them in the comparison with the ion engine.

B. Flight Configurations

1. Electromagnets. A number of preliminary studies of magnet configurations that would be suitable for space flights have been made. These studies include the use of permanent magnets, electromagnets, and combinations of these two types. The analysis of Ref. 29 is devoted to an electromagnet with a nominal field strength of 1000 G. An electromagnet capable of producing fields of 5000 G is considered in Ref. 48, and the design of and some experimental results obtained with a permanent magnet are presented in Ref. 105. The results of these analyses are expressed as the weight of the magnet plus the power supply that

is required to supply a given field and not as the reduction of the overall efficiency as was done above. The analyses include calculations of the magnet weight and the power required to produce a given magnetic field. The determination of the weight of the power supply required is made through the use of an assumed specific weight of the power supply.

Solenoidal electromagnets are generally analyzed with the aid of the Fabry relation.

$$B_z = G\,(P\lambda/\rho r_i)^{1/2} \tag{66}$$

where

B_z = axial magnetic field strength at the center of the coil

G = a geometric factor that depends on the coil geometry

P = magnet input power

λ = the fraction of the coil that is occupied by the conductor

ρ = the conductor resistivity

r_i = inside radius of the coil

The geometric factor G has a maximum value of about 0.2, and depends on coil geometry through two parameters: α, the ratio of the outside to inside coil radii, r_o/r_i, and β, the ratio of the coil length to the coil diameter, $L/2r_i$. The factor G is a relatively weak function of α and β. The water passages of the copper tubing coils reduce the value of λ to about ½, but solid conductors, with the insulation between windings occupying a negligible value, have been assumed for the problem at hand, and the value of λ is taken as unity.

The power dissipated in the coil must be radiated away, either from the surface of the magnet or from an auxiliary radiator. For the self-cooled solenoid, Eq. 66 is solved simultaneously with the Stefan–Boltzmann equation for the radiated power:

$$P = \varepsilon A \sigma T^4 \tag{67}$$

where

P = power radiated from magnet

ε = surface emissivity of the coil

σ = Stefan–Boltzmann constant

A = radiating surface $= 2\pi\,[(r_o^2 - r_i^2) + r_o L]$

$= 2\pi r_i^2\,(2\alpha\beta + \alpha^2 - 1)$

T = coil surface temperature

The temperature dependence of the conductor resistivity ρ must also be known to obtain a solution for the magnet power and the coil operating temperature.

The analysis reported in Ref. 29, in which both copper and aluminum were considered, was based on the following approximations and assumptions:

$\lambda = 1.0$

$G = 0.2$

α, β = between 2 and 3

$r_i = 1.0$ in.

$B_z = 1000$ G

Power supply specific weight = 50 lb/kW (22.6 kg/kW)

$\varepsilon_{Al} = 0.11$ to 0.19

$\varepsilon_{Cu} = 0.6$

The results obtained show that the copper magnet will operate at a surface temperature of about 300°C, will require about 225 W of power, and, together with the power supply, will weigh about 35 lb. Because of its low emissivity, the aluminum magnet would melt before it reached a temperature high enough to radiate the input power. If the emissivity of aluminum could be increased to 0.6, by, for example, plating with a material of high emissivity, the aluminum magnet would operate at 425°C, require 525 W, and, together with the power supply, weigh about 33 lb.

The required power, and therefore system weight, increases rapidly with increasing field strength. The required current is proportional to the square of the field (see Eq. 66); however, the power increases more rapidly than this because the conductor resistivity increases with temperature, and an increased surface temperature is required to radiate the additional power. Because the resistivity of aluminum increases more rapidly with temperature than does that of copper, the analysis indicates that copper would be preferable for fields greater than 1000 G and that aluminum would be preferable for fields less than 1000 G.

It should be noted that the magnetic system weight increases rapidly as the inner diameter of the coil radius is increased. From Eq. (66) it may be seen that the power, and therefore the weight of the power supply, required to produce a given field (with the conductor resistivity held constant) increases directly with the inside diameter of the coil. The weight of the magnet, however, increases as r_i^3 provided the geometric factors α and β remain unchanged.

It was shown in Ref. 29 that the required outer diameter of a radiation-cooled anode increases with the arc power level. For example, the maximum power of the AVSSD ammonia-fed X-7CR thrustor with a 2-in. anode was about 22 kW, whereas the maximum power of a 4-in.-diam anode was about 55 kW.

The magnet analysis assumes that the magnet can be adequately shielded from the heat radiated from the thrustor itself.

The analysis presented in Ref. 48 is for a field strength of 5000 G and for a coil inside radius of 3 cm. For this analysis, ϵ was assumed to be unity and the specific weight of the power supply was taken as 10 kg/kW. The value of β was fixed at 3.0 and the analysis proceeded by finding the value of α at which the system weight, which included the magnet plus the power supply, was minimized. For copper, which produced a lighter system than aluminum, the minimum system weight for a 5000-G field was about 550 lb.

Because of the different values of the emissivity and the specific weight of the power supply used in the two analyses, a direct comparison cannot be made. However, from a rough qualitative observation it may be seen that if the emissivity of 1.0 as used in Ref. 48 is lowered to 0.6 as used in Ref. 29 and if, similarly, the specific weight of the power supply is increased from 10 kg/kW to over 20 kg/kW, the system described by Cann would be significantly increased. Thus, a requirement of a field strength of 5000 G is accompanied by a rather severe weight penalty.

Cann also considered an externally cooled solenoid in which the power dissipated in the coil is removed to an auxiliary radiator by a coolant. The results of this study indicate that the weight of the total magnet system, which includes the magnet, radiator, and power supply, was less than the self-cooled solenoid by a factor of 3.

In a recent report of the Hall accelerator performance (Ref. 51), Cann states that the magnetic field can be reduced by nearly a factor of 5, i.e., from 5000 to 1000 G, without detrimental effects on the thrustor performance.

2. Permanent magnets. The use of permanent magnets instead of the solenoidal electromagnets, particularly for low thrustor power levels, has been considered (Refs. 48 and 105). The studies reported in Ref. 105 included investigations of simple, cylindrical bar magnets and a magnet configuration in which a soft iron flux-return circuit is used. The design specifications of the study required a volume 2 in. in diameter by 4 in. long (into which the MPD thrustor would be placed) in which the magnetic field is approximately solenoidal and exhibits no field-reversal points. The design field strength was 2000 G at the midpoint of this volume. The results for three magnetically active materials are shown in Table 8 for both 1000 and 2000 G.

Table 8. Estimated weights of cylindrical bar magnets to produce the field for MPD thrustors[a]

Magnet material	Magnet weight, lb	
	1000 G[b]	2000 G[b]
Alnico 9	9.5	168
Alnico 5	22.9	725
Alnico 8	23.5	Not possible

[a]Results from Ref. 105.

[b]On-axis field strength 2 in. from magnet face.

Alnico 9, an improved version of Alnico 8, was not available in sufficient quantities to conduct the experiments reported in Ref. 105. It was noted (Ref. 105) that the thermal stability characteristics of Alnico 9 were not well known at that time. Consequently, Alnico 8 was used for the experimental magnet with a flux-return circuit. The experimental results were used to estimate a weight of 467 lb to produce the design field of 2000 G. If Alnico 9 were to be used, the calculations indicated a weight of 261 lb, which is greater than the 168 lb (see Table 8) required for a simple bar magnet. Eckert and Miller (Ref. 105) suggest the use of a combination consisting of a bar magnet, producing 1000 G, plus an electromagnet solenoid to obtain the desired 2000 G.

C. Summary

Both solenoidal electromagnets and permanent magnets have been considered to produce the required field

for MPD thrustors. All of the investigations have indicated that a severe weight penalty is associated with field requirements in excess of about 1000 G. The lowest estimated magnet weight, 9.5 lb, was for a permanent bar magnet made of Alnico 9 that is capable of producing a field of 1000 G at a position 2 in. from the magnet face.

Part VI. Conclusions

The MPD thrustor continues to show potential as a very promising propulsion device for space exploration missions. However, continued testing, in a suitable test environment, and further development are needed to establish the full potential and to determine the limitations of the thrustor.

At the present time, one useful evaluation of the MPD thrustor as a spacecraft propulsion system is to compare its capacity to perform specific missions with that of the ion engine. Detailed mission analysis for a spacecraft propelled by an ion engine have demonstrated the advantages to be gained by using electric propulsion. An electric propulsion system thrustor must meet a number of requirements to be used successfully as a spacecraft accelerator. These requirements were discussed in Part I of this report, where some of the potential advantages of the MPD engine were listed. The conclusions reached in this study that concern the capacity of the MPD thrustor to meet the requirements are presented below as a comparison of the MPD and ion engines. Included in the following discussion is a summary of the conclusions that concern the present status of the experimental and theoretical efforts in the development of the MPD thrustor.

I. High Thrust Density

Although high thrust density is of minor importance for the solar electric power systems contemplated at present, this characteristic of MPD thrustors would be an advantage of considerable importance for missions requiring much larger power levels. Reported thrust levels of more than 100 gf are not uncommon for the experimental MPD engines, whereas the nominal thrust of a 20-cm-diameter ion engine is less than 10 gf. Qualitative theoretical considerations have indicated that the MPD thrust should be proportional to the square of the magnetic field and possibly from 10^2 to 10^3 times as large as the thrust density of the ion engine. However, the experimental results indicate that the limitation on the thrust of a single MPD engine is associated with the maximum power that can be absorbed by the anode and, further, is not proportional to the square of the applied field. The limitation is more severe for radiation-cooled anodes, which is a likely configuration for space missions, than for water-cooled anodes.

II. Favorable Current–Voltage Operating Characteristics

The MPD thrustor operates at low voltage and high current, whereas the ion engine operates at high voltage and low current. Because solar electric power systems are typically low-voltage devices, it is likely that less weight would be required for the power-conditioning equipment to match the power supply to the MPD thrustor than to the ion engine. A cursory inspection of the solar panel characteristics reveals a striking similarity with the "drooping" current–voltage characteristics of

the electric arc welding machines that are widely used to power the experimental MPD engines. Although no studies have been made to match the solar panel output to the MPD engine, this similarity suggests that the matching of the power supply could be made easily and with a substantial saving in the power-conditioning weight requirements. Another favorable characteristic of the MPD engine is the ability to control the arc voltage to some extent by changing the strength of the applied magnetic field. This could be used to advantage in adjusting the thrustor operating point so that it will remain near the condition at which the solar electric power supply delivers maximum power as the power supply voltage changes. Nuclear power supplies are planned to deliver constant power, at constant voltage, in contrast to the solar electric system. However, it is likely that the nuclear electric power system will also be a low-voltage supply.

III. Lifetime

At present, there are not enough data from endurance tests to predict MPD thrustor lifetime with any degree of accuracy. Minimum lifetimes of around 10,000 h are required for the contemplated missions. Endurance tests of 50 and 75 h have been conducted with MPD thrustors, whereas ion engines have been operated continuously for over 8000 h.

IV. Throttlability

The requirement for a throttlable engine is primarily a consequence of the decreased power level of solar panels as the distance from the spacecraft to the sun increases. To maintain a constant specific impulse, the propellant feed rate must be reduced as the power decreases. The initial performance results indicated that the MPD thrustor could be operated over a wide power range and that there was no dependence of the feed rate on the thrustor performance. However, the more recent results indicate a decrease in the overall efficiency at the lowest feed rates that were used. Nonetheless, it appears that operation down to at least 25% of full thrust can be accomplished without serious degradation of performance. The reduction of the ion engine efficiency as the thrust level is reduced is not well documented; however, the ion engine is probably less versatile in this respect than is the MPD thrustor.

V. Thrust Level

As discussed in Part I, the required thrust level of a single engine is closely associated with the throttling, redundancy, and thrust-vector control requirements, in addition to the basic requirement of the total power needed to perform a specified mission. At very high power levels, the MPD engine has a distinct advantage because of its higher thrust density. However, at low power levels, it is likely that the ion engine maintains an advantage. Most of the experimental MPD engines have been designed to be operated at between about 20 and 100 kW. Smaller engines, some designed to operate at nominal power levels as low as 2 kW, have also been tested. With few exceptions, the reported performance of the low-power engines has been less efficient than that of the larger engines. The ability to scale MPD thrustors from one size to another, without degrading the performance, remains one of the problems in the development of MPD thrustors.

VI. Performance

Because of the experimental uncertainties associated with the testing of the MPD thrustor, the performance of this engine remains questionable. Electrode losses, which account for 30 to 50% of the input power, severely limit the efficiency of the MPD thrustor. Frozen-flow losses also contribute to the inefficiency of the MPD engine, but the limitations imposed by these losses are not well understood because of experimental ambiguities. Specific impulse limitations cannot be predicted from the available theoretical studies or ascertained from the experimental results because of entrainment and other factors. A number of specific conclusions concerning the experimental and theoretical development and pertaining to the demonstrated performance and basic understanding of the MPD thrustor are summarized below. The basis for these conclusions is discussed in Part V.

(1) Much of the reported performance data of MPD thrustors is questionable because of the probability of entrainment or other interactions with the test environment. The probability of experimental anomalies appears to be greatest for the data that indicate the "best" performance.

(2) A suitable test environment for MPD thrustors has yet to be defined.

   (a) Evidence of the effect of entrainment on the measured performance cannot be detected

from the usually observed performance parameters unless the indicated overall efficiency exceeds the thermal efficiency. However, the data indicating decreasing ionization fraction as the power is increased or as the applied magnetic field strength is increased probably indicate anomalous measurements.

(b) Entrainment of ambient gas into the thrustor exhaust plume affects the calculated performance only if the gas is entrained into the region in which the acceleration occurs. The danger of entrainment increases as the size of the acceleration region in the downstream exhaust plume increases. The size of the acceleration volume in the exhaust probably is a function of the engine geometry and probably increases with increasing applied magnetic field strength and with increasing power-to-feed-rate ratio.

(c) The available evidence of the effect of entrainment at very low test pressures is inconclusive but is consistent with the argument that entrainment is reduced at very low test pressures.

(3) The highest overall efficiencies, at values of specific impulse above about 1500 s, have been reported for lithium. At values of specific impulse less than 1500 s, the efficiencies of sodium and potassium exceed that of lithium. The overall efficiency of ammonia is slightly higher than that of hydrogen, and the use of ammonia as a propellant for MPD thrustors continues to be of interest.

(4) MPD thrustors have been operated both with and without an applied magnetic field. The advantages of operation with an applied magnetic field favor this mode of operation for most practical applications. These advantages include:

(a) Longer lifetime of the electrodes.

(b) Increased arc stability.

(c) More favorable current–voltage characteristics. When a field is applied, the thrustor operates at a higher voltage, and some independent control of the voltage may be exercised.

(d) At lower power levels, more efficient operation may be obtained if an external magnetic field is applied.

(5) The total thrust produced by MPD thrustors results from the combination of a number of mechanisms that have been classified as aerodynamic (the thermal expansion of electrothermally heated propellant by pressure forces) and various electromagnetic mechanisms. The acceleration mechanisms have generally been treated separately and are usually uncoupled from all other processes. Some recent effort is devoted to obtaining self-consistent solutions in which the individual mechanisms are not treated separately.

(a) A quantitative and satisfactory theoretical description of the thrust production by aerodynamic forces has not been formulated.

(1) For thrustor operation without an applied field, empirically determined thrust coefficients of less than unity are not consistent with qualitative arguments based on the proposed similarity of the expansion in MPD engines to that in conventional nozzles.

(2) For thrustor operation with an applied field, the concept of thrust coefficient, as customarily used for conventional nozzle expansions, cannot be applied to MPD thrustors to separate the aerodynamic from the electromagnetic contributions to the total thrust.

(b) A general expression for the electromagnetic thrust production that results from the interaction of the applied current and its self-induced magnetic field has been derived.

(c) The theoretical description of the energy addition and acceleration mechanisms of MPD thrustor operation with an applied magnetic field is poorly understood at the present time. This is illustrated by the number of different, and sometimes conflicting, mechanisms that have been proposed. The proposed mechanisms are based on numerous assumptions, of which only a few have been verified experimentally. In particular, the role of Hall currents in the operation of MPD thrustors has not been clarified.

(6) At present, the level of understanding of the basic thrustor mechanisms and their dependence on the thrustor operating variables is insufficient to:

(a) Permit a critical evaluation of the performance data.

(b) Predict thrustor operation in the environment of the hard vacuum of space.

(c) Aid appreciably in the design of an "optimum" engine.

(d) Select the optimum propellant for a specific mission.

(e) Permit scaling of experimental engines to other sizes, either larger or smaller.

(7) The formulation of a realistic theory of the many complex processes that occur in MPD thrustor operation is hampered by the questionable nature of much of the performance data because of the possibility of entrainment or other interactions with the test environment, and by the small amount of necessary and sufficiently accurate diagnostic measurements.

VII. Summary

In spite of the uncertainties associated with the MPD engine, it may be concluded that, with the possible exception of operation at values of specific impulse less than 3000 s, the ion engine operates more efficiently than does the MPD thrustor. If the MPD thrustor is to be competitive with the ion engine as a spacecraft propulsion system, it is necessary that the weight savings gained from the reduced power conditioning requirement and other sources be sufficient to offset the advantage of higher overall efficiency that may presently be attributed to the ion engine. Before such a comparison can be meaningful, it will be necessary to eliminate experimental uncertainties and establish the true performance of the MPD engine.

References

1. Stearns, J. W., and Kerrisk, D. J., "Solar-Powered Electric Propulsion Systems – Engineering and Applications," Paper 66-576, presented at the AIAA Second Propulsion Joint Specialist Conference, Colorado Springs, Colo., June 13–17, 1966.

2. *Solar Powered Electric Propulsion Spacecraft Study,* Final Report SSD50094R. Hughes Aircraft Company, El Segundo, Calif., Dec. 1965.

3. Toms, R. S., Waddell, R. L., and Fine, S. B., *Feasibility Study of an Ion-Propelled Mars Orbiter/Lander Spacecraft With Solar Photovoltaic Power,* Report 4816-Final. Electro-Optical Systems, Pasadena, Calif., May 1966.

4. Stewart, H. J., "New Possibilities for Solar-System Exploration," *Astronaut. Aeronaut.*, Vol. 4, pp. 26–31, Dec. 1966.

5. Sohl, G., Fosnight, V. V., and Goldner, S. J., *Electron Bombardment Cesium Ion Engine System,* Report 6954-Summary. Electro-Optical Systems, Pasadena, Calif., Apr. 1967. Also available as NASA CR-54711.

6. Ducati, A. C., *Study of the Factors Affecting the Efficiency in Thermal Acceleration of Propellants,* Sixth Quarterly Technical Report 6QS-113-1161. Giannini Scientific Corporation, Santa Ana, Calif., Oct. 1963.

7. *High Specific Impulse Thermo-Ionic Acceleration,* PRE-114-a. Giannini Scientific Corporation, Santa Ana, Calif., Dec. 1963.

8. Ducati, A. C., Giannini, G. M., and Muehlberger, E., "Experimental Results in High-Specific-Impulse Thermo-Ionic Acceleration," *AIAA J.*, Vol. 2, No. 8, pp. 1452–1454, Aug. 1964.

References (contd)

9. Ducati, A. C., Muehlberger, E., and Giannini, G., "High Specific Impulse Thermo-Ionic Acceleration," Paper 64-668, presented at the AIAA Fourth Electric Propulsion Conference, Philadelphia, Pa., Aug. 31–Sept. 2, 1964.

10. Ducati, A. C., Muehlberger, E., and Todd, J. P., *Design and Development of a Thermo-Ionic Electric Thrustor,* Interim Report 1QS094-968. Giannini Scientific Corporation, Santa Ana, Calif., Sept. 1964.

11. Ducati, A. C., Muehlberger, E., and Todd, J. P., *Design and Development of a Thermo-Ionic Electric Thrustor,* Interim Report 2QS114-968. Giannini Scientific Corporation, Santa Ana, Calif., Nov. 1964.

12. Ducati, A. C., Muehlberger, E., and Todd, J. P., *Design and Development of a Thermo-Ionic Electric Thrustor,* Interim Report 3QS025-968. Giannini Scientific Corporation, Santa Ana, Calif., Feb. 1965.

13. Ducati, A. C., and Muehlberger, E., *Design and Development of a Thermo-Ionic Electric Thrustor,* Interim Report 4QS055-968. Giannini Scientific Corporation, Santa Ana, Calif., May 1965.

14. Jahn, R. G., *Design and Development of a Thermo-Ionic Electric Thrustor,* Interim Report 5QS085-968. Giannini Scientific Corporation, Santa Ana, Calif., Aug. 1965.

15. Ducati, A. C., et al., *Design and Development of a Thermo-Ionic Electric Thrustor,* Final Report FR-056-968. Giannini Scientific Corporation, Santa Ana, Calif., May 1966. Also available as NASA CR-54703.

16. Ducati, A. C., *Electrothermally Accelerated Plasma Jets,* Final Technical Report FR 096-1572 covering june 1, 1965, to May 31, 1966. Giannini Scientific Corporation, Santa Ana, Calif., Sept. 30, 1966.

17. Ducati, A. C., Giannini, G. M., and Muehlberger, E., *Recent Progress in High Specific Impulse Thermo-Ionic Acceleration,* Paper 65-96, presented at the AIAA 2nd Aerospace Sciences Meeting, New York, Jan. 25–27, 1965.

18. John, R. R., and Bennett, S., *Arc Jet Technology Research and Development,* AVCO/RAD SR 64-239. Avco Corporation, Research and Advanced Development Division (now AVSSD), Wilmington, Mass., Oct. 1964.

19. John, R. R., and Bennett, S., *Arc Jet Technology Research and Development,* Second Quarterly Progress Report, AVCO/RAD SR 65-5. Avco Corporation, Research and Advanced Development Division (now AVSSD), Wilmington, Mass, Dec. 1964.

20. John, R. R., and Bennett, S., *Arc Jet Technology Research and Development,* Fourth Quarterly Progress Report, AVCO/RAD SR 65-20. Avco Corporation, Research and Advanced Development Division (now AVSSD), Wilmington, Mass., June 1965.

21. John, R. R., and Bennett, S., *Arc Jet Technology Research and Development,* AVCO/RAD SR-65-37, Final Report. Avco Corporation, Research and Advanced Development Division (now AVSSD), Wilmington, Mass., Dec. 1965. Also available as NASA CR-54687.

References (contd)

22. John, R. R., Bennett, S., and Connors, J., "Experimental Performance of a High Specific Impulse Arc Jet Engine," Paper 64-669, presented at the AIAA Fourth Electric Propulsion Conference, Philadelphia, Pa., Aug. 31–Sept. 2, 1964.

23. John, R. R., and Bennett, S., "Recent Advances in Electrothermal and Hybrid Electrothermal–Electromagnetic Propulsion," presented at the AFOSR Fourth Symposium on Advanced Propulsion Concepts, Palo Alto, Calif., Apr. 1965.

24. Bennett, S., et al., "Cesium Fueled MPD Arcjet Engine Performance," Paper 65-296, presented at the 2nd Annual AIAA Meeting, San Francisco, Calif., July 26–29, 1965.

25. Powers, W. E., "Measurements of the Current Density Distribution in the Exhaust of an MPD Arc Jet," Paper 66-116, presented at the 3rd AIAA Aerospace Sciences Meeting, New York, Jan. 24–26, 1966.

26. Bennett, S., et al., "Experimental Investigation of the MPD Arcjet," Paper 66-239, presented at the AIAA Fifth Electric Propulsion Conference, San Diego, Calif., March 7–9, 1966.

27. Malliaris, A. C., "Phenomena in the Cathode Region of an MPD Accelerator," Paper No. 67-47, presented at the AIAA 5th Aerospace Sciences Meeting, New York, Jan. 23–26, 1967; also, *AIAA J.*, Vol. 5, No. 7, pp. 1325–1328, July 1967.

28. Malliaris, A. C., "Plasma Acceleration in an Electrical Discharge by the Self-Induced Magnetic Field," *J. Appl. Phys.*, Vol. 38, No. 9, pp. 3611–3619, Aug. 1967.

29. John, R. R., and Bennett, S., *Magnetoplasmadynamic Arcjet Thrustor*, Semi-annual Report, AVSSD-0161-67. Avco Space Systems Division, Wilmington, Mass., Mar. 1967.

30. Powers, W. E., and Patrick, R. M., "A Magnetic Annular Arc," presented at the Second Symposium on Engineering Aspects of Magnetohydrodynamics, University of Pennsylvania, Mar. 1961.

31. Powers, W. E., and Patrick, R. M., "Magnetic Annular Arc," *Phys. Fluids*, Vol. 5, No. 10, pp. 1196–1206, Oct. 1962.

32. Patrick, R. M., and Powers, W. E., "Plasma Flow in a Magnetic Arc Nozzle," presented at the Third Symposium on Advanced Propulsion Concepts, Cincinnati, Ohio, Oct. 1962.

33. Patrick, R. M., *Study of Magnetic Annular Plasma Accelerator*, Second Quarterly Progress Report, Contract NAS 3-5748. Avco-Everett Research Laboratory, Everett, Mass., Sept. 1964.

34. Patrick, R. M., and Schneiderman, A. M., *Study of Magnetic Annular Plasma Accelerator*, Third Quarterly Progress Report, Contract NAS 3-5748, Oct. 1–Dec. 31, 1964. Avco-Everett Research Laboratory, Everett, Mass.

References (contd)

35. Patrick, R. M., and Schneiderman, A. M., *Study of Magnetic Annular Plasma Accelerator,* Fourth Quarterly Progress Report, Contract NAS 3-5748, Jan. 1–Mar. 31, 1965. Avco-Everett Research Laboratory, Everett, Mass.

36. Patrick, R. M., and Schneiderman, A. M., *Performance Characteristics of a Magnetic Annular Arc,* Research Report 209, Contract AF 49(638)-659 and Contract NAS 3-5748, Mar. 1965. Avco-Everett Research Laboratory, Everett, Mass.

37. Schneiderman, A. M., and Patrick, R. M., "Optimization of the Thermal Efficiency of the Magnetic Annular Arc," Paper 66-115, presented at the AIAA 3rd Aerospace Sciences Meeting, New York, Jan. 24–26, 1966.

38. Patrick, R. M., and Schneiderman, A. M., *Axial Current Distribution in the Exhaust of the Magnetic Annular Arc,* Research Report 231, Contract NAS 3-5748. Avco-Everett Research Laboratory, Everett, Mass., Feb. 1966.

39. Patrick, R. M., and Schneiderman, A. M., "Performance Characteristics of a Magnetic Annular Arc," *AIAA J.*, Vol. 4, pp. 283–290, Feb. 1966.

40. Patrick, R. M., and Schneiderman, A. M., *Study of Magnetic Annular Plasma Accelerator,* Summary Report, Contract NAS 3-5748, Apr. 15, 1964–Jan. 14, 1966. Avco-Everett Research Laboratory, Everett, Mass. Also available as NASA CR-54686.

41. Cann, G. L., and Marlotte, G. L., "Hall Current Plasma Accelerator," *AIAA J.*, Vol. 2, No. 7, pp. 1234–1241, July 1964.

42. Cann, G. L., and Harder, R. L., *Follow-On Investigation of a Steady State Hall Current Accelerator,* Report 4010-Final. Electro-Optical Systems, Pasadena, Calif., Oct. 30, 1964. Also available as NASA CR-54062.

43. Cann, G. L., "Annular Magnetic Hall Current Accelerator," Paper 64-670, presented at the AIAA Fourth Electric Propulsion Conference, Philadelphia, Pa., Aug. 31–Sept. 2, 1964.

44. Cann, G. L., Lenn, P. D., and Harder, R. L., *Hall Current Accelerator,* First Quarterly Progress Report, 5470-QL-1. Electro-Optical Systems, Pasadena, Calif., Oct. 5, 1964.

45. Cann, G. L., Lenn, P. D., and Harder, R. L., *Hall Current Accelerator,* Second Quarterly Progress Report, 5470-Q-2. Electro-Optical Systems, Pasadena, Calif., Dec. 20, 1964.

46. Cann, G. L., Lenn, P. D., and Harder, R. L., *Hall Current Accelerator,* Report 5470-Q-3. Electro-Optical Systems, Pasadena, Calif., Mar. 20, 1965.

47. Cann, G. L., et al., *Hall Current Accelerator,* Report 5470-Final, Electro-Optical Systems, Pasadena, Calif., Feb. 4, 1966. Also available as NASA CR-54705.

48. Cann, G. L., et al., *High Specific Impulse Thermal Arc Jet Thrustor Technology,* Interim Report on Contract AF 33(615)-1579. Electro-Optical Systems, Pasadena, Calif., Dec. 1964.

References (contd)

49. Moore, R. A., Cann, G. L., and Gallagher, L. R., *High Specific Impulse Thermal Arc Jet Thrustor Technology,* Report 5090-Phase I Final. Electro-Optical Systems, Pasadena, Calif., June 1965. Also available as AFAPL-TR-65-48.

50. Cann, G. L., et al., *High Specific Impulse Thermal Arc Jet Thrustor Technology,* Report 5090-IR-2. Electro-Optical Systems, Pasadena, Calif., Sept. 1965.

51. Cann, G. L., et al., *High Specific Impulse Thermal Arc Jet Thrustor Technology,* Report on Phase II of Contract AF 33(615)-1579. Electro-Optical Systems, Pasadena, Calif., Jan. 1967. Also available as AFAPL-TR-65-48, Part II.

52. Jacobs, P. F., and Cann, G. L., *Diagnostics of an Alkali Plasma Hall Current Accelerator,* Report 7055-SA-1. Electro-Optical Systems, Pasadena, Calif., Sept. 1966.

53. Jacobs, P. F., Gallagher, L. R., and Pritchard, R. W., "Diagnostic Measurements in an Alkali Plasma Hall Accelerator," Paper 67-46, presented at the AIAA 5th Aerospace Sciences Meeting, New York, Jan. 23–26, 1967.

54. Hess, R. V., "Experiments and Theory for Continuous Steady Acceleration of Low Density Plasmas," *Proceedings of the Eleventh International Astronautical Congress,* August 1960: Vol. I, pp. 404–411. Edited by C. W. P. Reutersward. Springer-Verlag, Vienna, 1961

55. Brockman, P., Hess, R. V., and Weinstein, R., "Measurements and Theoretical Interpretation of Hall Currents for Steady Axial Discharges in Radial Magnetic Fields," Paper 63-382, presented at the AIAA Fifth Biennial Gas Dynamics Symposium, Northwestern University, Evanston, Ill., Aug. 14–16, 1963.

56. Brockman, P., et al., "Diagnostic Studies in a Hall Accelerator at Low Exhaust Pressure," Paper 65-297, presented at the AIAA Second Annual Meeting, July 26–29, 1965; also, *AIAA J.,* Vol. 4, No. 7, pp. 1209–1214, July 1966.

57. Grossman, W., Hess, R. V., and Hassan, H. A., "Experiments with Coaxial Hall Current Plasma Accelerator," Paper 64-700, presented at the AIAA Fourth Electric Propulsion Conference, Philadelphia, Pa., Aug. 31–Sept. 2, 1964; also *AIAA J.,* Vol. 3, No. 6, pp. 1034–1039, June 1965.

58. Burlock, J., et al., "Measurement of Velocities and Acceleration Mechanism for Coaxial Hall Accelerators," Paper 66-196, presented at the AIAA Fifth Electric Propulsion Conference, San Diego, Calif., March 7–9, 1966; also *AIAA J.,* Vol. 5, No. 6, pp. 558–561, March 1967.

59. Hoell, J. M., and Brooks, D. R., "Effect of Propellant Injection Through Electrodes on Potential Distribution in an MPD Arc," Paper 67-49, presented at the AIAA Fifth Aerospace Sciences Meeting, New York, Jan. 23–26, 1967.

References (contd)

60. Hassan, H. A., "Thrust From an MPD Arc Jet," *AIAA J.*, Vol. 5, No. 2, pp. 338–339, Feb. 1967.

61. Hassan, H. A., Hess, R. V., and Grossman, W., Jr., *Study of Coaxial Hall Current Accelerators at Moderate Pressures*, NASA TN D-3286. National Aeronautics and Space Administration, Washington, D. C., Oct. 1966.

62. Coleman, R. L., Hassan, H. A., and Garcia, B. H., Jr , "Potential and Current Distribution in MPD Arcs," Paper 67-48, presented at the AIAA Fifth Aerospace Sciences Meeting, New York, Jan. 23–26, 1967.

63. Hassan, H. A., and Garrison, G. W., Jr., "Anode Losses in Coaxial Hall Current Accelerators," *AIAA J.*, Vol. 5, No. 5, pp. 840–843, May 1967.

64. Finke, R. C., Holmes, A. D., and Keller, T. A., "Space Environment Facility for Electric Propulsion Systems Research," NASA TN D-2774, National Aeronautics and Space Administration, Washington, D. C., May 1965.

65. Jones, R. E., and Walker, E. L., "Status of Large Vacuum Facility Tests of MPD Arc Thrustor," Paper 66-117, presented at the AIAA 3rd Aerospace Sciences Meeting, New York, Jan. 24–26, 1966.

66. Connolly, D. J., et al., "Low Environmental Pressure MPD Arc Tests," Paper 67-685, presented at the AIAA Electric Propulsion and Plasma-Dynamics Conference, Sept. 11–13, 1967, Colorado Springs, Colo.

67. Connolly, D. J., et al., "Status of Large Vacuum Facility H_2, NH_3, and Li MPD Arc Tests," presented at the NASA OART Fifth Intercenter and Contractors Conference on Plasma Physics, Part III, NASA Lewis Research Center, Washington, D. C., May 24–26, 1966.

68. Jones, R. E., "Results of Large Vacuum Facility Tests of an MPD Arc Thrustor," *AIAA J.*, Vol. 4, No. 8, pp. 1455–1456, Aug. 1966.

69. Seikel, G. R., Bowditch, D. N., and Domitz, S., "Application of Magnetic-Expansion Plasma Thrustors to Satellite Station Keeping and Attitude Control Missions," Paper 64-677, presented at the AIAA Fourth Electric Propulsion Conference, Philadelphia Pa., Aug. 31–Sept. 2, 1964.

70. Johansen, A. E., Bowditch, D. N., and Burkhart, J. A., "Experimental Performance of a Low-Power MPD Arc Thrustor," Paper 67-50, presented at the AIAA Fifth Aerospace Sciences Meeting, New York, Jan. 23–26, 1967.

71. Lovberg, R., *Physical Processes in the Magneto-Plasmadynamic Arc*, First Semiannual Report, NASA Grant NGR-05-009-030. University of California, La Jolla, Calif., Nov. 1966.

72. Lovberg, R., *Physical Processes in the Magneto-Plasmadynamic Arc*, Second Semiannual Report, NASA Grant NGR-05-009-030. University of California, La Jolla, Calif , Mar. 1967.

73. Mickelsen, W. R., "Advanced Concepts in Electric Propulsion," Paper 67-426, presented at the AIAA Third Propulsion Joint Specialist Conference, Washington, D. C., July 17–21, 1967.

References (contd)

74. Domitz, S., et al., *Survey of Electromagnetic Accelerators for Space Propulsion*, NASA TN D-3332. National Aeronautics and Space Administration, Washington, D. C., Mar. 1966.

75. Noeske, H. O., "The Co-Axial MPD-Engine: A State-of-the-Art Review," Paper 66-242, presented at the AIAA Fifth Electric Propulsion Conference, San Diego, Calif., Mar. 7–9, 1966.

76. John, R. R., Bennett, S., and Jahn, R. G., "Current Status of Plasma Propulsion," Paper 66-565, presented at the AIAA Second Propulsion Joint Specialist Conference, Colorado Springs, Colo., June 13–17, 1966.

77. Clark, K. E., and Jahn, R. G., "The Magnetoplasmadynamic Arcjet," *Astronaut. Acta*, to be published.

78. Connolly, D. J., NASA Lewis Research Center, Cleveland, Ohio, private communication.

79. Treat, R. P., Giannini Scientific Corporation, Santa Ana, Calif., private communication.

80. Larson, A. V., "Experiments on Current Rotations in an MPD Engine," Paper 67-689, presented at the AIAA Electric Propulsion and Plasmadynamics Conference, Sept. 11–13, 1967, Colorado Springs, Colo.

81. Hess, R. V., NASA Langley Research Center, Hampton, Va., private communication.

82. Malliaris, A. C., "Induction Velometry in an Ionized Gas," *J. Appl. Phys.*, Vol. 37, No. 11, pp. 4159–4168, Oct. 1966.

83. Brooks, D. R., "Use of Rotating Langmuir Probes in Flowing Plasmas," *Rev. Sci. Instr.*, Vol. 37, No. 12, p. 1731, Dec. 1966.

84. Sonin, A. A., "Free-Molecule Langmuir Probe and Its Use in Flowfield Studies," *AIAA J.*, Vol. 4, No. 9, pp. 1588–1596, Sept. 1966.

85. Smetana, F. O., "On the Current Collected by a Charged Circular Cylinder Immersed in a Two-Dimensional Rarefied Plasma Stream," in *Rarefied Gas Dynamics*, Vol. II, p. 65. Edited by J. A. Laurmann. Academic Press Inc., New York, 1963.

86. Bowen, F. W., et al., "Optical Measurements of Temperature and Velocity in Low Density Plasma Streams," presented at the NASA OART Fifth Intercenter and Contractors Conference on Plasma Physics, Part II, NASA Langley Research Center, Washington, D. C., May 24–26, 1966.

87. Kelly, A. J., Nerheim, N. M., and Gardner, J. A., "Electron Density and Temperature Measurements in the Exhaust of a MPD Source," Paper 65-298, presented at the AIAA Second Annual Meeting, San Francisco, Calif., July 26-29, 1965; also *AIAA J.*, Vol. 4, No. 2, p. 291, Feb. 1966.

88. Nerheim, N., "Spectroscopic Measurement of Plasma Electron Temperature Using the Relative Intensities of Argon II Lines," *Supporting Research and Advanced Development*, Space Programs Summary 37-35, Vol. IV, pp. 174–180. Jet Propulsion Laboratory, Pasadena, Calif., Oct. 31, 1965.

References (contd)

89. Workman, J., Avco-Everett Research Laboratory, Everett, Mass., private communication.

90. Spitzer, L., Jr., *Physics of Fully Ionized Gases,* Interscience Publishers, Inc., New York, 1962.

91. Maecker, H., "Plasmastromügen in Lichtobogen infloge eigen Magnetioischer Kompression," *Z. Phys.*, Vol. 141, pp. 198–216, 1955.

92. Stratton, T. F., "High Current Steady State Coaxial Plasma Accelerators," *AIAA J.*, Vol. 3, No. 10, pp. 1960–1963, Oct. 1965.

93. Ellis, M. C., Jr., "Survey of Plasma Accelerator Research," Paper 62, *Proceedings of the NASA–University Conference on the Science and Technology of Space Exploration,* Vol. 2. National Aeronautics and Space Administration, Washington, D. C., Nov. 1963.

94. Seikel, G. R., and Reshotko, E., "Hall Current Ion Accelerator," *Bull. Am. Phys. Soc.*, Vol. 7, No. 6, 1962.

95. Brandmaier, A. E., et al., "An Investigation of Hall Propulsor Characteristics," *AIAA J.*, Vol. 2, pp. 674–681, 1964.

96. Rosciszewski, J., "Acceleration Process in the Hall Current Device," *Phys. Fluids,* Vol. 10, No. 5, pp. 1095–1099, May 1967.

97. Fahleson, U. V., "Experiments with Plasma Moving Through Neutral Gas," *Phys. Fluids,* Vol. 4, No. 1, pp. 123–127, Jan. 1961.

98. Alfvén, H., "Collision Between a Nonionized Gas and a Magnetized Plasma," *Rev. Mod. Phys.*, Vol. 32, pp. 710–713, 1960.

99. Lin, S. C., "Limiting Velocity for a Rotating Plasma," *Phys. Fluids,* Vol. 4, No. 10, pp. 1277–1288, Oct. 1961.

100. Allis, W. P., "Motions of Ions and Electrons," *Encyclopedia of Physics,* Vol. 21, Springer-Verlag, Berlin, 1956.

101. Hügel, H., Kruelle, G., and Peters, T., "Investigations on Plasma Thrustors with Thermal and Self-Magnetic Acceleration," *AIAA J.*, Vol. 5, No. 3, pp. 551–558, Mar. 1967.

102. Giovanelli, R., "Comment on 'Performance Characteristics of a Magnetic Annular Arc'," *AIAA J.*, Vol. 5, No. 8, p. 1530, Aug. 1967.

103. Patrick, R. M., and Schneiderman, A. M., "Reply by Authors to R. Giovanelli," *AIAA J.*, Vol. 5, No. 8, p. 1531, Aug. 1967.

104. Herrnegger, F., *The Magnetic Lavel Nozzle,* Scientific Report 34. Institute for Theoretical Physics, University of Innsbruck, Austria, May 24, 1966.

105. Eckert, A. C., and Miller, D. B., *Initial Design Study of a Permanent Magnet for Use with an MPD Arc Thruster,* Final Report. Space Sciences Laboratory, General Electric Company, Philadelphia, Pa., Jan. 11, 1967. Also available as NASA CR-54690.